Variations in GDGT flux and TEX_{86} thermometry in three distinct oceanic regimes of the Atlantic Ocean: a sediment trap study

Dissertation
Zur Erlangung des Doktorgrades der Naturwissenschafen
am Fachbereich Geowissenschaften
der Universität Bremen
- Dr.rer.nat. -

Vorgelegt von:

Eun Mi Park

Bremen
März 2019

Universität Bremen

Gutachter der Dissertation:

Prof.Dr. Gesine Mollenhauer
Department of Geosciences
University of Bremen &
Alfred Wegener Institute
Am Handelshafen 12
27570 Bremerhaven
Germany
gesine.mollenhauer@awi.de

Prof.Dr. Ann Pearson
Department of Earth and Planetary Sciences
Harvard University
Cambridge, MA 02138
USA
apearson@eps.harvard.edu

To my parents

This Ph.D. project was conducted at the Marine Geochemistry group at the Alfred Wegener Institute Helmholtz Center for Polar and Marine Research, Bremerhaven, Germany and at the Department of Geosciences, University of Bremen under the supervision of Prof.Dr. Gesine Mollenhauer. This project was funded through the German Science Foundation (DFG) Research Center/Cluster of Excellence “The Ocean in the Earth System” MARUM – Center for Marine Environmental Sciences. The Bremen International Graduate School for Marine Sciences (GLOMAR) provided financial support for participation in summer schools and international conferences.

Table of Contents

ABSTRACT

The global climate change and global warming have been observed since the pre-industrial times. This phenomenon calls for immediate actions to fight climate change. The climate change of the Earth´s history is preserved in the ocean, covering ~70% of the Earth, and the understanding of this history is the significant way to predict the future climate. The temperature changes in the past ocean can be estimated using several proxies. One of the most extensively applied temperature proxy to the paleoclimate is the TEX_{86} (tetraether index of tetraethers consisting of 86 carbons). It is based on the relative compositions of thaumarchaeotal membrane lipids, glycerol dialkyl glycerol tetraethers (GDGTs), in marine surface sediments, allowing us to estimate sea surface temperature (SST). The ubiquities of Thaumarchaeota, one phylum of the Archaea domain, and their dominant abundance in the ocean have made them a novel proxy. However, it has been recognized that the composition of GDGTs can be altered by non-thermal factors, leading the unconventional relationship between TEX_{86} and SST. This thesis shall contribute to a better understanding of TEX_{86} thermometry and the controlling environmental factors in various oceanic provinces by evaluating the GDGT flux and TEX_{86} related temperature estimate in sinking particles. The sinking particles collected using a time-series sediment trap system can be a great value to understand the export mechanism of lipids and to estimate the seasonal variability of the proxy signal. Three different ocean regimes from the upwelling (the Guinea Basin and Lüderitz off Namibia), high latitude (the eastern Fram Strait and the Antarctic Polar Front), and the oligotrophic oceans (the central Brazil Basin) in the Atlantic Ocean are investigated.

In the first part of the thesis, TEX_{86} values are converted to temperatures using the TEX_{86}^{H} calibration. The results in the eastern equatorial Guinea Basin (GBN3) show that GDGTs are mainly transported by particles containing opal. The TEX_{86}^{H}-derived temperatures at both different depth traps correspond to the subsurface water depth (~50 m), where the nutricline exists, implying the favorable habit depth of thaumarchaeotal communities and thus the record of the water temperature. In the coastal upwelling area off Lüderitz (LZ), the export mechanism of GDGT is yet unclear due to the shortage of the sampling period. The results show that the TEX_{86}^{H}-derived temperatures resemble the satellite-derived SSTs with a delay of 26 days during the warmer season while the warm-biased estimates occur during the colder season. As relatively higher TEX_{86} values were found in oxygen-depleted waters, it explains the warm-bias of TEX_{86}^{H} temperature in the Lüderitz, where the oxygen minimum zone is pronounced. This result is in agreement with the finding from off Cape Blanc, Northwest Africa.

The second part of the thesis focuses on the high latitude cold regions. The TEX_{86} values are converted to temperatures using the TEX_{86}^{L} calibration. In the eastern Fram Strait (79° N; FEVI16),

GDGT fluxes are correlated with biological and non-biological component fluxes. The best correlations are found between GDGT and opal/ carbonate fluxes, implying that opal and carbonate are the major transport of GDGTs to the deep ocean. The TEX_{86}^{L}-derived temperatures display the strong variability due to temporal variability of transporting materials and their different sinking velocities for particles carrying the lipids. The TEX_{86}^{L} signal corresponds to water temperature at 30-80 m depth, where nitrification might occur, and the almost identical is found in the underlying surface sediment. In the Antarctica Polar Front (50° S; PF3), the TEX_{86}^{L}-derived temperatures at the shallow trap display the cold and warm biases relative to the SSTs and the latter has a tendency to occur during periods of relatively low GDGT flux, which may be more dominant in the deep trap. The warm biased TEX_{86}^{L} signal (~7 °C) compared to the SST at the deep trap and in the underlying surface sediment might be due to the contribution of Euryarchaeota or the non-liner relationship of TEX_{86}^{L} with SST in the Southern Ocean. In both polar regions, hydroxylated-GDGT related temperature proxy seems applicable.

The third part of the thesis contributes to the oligotrophic regions, where usually attract less attention compared to two previous regimes despite its size and the impact on global biogeochemical budgets. The TEX_{86} values at two depths from two sites are examined (WAB1 and WA9). Good correlations between GDGT and opal/carbonate at both shallow traps reveal the preferential incorporation of GDGTs in opal- and carbonate-rich aggregates. At WAB1, which was located in the fringes of the gyre system, the TEX_{86}^{H}-derived temperatures of the shallow trap resemble the SSTs. The WA9 trap was collected in the more nutrient-depleted location of the central oligotrophic gyre relative to the site WAB. The warm biased TEX_{86}^{H}-derived temperature of the shallow trap relative to the SST can be caused by the response of Thaumarchaeota under the energy stressed condition. In the deep traps of both sites, the TEX_{86}^{H}-derived temperatures record the deep subsurface temperature. It is assumed that these signals are caused by the relatively dominant contribution of colder signal from deep *in situ* production and the smaller contribution of warmer signal from shallow waters.

The last part of the thesis investigates the alkenone-based temperatures (U_{37}^{k} or $U_{37}^{k'}$) in all three oceanic regimes, where GDGT based temperatures are discussed in previous chapters. Most of $U_{37}^{k'}$-derived temperatures display the SSTs of the tropical regions (i.e. the equatorial Guinea Basin, Lüderitz, the central Brazil Basin). It implies the regional geochemical characteristics (e.g., availability of nitrogen or oxygen), which probably affect the TEX_{86} thermometry, would not have an impact on the $U_{37}^{k'}$ thermometry. In the shallow trap of the Antarctic Polar Front, the $U_{37}^{k'}$-derived temperatures record the clear SST seasonality with a delay time of 10 weeks. However, the mixture of cold- and warm-biased temperature estimates of the deep trap is underconstrained. Samples from the eastern Fram Strait yield U_{37}^{k}- and $U_{37}^{k'}$-derived temperature estimates fall outside the expected

temperature range with the warm biases. It is in line with other studies that the applicability of alkenone proxies is limited in low temperature regions that disfavor alkenone producers. This chapter shows that the $U^{k'}_{37}$ proxy provides an additional temperature record complementary to the TEX_{86} proxy because of different responses of each source organism to environmental conditions in the tropical oceans.

KURZFASSUNG

Seit dem Beginn der Industrialisierung lassen sich Klimaveränderung und globale Erwärmung beobachten. Dieses Phänomen erfordert Strategien zur Minderung der Erderwärmung. Die Ozeane, die 70% der Erdoberfläche ausmachen, zeichnen in ihren Sedimenten klimatische Veränderungen der Erdvergangenheit auf. Diese Veränderungen zu verstehen, ist eine essenzielle Methode, zukünftige Temperaturanstiege vorherzusagen. Ozeanische Temperaturveränderungen aus der Vergangenheit können anhand verschiedener Proxies rekonstruiert werden. Einer der am häufigsten verwendeten Proxies in der Paläoklimatologie ist der sogenannte TEX_{86} (engl.: tetraether index of tetraethers consisting of 86 carbon atoms). Dieser basiert auf der relativen Häufigkeit sogenannter Glycerol Dialkyl Glycerol Tetraether (GDGTs), Membranlipide der Thaumarchaeota (Phylum innerhalb der Archaeendomäne). Anhand der GDGT Verteilung in marinen Sedimenten lässt sich die Wasseroberflächentemperatur (SST – engl.: sea surface temperature) abschätzen. Die Allgegenwärtigkeit und das dominante Auftreten der Thaumarchaeota in den Ozeanen machen die Lipide zu einem vielversprechenden Proxy. Jedoch ist er noch relativ jung. Es hat sich gezeigt, dass neben Temperaturveränderungen weitere Umweltbedingungen die Verteilung der GDGT beeinflussen und zu einem unkonventionellen Zusammenhang zwischen Temperatur und TEX_{86} führen können. Diese Arbeit soll zu einem besseren Verständnis des TEX_{86} -Temperaturproxies und dessen Abhängigkeit von diversen Umweltparametern in verschiedenen ozeanischen Regimen beitragen. Dazu werden GDGT-Verteilungen sowie TEX_{86} -basierte Temperaturen an sinkenden Partikeln bewertet und Partikelflüsse verschiedener Materialien durch die Wassersäule bestimmt. Zeitreihen, die mittels solcher Sedimentfallen an sinkenden Partikeln gewonnen werden, sind für das Verständnis von Exportmechanismen von Lipiden sowie der Abschätzung saisonaler Variabilität im Proxysignal von großem Wert. In dieser Arbeit werden die drei folgenden Ozeanregime im Atlantik untersucht: Upwelling-Zonen (Guineabecken, und Küstenregion vor Lüderitz, Namibia), hohe Breiten (östliche Framstraße und antarktische Polarfront) und die oligotrophen Gyren (Zentral Brasilianisches Becken).

Im ersten Teil der Arbeit werden mittels der TEX_{86}^{H}-Kalibration Temperaturen für die Upwelling-Zonen berechnet. Die Ergebnisse zeigen, dass die GDGTs im östlichen äquatorialen Guineabecken (GBN3) hauptsächlich durch opaltragende Partikel transportiert werden. Die TEX_{86}^{H} -basierten Temperaturen entsprechen in beiden beprobten Wassertiefen den Temperaturen unterhalb der Wasseroberfläche (engl.: subsurface) in ~50 m Wassertiefe, und damit gleichzeitig der Position der Nutrikline. Dieses Ergebnis impliziert, dass sich die bevorzugte Habitattiefe der Thaumarchaeota in diesem Tiefenbereich befindet. In der küstennahen Upwelling-Zone (Lüderitz, LZ) bleiben die Exportmechanismen der GDGTs auf Grund eines verkürzten Beprobungszeitraums unklar. Die TEX_{86}^{H} -basierten Temperaturen entsprechen den mit Satelliten aufgezeichneten SSTs, wobei das

TEX_{86}^{H}-Signal in der wärmeren Saison gegenüber den Satellitendaten um 26 Tage verzögert auftritt. Während der kalten Jahreszeiten überschätzt TEX_{86}^{H} die SST. Da relativ hohe TEX_{86}-Werte häufig in sauerstoffarmen Wassermassen auftreten, könnte die stark ausgeprägte Sauerstoffminimumzone vor Lüderitz die Temperaturüberschätzung erklären. Dieses Ergebnis stimmt mit vorherigen Arbeiten vor Cap Blanc, Nordwestafrika, überein.

Der Fokus des zweiten Teils dieser Arbeit liegt auf den kalten Ozeanen in den hohen Breiten. In diesem Fall wird die TEX_{86}^{L}-Kalibration zur Temperaturberechnung angewendet. In der östlichen Framstraße (79° N; FEVI16) korrelieren die GDGT-Flüsse sowohl mit Flüssen biologischer als auch nicht-biologischer Partikel. Die beste Korrelation ergibt sich zwischen GDGTs und Opal/Karbonat, was nahelegt, dass die Sedimentation der GDGTs hauptsächlich von Opal- und Karbonatpartikeln vollzogen wird. Die TEX_{86}^{L}-basierten Temperaturen zeigen eine starke Variabilität, die vermutlich auf variierender Zusammensetzung des sinkenden Materials und der unterschiedlichen Sinkgeschwindigkeiten der GDGT-tragenden Partikel beruht. Das TEX_{86}^{L} Signal reflektiert die Wassertemperatur in 30-80 m Tiefe, dem Tiefenbereich, in dem eventuell Nitrifizierung stattfindet. In der antarktischen Polarfront (50° S; PF3) zeigen die TEX_{86}^{L}-basierten Temperaturen aus der flachen Sedimentfalle sowohl Über- als auch Unterschätzungen der SST, wobei die Unterschätzungen tendenziell zu Zeiten geringen GDGT-Flusses auftreten. Dieser Effekt scheint in der tieferen Falle stärker ausgeprägt zu sein. Überschätzungen der SST von ~7 °C treten sowohl in der tiefen Falle als auch dem darunter befindlichen Oberflächensediment auf. Diese sind vermutlich auf Beiträge von Euryarchaeota zurückzuführen oder auch durch einen non-linearen Zusammenhang von TEX_{86}^{L} und der SST im Südozean zu erklären. In beiden polaren Regionen scheinen hydroxylierte GDGT als Temperaturproxy anwendbar zu sein.

Der dritte Teil der Arbeit befasst sich mit den oligotrophen Gyren, die im Vergleich zu den in Teil eins und zwei betrachteten ozeanischen Regimen trotz ihrer Größe und ihres Einflusses auf biogeochemische Budgets relativ wenig wissenschaftliche Aufmerksamkeit erlangen. In dieser Arbeit werden die TEX_{86}-Werte aus zwei Tiefen an zwei Lokationen im Brasilianischen Becken untersucht (WAB1 and WA9). An beiden Lokationen zeigen die flachgelegenen Fallen gute Korrelationen zwischen GDGTs und Opal/Karbonat, was als Zeichen präferenzieller Aufnahme von GDGTs durch opal- und karbonatreiche Aggregate interpretiert wird. An WAB1, die sich im Randgebiet des Gyre-Systems befindet, ähneln die TEX_{86}^{H}-basierten Temperaturen den SSTs. Im Gegensatz zu WAB1, wird mit Falle W9 Material aus den nährstoffärmeren Gebieten im Zentrum des oligotrophen Gyres beprobt. Dort tritt in der flachen Falle eine Überschätzung der SST auf, die möglicherweise durch Energiestress der Thaumarchaeota hervorgerufen wird. An beiden Lokationen entsprechen die TEX_{86}^{H}-basierten Temperaturen aus der tiefen Falle dem tieferen Subsurface. Grund dafür ist vermutlich ein

starker Beitrag von GDGTs, die in tieferen, kälteren Wassermassen gebildet werden, gegenüber GDGTs aus flachen, wärmeren Wassermassen.

Während sich die ersten drei Teile dieser Arbeit mit GDGT-basierten Temperaturrekonstruktionen beschäftigen, werden im letzten Teil Alkenone und die darauf basierenden SST-Proxies (U^{k}_{37} or $U^{k'}_{37}$) in den drei ozeanischen Regimen betrachtet. In den tropischen Gebieten, dem äquatorialen Guineabecken, dem Atlantik vor Lüderitz sowie dem zentralen Brasilianischen Becken, spiegeln die $U^{k'}_{37}$-basierten Temperaturen die regionalen SST wider. Dies impliziert, dass regional-spezifische geochemische Charakteristika (z. B. Sauerstoffkonzentration und Verfügbarkeit von Nährstoffen), die wahrscheinlich TEX_{86} in den Untersuchungsgebieten beeinflussen, dagegen keine Auswirkungen auf das Temperatursignal des $U^{k'}_{37}$ haben. In der flachen Falle der antarktischen Polarfront zeichnen die $U^{k'}_{37}$-basierten Temperaturen deutlich die Saisonalität der SST auf, allerdings mit einem zeitlichen Versatz von zehn Wochen. In der tiefen Falle treten Über- und Unterschätzungen der SST auf, deren Ursprung nicht eindeutig geklärt werden kann. In der östlichen Framstraße liefern sowohl U^{k}_{37} als auch $U^{k'}_{37}$ zu warme SSTs. Diese Ergebnissr unterstützten Schlussfolgerungen anderer Arbeiten, wonach die Anwendung der Alkenon-Proxies in kalten Ozeanen wegen ungeeigneter Umweltbedingungen für alkenonproduzierende Organismen limitiert ist. Dieses Kapitel zeigt, dass sich TEX_{86} und $U^{k'}_{37}$ in den tropischen Ozeanen als Temperaturproxies ergänzen, da Thaumarchaeota und Alkenonproduzenten die Bedingungen unterschiedlicher Habitate reflektieren. In den polaren Ozeanen ist TEX_{86} jedoch besser zur Temperaturrekonstruktion geeignet als die Alkenon-Proxies.

CHAPTER 1

Introduction

1 Introduction

1.1 Climate change and ocean warming

The climate is the long term condition of weather, which is defined by temperature, precipitation, wind, and the frequency and intensity of weather events. Solar radiation and the chemical composition of the atmosphere play key roles in controlling the earth's climate and temperature. The natural oscillation in atmospheric CO_2 concentration is linked to the solar energy cycle. However, the rate of current CO_2 increase is out of line with the rate that has applied at any time in the past 800,000 years (IPCC, 2014). The atmospheric CO_2 level has increased consistently since the first measurement in 1958 and it reached over 400 parts per million (ppm) in 2013 (Figure 1.1). Furthermore, the average global temperature recorded in 2017 was about 1.1 °C above the pre-industrial levels; this rise closely correlates with the rise in CO_2. Natural sources of CO_2 cannot account for the observed rise. Instead, it is now recognized that the recent abrupt climate change and warming are ultimately caused by human activities (IPCC, 2014). Reliable prediction of future climate change is essential to develop appropriate mitigation and adaptation strategies. The precise scenario for future change can be established when natural climate changes and anthropogenic changes arising from human activity are properly distinguished, and interlinked changes of the earth's climate system are fully comprehended. Therefore, understanding the long-term evolution of the climate is one of the key issues in geoscience that must be addressed to allow us to predict the effects of climate change that we cannot circumvent.

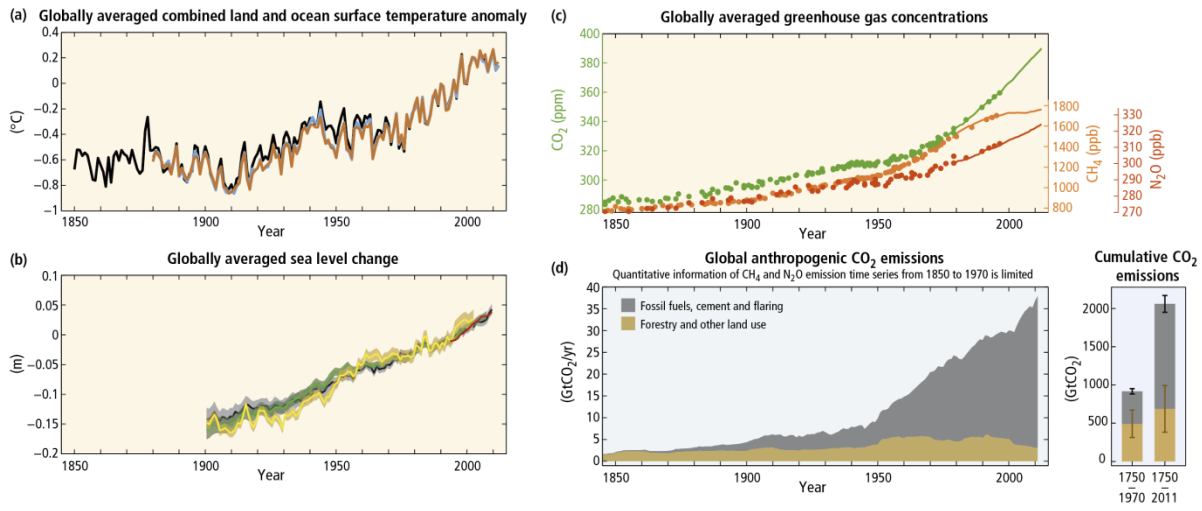

Figure 1.1 Observation of (a) global temperature anomalies, (b) sea level change relative to the average over the period 1986-2005, (c) concentration of greenhouse gasses, and (d) global anthropogenic CO_2 emission. (adapted from: IPCC, 2014 and references therein)

The atmosphere and oceans interact and exchange energy. As the oceans cover about 70% of the earth's surface, they play a significant role in regulating the climate and atmosphere as a heat and carbon reservoir. The ocean absorbs approximately 30% of anthropogenic CO_2 from the atmosphere. The rise of sea surface temperatures is accompanied by a rise in atmospheric CO_2. The projected changes in ocean temperature and uptake of CO_2 pose several direct and indirect problems such as ocean acidification; a decrease in O_2 solubility; altered distribution and abundance of marine resources; and further risks to human life (IPCC, 2014).

The temperature of the oceans is the principal parameter that is interconnected with other biological- and non-biological parameters, and it represents the status of the climate's condition. The recent history of ocean temperature has been recorded by field and satellite-derived measurement. However, the long-term history of temperature evolution can be determined by establishing temperature proxies through the study of marine sediments. Establishing a proxy is based on an assumption that the relationship between geochemical parameters and the proxy in the modern climate is the same as it was in the past and that changes in the proxy are well preserved within the geological records. Hence, an understating of the proxy system and precise historical temperature reconstruction are fundamental to the accurate prediction of future climate change.

1.2 Temperature proxy

Several inorganic and organic seawater temperature proxies have been developed and applied to paleoclimate studies (Table 1.1). Inorganic temperature proxies ($\delta^{18}O$, Mg/Ca, Sr/Ca) have a longer history relative to organic temperature proxies ($U^{k'}_{37}$, TEX_{86}, LDI). When organisms (Foraminifera, Coral, Diatom) build their shells, the isotope fractionation (e.g. $\delta^{18}O$) controlled by temperature is archived in the shell material (Leclerc and Labeyrie, 1987; Urey, 1947; Weber and Woodhead, 1972). However, there are some uncertainties associated with the use of an isotope proxy. For example, changes in $\delta^{18}O$ of seawater experiencing evaporation and precipitation have an effect on oxygen isotope thermometry. Also, the diagenesis of source organisms, the formation and preservation of shells, and the composition of unknown species in each source organism have to be considered (Lea, 2014 and reference therein). The Mg/Ca ratio measured in foraminifera and ostracods, and Si/Ca ratio measured in coral (Chave, 1954; Dwyer et al., 1995; Kinsman and Holland, 1969) are more recent inorganic temperature proxies. These elemental proxies can be affected by the dissolution of elements (Mg, Sr), contamination (Mg), species-specific control, and the growth rate of the source organism (Lea, 2014 and reference therein).

The first organic temperature proxy U^{k}_{37} containing di- ($C_{37:2}$), tri- ($C_{37:3}$) and tetra-unsaturated alkenones ($C_{37:4}$) was developed by Brassell et al., (1986) and later modified as $U^{k'}_{37}$ (= $C_{37:2}$ / ($C_{37:2}$ + $C_{37:3}$)) after excluding $C_{37:4}$ (Prahl and Wakeham, 1987; Table 1.1). The proxy values in surface

sediments showed the strongest correlation with mean annual Sea Surface Temperature (ma SST) ($U^{k'}_{37}$ = 0.033 × SST + 0.044, R^2 = 0.958; Müller et al., 1998). It has been confirmed that SST is a primary controller for the relative ratio ($U^{k'}_{37}$) of alkenones synthesized by Haptophyte algae (*Emiliania huxleyi*) living near the sea surface (Prahl and Wakeham, 1987). Despite the strong dependence of $U^{k'}_{37}$ on SST, discrepancies between the records of surface sediments and overlying SSTs have been investigated. The season of maximum production, export depth, selective degradation and other physical factors have been discussed as major reasons for the discrepancies in paleotemperature reconstruction using $U^{k'}_{37}$ (Prahl et al., 2000 and reference therein; Zabeti et al., 2010; Rosell-Melé and Prahl, 2013 and reference therein).

Table 1.1 Summary of major seawater temperature proxies

	Proxy	Organism	Non-thermal effects	References
Inorganic	$\delta^{18}O$	Foraminifera	Evaporation, precipitation, diagenesis, Species control [a] Dehydration [a]	(Urey, 1947) (Epstein and Mayeda, 1953)
		Coral[a]		(Weber and Woodhead, 1972)
		Diatom		(Leclerc and Labeyrie, 1987)
	Mg/Ca	Foraminifera	Dissolution Contamination (Mg) Species control	(Chave, 1954)
		Ostracods		(Dwyer et al., 1995)
	Sr/Ca	Corals	Growth rate Symbiosis	(Kinsman and Holland, 1969)
Organic	$U^{k'}_{37}$ [b]	*Emiliania huxleyi*	Community composition Seasonal of production Export depth Selective degradation [b] Lateral transport [b] Terrestrial input [c] Energy level [c]	(Brassell et al., 1986) (Prahl and Wakeham, 1987)
	TEX_{86} [c]	Thaumarchaeota		(Schouten et al., 2002)
	LDI	Eustigmatophyte algae (?)	On-going research	(Rampen et al., 2012)

The most recently proposed temperature proxy, a long chain diol index (LDI), is based on the distribution of C_{28} and C_{30} 1,13- and 1,15-diols (Rampen et al., 2012; Table 1.1). The proportional abundance of C_{30} 1,15 to total diols (Σ C_{28} 1,13 + C_{30} 1,13 + C_{30} 1,15) in marine sediments displayed a good correlation with ma SST (LDI = 0.033 × SST + 0.09, R^2 = 0.969; Rampen et al., (2012)). These diols and C_{32} 1,15-diols have been found in Eustigmatophyte algae (Méjanelle et al., 2003), which are likely to be a source organism of diols in the freshwater system (Shimokawara et al., 2010). However, a mismatch has been observed between the diol compositions of cultured Eustigmatophytes and those found in natural marine environments (Versteegh et al., 1997; Volkman et al., 1992). LDI-derived temperatures reflected neither ma SST nor any seasonal environment in sinking particles and

surface sediment around Iceland (Rodrigo-Gámiz et al., 2015), although they did correspond to SST in Late Quaternary sediments from the Chilean margin (de Bar et al., 2018). The source organism of diols and their role in marine sediments may need to be investigated further to constrain uncertainties when applying the LDI proxy.

TEX_{86} index (TetraEther indeX consisting of 86 carbon atoms), which was introduced later than the $U_{37}^{k'}$ and earlier than the LDI, has received a great deal of attention in paleoclimate studies (Schouten et al., 2002; Table 1.1). TEX_{86} quantifies the relative distribution of isoprenoid glycerol dialkyl tetraethers (GDGTs) produced by marine Thaumarchaeota, which are ammonia oxidizing chemoautotrophs (Wuchter et al., 2003; Francis et al., 2005; Könneke et al., 2005; Martens-Habbena et al., 2009). Their presence in many different environments and on a longer time scale compared to Haptophyte algae (*Emiliania huxleyi*) makes the TEX_{86} more applicable as a temperature proxy than the $U_{37}^{k'}$ (Schouten et al., 2013, 2000). The TEX_{86} was originally calibrated to ma SST (Table 1.2; Schouten et al., 2002), but warm- or cold biases compared to SST have been observed in different ocean regimes (see Section 1.4.1). Such anomalies could be caused by similar factors (e.g. the spatial and temporal variability of source organism) (see Section 1.5) to those that account for the ambiguous $U_{37}^{k'}$ calibration. Although the weakness of TEX_{86} calibration can be mitigated by applying other proxies (Lopes dos Santos et al., 2010; McClymont et al., 2012), it is important to investigate additional factors, which can alter GDGT compositions and the temperature estimates.

1.3 General biology of Thaumarchaeota

Thaumarchaeota were previously designated within the marine group I (MG-I) Crenarchaeota but are now affiliated with a phylum of the domain Archaea (Brochier-Armanet et al., 2008). This group is ubiquitously distributed in various ocean regions (Church et al., 2010; Francis et al., 2005; Karner et al., 2001; Mincer et al., 2007; Alison E Murray et al., 1999). The isolation of the cultured representative of this phylum, *Nitrosopumilus maritimus*, confirms that Thaumarchaeota are chemoautotrophs generating energy by oxidizing ammonia to nitrite (Könneke et al., 2005). Consequently, the high abundance of Thaumarchaeota as an ammonia oxidizer accounting for up to 30% of the total picoplankton in the oceans reveals their significant role in marine nitrogen cycles (Francis et al., 2005; Ingalls et al., 2006; Wuchter et al., 2006a). The isolated strain highlights a high affinity of Thaumarchaeota for ammonia (Horak et al., 2013; Martens-Habbena et al., 2009; Urakawa et al., 2014) allowing them to adapt to oligotrophic conditions. However, Achaea with mixotrophic or heterotrophic metabolism have also found in mesopelagic oceans (Agogué et al., 2008; Herndl et al., 2005; Ingalls et al., 2006).

Several pieces of evidence using the ammonia monooxygenase subunit A (*amoA*), 16S rRNA genes, and mRNA transcripts suggest that Thaumarchaeota preferentially dwell below the photic zone

(Beman et al., 2008; Church et al., 2010; Delong, 1992; Fhurmann et al., 1992; Mincer et al., 2007). These observations support the results from thaumarchaeotal membrane lipids, GDGTs (see Section 1.4), which also show the subsurface depth habit of Thaumarchaeota (Huguet et al., 2007; Karner et al., 2001; Turich et al., 2007; Wuchter et al., 2005). The abundance of Thaumarchaeota varies seasonally in widely different regions. The winter bloom occurs in the North Sea (Herfort et al., 2007; Pitcher et al., 2011), in Antarctic coastal waters (Tolar et al., 2016), and in the Santa Barbara Basin (Massana et al., 1997) whilst the upwelling period bloom occurs in the Arabian Sea (Wuchter et al., 2006b). The winter boom implies that winter time provides more favorable conditions for Thaumarchaeota due to ammonia availability together with reduced competition from phytoplankton, which suffer from the favorable water temperature and light intensity. However, the bloom during the upwelling season indicates that other factors also play a part.

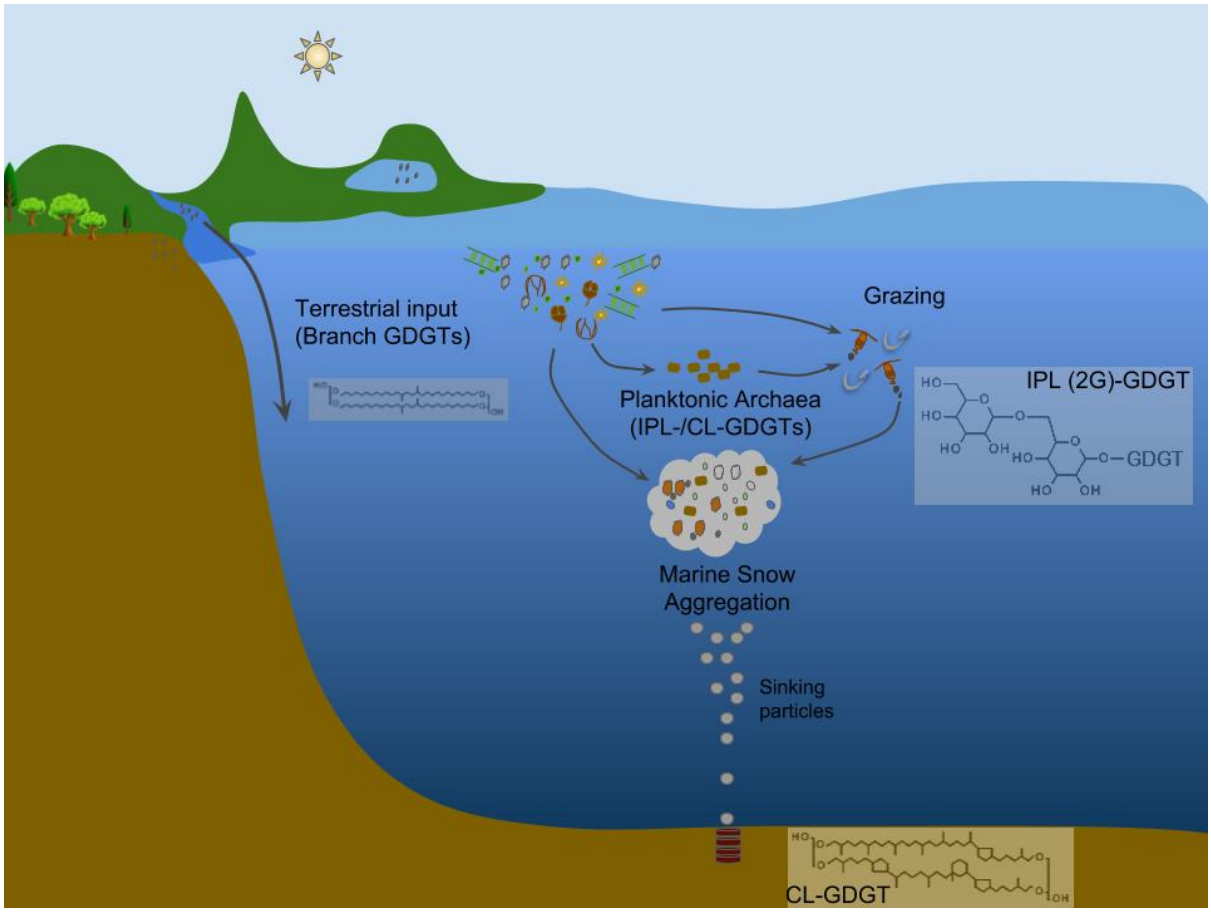

Figure 1.2 Sources of GDGTs in the marine environment. The detailed structure of GDGTs can be found in Figure 1.3. GDGTs synthesized in upper waters are exported to deep waters in the form of aggregated particles and buried in sediments.

The neutrally buoyant and small Thaumarchaeota (<1 μm) cannot sink by themselves (Schouten et al., 2013); they can only sink when they have gained enough density through aggregation with

phytoplankton debris, incorporation into other suspended particles, and/or through grazing by zooplankton (Wakeham et al., 2003; Figure 1.2). Together with the seasonal production and depth distribution of Thaumarchaeota, an investigation into the sinking mechanism that exports Thaumarchaeota to deep oceans is essential to understand the TEX_{86}-temperature relationship.

1.4 GDGTs

GDGTs, which are thaumarchaeotal membrane lipids, comprise zero to three cyclopentane moieties (GDGT-0−3) and crenarchaeol which has four cyclopentane moieties with a cyclohexane (Japp S. Sinninghe et al., 2002; Figure 1.3). The absence of crenarchaeol in hyperthermophilic Crenarchaeota and its unique presence in Thaumarchaeota (previously known as Crenarchaeota) means that crenarchaeol is a biomarker of Thaumarchaeota. The cyclization of GDGTs (i.e. the number of ring structures) is known to be an adaption to changes in temperature (Schouten et al., 2002). Although the formation process of GDGTs and cyclopentane moieties has been poorly elucidated, the relative abundances of different GDGTs are clearly seen in different oceans (Pearson and Ingalls, 2013; Schouten et al., 2013). GDGT-1 to -3 are more pronounced in warm-water environments, while the low abundance of GDGT-1 to -3 and higher abundance of GDGT-0 than crenarchaeol are found (Figure 1.3 in this study).

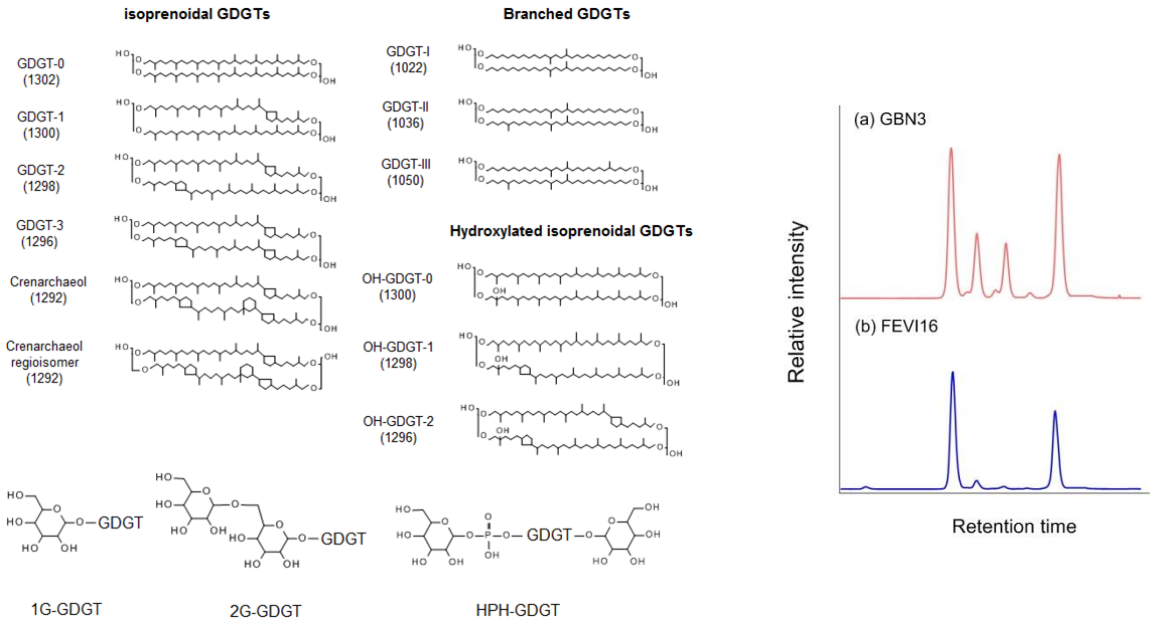

Figure 1.3 Structure of GDGTs and base peak chromatogram of GDGTs. Monolgycosidic (1G)-GDGT-GDGT), diglycosidic (2G)-GDGT, and hexosephosphohexose (HPH)-GDGT represent intact polar lipids (IPLs). The chromatograms are extracted from (a) the equatorial (warm; discussed in Chapter 2) and (b) polar (cold; discussed in Chapter 3) regions and their GDGT compositions are different. Abbreviations: GDGT, glycerol dialkyl glycerol tetraethers.

GDGTs are bound to polar head groups (intact polar lipids, IPLs) when the organisms are alive, and the head groups are detached from core GDGTs after cell death. Thus, IPLs are used as indicators of living populations (Herfort et al., 2007; Huguet et al., 2007; Japp S. Sinninghe et al., 2002; Turich et al., 2007). However, Schouten et al., (2010) demonstrated that IPLs can be preserved and buried in sediments. In terms of TEX_{86} thermometry, it is still debatable whether or not the viability of IPLs and the preferential degradation of certain head groups can influence core lipids (CL) GDGT distributions in the water column and sediments (Lengger et al., 2012; Schouten et al., 2012).

Recently Liu et al., (2012) reported a new set of GDGTs, the hydroxylated-GDGTs (OH-GDGTs) with one or two additional hydroxyl groups on the alkyl chain of GDGTs in core and intact forms (Figure 1.2; Liu et al., 2012). The relatively higher proportion of OH-GDGTs to the total (OH- and CL-) GDGT pool was determined in (sub) polar regions, suggesting 'OH-GDGTs' as a potential indicator for polar waters (Fietz et al., 2013). A similar finding was made by comparing samples distributed by latitude, showing an increasing proportion of OH-GDGTs in colder oceans (Huguet et al., 2013).

As a consequence, Fietz et al., (2013) and Huguet et al., (2013) suggested several SST calibrations using OH-GDGTs for the polar ocean. On the other hand, two previous studies indicate that OH-GDGTs can also play a role as a temperature proxy in subtropical and tropical marine environments (Lü et al., 2015; Yang et al., 2018).

1.4.1 Global calibration

Culture experiments have found that the number of cyclopentane rings in GDGTs of hyperthermophilic Archaea strongly depends on growth temperatures (Schouten et al., 2002). A finding of phylogenetically related Archaea in the ocean, and their ubiquity (Delong, 2003; Karner et al., 2001) led to the idea of GDGT composition as a temperature proxy (Schouten et al., 2002).

Schouten et al., (2002) plotted TEX_{86} values of 44 surface marine sediments against ma SSTs extracted from the World Ocean Atlas. The relationship displays a linear correlation as follows:

$$TEX_{86} = ([GDGT\text{-}2]+[GDGT\text{-}3]+[Cren']) / ([GDGT\text{-}1]+[GDGT\text{-}2]+[GDGT\text{-}3]+[Cren']) \quad (1)$$

$$TEX_{86} = 0.015 \times SST + 0.28 \ (R^2 = 0.92, n = 44) \quad (2)$$

The later mesocosm study also showed a linear correlation with the same slope and a higher intercept at temperatures ranging from 5 to 35 °C, thus confirming that temperature is a main controlling factor of GDGT composition (Wuchter et al., 2004; $TEX_{86} = 0.015 \times T + 0.010$, $R^2 = 0.79$).

Table 1.2 Most commonly used TEX_{86} related calibration.

Calibration		*n*	R^2	Standard deviation of Residuals (°C)	Remarks	Reference
$SST = -10.78 + 56.2 \times TEX_{86}$		223	0.84	1.7	w/o[1] Red Sea & residuals<1σ	Kim et al., (2008)
$SST = 50.475 - 16.332 \times (1/TEX_{86})$		287	0.82	3.7	All data	Liu et al., (2009)
$SST = 46.9 + 67.5 \times TEX_{86}^{L}$		396	0.87	4.0	w/o Red Sea	Kim et al., (2010)
$SST = 38.6 + 68.4 \times TEX_{86}^{H}$		255	0.86	2.5	w/o Red Sea & <5 °C	Kim et al., (2010)
$0\text{-}200m\ T = 36.1 + 50.8 \times TEX_{86}^{L}$		396	0.87	2.8	w/o Red Sea	Kim et al., (2012a)
$0\text{-}200m\ T = 30.7 + 54.7 \times TEX_{86}^{H}$		255	0.84	2.2	w/o Red Sea & <5 °C	Kim et al., (2012b)
Baysain Model	SST	1095	-	1.2-10	w/o> 70° N	Tierney and Tingley, (2015)
	0-200 mT		-	1.4-9		

[1] ´w/o´ ís an abbreviation of ´without´

The original TEX_{86} linear calibration has been updated by expanded data sets and/or a non-linear regression approach. After removing TEX_{86} values from the cold regions (<5 °C) and the Red Sea, Kim et al., (2008) updated the linear calibration (Table 1.2; Kim et al., 2008). Using Kim et al., (2008)´s dataset, Liu et al., (2009) reformulated TEX_{86} (the relative amount of GDGT-2 to the sum of GDGT-1, -2 and -3) and the reciprocal of TEX_{86}. Later, two non-linear calibrations were suggested to overcome the scattered relationship between TEX_{86} and SST at both ends of the linear regression. The base 10 logarithmic function of TEX_{86} in two different forms was developed to resolve these issues for the warm area (named TEX_{86}^{H}; Figure 1.4a) and for the cold area (named TEX_{86}^{L}; Figure 1.4b) (Table 1.2; Kim et al., 2010). The latter index, TEX_{86}^{L}, does not contain the Crenarchaeol regioisomer due to its scattered distribution in polar regions, revealing their insignificant role in cold environments.

$$TEX_{86}^{L} = \mathrm{Log}_{10}([GDGT\text{-}2]/([GDGT\text{-}1]+[GDGT\text{-}2]+[GDGT\text{-}3])) \quad (3)$$

Rea Sea and (sub)polar regions, where the relationship between TEX_{86} and SST is not likely to be linearly correlated, are excluded from the TEX_{86}^{H} calibration (Figure 1.4a). When the residuals (Residual (°C) = TEX_{86}/ TEX_{86}^{L}/ TEX_{86}^{H}-derived temperature − satellite SST) are compared, smaller residuals are evident in the logarithmic calibrations than in the linear calibration. However, the residuals do not seem to have any trend in their latitude or proxy values; rather, they are distributed randomly (Figure 1.4c, d). The depth distribution of Thaumarchaeota and the reflection of the subsurface in TEX_{86}-derived records promote depth-integrated calibrations, in which TEX_{86}^{L} and TEX_{86}^{H} are plotted against 0200 m depth-integrated water temperatures (Table 1.2; Kim et al., 2012a, 2012b).

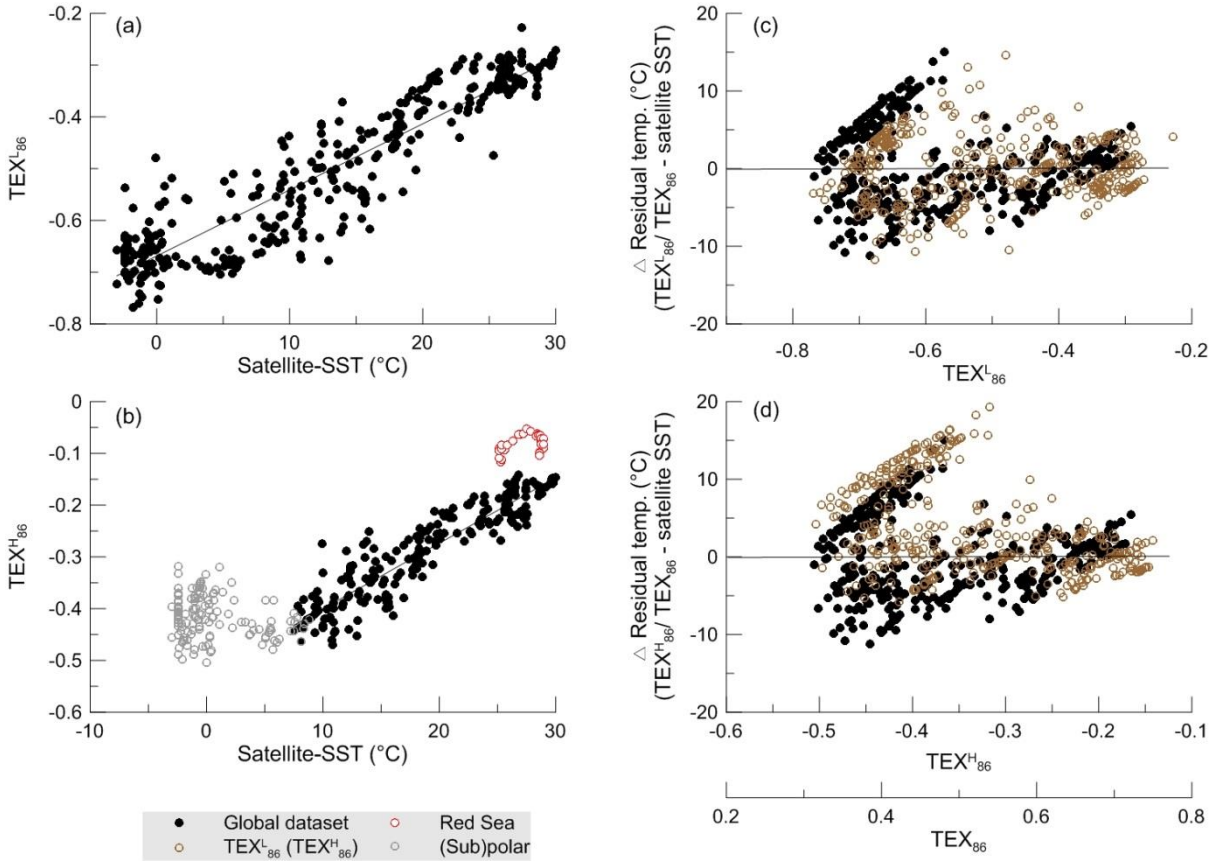

Figure 1.4 Global calibration of TEX_{86}^{L} (a) and TEX_{86}^{H} (b) (Kim et al., 2010). Black dots represent the calibration data set. Red and grey indicate the Red Sea and (sub) polar regions, respectively, which are excluded for the TEX_{86}^{H} based calibration (b). (c) and (d) display the residual temperatures between the calibrated ones and the satellite ones. Brown dots represent the original linear calibration. Note that SSTs as the independent variable (X-axis) and TEX_{86} as the dependent variable (Y-axis) are treated.

1.4.2 Regional calibrations

Previously developed TEX_{86} based calibrations (see Section 1.4.1) have been made with the assumption that the response of TEX_{86} (e.g. GDGT compositions) to temperature is constant across the earth's oceans. However, its response seems to vary depending on the environmental regimes, as revealed in the scattered residuals (Figure 1.4).

For temperature prediction, Tierney and Tingley, (2015) suggested the Bayesian, spatially-varying regression (BAYSPAR) model, which provides a compromise between a global calibration and a regional calibration, excluding data north from 70° N. In the BAYSPAR model, calibration parameters for each independent locale are decided within a 20° by 20° longitude-latitude grid box. Regionally distinct archaeal communities, which may respond differently to SST, result in regionally specified calibrations. In the deeply isolated basin of the Red Sea, where TEX_{86} values are clearly distinguished from the global calibration (Figure 1.4b), a new 'Red Sea' TEX_{86} calibration was suggested (Trommer et al., 2009). Later, Kim et al., (2015) identified a similar controlling mechanism of GDGT

to that found in the Red Sea in the Mediterranean Sea, where the global calibration shows warm-biased temperatures. In the Baltic Sea, Kabel et al., (2012) drew a regional calibration for the last 1000 years and found that TEX_{86} temperatures increased by up to 2 °C between the Little Ice Age and the Modern Warm Period when the anoxic area was expanded. Seki et al., (2014) made a local TEX_{86}^{L} calibration in the Sea of Okhotsk and North Pacific sub-polar region and generated reliable Last Glacial Maximum and Holocene temperatures for the region. Following this regional TEX_{86}^{L} calibration, which displayed the best fit between TEX_{86}^{L} values and the shallow subsurface temperature in the summer months, Meyer et al., (2016) reconstructed the glacial-Holocene temperatures for the subarctic northwest Pacific and the western Bering Sea. Shevenell et al., (2011) also suggested that a regional calibration is a right approach for TEX_{86} calibration in the western Antarctic Peninsula, demonstrating a cooling of 3−4 °C over the last 12,000 years. Furthermore, Ho et al., (2014) suggested that the regional TEX_{86}^{L} calibration could be a suitable approach for the Southern Ocean and the Pacific Subarctic Front Zone.

These observations of TEX_{86} thermometry in different regions challenge the efficacy of global calibration and emphasize the importance of understanding regionally specified environmental factors, which may lead the systematic offsets between proxy and measured temperatures.

1.5 Constraints of TEX_{86} thermometry

1.5.1 GDGTs-derived from Euryarchaeota

The ubiquity of Thaumarchaeota synthesizing GDGTs in a wide range of ocean environments makes TEX_{86} a good proxy for reconstructing temperatures in geological history. GDGTs are assumed to be predominantly produced by Thaumarchaeota, which are the dominant archaeal group in the ocean (Karner et al., 2001). However, there is a debate as to whether mesophilic Euryarchaeota could contribute to GDGT compositions (Lincoln et al., 2014; Schouten et al., 2014). This was one of the main reasons that GDGT-0 was excluded from the TEX_{86} calculation (Schouten et al., 2002).

Turich et al., (2007) suggested that GDGTs in suspended particulate matters (SPM) from mesopelagic water, as opposed to shallow waters (<100 m), can be attributed to GDGTs derived from Group II Euryarchaeota, producing GDGT-0 to -3. Schouten et al., (2008) did not agree with Turich et al., (2007) citing the temporal offset between the GDGT abundances (GDGT-0 and crenarchaeol) and the cell abundances of Euryarchaeota in the North Sea, which was one of the areas that Turich et al., (2007) used as an example. In the epipelagic zone of the North Pacific subtropical gyre, Lincoln et al., (2014) showed that Group II Euryarchaeota were a major source of GDGTs as determined through rRNA analysis in SPM samples. Although a bias caused by differing sampling processes is unavoidable, a relatively large abundance of Euryarchaeota in surface water was also found in the

eastern tropical North Pacific (Podlaska et al., 2012). GDGT-1 to -4 have also been detected in many strains of Euryarchaeota (Schouten et al., 2013 and reference therein).

In general, several lines of evidence detailed above illustrate that Euryarchaeota can contribute to GDGT production and, therefore, to TEX_{86} thermometry. However, much is still unknown remains regarding the proportional contribution of GDGTs solely produced by Euryarchaeota and the organism's physiological response to environmental parameters. Cultured mesophilic Euryarchaeota may help to answer these questions in the future.

1.5.2 Shallow vs. deep origin of GDGTs

The strong correlation between TEX_{86} in surface sediments and overlaying SSTs has been originally explained by GDGTs that were mostly exported from the surface waters (Schouten et al., 2002; Wakeham et al., 2003) via zooplankton grazing and the formation of fecal pellets (Huguet et al., 2006; Wuchter et al., 2005). However, the TEX_{86} -derived temperature often corresponds to subsurface temperature rather than SST (Lee et al., 2008; Lopes dos Santos et al., 2010; McClymont et al., 2012; Seki et al., 2014). The distribution (preferentially at the subsurface level) of Thaumarchaeota in the water column has been invoked to explain the TEX_{86} subsurface temperature. Archaea are found throughout the water column (Karner et al., 2001), but their maximum abundances tend to occur below the surface water (Church et al., 2010; Delong, 1992; Fhurmann et al., 1992; Massana et al., 1997; Mincer et al., 2007). These findings are associated with a generally high ammonia oxidation rate in the subsurface (Beman et al., 2008; Church et al., 2010). Significant production of GDGTs in waters deeper than subsurface was also observed by radiocarbon measurements in some settings (Ingalls et al., 2006; Shah et al., 2008).

Taylor et al., (2013) observed that GDGT [2]/[3] ratio in the SPMs and surface sediments increases with depth, indicating a potential contribution of deep-dwelling Archaea to sedimentary GDGT distributions. Although it has not yet been clearly explained what causes the increase in the GDGT [2]/[3] ratio by depth, the contribution of GDGTs derived from deep-dwelling Archaea is relatively higher in deep settings compared to shallower settings (Hernández-Sánchez et al., 2014; Kim et al., 2016). Different ecotypes of Archaea (shallow vs. deep) have been distinguished based on the ammonia monooxygenase (amoA) α-subunit genes (Francis et al., 2005; Sintes et al., 2013; Villanueva et al., 2014). Sintes et al., (2013) showed that two phylogenetically distinct clusters are separated by depth and regions, where ammonia availability differs. In the Arabian Sea and the Atlantic Ocean, ammonia availability appears to be an important factor affecting the distribution of two archaeal ecotypes (Sintes et al., 2016; Villanueva et al., 2014). By extension, sedimentary TEX_{86}-derived temperature reflects SST at shallow setting and subsurface temperature at deep setting. However, there is an offset between TEX_{86}-derived temperature measured in SPMs and *in situ*

temperature increases by depth, indicating that the adaptation mechanism of deep-dwelling Archaea to temperature is different to that of shallow-dwelling Archaea (Hernández-Sánchez et al., 2014; Schouten et al., 2012).

1.5.3 Environmental factors

The influence of physiological parameters on TEX_{86} thermometry was tested using a thaumarchaeotal culture by Elling et al., (2015). The authors determined that a response of TEX_{86} (i.e. GDGT compositions) to growth temperature occurred differently; a linear response in *Nitrosopumilus maritimus* but no correlation in the other strain culture. Thus, the authors suggested that community composition may be a crucial factor determining GDGT distributions rather than salinity or pH, which did show no systematic effect on TEX_{86} in all strains. Another culture experiment compared TEX_{86}-derived temperatures for individual core and IPL-GDGTs in different stationary phases (Elling et al., 2014). Between the early and late growth phase, the reconstructed temperatures increased in all GDGTs, while the temperature changes were rather smaller between the early and late stationary phase. It seems clear that TEX_{86}-derived temperature can be affected by the growth status of Thaumarchaeota. However, it is assumed that Thaumarchaeota aggregated with particles and sunk into deep waters are considered to be in the late stationary phase. Therefore, this finding may not be applicable in the field.

Nutrients and light conditions are commonly invoked explanations for the tendency to maximum values of the abundance of Thaumarchaeota and their ammonia oxidation at the base of the euphotic zone and the higher production in winter, agreeing with TEX_{86} reconstruction of subsurface temperatures (see Section 1.3 and 1.5.2). Turich et al., (2007) observed that the change in GDGT distribution is induced by nutrient enrichment. Ammonia oxidation rate was inhibited by low light intensity (Qin et al., 2014) or the presence of reactive oxygen species (Horak et al., 2017; Tolar et al., 2016). The vertical distribution of nutrients was also found to be a controlling factor of the niche segregation (Lopes dos Santos et al., 2010; Sintes et al., 2016). Using continuous cultures of *Nitrosopumilus maritimus*, Ring index (RI) value, the weighted average of cyclopentane moieties, and TEX_{86}-derived temperature increased at low ammonia oxidation rate while the opposite trend occurred at high ammonia oxidation rate (Hurley et al., 2016). A similar finding was made by Qin et al., (2015), implying an alteration of TEX_{86} temperature under energy stress condition.

1.5.4 Indices for non-thermal factors on TEX_{86}

GDGTs derived from soil or euryarchaeotal communities are known to be able to modify sedimentary GDGT composition. To evaluate non-thermal factors on TEX_{86}, a number of GDGT based indices have been proposed (Table 1.3). The input of terrestrial GDGTs on TEX_{86} can be examined by applying the BIT (branched and isoprenoid tetraether) index, which provides the relative

ratio of soil-derived branched GDGTs to crenarchaeol representing marine GDGTs (Hopmans et al., 2004; Weijers et al., 2006) (Figure 1.2 and 1.3). When the BIT value is higher than 0.3, TEX_{86} is influenced by soil-derived GDGTs. As explained in Section 1.5.1, methanogenic Euryarchaeota can produce mainly GDGT-0 with a minor portion of GDGT-1 to -3. The percentage of GDGT-0 to crenarchaeol, %GDGT, which indicates a relative extra contribution of GDGT-0 from methanogenic Euryarchaeota to the sedimentary GDGTs, should not exceed 67% (Blaga et al., 2009; Inglis et al., 2015; Sinninghe Damsté et al., 2012). Methanotrophic Euryarchaeota in marine gas hydrate or methane-rich sites characterized by diffusive methane flux can synthesize GDGT-1 to -3. Zhang et al., (2011) observed that TEX_{86} values represent normal marine signals when the methane index (MI) is below 0.3. The most recently proposed non-thermal index is the RI (Table 1.3; RI; Zhang et al., 2016). The authors found a significant correlation between TEX_{86} and RI values in the global marine. They suggested that GDGT distributions are influenced by GDGTs derived from soil, methanotrophic Euryarchaeota, or any other non-thermal factors when the discrepancy (ΔRI) between the measured RI value and the calculated one from the modern TEX_{86}-RI regression is higher than 0.3 (Table 1.3).

Table 1.3 Indices for assessing non-thermal influences on TEX_{86}

Index	Non-thermal source	Limit value	Reference
BIT, Branched and Isoprenoid Tetraether index = ([I] + [II] + [III])/([I] + [II] + [III] + [Cren])	Soil	<0.3	(Hopmans et al., 2004; Weijers et al., 2006)
%GDGT-0/Cren	Methanogenic Euryarchaeota	<67	(Blaga et al., 2009; Inglis et al., 2015; Sinninghe Damsté et al., 2012)
MI, Methane Index = ([1] + [2] + [3])/([1] + [2] + [3] + [Cren] + [Cren´])	Methanotrophic Euryarchaeota	<0.3	(Zhang et al., 2011)
RI, Ring Index = (0×[0] + 1×[1] + 2×[2] + 3×[3] + 4×[Cren] + 4×[Cren´] RI_{TEX} = -0.77(±0.38)×TEX_{86}+ 3.32(±0.34)×$(TEX_{86})^2$ + 0.59(±0.10) ΔR = RI_{TEX} − RI_{sample}	Non-thermal input	<|0.3|	(Zhang et al., 2016)

* [I] and [numbers] refer to branch- and isoprenoid GDGTs, respectively. GDGT structures are shown in Figure 1.3
* For RI, each GDGT indicates a relative proportion to the sum of all isoprenoidal GDGTs.

1.6 Trap study

1.6.1 Trapping efficiency

Determining the particle flux is essential to understand the biological pump in the ocean. The considerable amounts of carbon synthesized in the surface ocean sink in the form of particles and finally reached to the sea floor. The time-series mooring system is equipped with a sediment trap with

20 (or 17) sample cups and 0.5 m^2 of honeycomb baffles at the top, as well as a current meter (A1. Figure 1). A time-series sediment trap allowing the direct measurement of the particle flux in the ocean has been used for biogeochemical studies including paleo proxy, carbon cycle, the link between the shallow and deep ocean, and the consequence of human impact on the benthic ecosystem. Nonetheless, several efforts have been made to overcome the low trapping efficiency and to introduce best practice into the trap system (Buesseler et al., 2007; Gardner, 2000, 1985; Scholten et al., 2001; Yu et al., 2001). The trapping efficiency appeared to be generally low in the mesopelagic zone relative to the bathypelagic zone, as calculated from radionuclide measurements (^{230}Th and ^{231}Pa) in sediment traps and the water column (Buesseler et al., 2007 and references therein). Buesseler et al., (2007) reviewed the capabilities and limitations of the trap system as well as the possible enhancements. Under and over trappings are attributed to zooplankton, the biological process, and tilting by the strong current in the vicinity of the trap. Zooplankton trapped as active migrants can be removed by sieving or manual picking. To avoid further biological process within the sample cup, formaldehyde or mercury chloride ($HgCl_2$) can be used to poison the collected samples. Hydrodynamics are of most concern, and can cause the physical failure of the trap system (Gardner, 2000, 1985; Scholten et al., 2001). For example, the measured current velocity using current meters attached to the mooring system was in the range of 1 to 8 m s^{-1} in the Antarctic Polar Front (Walter et al., 2001). According to Gardner, (1985), this would not affect the trapping efficiency because the current velocity was below the critical value of >10 m s^{-1}. On the other hand, Yu et al., (2001) tested the trapping efficiency using radionuclides (^{230}Th and ^{231}Pa) and estimated that it was only 44%.

For all the trap samples used in the manuscripts of this thesis, swimmers were removed by sieving or picking after traps were recovered. Formaldehyde or $HgCl_2$ solutions were added to inhibit microbial activity before and after the mooring system deployment. Even if the trap sampling was biased by hydrodynamics around the trap, it would not affect the paleo proxy, which deals with the relative composition of the respective lipids captured in the trap. Longer term trap studies (made over several years) would be needed to measure long-term trends of particle flux and trap efficiency.

1.6.2 TEX_{86} thermometry with time-series sediment traps

It has been recognized that sinking particles collected using a sediment mooring system can be of great value in helping us to understand the progress of lipid biomarkers on their way to the sea-floor and for comparison with the sediment signal (Rosell-Melé and Prahl, 2013; Schouten et al., 2013). In particular, results from time-series sediment traps allow us to examine the seasonality of material flux as well as the lipid biomarker signal in a certain environment.

For GDGTs and TEX_{86} thermometry, time-series sediment trap studies have helped us to understand the ecology of GDGT synthesizers such as the seasonal variation of their production, the

corresponding water depth of TEX_{86}-derived temperature, the transport mechanism of lipid signal to the deep water, and potential environmental impacts on TEX_{86} thermometry. Despite the great value of trap studies, the seasonality of TEX_{86} using a sediment trap has been reported from only ten different regions (Figure 1.5, Table 1.4); the Arabian Sea (Wuchter et al., 2006b), the Santa Barbara Basin (Huguet et al., 2007), the Mozambique Channel (Fallet et al., 2011), the Gulf of California (McClymont et al., 2012), the western North Pacific (Yamamoto et al., 2012), the eastern Cariaco Basin (Courtney Turich et al., 2013), the Northwest Africa (Mollenhauer et al., 2015), around Iceland (Rodrigo-Gámiz et al., 2015), the South of Java (Chen et al., 2016), and the northern Gulf of Mexico (Richey and Tierney, 2016).

The variability of TEX_{86} thermometry has been revealed in various environmental ocean regimes. TEX_{86}-derived temperatures either showed the clear seasonality of SST with a few weeks of delay (e.g. Wuchter et al., 2006; Mollenhauer et al., 2015), or its Flux-weighted mean TEX_{86} temperature reflected the ma SST or SST in a specific season without a seasonal pattern (e.g. Yamamoto et al., 2012; Turich et al., 2013). The delay time or non-seasonality of TEX_{86} signal in the sediment trap was explained by the different season of GDGTs production or the enhanced sinking flux of GDGTs. On the other hand, several trap studies showed that TEX_{86}-based temperatures in sinking particles corresponded to the subsurface water temperature (Huguet et al., 2007; McClymont et al., 2012; Rodrigo-Gámiz et al., 2015; Chen et al., 2016; Richey and Tierney, 2016), even though TEX_{86} is calibrated to ma SST. This is in a good agreement with other studies that the TEX_{86} temperature-derived temperature represents the subsurface temperatures in surface sediments of upwelling regimes (Lee et al., 2008; Lopes dos Santos et al., 2010). Rodrigo-Gámiz et al., (2015) and Richey and Tierney, (2016) found the best temperature estimates by applying the TEX_{86} depth-integrated (0-200 m) calibration, indicating that most GDGTs are synthesized in upper water columns including subsurface and thus TEX_{86} record the depth-integrated water temperature.

The covariance between GDGTs and mass fluxes is attributed to the transport mechanism of GDGTs through water columns, which are incorporated with the particles. GDGT fluxes were enhanced when total mass fluxes peaked (Huguet et al., 2007; Courtney Turich et al., 2013). In the west North Pacific, the authors suggested that GDGTs are transported by organic materials aggregated with diatom frustules and lithogenic materials (Yamamoto et al., 2012). In the South of Java and around Cape Blanc off Northwest Africa, GDGT fluxes had a correlation with opal flux, implying preferential incorporation with opal-dominant aggregates (Chen et al., 2016; Mollenhauer et al., 2015).

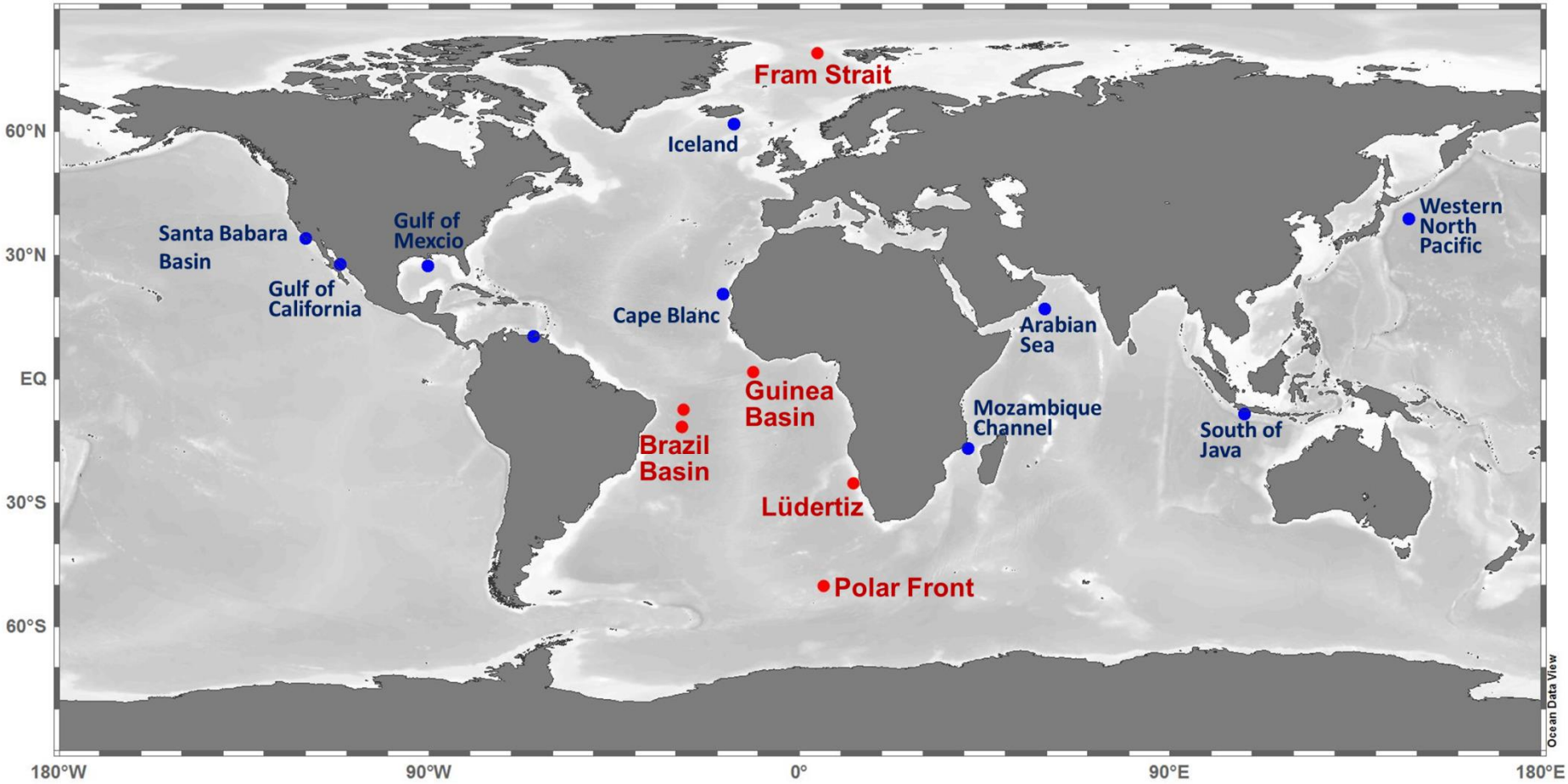

Figure 1.5 Locations of time-series sediment trap studies. Blue dots indicate the previous studies summarized in Table 1.4. Red dots are the trap locations in this thesis.

Table 1.4 Summary of TEX_{86} time-series sediment trap studies.

Study area	Location		Deployment period		Water depth	Trap depth	TEX_{86} calibration	TEX_{86} thermometry	Reference
	Latitude	Longitude	Start	End					
	(° N)	(° E)	(mm/yyyy)		(m)	(m)			
Arabian Sea	17.2	59.6	Nov/1994	Jan/1996	3,465	500 1500 3000	TEX_{86} [a]	• Seasonal SST with 1-3 weeks delay • Similar TEX_{86} among traps	(Wuchter et al. 2006)
Cape Blanc off Mauritania	20.75	-18.7	June/2003	Mar/2007	2,690	1,300	TEX_{86}^{H} [b]	• Seasonal SST with delay • Similar TEX_{86} in the core-top	(Mollenhauer et al., 2015)
Eastern Cariaco Basin	10.5	- 64.667	May/1999 July/2002	May/2000 July/2003	1,400	275 455	TEX_{86}^{H} [b]	• Seasonal SST • Similar TEX_{86} among traps	(Courtney Turich et al., 2013)
Gulf of California	27.883	-111.667	Feb/1996	Feb/1997	700	500	TEX_{86}^{H} [b]	• No seasonality • Subsurface (below the thermocline)	(McClymont et al., 2012)
Gulf of Mexico	27.5	-90.3	Jan/2010	Dec/2013	700	1,150	TEX_{86}^{H} [b] BAYSPAR[c]	• No seasonality, 0-200 m temperature • Similar TEX_{86} in the core top	(Richey and Tierney, 2016)
Iceland	61.996	-16.00	July/2011	June/2012	2,255	1,850	TEX_{86} [b] TEX_{86}^{L} [b]	• No seasonality, 0-200 m temperature • Similar TEX_{86} in the core top	(Rodrigo-Gámiz et al., 2015)
Mozambique Channel	-16.8	40.8	Oct/2003	Nov/2007	2,500	2,250	TEX_{86}^{H} [b]	• No seasonality • ma SST	(Fallet et al., 2011)
Santa Barbara Basin	34.333	-120.033	Dec/1995	Dec/1997	540	490	TEX_{86} [a]	• No seasonality • Subsurface (below 75 m)	(Huguet et al., 2007)
South of Java	8.292	108.033	Dec/2001	Nov/2002	2,200	1,400	TEX_{86}^{H} [b]	• No seasonality • Subsurface (upper thermocline ~50m)	(Chen et al., 2016)
Western North Pacific	39.017	147.994	Nov/1997	Aug/1999	5,356	1,366 3,056 4,789	TEX_{86}^{H} [b] TEX_{86}^{L} [b]	• No seasonality • 0-40 m (July-November) • Similar TEX_{86} in the core-top	(Yamamoto et al., 2012)

[a] Schouten et al., (2002)´s calibration

[b] Kim et al., (2010)´s calibration

[c] Tierney and Tingley, (2015)´s Bayesian calibration

* Calibrations used for each study can be found in the reference

When the TEX_{86}-derived temperatures reflect seasonality and its signals are delayed with respect to satellite-derived SST, the delay time can be used to calculate the sinking velocities of particles containing the relevant lipids. In the Arabian Sea, the TEX_{86}-derived temperatures resembled the *in situ* SSTs with a 1−3 weeks of delay at 500 m depth, showing a sinking velocity of approximately 25−75 m d^{-1} for the sinking particles (Wuchter et al., 2006b). In a four year trap in the filamentous upwelling zone of the Cape Blanc, Northwest Africa, the time lag (>1−3 months) of the TEX_{86} signal at the 1300 m depth trap relative to the satellite SST indicated a GDGT sinking velocity of approximately 9−17 m d^{-1} (Mollenhauer et al., 2015).

The similar TEX_{86} values among traps at multiple depths in a given study area and/or in the underlying surface sediment indicate that TEX_{86} does not alter significantly at different depths throughout the water column (Wuchter et al., 2006; Yamamoto et al., 2012; Mollenhauer et al., 2015; Rodrigo-Gámiz et al., 2015; Richey and Tierney, 2016; Chen et al., 2016). The study of temperature proxy ($U^{k'}_{37}$ and TEX_{86}) in sinking particles contributes to the understanding of the process and mechanism of past climate changes (Huguet et al., 2007; McClymont et al., 2012). For instance, the changes of the offset between surface ($U^{k'}_{37}$) and subsurface (TEX_{86}) signals allowed the assessment of the relative strength of seasonal upwelling and stratification in the Last Glacial Maximum and Termination 1 (McClymont et al., 2012).

1.7 Objectives of this thesis

Time-series trap studies to date reveal the influence of environmental variables other than temperature and stimulate the importance of TEX_{86} studies in sinking particle. Hence, many more studies on spatial and temporal compositions and productions of archaeal lipids will be needed to understand TEX_{86} thermometry dynamics.

In this sense, this thesis will contribute to broadening the knowledge regarding the seasonality of GDGTs production, TEX_{86} thermometry, and its regional environmental impacts on TEX_{86} in the Atlantic Ocean. This will shed the light on the interpretation of changes in estimated temperatures based on TEX_{86} in paleo climate variability.

The major emphasis of this thesis is given to the following research questions, which are addressed in the following manuscripts:

1) Do TEX_{86} signals reflect the temperature seasonality of the region? Does the seasonal variation of GDGT production affect the TEX_{86} thermometry?

2) What are the major causes of discrepancies between TEX_{86}-based temperature estimates and the satellite-derived SSTs?

3) At which depth archaeal lipids and TEX_{86} signals are originated?

4) Which processes govern the export of GDGTs from their production zone to deep waters?

The above-mentioned research questions are addressed in three different ocean regimes from the Atlantic Ocean.

1.8 Materials and analytical techniques

Sediment trap particle samples investigated in this thesis were retrieved from six mooring systems across the Atlantic Ocean from three distinct oceanic regimes (upwelling regimes, high latitude regions, oligotrophic system) (Figure 1.5). When there is no comparable data point in underlying surface sediments from the global TEX_{86} dataset, additional surface sediments in the respective trap location were also analysed to compare with the TEX_{86} signal in sinking particles.

The analysis process of samples can be found in the respective sections in each manuscript. Figure 1.6 shows the schematic flowchart of the GDGT analysis.

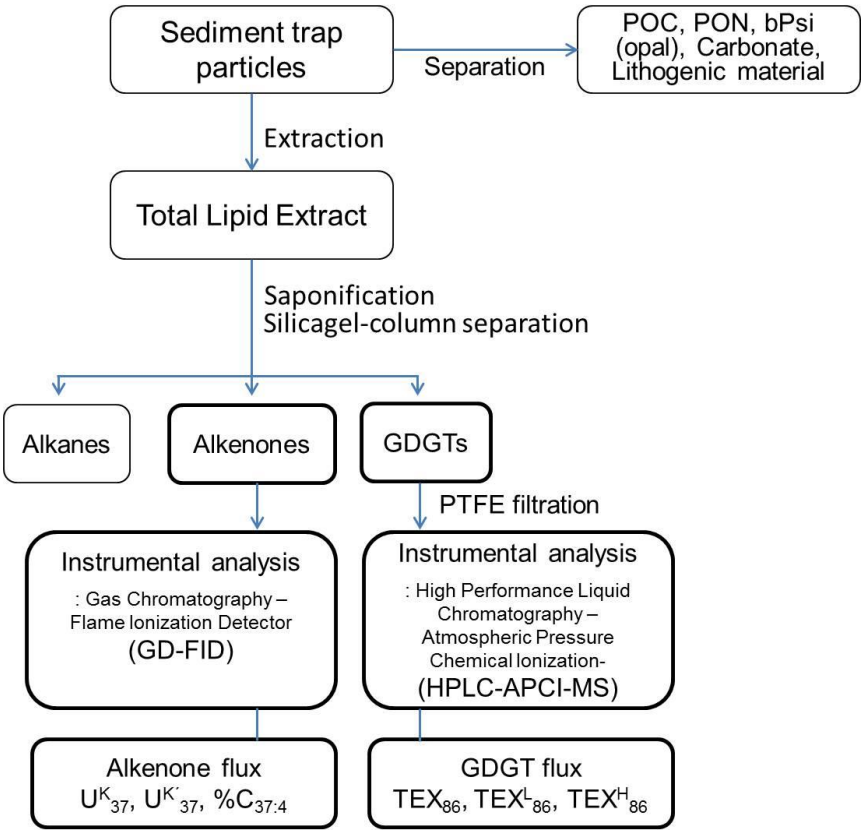

Figure 1.6 Schematic view of the GDGT analysis

1.9 Description of own contributions

The sediment trap and surface sediment samples had already been retrieved and stored at MARUM and AWI when I started my PhD. Surface sediment samples were provided by MARUM.

I conducted all the lipid extractions, and alkenone and GDGT measurements using the GC-FID and HPLC-APCI-MS with the help of Jens Hefter in the laboratories at the university of Bremen and Alfred Wegener Institute.

This project was initially designed by Gesine Mollenhauer and developed by myself. I interpreted all generated data, created all figures and tables, wrote all sections of the manuscripts, with suggestions and inputs from all the co-authors. Gesine Mollenhauer dedicated to the interpretation of TEX_{86} signal in all manuscripts (in Manuscript II, III, IV, V). Gerhard Fischer (in Manuscript II, III, IV) and Morten H. Iverson (in Manuscript III) contributed to the parts of sinking mechanisms of particles. Eva-Maria Nöthig and Simon Ramondenc helped to describe the oceanographical setting and to interpret the data in the Fram Strait (in Manuscript III).

1.10 Outline of the thesis

The study of GDGT flux and TEX_{86} thermometry from the Atlantic Ocean is addressed in four manuscripts (Chapters 2-4) which is published, in the process or in preparation for publishing in peer-reviewed journals. To answer the objectives mentioned above, each manuscript deals with each distinct oceanic regime; first manuscript in the eastern Atlantic upwelling regimes (the equatorial Guinea Basin and Lüderitz off Namibia; Chapter 2), second manuscript in high latitude regions (the eastern Fram Strait and Antarctic Polar Front; Chapter 3), and third manuscript in the south Atlantic oligotrophic system (in the central Brazil Basin; Chapter 4). In the last manuscript (Chapter 5), the $U^{k'}_{37}$-derived temperatures in all trap locations where GDGT based temperatures are discussed in previous chapters are investigated.

CHAPTER 2

TEX_{86} in sinking particles in three eastern Atlantic upwelling regimes

Organic Geochemistry (Park et al., 2018)

Vol. 124 (2018), pages 151-163. doi: https://doi.org/10.1016/j.orggeochem.2018.07.015

2 Manuscript I

TEX_{86} in sinking particles in three eastern Atlantic upwelling regimes

Eunmi Park[a,b,c,*], Jens Hefter[a], Gerhard Fischer[b,c], Gesine Mollenhauer[a,b,c]

[a] Alfred Wegener Institute, Helmholtz Center for Polar and Marine Research, D-27570 Bremerhaven, Germany
[b] MARUM Centre for Marine Environmental Sciences, University of Bremen, D-28334 Bremen, Germany
[c] Department of Geosciences, University of Bremen, D-28334 Bremen, Germany
*Corresponding author (eunmi.park@awi.de)

Abstract

Seasonal variations in fluxes of isoprenoid glycerol dialkyl glycerol tetraethers (GDGTs) and the estimated temperatures based on TEX_{86} are examined in sinking particles collected using moored sediment traps in the eastern Atlantic upwelling regions. In the equatorial Guinea Basin, GDGT fluxes show a correlation with opal fluxes, implying that GDGTs are mainly transported via aggregation with diatoms. The Flux-weighted mean TEX_{86}^{H} temperatures derived from particles collected both at 853 m and 3,921 m depth correspond to the water temperature (24.1 °C) of ca. 50 m depth, where nitrate concentration starts to increase. This suggests that nutrient concentrations may affect the depth habitat of Thaumarchaeota, thereby influencing the TEX_{86} derived water temperatures. In the coastal upwelling off Namibia, TEX_{86}^{H} temperatures are similar to satellite-derived sea surface temperature (SST) during the warm season, but the record derived from the trap is delayed relative to the SST by approximately 26 days. Warm biases, however, occur during the cold season. Higher TEX_{86} values have been found within the oxygen minimum zones (OMZs) in the water column of coastal upwelling regions. Thus, contributions from GDGTs produced in OMZs might explain the warmer temperature estimates during the cold season in regions, where OMZs are pronounced. This scenario could explain the observed warm bias off Namibia. We, therefore, suggest that in the eastern Atlantic upwelling systems, nutrient depth distribution and GDGTs produced in OMZs can be potential environmental factors influencing TEX_{86} in sinking particles. In paleoenvironmental records of TEX_{86}, non-thermal signals have to be considered on regional scales.

2.1 Introduction

The TEX_{86} is a temperature proxy based on the relative abundance of glycerol dialkyl glycerol tetraethers (GDGT) mainly synthesized by marine planktonic Thaumarchaeota, which are known as

chemoautotrophic ammonia-oxidizers in the ocean (e.g. Karner et al., 2001; Schouten et al., 2002; Sinninghe Damsté et al., 2002). Since the original linear calibration between TEX_{86} index and SST (Schouten et al., 2002), several modified and, partly, non-linear TEX_{86} calibrations have been suggested with expanded data sets to minimize the uncertainty of the global calibration and give the best absolute temperature estimates (Kim et al., 2008; Liu et al., 2009). Dedicated and logarithmic calibrations for low (<15 °C) and high (>5 °C) temperature regions, TEX_{86}^{L} and TEX_{86}^{H}, respectively, were suggested by Kim et al., (2010) and for 0-200 m water depth-integrated temperature by Kim et al., (2012). In the BAYSPAR approach using Bayesian statistics and allowing for spatial variability of TEX_{86} responding to temperature, SST and 0-200 m depth-integrated temperature calibrations were developed (Tierney and Tingley, 2015).

Despite the availability of various TEX_{86} calibrations and extensive applications in marine sediments (e.g., Lopes dos Santos et al., 2010; Rommerskirchen et al., 2011; McClymont et al., 2012; Hertzberg et al., 2015), many issues regarding (i) the mechanisms leading to the export of GDGTs to the deep oceans, (ii) the water depth and the seasonality of GDGT production, (iii) the contribution of different archaeal groups, and (iv) additional factors like nutrient or oxygen concentrations other than temperature influencing the proxy signals (Hurley et al., 2016; Lincoln et al., 2014; Qin et al., 2015; Turich et al., 2007; Wuchter et al., 2005) are still discussed.

Several studies on sinking particles collected by sediment traps reveal a correlation between GDGT concentrations and biogenic components in sinking particles, confirming that particles rich in organic matter are the major transport mechanisms for lipids (Chen et al., 2016; Huguet et al., 2007; Mollenhauer et al., 2015; Yamamoto et al., 2012). It appears that the lipids are aggregated or packed into larger particles and subsequently exported to deep waters and buried in the sediment. Additionally, the sinking rate depends on the dominant type of particles that the lipids are preferentially attached to. Even when there is no clear correlation between GDGTs and organic matter fluxes, TEX_{86}^{H} temperatures derived from sinking particles nevertheless correspond to the measured sea surface temperatures in the Cariaco Basin (Courtney Turich et al., 2013) and in the Gulf of Mexico (Richey and Tierney, 2016). The complexity of the sinking process of lipids and the transfer of its signal to the deep ocean require further investigation.

It has been reported that Thaumarchaeota reach their maximum abundance near 200 m water depth (Church et al., 2010; Hurley et al., 2016; Karner et al., 2001; Santoro et al., 2010), and enhanced GDGT production has been revealed in the subsurface oceans (Ingalls et al., 2006; Pearson et al., 2001; Shah et al., 2008). This supports the idea that Thaumarchaeota record the water temperature of the depth where they mainly dwell. Especially in many upwelling settings, TEX_{86}^{H} estimates reflected subsurface temperatures (Chen et al., 2016; Kim et al., 2012b; Lopes dos Santos et al., 2010; McClymont et al., 2012; Richey and Tierney, 2016).

Non-thermal environmental factors influencing TEX_{86} thermometry have been reported elsewhere. Higher TEX_{86} values than expected from ambient or surface temperatures are found in OMZs in water column studies (Basse et al., 2014; Schouten et al., 2012b; Xie et al., 2014; Qin et al. 2015), suggesting a typical warm bias of TEX_{86}-derived water temperatures under oxygen limitation. Hurley et al., (2016) recently showed that GDGT cyclization of *Nitrosopumilus maritimus* SCM1 in a culture experiment is enhanced when the ammonia oxidation rate is low, resulting in higher TEX_{86}signals in response to energy stress. Zhang et al. (2016) proposed an indicator, the Ring Index (RI), of potential non-thermal impacts of TEX_{86}, such as terrestrial input, contributions of GDGTs from non-planktonic Thaumarchaeota, nutrient, and/or dissolved oxygen levels. It is suggested that non-thermal effects on GDGT composition have occurred when the RI values, the weighted average of ring number of GDGTs, deviate from the typical TEX_{86} and RI relationship as observed in the modern ocean. It is important to understand the potential factors determining the TEX_{86} proxy in different oceanic realms in order to obtain reliable paleoenvironmental reconstructions. Samples of sinking particles collected by sediment traps can be of great value to study the proxy signal, resolving its seasonal and vertical variability.

Here we present TEX_{86} values in sinking particles collected in sediment traps deployed in eastern Atlantic upwelling systems, i.e., in the Guinea Basin within a region of equatorial upwelling activity (GBN3), and off Namibia within the Benguela coastal upwelling system near Lüderitz (LZ). We focus on high productivity settings, as they are often chosen for palaeoceanographic studies, yielding high-resolution sediment archives. Our results are compared to the sediment trap record from the eutrophic coastal upwelling system in Cape Blanc off Mauritania (CBeu; Mollenhauer et al., 2015).

2.2 Oceanographic setting

In the Eastern Atlantic Ocean, upwelling of nutrient rich-water masses resulting in high primary productivity occurs either along the coasts (coastal upwelling), or in the open ocean of the equatorial divergence zone (equatorial upwelling). The prevailing trade wind systems are responsible for upwelling in both types of settings. The north-easterly (NE) and south-easterly (SE) trade winds drive the Canary Current (CC) and the Benguela Current (BC), respectively, along the northwest and southwest African coasts, (Figure 2.1). Those two coastal upwelling systems belong to the four major Eastern Boundary Upwelling Ecosystems (EBUEs), which are well known for their highly productive ecosystems and their contribution to global primary production (Carr, 2002; Carr and Kearns, 2003; Shannon and Nelson, 1996).

The Intertropical Convergence Zone (ITCZ), where the NE and SE trade winds converge near the equator, is displaced to the North in response to the seasonal changes in trade winds and land configuration (Figure 2.1). During boreal summer (June - September), the SE trades are most strongly

developed and push the ITCZ to its northernmost location (10−15° N). This stimulates the South Equatorial Current (SEC) and maximum eastward advection of the North Equatorial Counter current (NECC), causing equatorial upwelling peaks and thermocline shoaling in the Guinea Basin. When the NE trades are most intense and the SE trades are weakened during boreal winter, the ITCZ is pushed to its southernmost location.

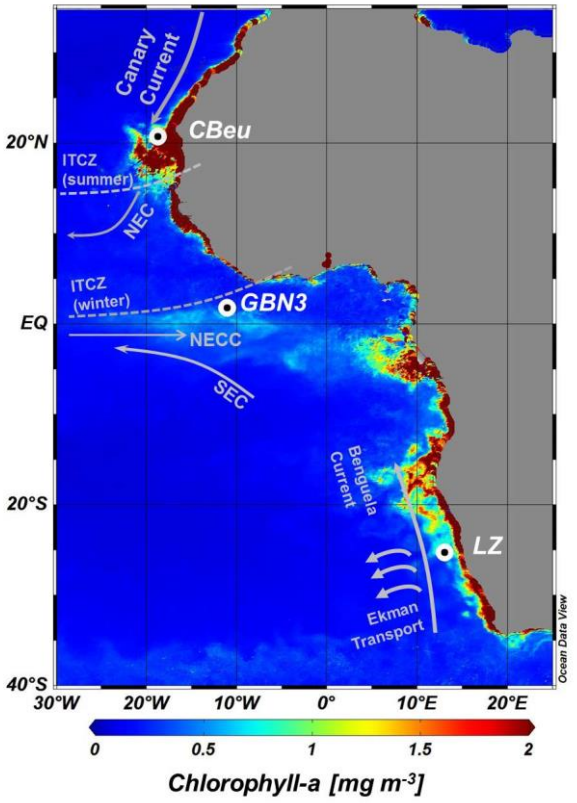

Figure 2.1 Location of GBN3, LZ, and CBeu sediment traps in the eastern Atlantic Ocean in context to the main current systems. The Canary Current and the Benguela Current induced by the trade winds lead the coastal upwelling along the northwest and southwest Africa, respectively, which belong to the four major Eastern Boundary Upwelling Ecosystems (EBUEs) in the world ocean. NEC and SEC represent the North and South Equatorial Currents. NECC represents the North Equatorial Counter Current. Dashed lines indicate the seasonal position of Inter Tropic Convergence Zone (ITCZ). The background ocean color map is shown for June 2004, displaying high chlorophyll-a concentrations near the trap locations. The Ocean Color Climate Change Initiative dataset, version 3.1, European Space Agency, available online at http://www.esa-oceancolour-cci.org/ was used. The map was produced using Ocean Data View (Schlitzer, 2017).

In the Guinea Basin, satellite SST reaches minimum values of approximately 24−25 °C, and chlorophyll-a and primary production are at their maximum between 0−20° W, and 0−10° S (Pérez et al., 2005). Except for this maximum production period, this region remains in a typical tropical condition characterized by a nutrient-depleted mixed layer and a stable thermocline of approximately 30−40 m depth (Lange et al., 1994). The maximum SST reaches 29 °C during boreal winter. This

region is characterized as “open ocean with moderate coastal influence” due to the presence of non-marine (fresh water) diatoms and enhanced lithogenic materials during boreal winter, which might be supplied by the Saharan dust plume (Lange et al., 1998).

We compare this equatorial upwelling setting with the Benguela coastal upwelling system off Namibia. Like the coastal upwelling off Cape Blanc, this upwelling area is active year-round with seasonally changing intensity. The BC flows northwards along the western coast of South Africa and causes strong coastal upwelling which is additionally strengthened by the south-easterly trade wind-driven Ekman transport, supplying cold and nutrient-rich South Atlantic Central Water (Shannon and Nelson, 1996) (Figure 2.1). The intense year-round trade winds induce perennial upwelling in the northern part of the BC system, in particular near Lüderitz (26° S), while upwelling is the strongest in austral spring and summer in the southern part of the system (Shannon and Nelson, 1996). The BC system with 0.37 Gt C/y is the most productive of the EBUEs followed by the CC system (0.33 Gt C/y) (Carr, 2002). A TOC maximum in surface sediments was found on the shelf off Lüderitz within the BC system (Mollenhauer et al., 2002).

Associated with the high productivity, oxygen minimum layers have been recorded in the Benguela system (Brüchert et al., 2003; Chapman and Shannon, 1987; Inthorn et al., 2006b; Monteiro et al., 2006, 2011). The seasonally oxygen depleted waters are developed mainly in austral summer and autumn at around 200 m depth (150−400 m) over the shelf region (Brüchert et al., 2003; Kalvelage et al., 2011). The seasonal variability of water temperature within the OMZs is ca. 1 °C at a given depth. Monteiro et al., (2006) reported year-round low-oxygen water (< 0.5 ml l^{-1}) in 2000-2001 caused by a greater contribution of the Eastern Tropical-South Atlantic Central Water (ET-SACW), which is characterized by strong hypoxia, rather than the Cape Basin-South Atlantic Central Water (CB-SACW), which is better ventilated. The oceanographic dynamics in the central Benguela are related to the relative contribution of the poleward ET-SACW and northward CB-SACW, which form the sub-thermocline boundary near 25° S off Namibia, (Monteiro et al., 2008, 2006).

2.3 Material and methods

2.3.1 Samples

Sediment trap moorings were deployed in the Guinea Basin (GBN3 at 1.8000° N, 11.1303° W, 4,481 m water depth) and off Lüderitz in the vicinity of the Lüderitz upwelling cell (LZ1 and LZ2 at 25.279° S. 13.052° E, 1,795 m depth) (Figure 2.1, Table 2.1). The GBN3 trap was deployed between March 1989 and March 1990 at 853 m and 3,921 m water depths. Each LZ trap deployment period covered 6 months. The last cup from the LZ1 deployment is excluded from the data sets, due to problems during trap servicing. In the LZ2 trap, particles were collected only in the first 4 sample bottles (mid-August to mid-September, 2000), while the remaining bottles were almost empty in spite

of correct functioning of the sediment trap programming. Exact sampling periods and locations of the sediment traps are summarized in Table 2.1. Additionally, a core-top sediment (GeoB1405-8; 1.7867° N, 11.14° W) recovered near the GBN3 trap site was analyzed.

Table 2.1 Trap names, locations, deployment depths and periods and sampling intervals.

Name	Location		Water depth	Trap deployment - depth	Deployment period		Sampling interval
	Latitude (° N)	Longitude (° E)			Start	End	
			(m)	(m)	(dd.mm.yyyy)		(d)
GBN3	1.8000	-11.1333	4,481	853/ 3,921	01.03.89	16.03.90	19
LZ1	-25.279	13.052	1,795	960	17.02.00	09.08.00	8.5, 13.5
LZ2			1,800	965	11.08.00	28.01.01	8.5
CBeu*	20.75	-18.7	2,690	1,296	15.07.03	23.03.07	7.5-23

* GDGT fractional abundances and TEX_{86} values for site CBeu were published by Mollenhauer et al., (2015)

Cone-shaped sediment traps (Kiel type) with a collection area of 0.5 m^2 were deployed for the collection of sinking particles. Each trap was equipped with 20 cups, poisoned with mercury chloride (HgCl2) before and after the deployment. The opening period of each cup was programmed before launching the mooring system. Materials were stored at 4 °C until further processing after servicing the trap. After recovery, wet samples were sieved (1 mm) to remove large particles, and swimmers were manually removed with tweezers. Samples were split (4–5 times) using a McLane wet samples at the University of Bremen and freeze-dried and homogenized afterwards. Prior to lipid analysis, samples were sealed and stored in the dark at room temperature. More details can be found in Wefer and Fischer (1993).

2.3.2 Mass fluxes

Samples of sinking particles collected with the sediment traps were weighed and analyzed for their geochemical composition. Total organic carbon (TOC) and total nitrogen (TN) contents were measured with a Heraeus CHN element analyzer. TOC content was determined after decalcifying the samples with 6N hydrochloric acid (HCl) and drying them on a hot plate at 80 °C. Calcium carbonate (carbonate) was estimated from the differences between non-decalcified and decalcified CHN analyzer measurements as carbonate = (total carbon – organic carbon) x 8.33. Biogenic opal was determined using a sequential leaching technique (Müller and Schneider, 1993). The flux of lithogenic material was calculated from total mass flux – (2 x organic carbon + carbonate + opal). Total mass

flux, TOC, TN, carbonate, opal, and lithogenic material fluxes for site GBN3 were reported by Wefer and Fischer (1993). Data from CBeu were shown in Mollenhauer et al., (2015).

2.3.3 Lipid analysis

Lipids were extracted from freeze-dried and homogenized samples (approximately 4-318 mg) with dichloromethane (DCM): methanol (MeOH) 9:1 (v/v) solvent using an ultrasonic bath for 10 min. The procedure was repeated three times. The extract was saponified at 80 °C for two hours with 0.1 M potassium hydroxide (KOH) in MeOH and purified water (9:1) from a Seralpur system extracted with DCM. Neutral lipids were recovered by partitioning into 1 mL hexane (Hex) (×3). This aliquot was separated into F1 (apolar), F2 (ketone), and F3 (polar) fractions eluted in 2 mL Hex, 4 mL DCM: Hex 2:1 (v/v), and 4 mL DCM: MeOH 9:1 (v/v), respectively, through a silica-gel column (deactivated with 1% distilled water, mesh size: 70−230 mm, length: 4 cm) prepared in a Pasteur pipette. To quantify GDGTs, known amounts (1µg for GBN3 and 5 µg for LZ) of an internal standard (C_{46} GDGT) were added to each sample before the extraction.

Polar fractions (F3) for GDGTs were filtered through 0.45 µm pore size polytetrafluoroethylene (PTFE) syringe filters and diluted to 2 mg ml^{-1} concentrations in Hex: isopropanol 99:1 (v/v) according to Hopmans et al. (2000). GDGTs were analyzed using high performance liquid chromatography/atmospheric pressure chemical ionization-mass spectrometry (HPLC/APCI-MS) as described by Meyer et al., (2016). GDGT flux was calculated as the sum of GDGTs used to calculate the TEX_{86} value.

The TEX_{86}/ TEX_{86}^{H} values were calculated according to Schouten et al. (2002, eq. 1) and Kim et al. (2010, eq. 2):

$$TEX_{86} = ([GDGT\text{-}2]+[GDGT\text{-}3]+[Cren']) / ([GDGT\text{-}1]+[GDGT\text{-}2]+[GDGT\text{-}3]+[Cren']) \quad (1)$$

$$TEX_{86}^{H} = Log_{10}(TEX_{86}) \quad (2)$$

,where the numbers indicate the number of cyclopentane moieties (GDGT-1-3) in the isoprenoid GDGTs, and Cren´ means the regio-isomer of Crenarchaeol containing 4 cyclopentane moieties and 1 cyclohexane moiety. When each bracket represents the relative abundance of individual GDGT in the GDGT pool (eq. 3), the Ring Index (RI) was calculated as follows (eq. 4; Zhang et al., 2016):

$$[GDGT\text{-}0] + [GDGT\text{-}1] + [GDGT\text{-}2] + [GDGT\text{-}3] + [Cren] + [Cren'] = 100\% \quad (3)$$

$$RI = 0\times[GDGT\text{-}0]+1\times[GDGT\text{-}1]+2\times[GDGT\text{-}2]+3\times[GDGT\text{-}3]+4\times[Cren]+4\times[Cren'] \quad (4)$$

Temperatures were calculated using the following TEX_{86} calibrations (Kim et al. 2010; 2012):

$$T = 68.4 \times TEX_{86}^{H} + 38.6 \quad (5)$$

$$T = 54.7 \times TEX_{86}^{H} + 30.7 \quad (6)$$

,which were suggested for regions with SSTs above 15 °C for SST (eq. 5) and for water depth of 0-200 m (eq. 6), respectively. Additionally, the BAYSPAR SST and subsurface temperature (SubT) calibrations were applied with the standard prediction mode and the default settings (Tierney and Tingley, 2015).

The standard deviation of replicate analyses of a lab-internal sediment standard is ± 0.01 units of TEX_{86}, corresponding to an uncertainty of ± 0.60 °C in the estimated temperatures based on the TEX_{86}^{H} calibration (Kim et al., 2010), and 6% for isoprenoid GDGT concentrations.

2.3.4 Environmental data

To compare the estimated SSTs based on TEX_{86}^{H} and BAYSPAR, Advanced Very High Resolution Radiometer (AVHRR) satellite-derived SSTs (http://www.ncdc.noaa.gov/oisst) were extracted and re-averaged according to the sampling periods. The satellite-derived SSTs have a spatial grid resolution of 0.25 degree and temporal resolution of 1 day. We also compare the seasonal and mean annual depth profile of water temperature and nitrate (NO_3^-) concentration in the vicinity of the trap locations extracted from the World Ocean Atlas 2013 (WOA13), representing the average value for the period from 1955 to 2012 (Garcia et al., 2013; Locarnini et al., 2013). The resolutions of WOA13 are 0.25 degree for temperature and 1 degree for nutrients. We used a definition of seasons according to WOA13 (i.e. boreal winter/austral summer: January−March, spring/autumn: April−June, summer/winter: July−September, autumn/spring: October−December; Garcia et al., 2013; Locarnini et al., 2013).

2.4 Results

2.4.1 Sinking particles in the northern Guinea Basin (GBN3)

2.4.1.1 TEX_{86} thermometry

TEX_{86} varied in the range 0.59−0.67 and 0.60−0.62 at the shallow and deep traps, respectively (Figure 2.2). The seasonality in the estimated temperatures based on TEX_{86}^{H} was similar to SST changes at the shallow trap while there was no clear seasonality at the deep trap (Figure 2.2). The Flux-weighted mean TEX_{86} values over the study period were identical at both depths with a value of 0.61 (Table 2.2).

BAYSPAR SST temperatures ranged from 25.3 to 32.3 °C and from 26.5 to 28.2 °C at the shallow and the deep traps, respectively. The estimated temperatures were higher than the satellite-derived SST from July to September 1989 at both depths, and the strongest overestimation of BAYSPAR SST compared to the satellite-derived SST occurred from November 1989 to March 1990 at the shallow

trap. BAYSPAR SubT (proposed to reflect weighted averages of 0-200 m water depth) estimates of 17.4-23.1 °C at the shallow trap and 18.4−19.7 °C at the deep trap resembled the estimates obtained with the TEX_{86}^{H} 0-200 m depth-integrated calibration (18.0−21.2 °C at the shallow trap and 18.7−19.5 °C at the deep trap) (Table 2.2, Figure 2.2).

RI values ranged from 2.19 to 2.56 and from 2.03 to 2.29 at the shallow and deep traps, respectively (Figure 2.3). Most values of TEX_{86}-RI from both depth traps reside well within the 95% prediction intervals of global TEX_{86}-RI correlation, except for one sample collected in September 1989 (Figure 2.3).

2.4.1.2 Mass and GDGT fluxes

Between March 1989 and March 1990, seasonal mass fluxes at the shallow trap (853 m) in the Guinea Basin were highest in boreal summer (240.5 mg m^{-2} d^{-1} in August−September 1989) and in spring (197.5 mg m^{-2} d^{-1} in March 1989) (Figure 2.2). The deep trap (3,921 m) recorded similar peaks of mass fluxes occurring in March and September 1989, but the fluxes were significantly higher than those at the shallow trap. Over the entire trap deployment period, the fluxes of GDGT were higher in the deep trap (0.15−0.73 μg m^{-2} d^{-1}) than in the shallow trap (0.01−0.38 μg m^{-2} d^{-1}) (Figure 2.2). The GDGT fluxes were correlated with opal fluxes (R^2 = 0.71 for the shallow trap, R^2 = 0.62 for the deep trap) when episodic GDGT pulses in late-October and late-December 1989 at the shallow trap and January−March 1990 at the deep trap were excluded in the correlations (Figure 2.2).

2.4.2 Sinking particles in the Benguela area off Namibia (LZ)

2.4.2.1 TEX_{86} thermometry

TEX_{86} values ranged from 0.47 to 0.54 in the Benguela upwelling region (Figure 2.4). TEX_{86}^{H} temperatures decreased from mid-February (20.0 °C) to early-June (16.4 °C), and increased to 19.2 °C in the remaining period while the satellite-derived SSTs decreased continuously from February to September. The BAYSPAR SST showed similar temperature trends as obtained from the TEX_{86}^{H} calibration, varying between 16.3 and 20.9 °C. The BAYSPAR SubT estimates ranged between 12.6 and 16.9 °C, which also had similar trends as obtained from TEX_{86}^{H} 0-200 m depth-integrated calibrations, but the amplitude of BAYSPAR temperature variations was higher (Figure 2.4).

RI values ranged from 1.70 to 1.97. Two samples collected in early and late May 2009 and four samples collected between early-August and mid-September 2009 are out of the 95% prediction intervals of TEX_{86}-RI global correlation (Figure 2.3).

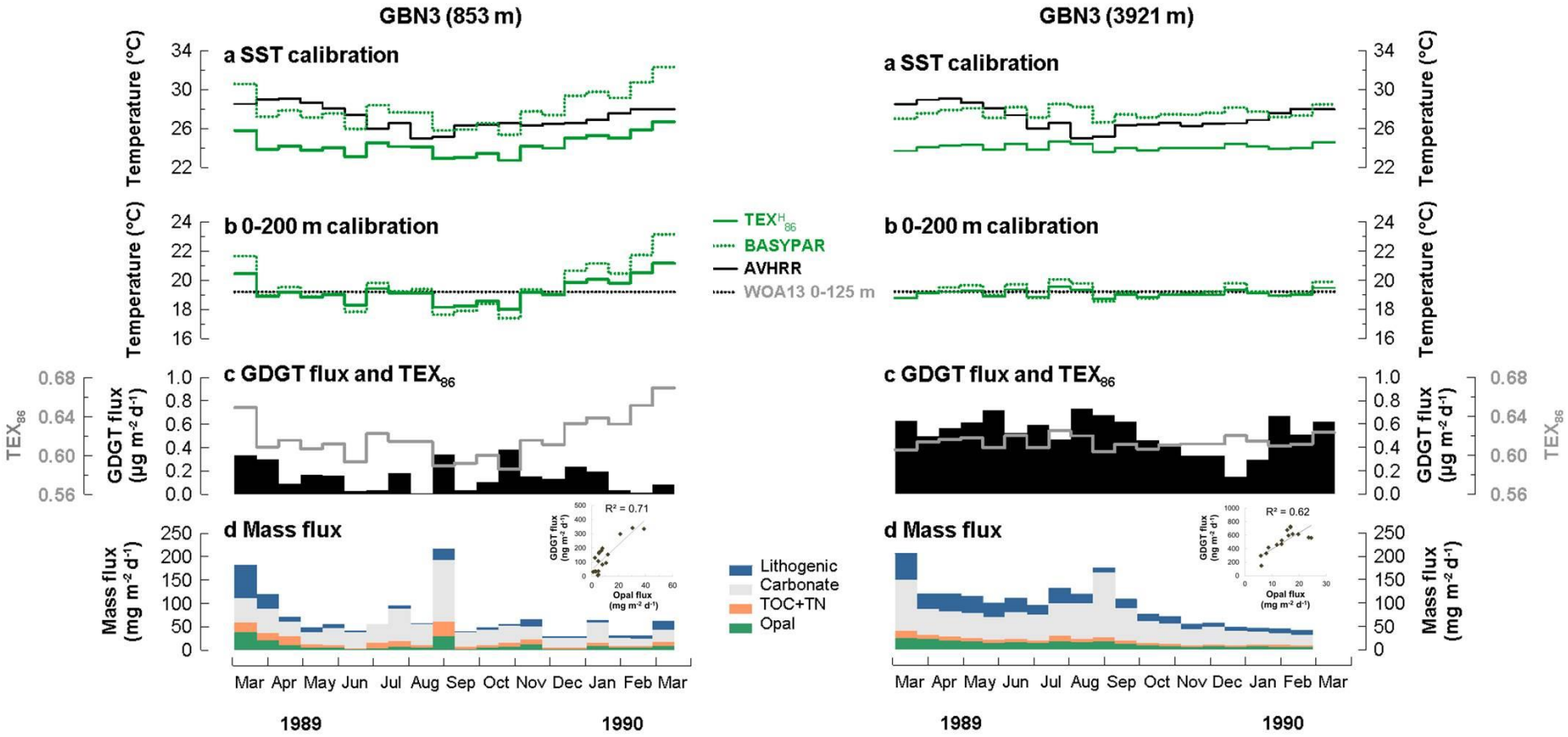

Figure 2.2 Changes in (a) estimated temperatures for SST, (b) estimated 0-200 m depth-integrated temperatures, (c) GDGT flux and TEX_{86} and (d) mass flux and the correlation of the fluxes between GDGT and opal at 853 m (left panel) and at 3921 m (right panel) water depth in the Guinea Basin (GBN3).

Table 2.2 Values of TEX_{86} (Flux-weighted mean values for trap time-series data) and estimated temperatures at GBN3 and LZ.

Region		Material	Location		TEX_{86}	Estimated temperature (°C)			
			Latitude (° N)	Longitude (° E)		TEX^{H}_{86} (1)		BAYSPAR (2)	
						SST	0-200m	SST	0-200m
Guinea Basin	GBN3 (853 m)	sinking particles	1.8000	-11.1333	0.61	24.1	19.1	27.7	19.3
	GBN3 (3,921 m)				0.61	24.1	19.1	27.6	19.3
	GeoB1405-8	core-top sediment	1.7867	-11.14	0.57	21.7	17.2	23.8	16.0
Lüderitz	LZ (960 m)	sinking particles	-25.279	13.052	0.50	18.3	14.5	18.6	14.8

(1) TEX_{86} temperatures are calculated by the TEX^{H}_{86} calibration for SST from Kim et al. (2010) and by the TEX^{H}_{86} 0-200m depth-integrated calibration from Kim et al., (2012).

(2) TEX_{86} temperatures are calculated by the Bayspar calibrations for SST and 0-200m depth-integrated temperature (Tierney and Tingley, 2015).

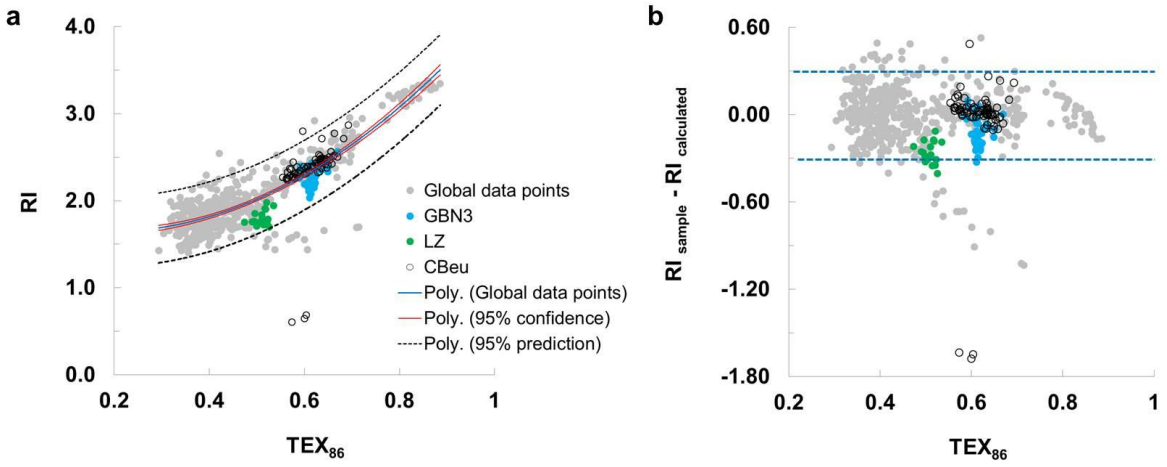

Figure 2.3 (a) Correlation between TEX_{86} and Ring index (RI) modified after Zhang et al., (2016). The grey, blue, green and black empty circles represent the global ocean core-top points, GBN3, LZ, and CBeu trap samples, respectively. (b) "$RI_{sample} - RI_{calculated}$" represents the difference of RI between the original sample value and the calculated value based on the relationship of TEX_{86}-RI in the global ocean by Zhang et al., (2016). TEX_{86} between two vertical blue lines on (b) displays thermal signal, while samples located outside of the lines possess non-thermal factors on TEX_{86} values.

2.4.2.2 Mass and GDGT fluxes

In the Benguela upwelling area off Lüderitz, mass fluxes ranged from 0 to 788 mg m^{-2} d^{-1} (Figure 2.4) with multiple peaks in February−May and August. The maximum in mass fluxes occurred in mid-May when opal and carbonate fluxes were enhanced. Carbonate fluxes mostly accounted for 26−78% of mass fluxes, but for only 9% when lithogenic flux was pronounced in early May. Between mid-August and mid-September, the relative proportion of opal to mass flux was higher than the one of carbonate. The seasonal variability of fluxes in TOC and TN was similar to the one of carbonate fluxes, but both accounted for only 5−15% and 1−3% of mass fluxes, respectively. The GDGT fluxes were not correlated to any of the biogenic fluxes due to maxima in different seasons. The flux of GDGTs varied between 0.41 and 4.2 µg m^{-2} d^{-1}, with two maxima in mid-April (3.9 µg m^{-2} d^{-1}) and late-May (4.2 µg m^{-2} d^{-1}) (Figure 2.4).

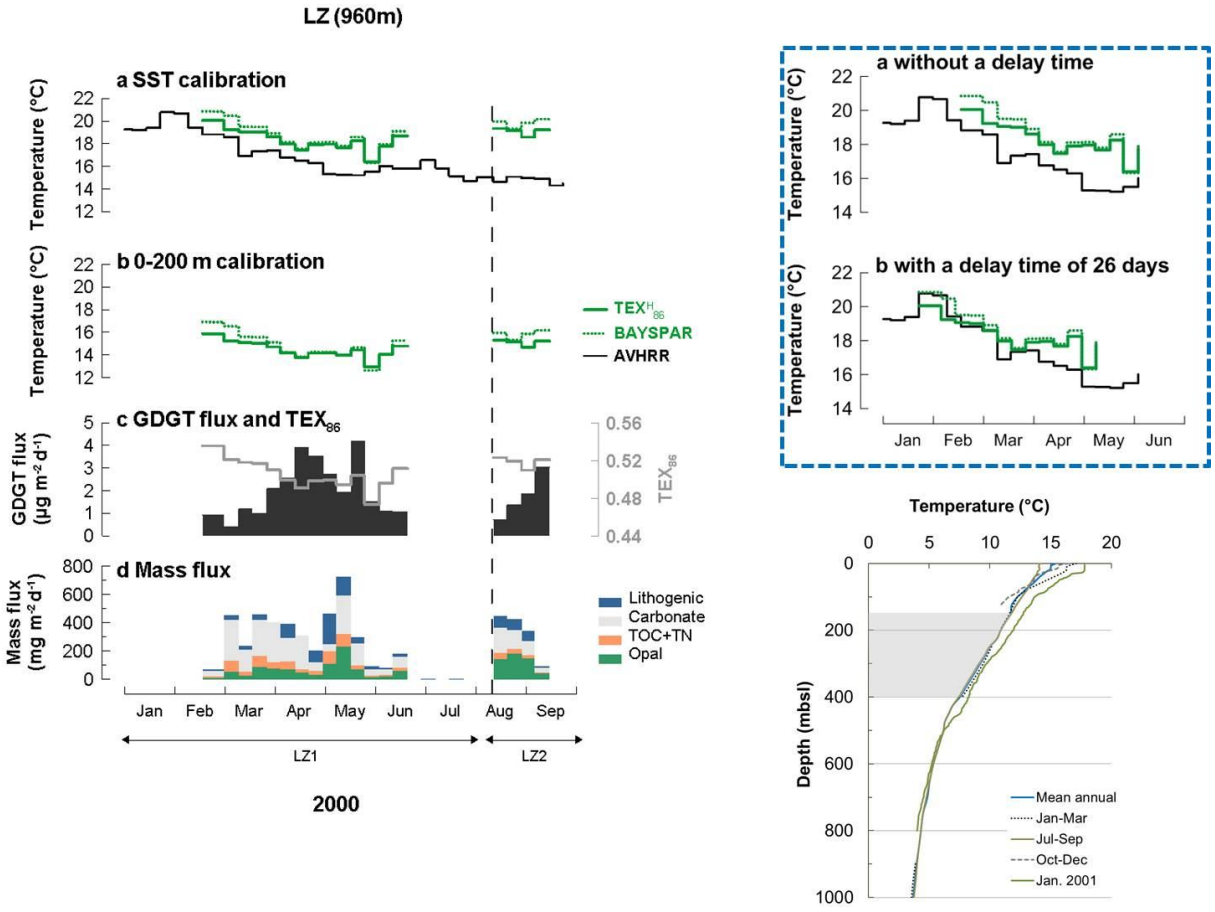

Figure 2.4 Changes in (a) estimated temperatures for SST, (b) estimated 0-200 m depth-integrated temperatures, (c) GDGT flux and TEX_{86}, and (d) mass flux at 960 m water depth in the Lüderitz bay (LZ) off Namibia on the left panel. The vertical dashed line represents the end of LZ1 trap and the start of the LZ2 trap. TEX^{H}_{86} signals in the trap between mid-February and early-June (right panel, a) have a good match with satellite-derived SSTs between mid-January and early-May when a 26 days delay time is considered (right panel b). Depth profile of temperature measured by a Seabird sensor during the 64PE174 MARE-3 cruise at the trap location and seasonal depth profile of temperature extracted from WOA13 in the Lüderitz are presented on the right bottom panel. No temperatures are available in April−June of WOA13.

2.5 Discussion

2.5.1 TEX_{86}-RI correlation

The TEX_{86} values were plotted against the RI values measured from GBN3 and LZ as well as from NW Africa (Mollenhauer et al., 2015) on the global TEX_{86}-RI regression (Figure 2.3a; Zhang et al., 2016). The TEX_{86} values were also plotted against the differences between the sample´s original RI values and calculated ones based on the global TEX_{86}-RI regression ($RI_{sample}-RI_{calculated}$, ΔRI; Figure 2.3b). Most trap samples fell within the 95% prediction intervals, but some samples had offsets greater than 0.3 of $|\Delta RI|$, which was suggested as an indicator of non-thermal factors (Zhang et al., 2016). One sample collected in September 1989 at the lower trap of GBN3 fell outside the area controlled by thermal factors (Figure 2.3b). Two samples in May 2000 and four consecutive samples in between mid-August and mid-September 2000 from LZ had offsets (Figure 2.3b). Four samples in CBeu were found outside the range of thermal factors; one sample collected in late-June 2003 with $|\Delta RI| = 0.49$ of and three samples collected in between mid-April and mid-May 2005, late-September and late-October 2005, and early-July and late-July 2006 with up to $|\Delta RI| = 1.68$ of (Figure 2.3). It appears that larger ΔRI do not systematically occur during a specific season. The samples from CBeu (within the 95% confidence intervals of the global regression) contained 19-35% GDGT-0 of total GDGTs. By contrast, those samples with low ring index values falling far off the global regression were attributed to relative abundances of >80% of GDGT-0 (Mollenhauer et al., 2015). Such a large proportion of GDGT-0 can be explained by GDGTs produced by methanogenic archaea (Weijers et al., 2011). The influence of methanogenic archaea on GDGT pools can be screened by the relative abundance of GDGT-0 to the sum of GDGT-0 and Crenarchaeol, represented by the %GDGT-0 index (Inglis et al., 2015). The %GDGT-0 values of samples with deviated ΔRI from CBeu were 85−87%, which exceeded 67% indicating the influence of methanogenic archaea, while the index values of the remaining samples ranged between 24−42%. However, it seems unlikely that methanogens thrive in the water column of the open ocean. The question also arises why such events occurred randomly only in a very short term (e.g. only within the collection time of one sample cup). Thus, the origin of these high GDGT-0 abundances remains unclear at this stage. Mollenhauer et al., (2015) suggested a potential contribution of GDGTs derived from subsurface communities at site CBeu, but predominantly during the upwelling season. Moreover, the authors pointed out that higher TEX_{86} values could be caused by GDGTs produced in the OMZs, where Basse et al., (2014) found high TEX_{86} values within suspended particles.

The above analysis showed that non-thermal effects are not directly obvious by using the TEX_{86}-RI relationship. Therefore, in the following sections we discuss TEX_{86}^{H}-derived temperature estimates and the possible non-thermal factors on GDGT distributions. We investigate GDGT fluxes and indices in the Guinea Basin characterized by equatorial upwelling and the Benguela coastal upwelling system

off Namibia and consider the respective regional conditions. This discussion includes implications for TEX_{86}^{H} observed in the eastern Atlantic upwelling settings.

2.5.2 Equatorial upwelling: Guinea Basin (GBN3)

In the Guinea Basin, the GDGT fluxes at the shallow GBN3 trap had multiple peaks in March, July−late-August, late-October, and December 1989 (Figure 2.2). The maxima of GDGT and mass fluxes in boreal spring and summer are associated with input of Saharan dust (lithogenic components) and seasonal upwelling, respectively (Wefer and Fischer, 1993; Figure 2.2). These seasonal maxima in GDGT and mass fluxes also occurred at the deep trap with less pronounced seasonality throughout the trap deployment period. No clear correlation was found between the fluxes of GDGTs and biogenic components at neither the shallow nor deep traps when all samples were considered. Surprisingly, the correlation between the fluxes of GDGTs and opal appeared to be better when two or three episodic GDGTs pulses at both depths were excluded (Figure 2.2; $R^2 = 0.71$ for the shallow trap, $R^2 = 0.62$ for the deep trap). This is in good agreement with other studies which showed good correlations between GDGTs and biogenic components fluxes in sinking particles in different environmental regimes (e.g., in the South of Java (Chen et al., 2016), off Cape Blanc (Mollenhauer et al., 2015), and in the western North Pacific (Yamamoto et al., 2012)). Based on those correlations it was suggested that GDGTs are primarily aggregated into opal dominant particles and exported to deep waters.

Opal is primarily contributed by diatoms to the sediment of the pelagic ocean by the formation and sinking of marine snow aggregates and zooplankton faecal pellets from the upper ocean (Ploug et al., 2008a). Diatoms and silicoflagellates are the most abundant groups of opal producing organisms in the Guinea Basin (Lange et al., 1994; Treppke et al., 1996). Diatoms release extracellular polymer substances which promote the formation of marine snow particles (Thornton, 2002). Planktonic Archaea that are very small (<1 μm) and neutrally buoyant can only sink and be buried in sediments when aggregated or packed into larger particles, similar to diatoms (Schouten et al., 2013). Indeed, Wuchter et al., (2005) found TEX_{86} temperatures resembling water temperatures exclusively in upper oceans (<100 m), implying a rapid sinking of GDGTs by aggregation and packaging. As mentioned earlier, this sinking mechanism of GDGTs has been reflected in good correlations between GDGT and opal fluxes in sinking particles. Therefore, our results support the idea that most GDGTs in the Guinea Basin are transported to the deep sea by packaging into opal-rich particles. The episodic GDGT pulses, which were not closely related to opal flux peaks, occurred in late-October and late-December 1989 at the shallow and in early 1990 at the deep trap. This might have been a consequence of enhanced GDGT production during periods of relatively lower primary production when there is no competition with phytoplankton for ammonia (Herfort et al., 2007; Pitcher et al., 2011; Wuchter et al., 2006a). However, the export mechanism of GDGTs during these times remains unresolved.

The relatively low mass and GDGT fluxes at the shallow trap could be due to the low sampling efficiency of the trap in the upper water column where the current velocities are generally higher than in the deeper water column (Figure 2.2). However, the current velocities measured at 905 m and 3960 m water depth varied around 15−20 cm s^{-1} at both depths (Wefer and Fischer, 1993). The sampling efficiency therefore might be similar at both depth levels. A more plausible explanation is that the deeper trap represents a larger source area, resulting in a higher organic material flux and a smoothed seasonal variability compared to the shallower trap (Wuchter et al., 2006b). This is supported by the observation of higher summer fluxes only north of the equator related to the oceanographic setting (e.g. the equatorial divergence) and increased fluxes of lithogenic materials with depth originating from topographic elevation in the Guinea Basin (Fischer and Wefer, 1996).

For temperature estimations, neither TEX_{86}^{H} nor BAYSPAR SST was successful in reproducing SST. TEX_{86}^{H}-derived temperatures were colder and BAYSPAR temperatures were warmer than the satellite-derived SSTs (Figure 2.2). However, both depth-integrated calibrations based on TEX_{86}^{H} 0-200 m and BAYSPAR SubT yielded realistic subsurface temperatures (Table 2.1, Figure 2.2). Given the fact that the BAYSPAR model takes calibration factors from the existing data near the study area, it is surprising that BASYPAR SubT displayed rather realistic subsurface temperatures although there are hardly any calibration points near the GBN3 trap site. However, considering that subsurface temperatures are less variable spatially and temporally compared to SST, it is expectable that depth-integrated calibrations generate more reasonable temperatures compared to SST calibrations irrespective of the number of core top data points in the vicinity of a study site.

The decreasing trend in TEX_{86}^{H} temperatures from March until early-September followed by an increase starting from late October at the shallow trap was similar to the satellite-derived SST variations (Figure 2.2). Due to the time required for GDGTs to become entrained into larger sinking particles, and subsequent transportation to deep waters, TEX_{86} variations are often delayed relative to the satellite-derived temperature variations (Ingalls et al., 2012; Mollenhauer et al., 2015; Wuchter et al., 2005; Yamamoto et al., 2012). The absence of a notable time-lag indicates shorter residence time (Ingalls et al., 2012) and faster transportation of core lipids in the water column here than in other settings. Fischer and Karakaş, (2009) found that sinking rates are relatively high in the eastern equatorial Atlantic and off NW Africa. Although these sinking rates are calculated based on the time delay of flux maxima between two traps and do not represent the sinking velocity in surface waters, this scenario explains particles tending to be transferred rapidly to the shallower trap of GBN3 (Fischer and Karakaş, 2009). Together with the high sinking rate of particles, 19 days of sample resolution might be too long to record a time shift of the TEX_{86}signal. Taking 19 days of sample resolution as a maximum travel time, and the travel distance between the depths of origin of the

TEX_{86} signal (50 m; see the discussion below) and the trap (853 m), the minimum sinking rate of particles containing GDGTs is 42 m d^{-1} ((853 – 50) m / 19 days) in the Guinea Basin.

TEX_{86}^{H} temperatures at the deep trap varied only by approximately 2 °C (22.6−24.6 °C), which is less than the temperature amplitude reconstructed from the shallow trap samples (22.7−26.7 °C) (Figure 2.2). Compared with higher fluxes and less pronounced seasonality of mass and GDGT fluxes at the deep trap relative to the shallow one, the deep trap records a homogenized signal and integrates sinking particles transported from a wide range of areas and long-time scales, comparable to finding in the Arabian Sea (Wuchter et al., 2006b). Thus, a larger catchment area can explain the smaller amplitude of estimated temperatures as well as higher mass and GDGTs fluxes at the deeper trap in the Guinea Basin.

In order to investigate a possible sub-surface origin of the temperature signal reflected in TEX_{86}^{H}, the TEX_{86}^{H} temperature estimates from both traps at GBN were compared to the depth profiles of water temperatures and nitrate (NO_3^-) concentrations (Figure 2.5). As no seasonally resolved temperature and nutrient data are available from the subsurface, we compared annual mean data with Flux-weighted mean values calculated from the sediment trap samples. The Flux-weighted mean TEX_{86}^{H} temperatures at both traps were 24.1 °C (Table 2.2), which corresponds to the temperatures below the surface mixed layer (approximately 50 m water depth). Notably, this coincides with the nutricline, where the nitrate concentration starts to increase (Figure 2.5). Known for their ability to oxidize ammonia to nitrite, marine planktonic Thaumarchaeota play a crucial role in the nitrogen cycle in the ocean (Wuchter et al., 2006a). In biological studies of Thaumarchaeota, correlations between copy numbers of amoA (the gene coding for the subunit of the ammonia monooxygenase), ammonia oxidation rate, and/or nutrient (NH_4^+, NO_2^-, and/or NO_3^-) concentrations have been reported with depth or through time (Beman et al., 2008; Church et al., 2010; Horak et al., 2013; Wuchter et al., 2006a). Beman et al. (2008) and Horak et al. (2013) showed increased nitrate (NO_3^-) concentrations at high ammonia oxidation rates and maximum amoA gene copies in the water column.

Intact polar lipid GDGTs (IPLs) are believed to reflect the living thaumarchaeal biomass, while the core GDGTs (breakup products of IPLs) are less suitable to describe the living *in situ* communities (Ingalls et al., 2012; Urakawa et al., 2014). However, a sediment mooring system collects particles with incorporated GDGTs after Thaumarchaeota die in the upper waters and exported into deep waters. Thus, the GDGT assemblage provides integrated information about the production of GDGTs, the formation of aggregates, and the transport mechanism to the trap. While no unambiguous information on the archaeal community can be deduced from our observations, the good agreement of the TEX_{86}^{H} temperatures with the water temperature at the onset of increasing nitrate concentrations suggest that the corresponding depth (~50 m) may be the predominant origin of GDGTs. GDGTs are expected to reflect the water temperature at the site of production, which may be the primary habitat

depth of the local thaumarchaeotal community. This habitat is suggested to be in the shallow subsurface (~50 m) in the Guinea Basin.

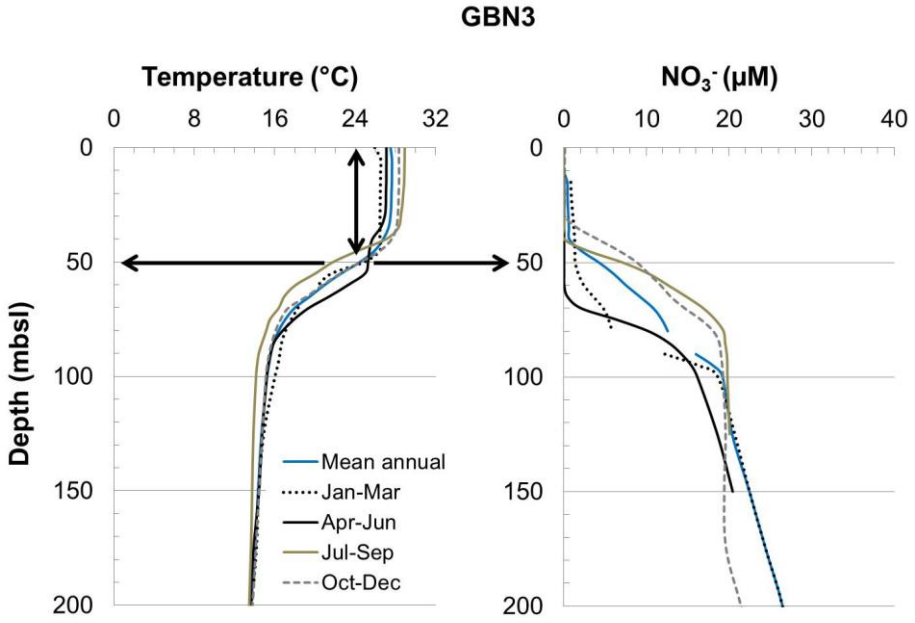

Figure 2.5 Depth profile of temperature and nitrate concentrations in the Guinea Basin (GBN3) extracted from WOA13. The arrows indicate the Flux-weighted mean TEX_{86}^{H} temperature (24.1 ℃) in sinking particles and the possible depth of (ca. 50 m) of major GDGT production.

Apart from the impact of nutrient distribution on the TEX_{86} value we suggest, other physiological and environmental factors like pH, salinity, growth phase of Archaea, or different archaeal community have been studied. Elling et al., (2015) found no significant impact of salinity and pH on TEX_{86} in a culture study. Considering a wide range of both parameters tested in the study and a small range of their variations in the open ocean, it seems that both parameters are negligible for TEX_{86} thermometry. Changes of GDGT compositions and TEX_{86} values were shown in response to the growth phase in Nitrosopumilus maritimus culture (Elling et al., 2014). However, we assume that particles captured in the sediment trap are derived from deceased planktonic Archaea cells after their final stage of the life cycle. Thus, the growth stage of planktonic Archaea can be ruled out as a physiological factor on TEX_{86} in sinking particles. As discussed earlier in section 2.5.2., we found no clear evidence of methanogenic Archaea in the trap samples of GBN3. Several studies using different approaches have revealed a contribution of subsurface GDGTs (deep-dwelling archaeal community) to TEX_{86} signals (Hernández-Sánchez et al., 2014; Huguet et al., 2007; Lengger et al., 2012; Shah et al., 2008; Taylor et al., 2013). This is consistent with our results in the Guinea Basin, which suggest that TEX_{86} is a reflection of planktonic archaeal GDGTs from the shallow subsurface.

In studies using sediment traps deployed at multiple water depths, TEX_{86} values are generally constant from the shallow to the deep waters across a range of different settings (Turich et al., 2007; Wuchter et al., 2006a; Yamamoto et al., 2012). This is in agreement with other observations carried out at different water depths and in various oxygen levels where TEX_{86} remains relatively constant and less susceptible to oxic degradation and transport (Kim et al. 2009; Mollenhauer et al. 2008; Schouten al. 2004; Wuchter et al. 2005). Moreover, when comparing TEX_{86} values (or an estimated water temperature) between sinking particles and underlying core-top sediments, it has been found that the TEX_{86} signal is transported through the water column and reaches the sediment without significant alteration (Chen et al. 2016; Mollenhauer et al. 2015; Rodrigo-Gámiz et al. 2015).

However, TEX_{86} temperature on underlying core-top sediment at GBN3 site (1.7867° N, 11.14° W, GeoB1405-8) was clearly lower (21.7 °C) than the Flux-weighted mean TEX_{86}^{H} temperatures (24.1 °C) from both traps (Table 2.1). Lateral transport from a substantially colder region could be one explanation. However, such a strong lateral gradient of temperature does not exist near the trap region, and there is evidence that GDGTs are less subjected to long distance lateral transport and they rather represent the local conditions (Kim et al., 2009; Mollenhauer et al., 2008; Shah et al., 2008). Moreover, SSTs are generally higher closer to the continental shelf regions than at open water location. One possible explanation may be *in situ* production of methanogenic Archaea, which are well known to contain relatively higher proportions of GDGT-1, -2 and -3 and can potentially contribute to the GDGT pools in sediments (Weijers et al., 2011). Liu et al., (2011) also report a relatively higher amount of GDGT-2 and -3 in the IPLs-GDGTs produced by methanogenic Archaea, which can alter the composition of core lipid GDGTs (CLs). However, methanogenesis is not expected in samples with a relatively low TOC content (0.5 wt.% of TOC in GeoB 1405-8 core-top sediment; Mollenhauer et al., 2004). Further insights could be obtained by analysing IPL-GDGTs in the surface sediments.

Our findings in the Guinea Basin agree well with other studies showing that TEX_{86}^{H} temperatures reflect a subsurface temperature rather than SST in tropical or subtropical upwelling regions where thermocline and nutricline are well developed (Huguet et al., 2007; Lee et al., 2008; Lopes dos Santos et al., 2010; McClymont et al., 2012; Rommerskirchen et al., 2011). This reveals that distribution of GDGTs is not solely determined by sea surface water temperature, but also by the regional environmental setting that determines the favorable dwelling depth of Thaumarchaeota.

2.5.3 Coastal upwelling: Benguela system (LZ) with comparisons to the Cape Blanc area

The mass fluxes peaked in March to early-April and mid-May 2000 (late austral summer to autumn), but the maxima in GDGT fluxes occurred in mid-April and late-May 2000 (austral autumn; Figure 2.4). Wefer and Fischer (1993) showed that mass fluxes peaked in austral autumn (May−June) and in spring (October−November) from a sediment trap deployed at 599 m water depth at Walvis

Ridge located 5° north of the LZ trap within the Benguela upwelling system. These observations suggest that the LZ trap recorded realistic peak fluxes in austral autumn, but it might miss the real fluxes in austral spring. During two periods (LZ1 + LZ2) of the trapping interval, the collection cups of the sediment traps were practically empty in mid-June to early-August 2000 from LZ1 and mid-September 2000 to late January 2001 from LZ2. This might be caused by a low trapping efficiency. Potential under-sampling in the rather shallow traps due to stronger currents in the more coastal site compared to the Walvis Ridge location seems plausible (Buesseler et al., 2007; Gardner, 1985). However, no current speed data from the LZ trap site were available. Considering the year-round high productivity at Lüderitz, the above mentioned periods of minimal or no flux at LZ may indeed be due to lower sediment trap efficiency.

Enhanced fluxes of GDGTs suggest a higher production of GDGTs at that time or an increased transport of GDGTs to the trap depth. The temperature depth profile measured using a CTD when the LZ2 was recovered in January 2001 showed a clear stratification in austral summer (Figure 2.4). It is likely that the mass flux maxima observed in austral autumn were triggered by the shoaling of the thermocline followed by the supply of nutrients (that accumulated during the stratification) to the surface waters and thus stimulating productivity (Louw et al., 2016; Vorrath et al., 2017). After the bloom, ammonia released by remineralization of organic matter may prompt ammonia oxidation by Thaumarchaeota and thus the production of GDGTs. At the same time, increased fluxes of phytoplankton debris after the bloom can transport GDGTs to the trap depth more effectively. In this case, GDGT fluxes should be parallel to the mass fluxes or other biogenic component fluxes (e.g., organic carbon, opal). A potential correlation between GDGTs and organic matters could be more obvious if both flux data sets cover the entire year, which unfortunately is not the case. Therefore, we cannot make any inferences regarding the main transport mechanism for GDGTs at site Lüderitz.

TEX_{86}^{H} temperatures agreed well with the satellite-derived SSTs changes from mid-February to early-June in 2000 when a delay-time of 26 days was considered, while the estimated temperatures were higher by 2.5−4.9 °C than the satellite-derived SSTs from early-June to mid-September (Figure 2.4). The sinking rate of particles to the LZ trap determined by the delay time between the satellite-derived SSTs and theTEX_{86} signals according to Müller and Fischer (2001) was approximately 37 m d^{-1} ((960 − 0) m / 26 days). This sinking rate is slightly slower than those for alkenone-associated particles within the Benguela regime at locations to the South (NU-2; 45 m d^{-1} at 2516 m) and North (WU 2−4; 48 m d^{-1} at 1648/1717 m) of the LZ site (Fischer and Karakaş, 2009). Sinking rates of particles tend to increase with depth (Berelson, 2002; Fischer and Karakaş, 2009), and particles containing alkenones have been reported to sink faster than those containing GDGTs (Mollenhauer et al., 2015). Thus, the estimated sinking rate of particles containing GDGTs at LZ seems reasonable within the Benguela system. This calculated sinking rate of GDGTs is much faster than the one in Cape Blanc site (9−17 m d^{-1}; Mollenhauer et al., 2015), where the trap was deployed at deeper water

depth. This could be due to higher productivity at Lüderitz compared to Cape Blanc resulting in generally high particle density, strong grazing and faster sinking (Carr, 2002). Due to a high interannual variability of fluxes, the limited time series at LZ make it difficult to compare among different regimes and periods in the upwelling system like the one off Cape Blanc (Fischer and Karakaş, 2009). A longer observation time of fluxes would be helpful to gain better insights into the sedimentation processes and sinking rate of particles in the Benguela coastal upwelling system off Lüderitz.

The temperature estimations based on TEX_{86}^{H} in particles collected in the LZ traps are different from previous studies that showed subsurface temperature estimations in the eastern Atlantic upwelling regions (Figure 2.4) (Lee et al., 2008; Kim et al., 2012; Lopes dos Santos et al., 2010; Rommerskirchen et al., 2011). Sinking particles collected from the strongest upwelling cell in the Benguela system were used in our study, while previous studies showing subsurface signals based on sediment samples and suspended particulate matter. Moreover, the samples used by Lee et al. (2008) were taken from the southern less productive part of the Benguela system. For this region, the authors concluded that TEX_{86} temperatures represent subsurface temperature both in particles from surface water as well as on the core-top sediments using the calibration from Kim et al. (2008). When TEX_{86} values in the study by Lee et al. (2008) are re-calculated with the TEX_{86}^{H} calibration (Kim et al., 2010) for the areas where mean annual SSTs are higher than 15 °C, the temperature estimates differ by only up to 0.8 °C, which is within the uncertainty range of both calibrations (± 1.7 °C for Kim et al., (2008) and ±2.5 °C for TEX_{86}^{H}), but TEX_{86}^{H} based estimates are still lower than mean annual SST. Therefore, it is unlikely that the difference between our findings and the interpretations made by the authors of the previous study are due to the fact that different sample types were used. The warm biases of TEX_{86}^{H}, we observed at LZ might be a reflection of the potential non-thermal effects in this region. Interestingly, TEX_{86}^{H} temperature estimates both in Lüderitz and off Cape Blanc agreed with SST observations during the warm season and a warm bias occurred only during the cold season (Figure 2.4 and 2.6). Basse et al., (2014) reported TEX_{86} values in suspended particles from various depths in the Cape Blanc region, showing higher TEX_{86} in the OMZs, and they used samples collected during the time of strongest upwelling off Cape Blanc. Based on these results, Mollenhauer et al., (2015) speculated that GDGTs produced by different ammonia oxidizing archaeal community in the OMZ might cause higher TEX_{86} values. This might explain the warmer temperature estimates in sinking particles collected during the cold season when the OMZs might be most pronounced (Figure 2.4 and 2.6). We suggest that a similar mechanism might be active in the Benguela region, where the OMZ expands from the Walvis ridge to off Lüderitz during the peak upwelling period (Chapman and Shannon, 1987; Monteiro et al., 2008).

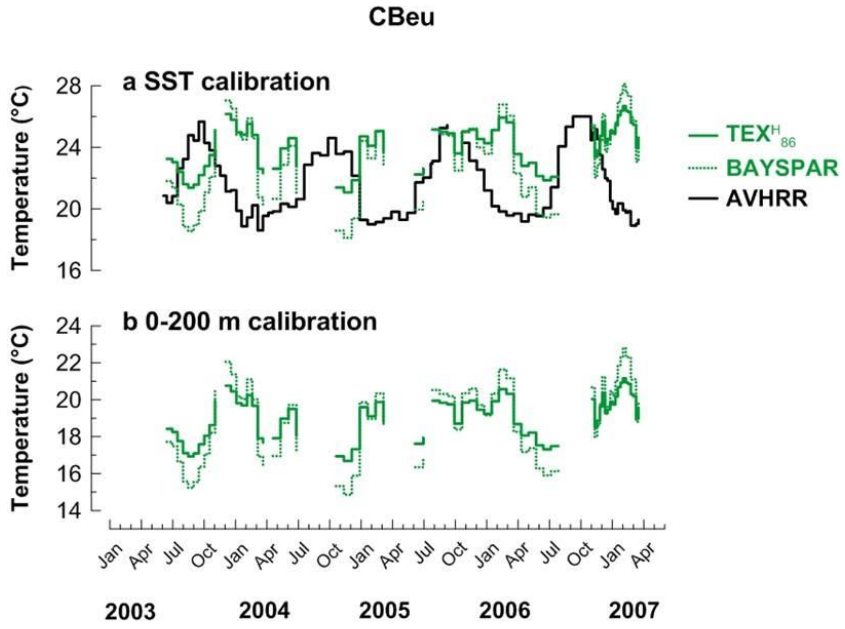

Figure 2.6. Changes in (a) estimated temperatures for SST, and (b) estimated 0-200 m depth-integrated temperatures off Cape Blanc, North West Africa at the water depth of approximately 1,300 m for between June 2003 and March 2007. Modified after Mollenhauer et al., (2015).

The archaeal community was mostly dominated by marine group I Crenarchaeota (now re-named to Thaumarchaeota) and their 16S rRNA gene sequences tightly clustered with Nitrosopumilus maritimus in the Namibian OMZ (Woebken et al., 2007), suggesting that the same archaeal community prevailed throughout the water column. Likewise, Schouten et al., (2012) observed no clear evidence for a substantial contribution on GDGT pools by archaeal communities other than Thaumarchaeota in the Arabian Sea OMZ. Indeed, archaeal communities in the Arabian Sea OMZ were not distinguished from the ones in oxygenated surface waters (Peng et al., 2013). This implies that GDGTs, leading to elevated TEX_{86} values in sinking particles, are more likely produced by an archaeal community adapted to OMZs (Martens-Habbena et al., 2009) rather than by different archaeal communities as suggested by Mollenhauer et al., (2015).

Oxygen-depleted waters are observed between 150 m and 400 m depth on the shelf of Lüderitz (Brüchert et al., 2003; Inthorn et al., 2006a). In the OMZs, a significant amount of oceanic nitrogen is fixed with the contribution of both aerobic- and anaerobic oxidation processes (Kalvelage et al., 2011; Kuypers et al., 2005). Intriguingly, high ammonia oxidation activity, amoA gene abundances as well as GDGTs in oxygen-depleted conditions have been observed in other field studies (Ingalls et al., 2006; Kim et al., 2015; Schouten et al., 2012b; Xie et al., 2014). Higher TEX_{86} values were measured under oxygen depleted and ammonia oxidation rate limited conditions in culture experiments (Hurley et al., 2016; Qin et al., 2015), exhibiting a high affinity of Thaumarchaeota for oxygen (Martens-Habbena et al., 2009; Urakawa et al., 2014). These findings support our interpretation that the warm

biased TEX_{86}^{H} temperatures can be attributed to the contributions of GDGTs synthesized within the OMZ, which differ by an increase in the relative abundance of GDGT-2 and GDGT-3 from the GDGT pools formed in surface waters in the Lüderitz region. Especially in 2000-2001 when the LZ traps were deployed, this region was characterized by advection of less ventilated ocean water onto the shelf, which resulted in intensified OMZs (Monteiro et al., 2008). This might have stimulated the GDGT production in the OMZs. It is, however, unclear how these GDGTs are exported through the water column and which proportions of GDGTs from the OMZs were collected in the sediment traps. It is paramount to study the composition of GDGTs and TEX_{86} not only in sinking particles covering a longer time period but also in sediments, ideally on transects crossing the depth range of the OMZs in order to quantify the influence of GDGTs in the OMZs on TEX_{86} thermometry in the Benguela coastal upwelling. The flux-weighted mean TEX_{86}^{H} temperature of the LZ trap was 18.3 °C, which was warmer than the averaged satellite-derived SSTs in 2000 (16.4 °C) (Table 2.2, Figure 2.4). This is due to the warm-biased TEX_{86}^{H} estimates relative to the satellite-derived SSTs, which we observed in the trap record from June to September 2000. The TEX_{86}^{H} temperature in a core-top sediment from about 1° north of the LZ trap location, was 15.3 °C (WW24080 at 24.002° S, 12.999° E; unpublished data; cf. Mollenhauer et al., 2007). This is relatively colder than the temperatures estimated from the LZ trap and the satellite-derived mean annual SST. However, as the trap records do not cover the entire year, the Flux-weighted mean TEX_{86}^{H} estimation cannot be compared with the TEX_{86}^{H} estimate from the underlying core-top sediment. The BAYSPAR SSTs were very similar to TEX_{86}^{H} estimations, showing a warm bias compared to the satellite-derived SSTs during the cold season in the LZ while it displayed a better match for the cold season at site CBeu (Figure 2.4 and 2.6). Although the BAYSPAR SST had different trends in the LZ and CBeu, it seems to work better than for the GBN3 region (Figure 2.2). For BAYSPAR calibration in the global TEX_{86} the database, there are more data points from the coast near Southwest Africa (off Namibia) and Northwest Africa (off Cape Blanc) than in the eastern Atlantic equatorial region (Tierney and Tingley, 2015). This illustrates that the quality of BAYSPAR SST calculations depends on the reference point density, which can provide representative calibration parameters within the region. Instead, the poor reference point density can lead to unrealistic temperature estimations based on BAYSPAR SST. BAYSPAR SubT demonstrated subsurface temperatures at both sites LZ and CBeu (Figure 2.4 and 2.6). As discussed in section 2.5.2 for the site GBN3 (Figure 2.2), BAYSPAR SubT is likely to be insensitive to the number of calibration points and it seems to work better.

Our findings from the Benguela coastal upwelling system and the Cape Blanc region suggest that a different physicochemical response of thaumarchaeotal communities in oxygen depleted waters can influence the TEX_{86} thermometry, resulting in a seasonal warm bias in TEX_{86}^{H} temperature estimates

during the upwelling season. This underlines that water column oxygenation as an environmental factor needs to be considered when the TEX_{86}^{H} calibration is applied in areas with OMZs.

2.6 Summary and conclusions

We studied the seasonal variability of GDGT fluxes and TEX_{86}^{H} thermometry in sinking particles in three eastern Atlantic upwelling regimes. TEX_{86}^{H} temperatures reflect temperatures at different depths and different absolute temperature ranges depending on the sites and the calibrations.

In the equatorial upwelling area (GBN), GDGTs appear to be exported mostly by particles containing opal. Due to the high particle sinking rate (>42 m d^{-1}) and relatively long sampling period, we did not observe a delay in TEX_{86}^{H}-based temperature estimates relative to satellite-derived SST data. TEX_{86}^{H}-based temperature estimates derived from particles collected at 853 m and 3,921 m water depth correspond to temperatures at ca. 50 m water depth where the nutricline exists. The depth profile of nutrient concentrations can thus play an important role in determining the favorable habitat depth of thaumarchaeotal communities and, as the result, the depth at which temperature is recorded by GDGTs sinking to the sediment. In the coastal upwelling area off Lüderitz (LZ, Benguela system), TEX_{86}^{H}-based temperature estimates resemble the satellite-derived SSTs with a delay of 26 days during the warmer season while it shows warmer estimations than satellite-derived SSTs during the colder season. Similar trends were recorded in the coastal upwelling off NW Africa (Cape Blanc, site CBeu), where higher TEX_{86} values were found in oxygen depleted water masses. As OMZs are pronounced in the Benguela coastal upwelling area, GDGTs synthesized by Archaea adapted to the OMZs are inferred to drive changes of TEX_{86} values in sinking particles.

Our findings in the high productivity upwelling systems of the eastern Atlantic prompt a re-thinking of paleotemperature estimations using the TEX_{86} proxy. In paleoclimate studies based on the TEX_{86} index, it should, therefore, be carefully considered that environmental conditions other than temperature (particularly oxygen depletion) and variable habitat depths under different ecological- and oceanographic settings may influence the sedimentary signals. This study furthermore suggests limitations of one single calibration for SST based on TEX_{86} for all settings which might have temporally and spatially varying nutrient and oxygen distributions in the water column.

Acknowledgments

We acknowledge the captains, crews, student assistants and scientists who participated in the cruises for collecting samples used in this study. We thank Marco Klann who was responsible for the sediment trap sample processing and bulk measurements and Götz Ruhland for preparation and deployments/recoveries of the mooring arrays. The trap samples and core-top sediments were supplied by the MARUM Centre of Marine Environmental Research at the University of Bremen.

This project is funded through DFG-Research Center / Cluster of Excellent “The Ocean in the Earth System” and supported by GLOMAR− Bremen International Graduate School for Marine Sciences, University of Bremen. The Royal Netherlands Institute for Sea Research is thanked for providing unpublished TEX_{86} value of WWW24080 core-top (24.002° S, 12.999° E) and CTD profile data in the Lüderitz Bay collected during the 64PE174 MARE-3 cruise. We also thank two anonymous reviewers for their constructive comments on an earlier version of this manuscript.

Data availability

The data presented here are available on the PANGAEA database (https://doi.pangaea.de/10.1594/PANGAEA.886701).

CHAPTER 3

Seasonality of archaeal lipid flux and GDGT-based thermometry in sinking particles of high latitude oceans: Fram Strait (79° N) and Antarctic Polar Front (50° S)

Submitted to Biogeosciences (Park et al., 2019)

3 Manuscript II

Seasonality of archaeal lipid flux and GDGT-based thermometry in sinking particles of high latitude oceans: Fram Strait (79° N) and Antarctic Polar Front (50° S)

Eunmi Park[1,2,3], Jens Hefter[1], Gerhard Fischer[2,3], Morten H. Iversen[1,2], Simon Ramondenc[1,2], Eva-Maria Nöthig[1], Gesine Mollenhauer[1,2,3]

[1]Alfred Wegener Institute, Helmholtz Center for Polar and Marine Research, D-27570 Bremerhaven, Germany
2MARUM Centre for Marine Environmental Sciences, University of Bremen, D-28334 Bremen, Germany
3Department of Geosciences, University of Bremen, D-28334 Bremen, Germany

Abstract

The relative abundance of individual archaeal membrane lipids, namely of glycerol dialkyl glycerol tetraethers (GDGTs) with the different number of cyclopentane rings, varies with temperature, which enabled their use as paleotemperature proxy. The first GDGT-based index in marine sediments called TEX_{86} is believed to reflect mean annual sea surface temperature (ma SST). The TEX_{86}^{L} is an alternative temperature proxy for ´low´ temperature regions (<15 °C), where the original TEX_{86} proxy suffers from scattering in a linear calibration with SSTs. However, TEX_{86}^{L}-derived temperatures still display anomalous estimates in polar regions. In order to elucidate the potential cause of the disagreement between TEX_{86}^{L} estimate and SST, we analyzed GDGT fluxes and TEX_{86}^{L}-derived temperatures in sinking particles collected with time-series sediment traps in high northern and southern latitude regions. At 1296 m depth in the eastern Fram Strait (79° N), a combination of various transporting mechanisms for GDGTs might result in seasonally different sinking velocities for particles carrying these lipids, resulting in strong variability in the TEX_{86}^{L} signal. The similarity of flux weighted TEX_{86}^{L} temperatures from sinking particles and surface sediments implies an export of GDGTs without alteration during transport in the Fram Strait. The estimated temperatures correspond to temperatures in water depths of 30−80 m, where nitrification might occur, indicating the favorable depth habitat of Thaumarchaeota. In the Antarctic Polar Front of the Atlantic sector (50° S), TEX_{86}^{L}-derived temperatures displayed warm and cold biases compared to satellite-derived SSTs at 614 m depth, and its flux-weighted mean signal differs from the deep signal at 3196 m. TEX_{86}^{L}-derived temperatures at 3196 m depth and the surface sediment showed up to 7 °C warmer

temperatures relative to satellite-derived SST. Such a warm anomaly might be caused by GDGT contributions from Euryarchaeota, which are known to dominate archaeal communities in the circumpolar deep water of the Antarctic Polar Front. The other reason might be that a linear calibration is not appropriate for this frontal region. Of the newly suggested SST proxies based on hydroxylated GDGTs (OH-GDGTs), only those with OH-GDGT-0 and Crenarchaeol or the ring index (RI) of OH-GDGTs yield realistic temperature estimates in our study regions, suggesting that OH-GDGTs could be applied as a potential temperature proxy in high latitude oceans.

3.1 Introduction

The knowledge that Thaumarchaeota, one phylum of Archaea, regulate the composition of their membrane lipids according to the surrounding water temperatures enabled the development of the paleothermometer TEX_{86} (Kim et al., 2010; Schouten et al., 2002). TEX_{86} is calculated based on the relative abundance of GDGTs containing 0−3 cyclopentane (GDGT-0−3) or 4 cyclopentane and one cyclohexane (Crenarchaeol) rings (Figure 3.1).

The ubiquity of Thaumarchaeota, even in the polar oceans where the widely applied $U^{k'}_{37}$ proxy for sea surface temperature (SST) reconstructions is often problematic, supports the use of TEX_{86} in high latitude regions (Bendle and Rosell-Melé, 2004; Ho et al., 2014). Nonetheless, the SST dependence of TEX_{86} in warm regions is stronger than in colder regions where SSTs are below 5 °C (Kim et al., 2010). Thus, a logarithmic calibration, excluding the Crenarchaeol region-isomer, of TEX^{L}_{86} was suggested for regions where ma SSTs are below 15 °C (see Eq. 2; Kim et al., 2010). The authors speculated that the lack of correlation between the Crenarchaeol regio-isomer and SST at low temperatures might be caused by genetically different GDGT producers.

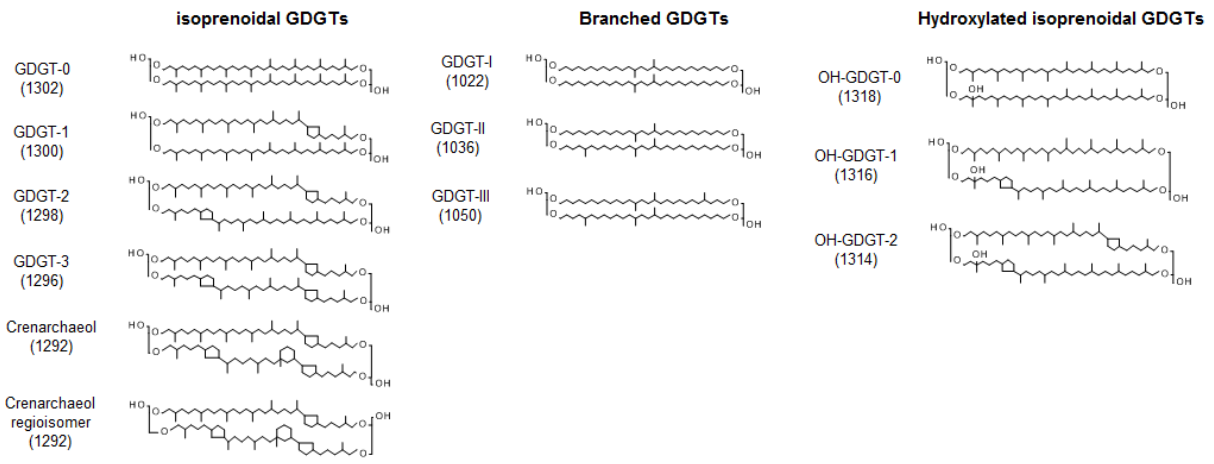

Figure 3.1 Chemical structures and molecular ion m/z values of the isoprenoid glycerol dialkyl glycerol tetraethers (GDGTs), branched GDGTs, and hydroxylated GDGTs.

It has been questioned whether temperature is the only factor influencing the lipid composition (i.e., TEX_{86}) particularly in the regions where strong cold or warm biases were observed between TEX_{86} reconstructed and measured ma SSTs. The biases of TEX_{86} calibrations have been attributed to enhanced production of GDGTs during seasons with favorable growth conditions for Thaumarchaeota (Pitcher et al., 2011; Wuchter et al., 2006b), a contribution of GDGTs from deep-dwelling communities (Kim et al., 2015; Lee et al., 2008; Taylor et al., 2013), terrestrial input (Weijers et al., 2006), influences of different archaeal communities (Lincoln et al., 2014; Turich et al., 2007), and/or other environmental factors (Huguet et al., 2006; Mollenhauer et al., 2015; Park et al., 2018; Turich et al., 2007).

To circumvent these problems, especially in cold regions, a handful of studies have developed dedicated calibrations on regional scales (Meyer et al., 2016; Seki et al., 2014; Shevenell et al., 2011). For the temperature estimate in the Eocene Arctic Ocean, a modified version of TEX_{86}, the index termed TEX'_{86} was proposed (Sluijs et al., 2006). It excludes GDGT-3 to eliminated contribution from terrestrial input, leading to significantly higher temperature estimates compared to the original TEX_{86} calibration. The TEX'_{86} values of 104 marine surface sediments showed a good linear correlation with ma SSTs ($R^2 = 0.93$) (Sluijs et al., 2006). Following the addition of 7 additional TEX_{86} values from surface sediments collected at the continental margin of the western Antarctic Peninsula, Shevenell et al., (2011) modified the Kim et al., (2008)'s TEX_{86} calibration for this region ($TEX_{86} = 0.0125 \times Temp + 0.3038$, $R^2 = 0.82$) and estimated water temperatures for the Holocene.

Ho et al., (2014) evaluated TEX_{86} and the different calibrations in an extended set of surface sediments from the polar regions of both hemispheres and found that the global TEX_{86} calibration is suitable for subpolar regions (e.g., the Pacific sector of the Southern Ocean and the Subarctic Front in the North Pacific). Additionally, the TEX_{86}^{L} yields reasonable temperature estimates if regional calibrations are developed for high latitude regions. Using a regression of water temperatures (at 20 m depth in August) versus TEX_{86}^{L} values, Seki et al., (2014) obtained plausible paleotemperature estimates for the Sea of Okhotsk and the subpolar North Pacific region. Meyer et al., (2016) confirmed later that this regional TEX_{86}^{L} calibration can also be applied to the subarctic northwest Pacific and the Western Bering Sea.

More recently, hydroxylated GDGTs (OH-GDGTs), which contain an additional hydroxyl group in one of the biphytanyl moieties of GDGT-0, -1, and -2, have been recognized in marine sediments (Liu et al., 2012; Figure 3.1). Based on the finding that the abundance of OH-GDGTs relative to the total isoprenoid GDGTs increase towards cold regions (Huguet et al., 2013), OH-GDGT based SST calibrations have been proposed for high latitude oceans (Fietz et al., 2013; Huguet et al., 2013).

Beside the biological, phylogenetic, and statistical studies of the temperature proxy, sinking particles collected in specific regions can provide new perspectives on the distribution of GDGTs and

TEX_{86} based temperature reconstructions. The study using time-series sediment traps can give insights on the seasonal variability of lipid flux and temperature signals, and allows comparing the lipid signal to those in underlying sediments. Only one TEX_{86} study using a time-series sediment trap in high latitude regions has been conducted near Iceland (Rodrigo-Gámiz et al., 2015), regardless of the interest in polar regions, where temperature reconstructions with lipid proxies are troublesome. Here, we examine the seasonal GDGT production and TEX_{86}^{L}-derived temperatures in comparison to measured SSTs in order to better understand the drivers influencing TEX_{86}^{L} values in sinking particles collected in two high latitude oceans (eastern Fram Strait, 79° N and Antarctic Polar Front of the Atlantic sector, 50° S). The temperatures derived from OH-GDGT proxies were also calculated to evaluate the applicability of these novel proxies for high latitude regions.

3.2 Study area

3.2.1 Fram Strait

The Fram Strait is located west of Spitsbergen, where the heat exchange occurs between the Arctic Ocean and the North Atlantic (Figure 3.2). Relatively warm and nutrient-rich Atlantic water (AW) is transported by the West Spitsbergen Current (WSC) to the central Arctic Ocean, while colder and less saline Arctic water is transported along the East Greenland Current (EGC) to the Nordic Seas (Figure 3.2). Part of the WSC is separated from the northward flow and recirculated within the region (Manley, 1995; Soltwedel et al., 2016). Eddies, mixing, and recirculating Atlantic water contribute to the hydrographic complexity observed in the Fram Strait (Walczowski, 2013). The volume transport of the WSC and AW within the WSC displays strong seasonality with maxima in March and minima in July for the WSC, and maxima in late autumn and winter and minima in June for the AW (Beszczynska-Möller et al., 2012b). The occurrence of sea ice and its variability has an effect on the particle fluxes as well as on benthic ecosystems (Bauerfeind et al., 2009; Hebbeln and Wefer, 1991; Soltwedel et al., 2016). Sinking particles in the Fram Strait, including organic and terrigenous material, are well known to originate not only from the photic zone in the upper water column, but also from the Svalbard archipelago and Siberian shelf, from where they are transported by sea ice (Hebbeln, 2000; Lalande et al., 2016). Phytoplankton blooms enhance the vertical flux of biogenic components (organic carbon, carbonate, and opal) in spring-summer, but the downward flux of particles is likely affected by the environmental conditions (e.g. hydrographic changes, sea ice extent, and atmospheric low-pressure) on an annual time scale (Wassmann et al., 2006). Based on oceanographic measurements from mooring arrays at multiple depths across the Fram Strait (from 7° W to 9° E, 78.3° N), Beszczynska-Möller et al., (2012) found two warm anomalies in the Atlantic water through the Fram Strait in 1999−2000 and 2005−2007. During the second warm anomaly, community structures of phytoplankton and zooplankton were affected by the decreased sea ice in this

region (Lalande et al., 2013; Nöthig et al., 2015) and had a profound influence on biogenic sediment fluxes.

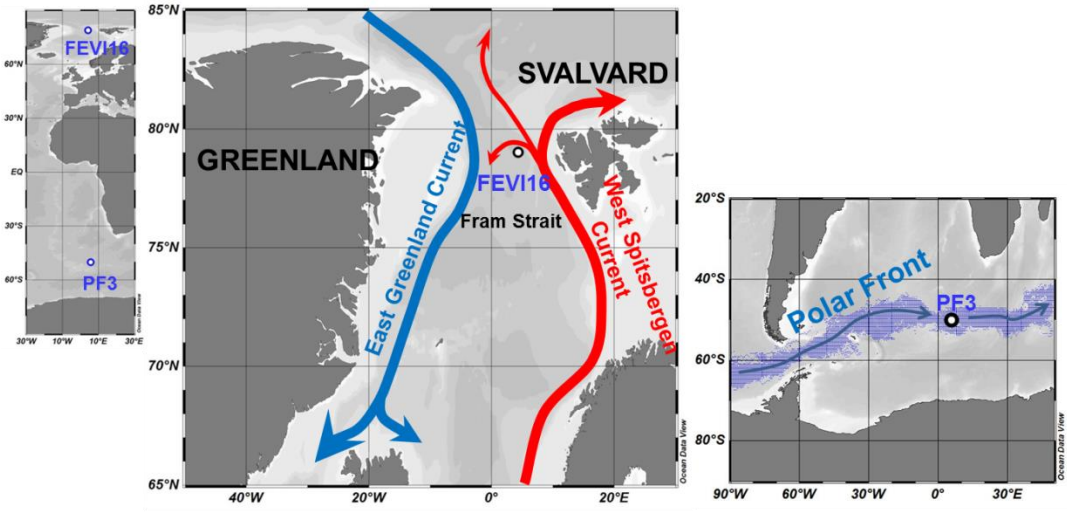

Figure 3.2 Map of sediment trap locations in the high northern latitude (FEVI16) and in the Antarctic Polar Front (PF3). In Fram Strait, the northward red arrow represents the West Spitsbergen Current bringing warm and saline Atlantic Waters to the Arctic and the southward blue arrow displays the East Greenland Current transporting cold and fresh water to the Norwegian Sea. Around the Antarctic, the digitized blue shadow exhibits the location of the Antarctic Polar Front for the year 2002−2014 at weekly resolution (Freeman and Lovenduski, 2016). The blue arrow indicates the clockwise Antarctic Circumpolar Current (ACC). Ocean Data View is used for mapping (Schlitzer, 2017; available at https://odv.awi.de).

3.2.2 Antarctic Polar Front

The Antarctic Polar Front (APF) region is one of the major frontal zones within the westerly wind driven Antarctic Circumpolar Current (ACC) (Figure 3.2). Spatial and temporal variability of the APF is strongly affected by seafloor topography. The APF has an average width of 43 km (1987−1993), which moves southward during the austral summer and reaches its northernmost position during the austral winter (Moore et al., 1999). The ACC is well known for its meandering jet flow and eddy formation (Moore et al., 1999; Orsi et al., 1995), which likely stimulate phytoplankton blooms and primary production in this region by supplying growths limiting nutrients, and/or bringing deeper dwelling phytoplankton into the photic zone (Abbott et al., 2001; Moore and Abbott, 2002, 2000). Thus, the hydrographic structure is an important factor controlling the distribution of phytoplankton and small zooplankton in this region (Read et al., 2002). The highest chlorophyll-a levels of up to 3.5 mg m^{-3} were recorded in the APF during the early austral summer 1990−1991, and it co-occurred with elevated silicate levels as well as water column stability (Laubscher et al., 1993). The current speed close to the PF3 trap was recorded to be up to 8 cm s^{-1} (Walter et al., 2001). Read et al., (2002) reported the vertical profile of currents measured between the surface and 400 m depth in the polar frontal regions in December 1995. The currents recorded at the surface and subsurface of the Polar

Front were much stronger (30−50 cm s^{-1}) than the ones measured at 700 m depth (1−8 cm s^{-1}) by Walter et al., (2001).

3.3 Material and Methods

3.3.1 Sediment trap

A time-series sediment trap system was moored to collect sinking particles at the eastern Fram Strait (FEVI16) between July 2007 and July 2008 at 1296 m water depth (Table 3.1, Figure 3.2). Two traps (PF3) were deployed in the permanent ice free-area of the APF in the Atlantic sector at 614 m and 3196 m water depth from November 1989 to December 1990 (Table 3.1, Figure 3.2). The cone-shaped funnel of the Kiel trap systems had a 0.5 m^2 collection area, and the collection periods of each individual sample cup were programmed depending on the expected time of ice cover and/or the seasonality of the production. The sampling cups were filled with filtered sea water enriched in sodium chloride (NaCl) to achieve a salinity of 40 psu, and they were poisoned with mercury chloride ($HgCl_2$; 0.14% final solution) for sample preservation. For FEVI16 samples, zooplankton 'large swimmers' were removed using forceps before splitting each sampling cup into smaller sub-samples (Lalande et al., 2016). For PF3 samples, large swimmers were removed using forceps and a sieve (mesh size: 1 mm mesh) in the laboratory (Fischer et al., 2002). Afterward, the samples were split for different purposes. A current meter (RCM 9/11) was attached to both trap moorings, and the data sets are available on PANGAEA (https://doi.org/10.1594/PANGAEA.845610; FEVI16) and in Walter et al., (2001; PF3)

3.3.2 Mass flux

Split FEVI16 samples were filtered onto GF/F filters (pre-combusted at 500 °C for 4 h) for organic carbon, organic nitrogen (PON), and carbonate, and onto cellulose acetate filters for biogenic opal quantification. Organic carbon (POC) and organic nitrogen (PON) were measured with a CHN elemental analyzer after 0.1 N HCl treatment. Carbonate was calculated by subtracting the weight from total mass after 0.1 N HCl treatments and re-corrected according to the aragonite contents. The detailed methods used for biogenic silica can be found in Lalande et al., (2016). Split PF3 samples were freeze-dried for further processing. Decalcified samples (6 N HCl) were analysed for POC using a CHN elemental analyzer. Total nitrogen (TN) was also determined. Carbonate was calculated by subtracting POC from total carbon (TC), which was directly measured without decalcification (carbonate = 8.33 × (TC - POC)). The methodology for the quantification of biogenic silica is described in Fischer et al., (2002).

Table 3.1 Information on FEVI16 and PF3 trap.

Name	Region	Location		Water depth	Trap depth	Deployment period		Sampling interval	Cruise reports
						Start	End		
		Latitude (° N)	Longitude (° E)	(m)	(m)	(dd.mm.yyyy)		(d)	
FEVI16	Eastern Fram Strait	79.02	4.35	2589	1296	23.07.2007	30.06.2008	10-31*	ARK-XXII/1c (Klages and Participants, 2007) ARK-XXIII/2 (Kattner and Participants, 2009)
PF3	Antarctic Polar Front	-50.13	5.83	3785	614 3196	10.11.1989	23.12.1990	21, 42*	ANT-VIII/3 (Gersonde and Participants, 1990) ANT-IX/2 (Fahrbach and Cruise Participants, 1992)

* The exact sampling interval of each sample at FEVI16 and PF3 can be found on PANGAEA (https://doi.pangaea.de/10.1594/PANGAEA.897268).

3.3.3 GDGT analyses

For GDGT analysis, total lipids were extracted with a solvent mixture (9:1 v/v dichloromethane (DCM): methanol (MeOH)) using an ultrasonic bath for 10 min and a centrifuge for 5 min, after which the supernatant was decanted. This process was repeated three times and the supernatants were combined. Before the extraction process, a known amount of C_{46}-GDGT (internal standard) was added to each sample for GDGT quantification.

Following saponification of total lipids with 1 mL of 0.1 M potassium hydroxide (KOH) in a mixture of MeOH: purified water 9:1 (v/v) at 80 °C for two hours, neutral lipids (NLs) were recovered with 1 mL hexane (3 times). NLs were separated into F1 (apolar), F2 (ketone), and F3 (polar) polarity fractions eluted in 2 mL hexane, 4 mL DCM: hexane (2:1 v/v), and 4 mL DCM: MeOH (1:1 v/v), respectively, using deactivated silica-gel chromatography (mesh size: 70-μm).

The F3 polar fraction containing GDGTs was re-dissolved in 500 μL hexane: isopropanol 99:1 (v/v) and filtered through a polytetrafluoroethylene (PTFE) filter (pore-size: 0.45 μm) into a glass insert of a 2 mL vial according to Hopmans et al., (2000). The filtered polar fraction was diluted with hexane: isopropanol 99:1 (v/v) to a concentration of approximately 2 mg ml^{-1} before the instrumental analysis.

GDGTs were analyzed using high-performance liquid chromatography/atmospheric pressure chemical ionization-mass spectrometry (HPLC/APCI-MS) according to Chen et al., (2014). Molecular ions *m/z* 1302, 1300, 1298, 1296, 1292 for isoprenoid GDGTs and 1050, 1036 and 1022 for branched GDGTs were determined and quantified in relation to the molecular ion *m/z* 744 of the C_{46}-GDGT. The late eluting peaks of OH-GDGT-0, -1, and -2 with *m/z* 1318, 1316, and 1314 were also determined in the *m/z* 1300, 1298, and 1296 scan, as described by Fietz et al., (2013).

3.3.4 GDGT flux and indices

TEX_{86}^{L} values were calculated according to Kim et al., (2010).

$$TEX_{86}^{L} = Log_{10} ([GDGT\text{-}2] / ([GDGT\text{-}1] + [GDGT\text{-}2] + [GDGT\text{-}3])) \quad (1)$$

where the numbers represent the number of cyclopentane moieties in the isoprenoid GDGTs.

TEX_{86}^{L} values were converted into temperatures using the following equation (Kim et al., 2010):

$$SST\ (°C) = 67.5 \times TEX_{86}^{L} + 46.9\ (R^2 = 0.86,\ n = 396) \quad (2)$$

GDGT flux represents the sum of fluxes of individual GDGTs, which are used for calculating TEX_{86}^{L}.

$$GDGT\ flux = [GDGT\text{-}1] + [GDGT\text{-}2] + [GDGT\text{-}3] \quad (3)$$

OH-GDGT based indices and estimated temperatures were calculated using the following equations (eq.4 by Fietz et al., 2013; eq. 5 and 6 by Lü et al., 2015):

$$\text{OH-GDGT-0/Cren} = 0.25 - 0.025 \times \text{SST (°C)} \ (R^2 = 0.58, n = 13) \quad (4)$$

$$\text{RI-OH}' = ([\text{OH-GDGT-1}] + 2\times [\text{OH-GDGT-2}]) / ([\text{OH-GDGT-0}] + [\text{OH-GDGT-1}] + [\text{OH-GDGT-2}]) \quad (5)$$

$$\text{RI-OH}' = 0.0382 \times \text{SST (°C)} + 0.1 \ (R^2 = 0.75, n = 107) \quad (6)$$

BIT, an index of relative contributions of terrestrial versus marine input, was calculated according to Hopmans et al., (2004).

$$\text{BIT} = [\text{I} + \text{II} + \text{III}] / [\text{I} + \text{II} + \text{III} + \text{Cren}] \quad (7)$$

The Roman numerals I, II and III refer to the branched GDGTs with 4, 5, and 6 methyl moieties, and Cren represents Crenarchaeol containing 4 cyclopentane moieties and 1 cyclohexane ring (Figure 3.1). A terrestrial effect on TEX_{86} can be significant when the BIT value is >0.3 (Weijers et al., 2006).

MI, the methane index indicating the relative contribution of GDGTs derived from methanotrophic archaea to those from planktonic Thaumarchaeota was calculated as follows (Zhang et al., 2011):

$$\text{MI} = ([\text{GDGT-1}] + [\text{GDGT-2}] + [\text{GDGT-3}]) / ([\text{GDGT-1}] + [\text{GDGT-2}] + [\text{GDGT-3}] + [\text{Cren}] + [\text{Cren}']) \quad (8)$$

Cren´ represents the regio-isomer of Crenarchaeol. Contributions from methanotrophic Archaea are considered to be significant when MI >3.

%GDGT-0, an indicator of a methanogenic source of GDGTs with a %GDGT value >67%, was calculated as follows (Inglis et al., 2015):

$$\%\text{GDGT-0} = ([\text{GDGT-0}] / ([\text{GDGT-0}] + [\text{Cren}])) \times 100 \quad (9)$$

RI, the ring index, is a tool for identifying a potential non-thermal influence on GDGT distributions. A sample´s ring index is defined as follows (Zhang et al., 2016):

$$\text{RI}_{\text{sample}} = 0\times[\text{GDGT-0}] + 1\times[\text{GDGT-1}] + 2\times[\text{GDGT-2}] + 3\times[\text{GDGT-3}] + 4\times[\text{Cren}] + 4\times[\text{Cren}'] \quad (10)$$

$|\Delta\text{RI}|$ indicates the residual of a sample´s RI ($\text{RI}_{\text{sample}}$) from a calculated RI ($\text{RI}_{\text{calculated}}$) based on the global TEX_{86}–RI regression. $\text{RI}_{\text{calculated}}$ and $|\Delta\text{RI}|$ are defined as follows:

$$\text{RI}_{\text{calculated}} = -0.77(\pm0.38)\times\text{TEX}_{86} + 3.32(\pm0.34)\times(\text{TEX}_{86})^2 + 1.59(\pm0.10) \ (R^2 = 0.87, n = 531) \quad (11)$$

$$|\Delta\text{RI}| = \text{RI}_{\text{calculated}} - \text{RI}_{\text{sample}} \quad (12)$$

Potential non-thermal influences on TEX_{86} can be recognized when $|\Delta\text{RI}|$ is >0.3 (Zhang et al., 2016).

3.3.5 Environmental parameters

TEX_{86}^{L}-derived temperatures were compared to satellite-derived SSTs obtained by Advanced Very High Resolution Radiometer (AVHRR), which has a spatial grid resolution of 0.25° and temporal resolution of 1 day (Reynolds et al., 2007). The satellite-derived SSTs were averaged over the collection period of each sample cup. The depth profiles of mean annual water temperature and nitrate

concentration were obtained from the World Ocean Atlas 2013 (WOA13) representing averaged values for the years 1955−2012 (Garcia et al., 2013; Locarnini et al., 2013).

3.4 Results

3.4.1 Eastern Fram Strait: FEVI16

3.4.1.1 Mass and GDGT fluxes

The mass flux data of the FEVI16 trap have been published previously by Lalande et al., (2016). In summary, the mass flux (opal + POC + PON + lithogenic fluxes) measured at 1296 m water depth varied in between 18.5−652.9 mg m^{-2} d^{-1}, with minima in the winter season (November 2007−February 2008; Figure 3.3a). Lithogenic flux is presented separately in Figure 3.3a due to its significantly higher contribution to total mass flux. The composition of sinking particles changed between seasons. Lithogenic material flux showed sudden pulses in spring (March and April−May 2008). POC was predominant in mid-July 2007. Carbonate flux was elevated in March, early-May and mid-June 2008. Opal was dominant in early-September 2007 and mid-May to June 2008.

GDGT fluxes varied between 7.2−85.9 ng m^{-2} d^{-1} (Figure 3.3b). Peaks of GDGT flux occurred in August−September 2007 and March, May−June 2008, while minima were observed in the winter season (November 2007−February 2008). The GDGT flux was strongly correlated with opal flux (R^2 = 0.82, $p<0.0001$) when two GDGT maxima in late-September 2007 and March 2008 were excluded, and with carbonate flux (R^2 = 0.86, $p<0.0001$) except for the last two months in May-June 2008 (Figure 3.3a, b).

3.4.1.2 TEX_{86}^{L} thermometry

TEX_{86}^{L} values varied between -0.70−-0.64 and their TEX_{86}^{L}-derived temperatures (Kim et al (2010) calibration) ranged between 0.6−3.7 °C (Figure 3.3b, f). The flux-weighted mean TEX_{86}^{L} temperature during the trap deployment period was 2.8 °C. Two surface sediment TEX_{86}^{L}values (-0.66 at PS68-251/2 (79.1° N, 4.6° E) and -0.65 at PS68-271/2 (79.3° N, 4.3° E)) are available near the FEVI16 trap (Ho et al., 2014). Most index values of BIT, MI, %GDGT-0, and $|\Delta RI|$ for samples from FEVI16 were below the critical values of each index (>0.3 for BIT and MI, >67% for %GDGT-0, >0.3 for $|\Delta RI|$). One sample with a $|\Delta RI|$ value >0.3 was found, indicating a non-thermal effect on TEX_{86} (Table A 3.1).

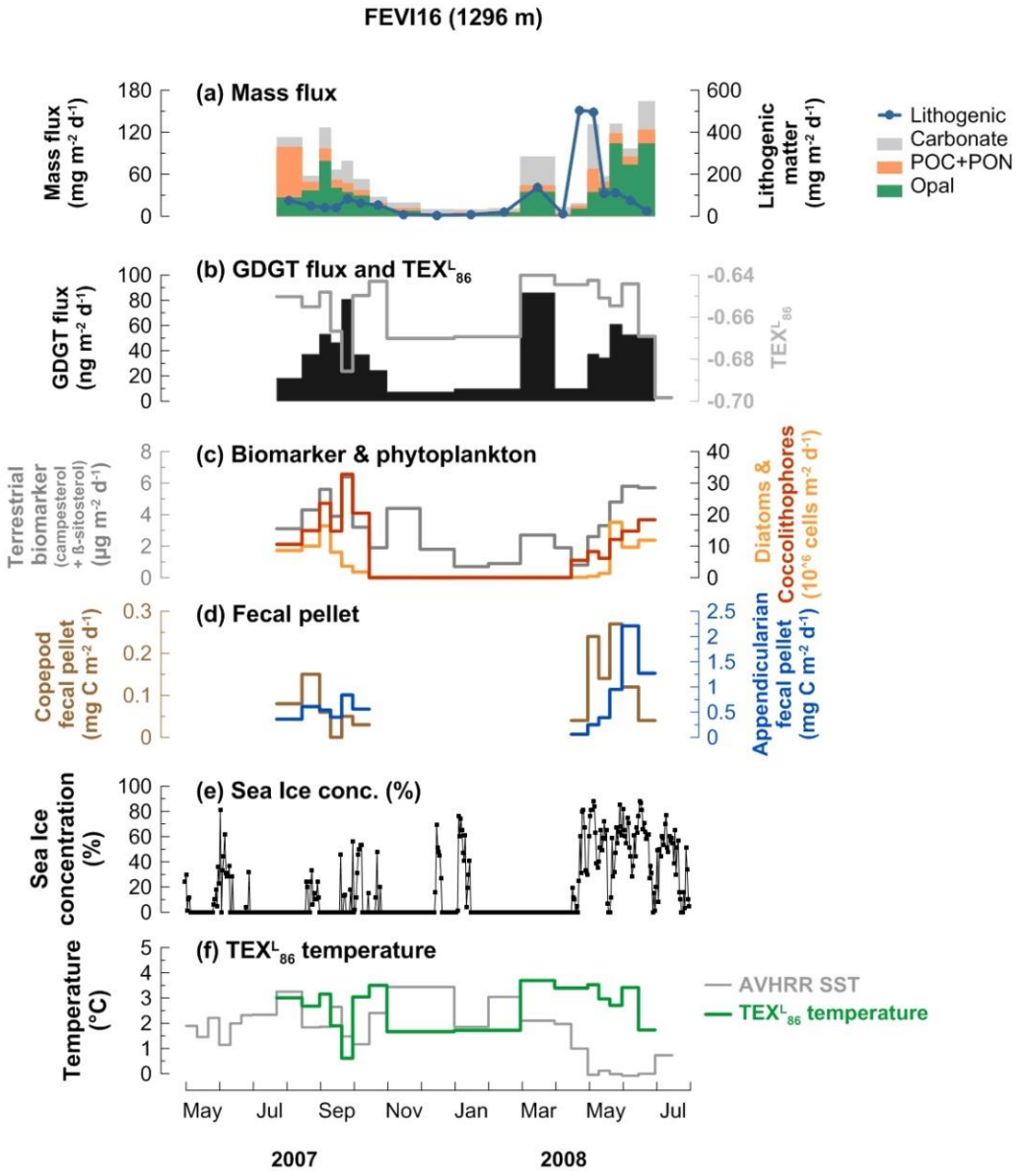

Figure 3.3 Changes in mass flux (a), GDGT flux (b), terrestrial biomarker flux and diatom and coccolithophore abundances (c), fecal pellet flux (d), sea ice concentration (e), TEX_{86}^{L}-derived temperatures and satellite-derived SSTs obtained at 79.125° N, 4.375° E near the trap site (f) at 1296 m water depth in the eastern Fram Strait site, FEVI16 during the deployment period (July 2007−July 2008). (a), (c), (d), and (e) are previously reported by Lalande et al., (2016).

3.4.1.3 Fractional abundance of OH-GDGTs

All OH-GDGTs were clearly present in FEVI16 samples. OH-GDGT-0 was predominant in the OH-GDGT pool, accounting for 87−95% (Figure 3.4a). The proportion of OH-GDGTs in the sum of iso- and OH-GDGTs ranged between 7 and 11% during the trap deployment period (Figure 3.4a). Estimated temperatures calculated using the calibrations as described in Eq. (4) and (6) (Fietz et al., 2013 and Lü et al., 2015) ranged between -0.3−2.5 °C and between -0.9−1.4 °C, respectively. The last two data points for the trap time-series were unusually low when using Eq. (4) (Figure 3.4b).

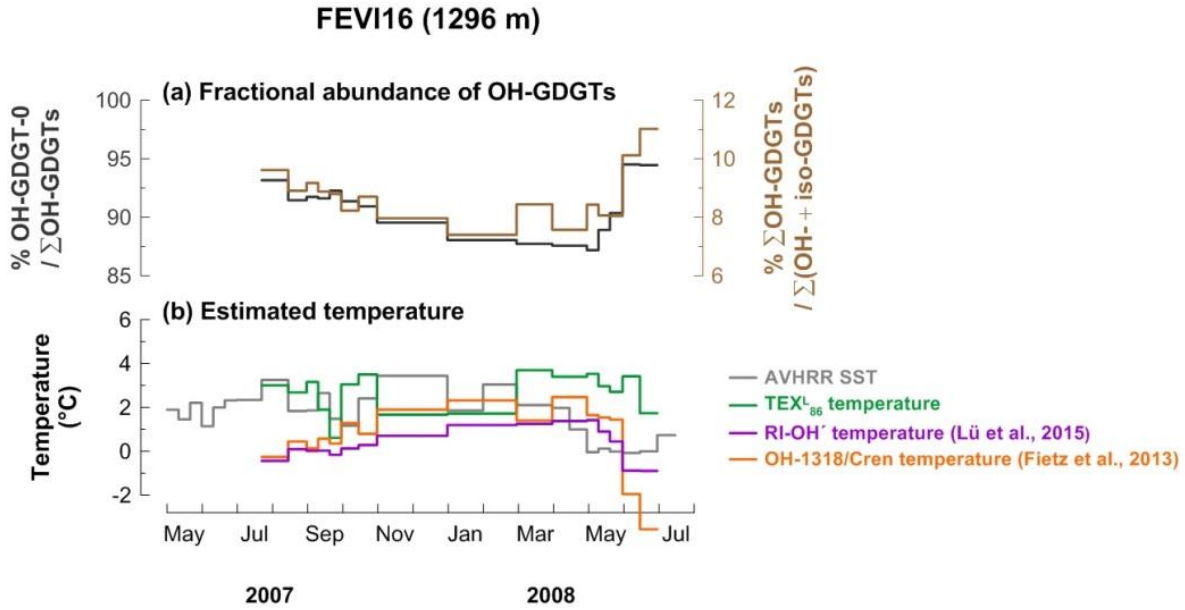

Figure 3.4 Changes in fractional abundance of OH-GDGTs (a) and estimated temperatures based on OH-related calibrations (b) at site FEVI16. The purple and orange lines indicate the calculated temperatures using the calibrations by Fietz et al., (2013) (Eq. 4) and Lü et al., (2015) (Eq. 6), respectively. The green line indicates the TEX^{L}_{86}-derived temperatures.

3.4.2 Southern Atlantic Polar Front: PF3

3.4.2.1 Mass and GDGT fluxes

The mass flux data of the PF3 trap have been published previously by Fischer et al., (2002). The mass flux at the shallow trap ranged between 19.7−592.1 mg m^{-2} d^{-1} with a distinct seasonal variability (Figure 3.5a). Flux maxima occurred in November 1989 to early-March 1990 and mid-October to November 1990, while it stayed relatively low from mid-March to mid-October 1990. At the deep trap, the mass flux varied between 0−516.6 mg m^{-2} d^{-1} (Figure 3.5d). The mass flux peaked in mid-December 1989−January and March 1990 but stayed low for the remaining sampling period except for mid-May 1990.

There was no clear correlation between organic material and GDGT fluxes at neither depth. The fluxes in GDGTs ranged from 10.5 to 73.9 ng m^{-2} d^{-1} at 614 m and from 0.5 to 153.9 ng m^{-2} d^{-1} at 3196 m depth (Figure 3.5b, e). GDGT fluxes were mostly enhanced during the low mass flux season at the shallow trap (Figure 3.5b). GDGT flux maxima occurred in November and December 1989, late-May and early-November 1990 at the deep trap (Figure 3.5e). GDGT analysis was not possible between late-July and October 1990 in the deep trap, since very little material was collected during this time period.

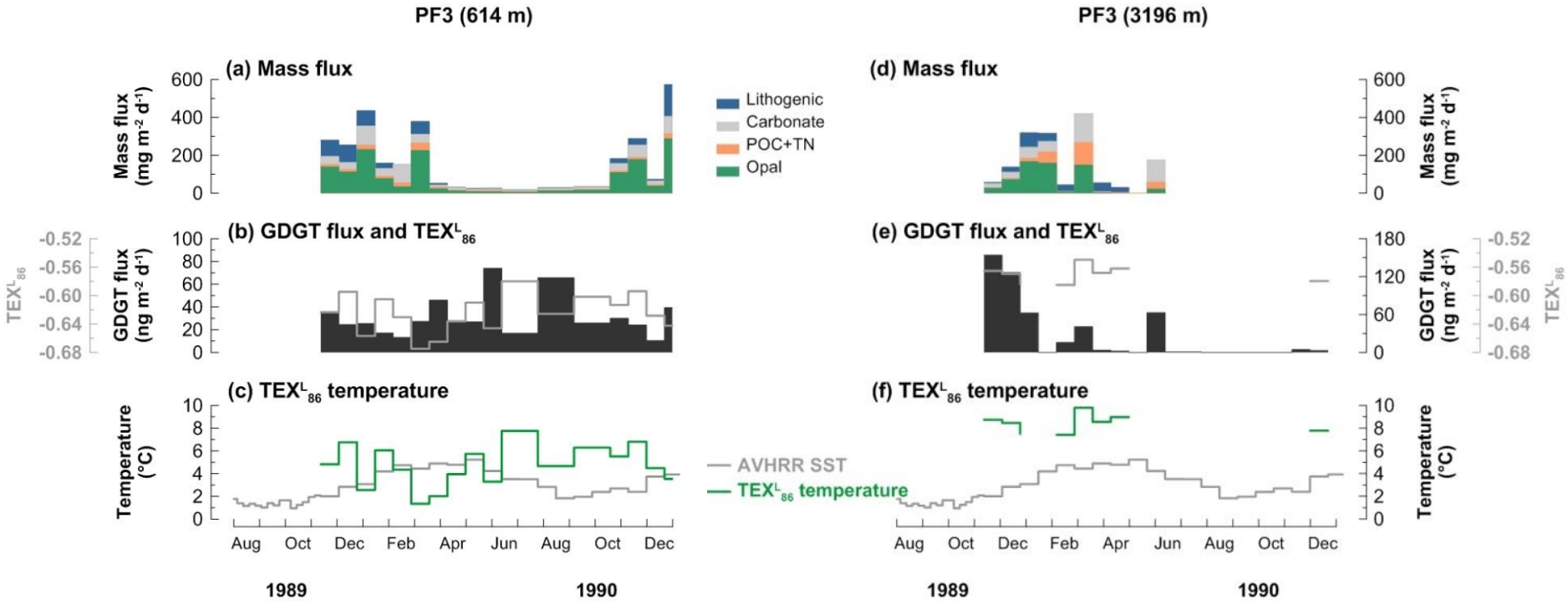

Figure 3.5 Changes in mass flux (a, d), GDGT flux (b, e) and TEX^{L}_{86}-derived temperatures and satellite-derived SSTs obtained at 50.125° S, 5.875° E near the trap site (c, f) at the 614 m (left panels) and 3196 m (right panels) water depth in the Antarctic Polar Front site (PF3) during the deployment period (November 1989−December 1990).

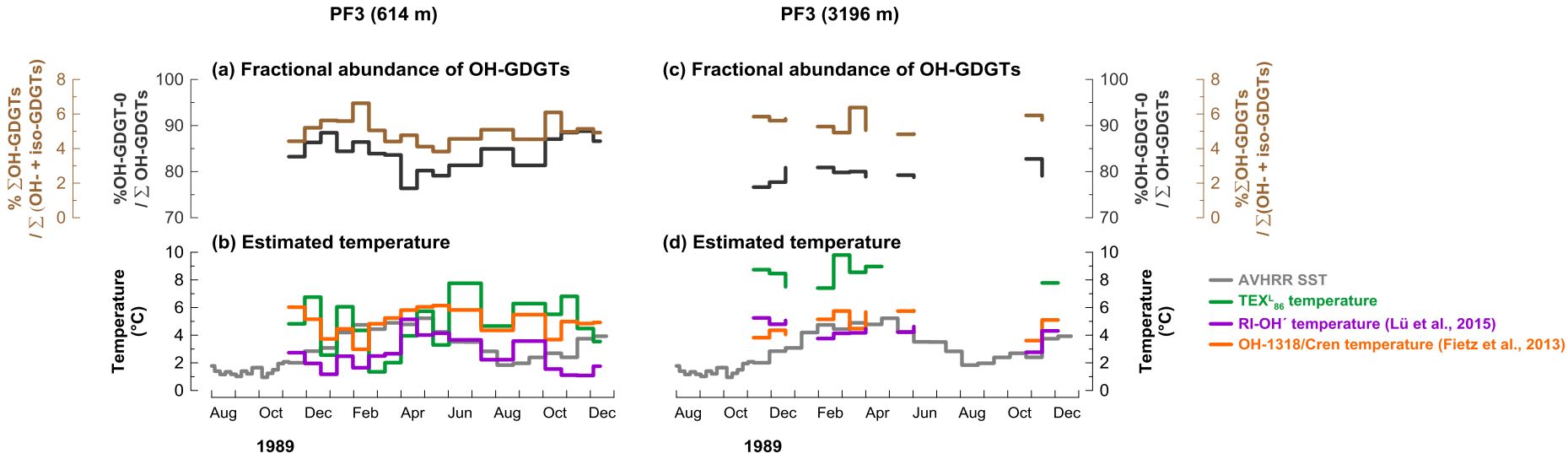

Figure 3.6 Changes in fractional abundance of OH-GDGTs (a, c) and estimated temperatures based on OH-related calibrations (b, d) at site PF3. The purple and orange lines indicate the calculated temperatures using the calibrations by Fietz et al., (2013) (eq. 4) and Lü et al., (2015) (eq. 6), respectively. The green lines indicate the TEX^{L}_{86}-derived temperatures.

3.4.2.2 TEX_{86}^{L} thermometry

TEX_{86}^{L} values varied between -0.58−-0.67, and -0.55−-0.59 at the shallow and deep trap, respectively (Figure 3.5b, e). The TEX_{86}^{L}-derived temperatures ranged between 1.3−7.8 °C for the shallow trap and 7.4−9.8 °C for the deep trap (Figure 3.5c, f). The flux-weighted mean TEX_{86}^{L} temperatures were 4.6 °C and 8.5 °C at the shallow and deep traps, respectively. In some samples, GDGT-3 was below the detection limit. In these cases, TEX_{86}^{L} values and estimated temperatures were not included on the figures, but GDGT flux was calculated. A surface sediment TEX_{86}^{L} value of -0.56 (CHN-115-4-34; 51.00° S, 5.33° E) in the vicinity of the PF3 trap site (50.13° S, 5.83° E) can be found in the TEX_{86} global calibration dataset (Kim et al., 2010), and its TEX_{86}^{L}-derived temperature estimate is 9.1 °C. Most samples did not exceed the index values indicating non-thermal impacts on TEX_{86} (see Section 3.3.4). Two samples from the deep trap between early November and late December 1989, however, showed MI values between 0.3 and 0.5 (Table A 3.1).

3.4.2.3 Fractional abundance of OH-GDGTs

All OH-GDGTs were clearly present in samples from both depths. OH-GDGT-0 was predominant in the OH-GDGT pool (76−8 % for the shallow trap, 77−8 % for the deep trap; Figure 3.6a, c). The proportion of OH-GDGTs in the sum of iso- and OH-GDGTs ranged from 4−7% and 5−6% at the shallow and deep trap, respectively, (Figure 3.6a, c). Estimated temperatures calculated according to Eq. (4) and (6) ranged between 3.0−6.1 °C and 1.1−5.1 °C in the shallow trap (Figure 3.6b). With the same calibrations, estimated temperatures varied between 3.6−5.8 °C and 2.8−5.2 °C in the deep trap (Figure 3.6d).

3.5 Discussion

3.5.1 Eastern Fram Strait (79° N)

3.5.1.1 GDGT flux and particle export

Organic matt Organic matter (including GDGTs), formed in the upper ocean, is exported to the bathypelagic mainly as zooplankton fecal pellets or marine snow aggregates (Fischer and Karakaş, 2009; Wuchter et al., 2006b). The velocities of the sinking aggregates vary in relation to their composition (Fischer and Karakaş, 2009; Iversen and Ploug, 2010) and physical characteristics. For instance, aggregates formed from coccolithophores are ballasted by carbonate and may sink faster than opal ballasted diatom aggregates (Iversen and Ploug, 2010). Still, fecal pellets formed from either coccolithophores or diatoms sink faster than fecal pellets formed from non-ballasted flagellates (Ploug et al., 2008a, 2008b). GDGTs have been suggested to be preferentially incorporated in opal-dominated particles (Mollenhauer et al., 2015). This is in agreement with observed TEX_{86}-derived temperatures

in sediment-trap samples off Cape Blanc being delayed relative to the SST signal, and this time delay was longer than for $U^{K'}_{37}$-derived temperatures (Mollenhauer et al., 2015).

GDGT fluxes co-varied with fluxes of biogenic- and non-biogenic components in the eastern Fram Strait (Fig. 3). GDGT fluxes were enhanced in summer 2007 and spring 2008 with two clear maxima in late September 2007 and March 2008 (Figure 3.3b). Without those two distinct GDGT flux maxima, GDGT flux showed a good correlation with opal (R^2 = 0.82, $p<0.0001$) throughout the deployment period. GDGT fluxes co-varied also with carbonate from the beginning of the deployment until April 2008 (R^2 = 0.8, $p<0.0001$) (Figure 3.3a, b). This agrees with the concept that GDGTs are transported by particles mainly containing opal and carbonate as previously shown in sediment trap studies (Chen et al., 2016; Huguet et al., 2007; Mollenhauer et al., 2015; Park et al., 2018; Yamamoto et al., 2012). This observation suggests that GDGTs are exported together with diatoms (opal) and coccolithophores (carbonate). Supporting this, diatom and coccolithophore fluxes both, previously reported by Lalande et al., (2016), showed good correlations with GDGT fluxes (R^2 = 0.64, $p<0.001$ for diatoms and R^2 = 0.68, $p<0.0001$ for coccolithophores) when excluding two GDGT flux maxima in the correlations with opal fluxes. The flux of terrestrial biomarkers (campesterol+ß-sitosterol), previously analyzed by Lalande et al., (2016), also showed a positive correlation with GDGT flux (R^2 = 0.64, $p<0.001$). The sterols (campesterol and ß-sitosterol), used frequently to assess the plant-derived organic matter input to aquatic systems (Moreau et al., 2002), reflect the input of terrestrial matter transported by sea-ice in the Fram Strait (Lalande et al., 2016). We thus assume that terrestrial material is aggregated into particles which carry GDGTs. However, the lithogenic flux, also representing terrestrial input, displayed a different trend with maxima only in mid-April−mid-May 2008, when the sea ice concentration abruptly increased (Figure 3.3e). The lithogenic material seems to be mainly supplied by downslope export from the nearby Svalbard archipelago (Lalande et al., 2016), with a significant input when the sea ice is present (Figure 3.3e).

GDGTs might also be exported with fecal pellets after grazing of Archaea by zooplankton. Indeed, GDGTs have been found in decapod guts and intestines, and their abundance ratios appear to be unaltered during gut passage (Huguet et al., 2006). The fecal pellet carbon (FPC) flux from appendicularians contributed more to the total carbon flux than copepod FPC flux. Both appendicularian and copepod FPC fluxes were higher during spring 2008 than during summer 2007 (Figure 3.3d; Lalande et al., (2016)). The correlation of GDGT fluxes with appendicularian FPC fluxes (R^2 = 0.67, $p<0.05$ in mid-July to mid-October 2007) implies grazing of Archaea by the appendicularians. Appendicularians are well known to ingest micro-size particles like Archaea (<1 µm) efficiently through a fine mucus filter (Conley and Sutherland, 2017).

Overall, it is reasonable to assume that seasonal changes in the relative proportion of materials that GDGTs can be aggregated with, may result in variable export velocities of particles carrying GDGTs

to deeper waters in the eastern Fram Strait.er (including GDGTs), formed in the upper ocean, is exported to the bathypelagic mainly as zooplankton fecal pellets or marine snow aggregates (Fischer and Karakaş, 2009; Wuchter et al., 2006b). The velocities of the sinking aggregates vary in relation to their composition (Fischer and Karakaş, 2009; Iversen and Ploug, 2010) and physical characteristics. For instance, aggregates formed from coccolithophores are ballasted by carbonate and may sink faster than opal ballasted diatom aggregates (Iversen and Ploug, 2010). Still, fecal pellets formed from either coccolithophores or diatoms sink faster than fecal pellets formed from non-ballasted flagellates (Ploug et al., 2008a, 2008b). GDGTs have been suggested to be preferentially incorporated in opal-dominated particles (Mollenhauer et al., 2015). This is in agreement with observed TEX_{86}-derived temperatures in sediment-trap samples off Cape Blanc being delayed relative to the SST signal, and this time delay was longer than for $U^{k'}_{37}$-derived temperatures (Mollenhauer et al., 2015).

GDGT fluxes co-varied with fluxes of biogenic- and non-biogenic components in the eastern Fram Strait (Fig. 3). GDGT fluxes were enhanced in summer 2007 and spring 2008 with two clear maxima in late September 2007 and March 2008 (Figure 3.3b). Without those two distinct GDGT flux maxima, GDGT flux showed a good correlation with opal (R^2 = 0.82, $p<0.0001$) throughout the deployment period. GDGT fluxes co-varied also with carbonate from the beginning of the deployment until April 2008 (R^2 = 0.8, $p<0.0001$) (Figure 3.3a, b). This agrees with the concept that GDGTs are transported by particles mainly containing opal and carbonate as previously shown in sediment trap studies (Chen et al., 2016; Huguet et al., 2007; Mollenhauer et al., 2015; Park et al., 2018; Yamamoto et al., 2012). This observation suggests that GDGTs are exported together with diatoms (opal) and coccolithophores (carbonate). Supporting this, diatom and coccolithophore fluxes both, previously reported by Lalande et al., (2016), showed good correlations with GDGT fluxes (R^2 = 0.64, $p<0.001$ for diatoms and R^2 = 0.68, $p<0.0001$ for coccolithophores) when excluding two GDGT flux maxima in the correlations with opal fluxes. The flux of terrestrial biomarkers (campesterol+ß-sitosterol), previously analyzed by Lalande et al., (2016), also showed a positive correlation with GDGT flux (R^2 = 0.64, $p<0.001$). The sterols (campesterol and ß-sitosterol), used frequently to assess the plant-derived organic matter input to aquatic systems (Moreau et al., 2002), reflect the input of terrestrial matter transported by sea-ice in the Fram Strait (Lalande et al., 2016). We thus assume that terrestrial material is aggregated into particles which carry GDGTs. However, the lithogenic flux, also representing terrestrial input, displayed a different trend with maxima only in mid-April−mid-May 2008, when the sea ice concentration abruptly increased (Figure 3.3e). The lithogenic material seems to be mainly supplied by downslope export from the nearby Svalbard archipelago (Lalande et al., 2016), with a significant input when the sea ice is present (Figure 3.3e).

GDGTs might also be exported with fecal pellets after grazing of Archaea by zooplankton. Indeed, GDGTs have been found in decapod guts and intestines, and their abundance ratios appear to be unaltered during gut passage (Huguet et al., 2006). The fecal pellet carbon (FPC) flux from

appendicularians contributed more to the total carbon flux than copepod FPC flux. Both appendicularian and copepod FPC fluxes were higher during spring 2008 than during summer 2007 (Figure 3.3d; Lalande et al., (2016)). The correlation of GDGT fluxes with appendicularian FPC fluxes (R^2 = 0.67, $p<0.05$ in mid-July to mid-October 2007) implies grazing of Archaea by the appendicularians. Appendicularians are well known to ingest micro-size particles like Archaea (<1 μm) efficiently through a fine mucus filter (Conley and Sutherland, 2017).

Overall, it is reasonable to assume that seasonal changes in the relative proportion of materials that GDGTs can be aggregated with, may result in variable export velocities of particles carrying GDGTs to deeper waters in the eastern Fram Strait.

3.5.1.2 Variability of TEX_{86}^{L}-derived temperature

TEX_{86}^{L} temperatures varied (-0.2−3.7 °C) within a similar range as the satellite-derived SSTs (-0.1−3.4 °C) during the trap deployment period in the eastern Fram Strait. Although it did not display a clear seasonality, the TEX_{86}^{L} signal is most likely to reflect the surface water environments without non-thermal effects influencing the TEX_{86}^{L} (Figure 3.3). First of all, the index values (e.g. BIT, MI, %GDGT-0, RI), which could indicate potential non-thermal factors influencing the distribution of GDGTs, suggest that TEX_{86}^{L} temperatures should reflect the upper water column temperature (Table A 3.1). The BIT index defined by Hopmans et al., (2004) as a tracer for the terrestrial organic matter input was very low (<0.02), showing that negligible amounts of soil-derived GDGTs are entrained in sinking particles. MI (Zhang et al., 2011) and %GDGT-0 (Inglis et al., 2015) have been suggested as indicators for the impact of methanotrophic Archaea even though it was questioned if the latter index can be applied in marine settings (Inglis et al., 2015). Both index values were consistently lower than the respective critical values of 0.3 for MI and 67% for %GDGT-0. $|\Delta RI|$ was suggested by Zhang et al., (2016) as an indicator for the integrated non-thermal factors on TEX_{86}. Most $|\Delta RI|$ values were lower than a value of 0.3, and only three samples collected in late September 2007 and June 2008 satisfied the criteria of being influenced by non-thermal factors. Secondly, although significant portions of particles transported to the mid-depth and deep water in the eastern Fram Strait originated off Svalbard and the Barents Sea (Lalande et al., 2016), it is known that GDGTs are most likely to reflect the local conditions rather than being affected by lateral transport (J. H. Kim et al., 2009; Mollenhauer et al., 2008). Therefore, we conclude that GDGTs are mainly transported from upper waters and non-regional sources of particles do not play a significant role in the TEX_{86}^{L} estimate in sinking particles of the eastern Fram Strait.

TEX_{86}^{L} temperatures varied strongly between mid-July−October 2007, with the minimum estimated temperature (0.6 °C) when the GDGT and terrestrial biomarker fluxes were highest (Figure 3.3b, c, f). This is the most productive period in the Fram Strait and also the period with the highest

export fluxes (e.g. Lalande et al., 2016). The material collected by deep ocean sediment traps is a mixture of many types of aggregates with different composition and settling velocities. Therefore, fluctuating TEX_{86}^{L} temperatures might be due to an average of signals from previous (before mid-July, i.e. slowly sinking particles) and current seasons (mid-July to October, i.e. fast settling aggregates), which were exported via different aggregation and sinking mechanisms with different horizontal displacements during particle descent. Due to the collection of aggregates sinking with different velocities, one sample cup in a sediment trap may collect GDGTs of different ages.

During the low flux period between November 2007−February 2008, TEX_{86}^{L} temperatures were constantly lower than the satellite-derived SSTs (Figure 3.3a, b, f). These signals might be derived from GDGTs synthesized in mid-August to October, which was a late-bloom period dominated by protists that do not produce biominerals, such as *Phaeocystis* sp., dinoflagellates, and nanoflagellates (Nöthig et al., 2015). Aggregates formed without biominerals have low sinking velocities (Iversen and Ploug, 2010; Ploug et al., 2008a, 2008b), which may explain why the satellite-derived SSTs from mid-August to October 2007 were similar to the TEX_{86}^{L}-derived temperatures in sinking particles collected during November 2007 and February 2008. In spring 2008, TEX_{86}^{L} temperatures stayed relatively warm until mid-April and suddenly dropped in May and June (Figure 3.3f). The relatively warm TEX_{86}^{L} temperatures in particles collected in March and April 2008 probably reflect the signal transported by GDGTs produced in November−December 2007. Like previous seasons, the lack of transporting materials for GDGTs delayed the TEX_{86}^{L} signal. The sudden drop of TEX_{86}^{L}-derived temperatures in mid-May to June 2008 was matched with the season of the enhanced flux of biogenic materials, GDGTs, phytoplankton, zooplankton fecal pellets and terrestrial biomarkers at the trap when the sea ice concentration was enhanced (Figure 3.3). Eddies around the ice-edge create upwelling and downwelling, which breaks the stratified surface water and supplies nutrients to the upper water column, fostering phytoplankton blooms (Lalande et al., 2013). The sea ice-edge bloom probably enhanced the GDGT production followed by zooplankton grazing. Additionally, the terrestrial materials as ballast were more available, which were derived from sea-ice as it melted during spring 2008. This process caused the fast export of TEX_{86}^{L} signal from the surface waters in mid-May to June 2008. Overall, the particles containing GDGTs captured at 1296 m depth in the eastern Fram Strait were likely delivered by a combination of packaging mechanisms involving biological and non-biological transport materials with different delay times over the season. Moreover, most GDGTs are exported vertically from the upper waters and reflect a regional TEX_{86}^{L} signal in the eastern Fram Strait, while significant particle supply from the south via lateral advection has been reported previously (Lalande et al., 2016). This result agrees with the finding that diatom and fecal pellet fluxes can be traced as the export of local production regardless of the lateral particle supply.

The average export velocity of particles containing GDGTs can be calculated by dividing the travel distance of particles (i.e., the depth of the sediment trap) by the temporal offset between TEX_{86}^{L}-derived temperature and the corresponding satellite-derived SST, greatly simplifying the complexity of sinking mechanisms and range of settling velocities throughout the season (Mollenhauer et al., 2015). When the TEX_{86}^{L}-derived temperatures are shifted by 82 days, we found the best fit to the satellite-derived SSTs (Figure 3.7b). Therefore, we see that GDGTs synthesized in the eastern Fram Strait likely travel to the trap (1296 m) approximately within 82 days. This translates into an average minimum export velocity of GDGT-containing particles of approximately 15 m d^{-1} when assuming export from 30-80 m water depth (see below Section 3.5.1.3). We have assumed that the export velocity includes the time of GDGT synthesis and transport time to the trap. The estimated sinking velocity of 15 m d^{-1} is within range (9−17 m d^{-1}) estimated at a similar water depth (~1300 m) in the filamentous upwelling zone off northwest Africa (Mollenhauer et al., 2015) and only slightly lower than settling velocities found previously for aggregates from the Fram Strait (Wekerle et al., 2018). Based on the seasonal succession of peaks in appendicularian fecal pellets in the same mooring system, their sinking velocity was estimated to be 5- to 11- fold higher (15−35 days to 2400 m depth; Lalande et al., 2016) compared to GDGTs. This is a realistic scenario because of the fast sinking velocity of a fecal pellet, being rather big and dense, and generally faster average export velocities to deeper ocean depths (Fischer and Karakaş, 2009; Iversen et al., 2017). Moreover, the average export velocity of GDGTs includes the time it takes to be incorporated into aggregates. A more rapid export of GDGTs to depth resulting in smaller temporal offsets of TEX_{86}^{L}-derived temperature to water temperature changes occurred in mid-May−June 2008 when the FPC flux of appendicularians was enhanced (Figure 3.3d). It has to be noted that the export velocity we calculated here may represent an averaged velocity of all the aggregates collected in the trap, as the export velocity of GDGTs can vary depending on the type of sinking materials GDGTs are incorporated into.

The flux-weighted mean TEX_{86}^{L} temperature over the mooring period was 2.8 °C. In the vicinity of the site FEVI16 (79.03° N, 4.35° E), two TEX_{86}^{L} values from surface sediments are available in the dataset published by Ho et al., (2014). The estimated temperatures based on TEX_{86}^{L} are 2.8 °C and 2.3 °C in PS68-251/2 (79.30° N, 4.30° E) and PS68-271/2 (79.10° N, 4.60° E), respectively. Considering the error of the TEX_{86}^{L} calibration (Kim et al., 2010), TEX_{86}^{L} estimates are almost identical between sinking particles and surface sediments. This suggests that GDGTs synthesized in the upper waters are propagated through the water column into the sediment without significant alteration even though the sinking process of GDGTs in the eastern Fram Strait seems quite complicated as discussed above. Iversen et al., (2010) and Jackson and Checkley Jr. (2011) also suggested that most biological activities resulting in aggregate alteration and degradation occur around the base of the photic zone. Our observations agree with previous studies, as TEX_{86} displays

consistent values at multiple depths and/or in the underlying surface sediments in various environmental regimes such as in the Arabian sea (Wuchter et al., 2006b), in the north western Pacific (Yamamoto et al., 2012), off Cape Blanc (Mollenhauer et al., 2015), near Iceland (Rodrigo-Gámiz et al., 2015), off southern Java (Chen et al., 2016), and in the northern Gulf of Mexico (Richey and Tierney, 2016).

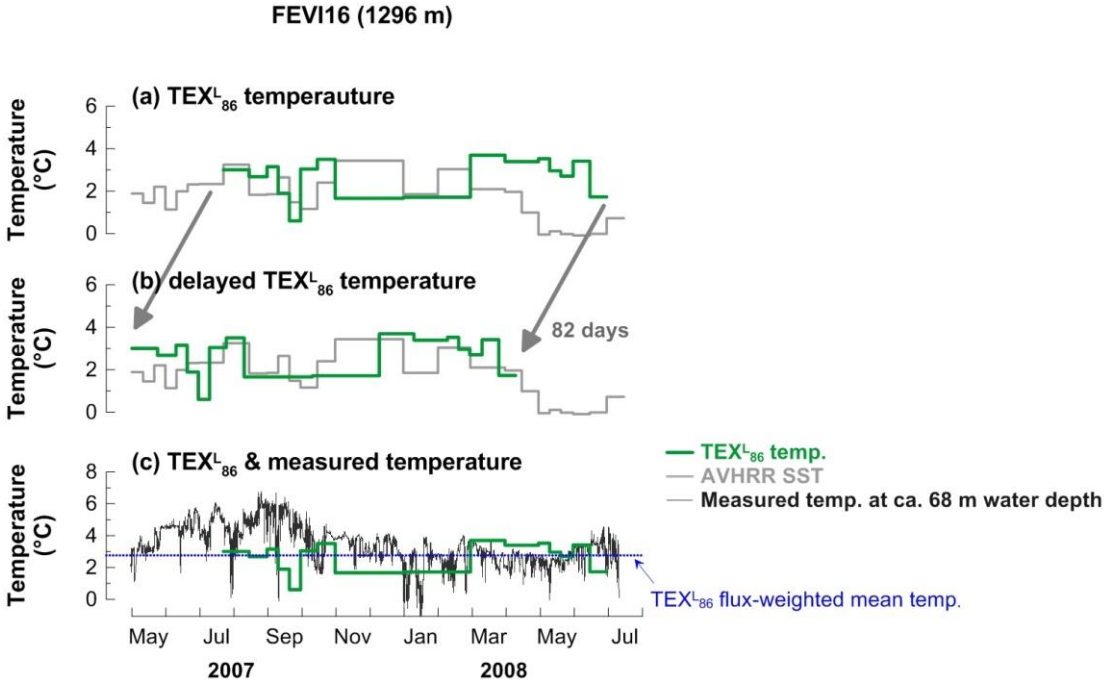

Figure 3.7 Changes in TEX^{L}_{86}-derived temperatures and satellite-derived SSTs (a), time-delayed TEX^{L}_{86} temperatures (b), sensor measured temperatures at approximately 68 m water depth at site FEVI16.

3.5.1.3 Potential depth of TEX^{L}_{86} signal origin

To determine the water depth where the TEX^{L}_{86} signal originated, the flux-weighted mean TEX^{L}_{86} temperature (2.8 °C) was compared to the depth profile of nutrient concentrations (NH_4^+, NO_2^-, and NO_3^-) measured in late June to early July 2010, 2011, and 2013, and water temperature extracted from WOA13 (79.125° N, 4.375° E) in the eastern Fram Strait (Figure 3.8). Unfortunately, ammonia data are unavailable in 2007 and 2008. The mean estimated temperature (2.8 °C) in sinking particles corresponds to the surface water in July−September or of 30−80 m subsurface waters in April−June (Fig. 8). Major production of GDGTs in both seasons is a possible scenario because GDGT flux peaked in both seasons (Figure 3.3b). However, the latter period (April−June) is the more plausible season dominantly supplying GDGTs to the sediment if we consider the delay time of the GDGT signal (approximately 82 days, see Section 3.5.1.2), which illustrates the initial time of GDGT production (Figure 3.3b). Furthermore, Thaumarchaeota, the primary synthesizers of GDGTs in the

ocean, are aerobic ammonia oxidizers (Könneke et al., 2005) and maximum GDGT concentrations have been found near the NO_2^- maximum, where maximum rates of ammonia oxidation and nitrification occur (Beman et al., 2008; Hurley et al., 2016). The depths of consumption of ammonia and production of nitrite as well as nitrate accumulation as a result of the nitrification process in the subsurface can be deduced from the nutrient profile (Figure 3.8).

Assuming that maximum thaumarchaeotal abundance occurs at the depth of highest substrate availability, we, therefore, infer that Thaumarchaeota mainly record the subsurface water temperature (30−80 m) during the warm season when the spring bloom may occur (April−June) in the eastern Fram Strait. Similar observations were made in the Sea of Okhotsk and the north-west Pacific (Seki et al., 2014) and in the western Bering Sea (Meyer et al., 2016), where the TEX_{86}^L-derived temperature is attributable to the regional season and water depth of GDGT production. The temperatures measured by a temperature sensor attached to the mooring array at approximately 68 m depth (Beszczynska-Möller et al., 2012a), which is approximately in the middle of the depth interval (30−80 m) corresponded to the TEX_{86}^L temperature (Figure 3.8), support our interpretation. The flux-weighted mean TEX_{86}^L temperature is well within the range of measured temperatures at this depth and it reflects well the temperatures in March−June as deduced from the nutrient depth profile (Figure 3.7c).

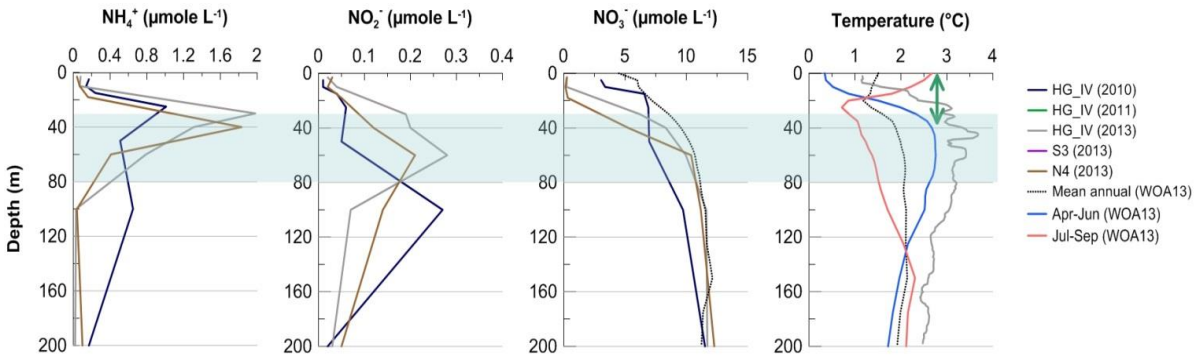

Figure 3.8 Depth profiles of nutrient concentration (NH_4^+, NO_2^-, NO_3^-), and temperature in the Fram Strait. The navy, green, and gray lines represent the central station of the Long-Term Ecological Research (LTER) observatory HAUSGARTEN (HG-IV), close to FEVI16 trap location. The purple and brown lines represent the southern and northern stations of HG-IV. Black dotted lines for NO_3^- and temperature, and blue and orange lines for temperature represent the datasets extracted from WOA13. Only two seasonal profiles (April to June and July to September) from WOA13 are available at the same location (79.125° N, 4.375° E) near the site FEVI16. Measured nutrient concentrations are reported on PANGAEA (Bauerfeind et al., 2014).

3.5.2 Antarctic Polar Front (50° S)

3.5.2.1 GDGT flux

At the shallow trap (614 m water depth) at site PF3, there was no clear correlation between fluxes of organic matter and GDGTs, which displayed their respective maxima in different seasons (Figure

3.5a, b). Peaks of mass flux occurred in November 1989−early-March 1990 and mid-October−December 1990, while GDGT fluxes were highest in mid-May−June and late July−August 1990 (late austral autumn and winter) (Figure 3.5a, b). Similar observations were made in the North Sea, where the abundance of Thaumarchaeota (previously known as marine group I Crenarchaeota) and GDGT concentrations were high in winter time, supported by the seasonality of Thaumarchaeotal 16S rRNA and amoA gene abundances in that region (Herfort et al., 2007; Pitcher et al., 2011; Wuchter et al., 2006a). An austral "winter bloom" of planktonic Archaea was also found near the Antarctic Peninsula (Church et al., 2003; Alison E Murray et al., 1999; Tolar et al., 2016). Austral winter blooms of planktonic Archaea can be explained by higher ammonia availability in winter, while the chemoautotrophic Archaea are outcompeted by photoautotrophic phytoplankton in spring and summer when the light is not limiting (Könneke et al., 2005; Pitcher et al., 2011). Laubscher et al., (1993) found that ammonia was highly depleted at the chlorophyll-a maximum across the Antarctic Polar Front in early austral summer, which might create less favorable conditions for ammonia-oxidizing planktonic Archaea. Additionally, Thaumarchaeota are known to be sensitive to photoinhibition (Horak et al., 2017). Therefore, the austral winter maxima in GDGT flux at the shallow trap of PF3 might be a consequence of the higher production of planktonic Archaea in surface waters of the APF during the time when ammonia is more available and photoautotrophs cannot compete due to light limitation.

At the deep trap (3196 m water depth) of PF3, GDGT flux peaked in November 1989 while mass flux was most pronounced in March 1990 (Figure 3.5d, e). Due to the lack of sinking particles captured in the deep trap in the period June to November 1990, it is unclear if a potential "winter bloom" of GDGTs was also exported to deeper waters. The trapping efficiency of PF3 was found to be below 50% at the deep trap using ^{230}Th as flux proxy (Walter et al., 2001). The negligible mass flux could thus be caused by low trapping efficiency. However, Fischer et al., (2002) observed a similar flux pattern in the following years at the same location of site PF3 including periods of almost no flux in July−December at a location further to the south in the marginal winter sea-ice zone. Thus, it is assumed that a low trapping efficiency or a failure of the trap system did not account for the lack of particle samples at the deep trap of PF3.

3.5.2.2 Variability of TEX_{86}^{L}-derived temperature

TEX_{86}^{L}-derived temperatures at the shallow trap did not display a clear seasonal variability. Only 1/3 of the data points were similar to the SSTs, while the remaining samples showed warm or cold biased temperatures relative to the satellite-derived SSTs during the sampling period (Figure 3.5c). All samples in the deep trap displayed warmer TEX_{86}^{L} temperatures by up to 7 °C relative to the satellite-derived SSTs (Figure 3.5f). As discussed above, the mismatch between lipid proxy-based temperature estimates and satellite-derived temperature could be explained by the delay time of the proxy signal,

due to the time needed between lipid synthesis and incorporation into sinking aggregates plus the sinking time (Mollenhauer et al., 2015; Müller and Fischer, 2003; Park et al., 2018). However, without a marked seasonality of the estimated temperature, it is difficult to determine a delay time of the TEX_{86} signal. The other explanation for the absence of covariance between the TEX_{86} signal and the satellite-derived SST is that we observe a mixed signal of Thaumarchaeotal GDGTs derived from surface and deep oceans. The warm biases have a tendency to occur during periods of lower GDGT flux and thus may include higher proportions of material from different sources (early-December, mid-June−July, September−November), which may be more dominant in the deep trap (see discussion below).

Warm-biased TEX_{86}^{L}-derived temperatures have been attributed to the contribution of different archaeal communities or GDGT input from terrestrial sources, which may alter the composition of pelagic GDGTs, leading to unusual TEX_{86}^{L}-derived temperature estimates (Hopmans et al., 2004; Inglis et al., 2015; Zhang et al., 2016, 2011). For example, several studies showed that anomalous TEX_{86} based temperature estimates can be caused by isoprenoid GDGTs produced by Group II Euryarchaeota as significant contributors to the archaeal tetraether lipid pool and, thus, TEX_{86} (Lincoln et al., 2014; Schouten et al., 2014, 2008; Turich et al., 2007), a suggestion that is controversial. A prevalence of marine Group II Euryarchaeota has been reported in Circumpolar Deep Waters (Alonso-Sáez et al., 2011) and in deep waters of the Antarctic Polar Front (López-García et al., 2001; Martin-Cuadrado et al., 2008; Moreira et al., 2004; Alison E Murray et al., 1999). Therefore, we would assume that GDGTs produced by deep-dwelling Euryarchaeota might have caused the warm-biased TEX_{86}^{L} signal at depth in the region. Alternatively, advection of particles from warmer ocean regions could potentially lead to warm biases. However, it is known that the impact of lateral transport of GDGTs on the local signal is insignificant (J. H. Kim et al., 2009; Mollenhauer et al., 2008).

BIT, MI, %GDGT-0, and $|\Delta RI|$ were examined to evaluate non-thermal factors on GDGT composition and TEX_{86} values at both PF3 traps. However, none of the values for BIT, %GDGT-0, and $|\Delta RI|$ exceeded the defined critical values (Table A 3.1). MI values were higher at the deep trap than at the shallow one. The first two samples at the deep trap reached values of 0.3−0.5 MI, suggesting that GDGTs are derived from a mixture of non-methanotrophic and methanotrophic communities (Zhang et al., 2011). However, these two samples alone cannot fully explain the episodic and continuous warm-biased TEX_{86}^{L} estimates at the shallow and deep trap. Therefore, those indices cannot explain the warm anomaly of TEX_{86}^{L} estimates in the APF. Like in the Gulf of Mexico (Richey and Tierney, 2016), a longer time-series of samples would be helpful to investigate inter-annual variability, paired with a direct assessment of the archaeal community in the region.

The flux-weighted mean TEX_{86}^{L} temperatures averaged over the trap deployment period were 4.6 and 8.5 °C at the shallow and deep traps, respectively. The TEX_{86}^{L} temperature in surface sediment

(CHN 115-4-34; 51.00° S, 5.33° E) from the vicinity of the PF3 trap was 9.1 °C, which is 4.5 °C warmer than the TEX_{86}^{L} estimate temperature in the shallow trap (4.6 °C), but is similar to the one in the deep trap (8.5 °C). This situation is different from the Fram Strait and other time-series trap studies which showed that TEX_{86} values in different depths are almost identical (Chen et al., 2016; Mollenhauer et al., 2015; Wuchter et al., 2006b). This implies that there is a clearly different origin of GDGTs in particles collected in the upper (<~600 m) and deeper ocean, yet the main explanation of the warm-biased TEX_{86}^{L} is still speculative.

3.5.3 Re-evaluation of TEX_{86}^{L} calibration in polar oceans

In the two previous sections, the TEX_{86}^{L} calibration developed by Kim et al., (2010) for regions where ma SSTs are below 15 °C was applied. This calibration is based on data from 396 surface sediments in the global ocean. Several studies have expanded the TEX_{86} and TEX_{86}^{L} surface sediment dataset. We revisited the latest global surface sediment dataset containing 1095 surface sediment measurements (Tierney and Tingley, 2015 and reference therein) to recalculate the TEX_{86}^{L} calibration and to examine the agreement of our results with the new calibration. From the dataset, the data points for which TEX_{86}^{L} values cannot be calculated or which were pointed out as problematic by Ho et al., (2014) (c.f. BIT>0.3 or ~1.0 and GDGT concentration below detection limit) were excluded to avoid potential biases. With approximately two times more data points for the TEX_{86}^{L} calibration than the original one (Kim et al., 2010; n = 396), the new calibration again shows a linear correlation with ma SSTs even though the correlation coefficient is slightly lower (Figure 3.9; TEX_{86}^{L} = 0.013 × SST - 0.657; R^2 = 0.80, n = 744) and the residual standard error (±5.0 °C) is higher than those of the Kim et al., (2010)'s calibration (R^2 = 0.86, ±4.0 °C).

It should be noted that our new linear calibration has SST on the x-axis as the control variable and TEX_{86}^{L} value on the y-axis as the dependent variable because the composition of GDGTs, membrane lipids of Thaumarchaeota, (i.e., TEX_{86}/ TEX_{86}^{L} value) is potentially affected by water temperature. This different regression might explain parts of the discrepancy between our and the original calibrations of Kim et al. (2010). More scattered plots towards the cold temperatures appear in the new calibration as shown in previous studies (Ho et al., 2014; Kim et al., 2010) (Figure 3.9).

It is obvious that the relationship of ma SSTs to TEX_{86}^{L} values in high latitude northern (>50° N) and southern (>50° S) oceans is significantly different when both regions are plotted separately (Fig. 9). The data from the north (>50° N) are scattered both on the right- and left-hand side of the regression line, resulting in potential warm and cold anomalies, respectively (Figure 3.9). This may reflect various sources of GDGTs in the high latitude northern oceans, which have direct geographical connections to Eurasia and North America.

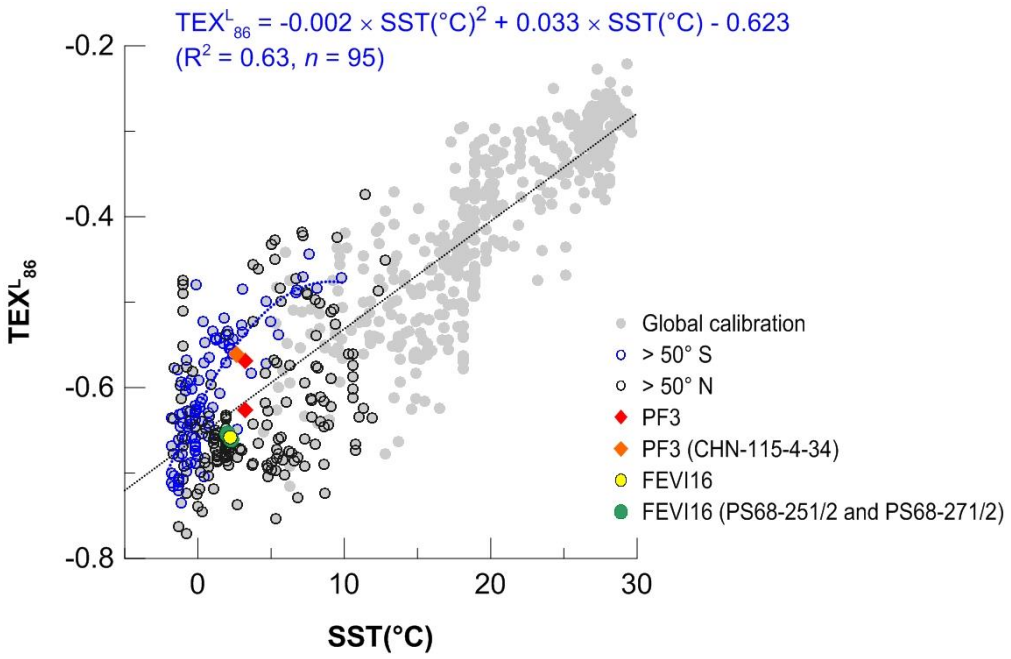

Figure 3.9 Correlation of TEX^{L}_{86} values with mean annual SSTs in the global ocean (gray symbols; Tierney and Tingley, (2015) and reference therein). Blue and black round symbols represent the high latitude regions higher than 50° S and 50° N, respectively. In the southern regions (>50° S), TEX^{L}_{86} values have a polynomial correlation with ma SSTs (R^2 = 0.63, n = 95). Red and orange diamonds represent the flux-weighted mean TEX^{L}_{86} of the two traps at the site PF3 and TEX^{L}_{86} on the surface sediment (CHN-115-4-34), respectively. Yellow and green round symbols represent the flux-weighted mean TEX^{L}_{86} at the site FEVI16 and TEX^{L}_{86} on the surface sediments (PS68-251/2 and PS68-271/2), respectively.

Warm biased TEX^{L}_{86} estimates in these regions might be caused by input of soil-derived GDGTs, which are picked up by the sea ice in the Arctic marginal seas (c.f. Laptev sea, Kara Sea, eastern Greenland), and released while the sea ice melts. Alternatively, TEX^{L}_{86}-derived temperatures might reflect warmer subsurface temperatures in the warm season as shown in the subarctic North Pacific region with the regional calibration by Seki et al., (2014) and Meyer et al., (2016). Cold-biased TEX^{L}_{86} estimates are mainly found in the Barents Sea, North Sea, and the Norwegian Sea. In the North Sea, a significantly enhanced abundance of planktonic Archaeal cells and high GDGT concentration in the winter time could account for colder TEX^{L}_{86}-derived temperature compared to SST (Herfort et al., 2007; Pitcher et al., 2011; Wuchter et al., 2006a). Hence, regional calibrations in the high latitude northern oceans seem to be a valid approach.

By contrast, most of the data from the south (>50° S) show higher TEX^{L}_{86} values than predicted by the regression line (*n* = 95). This explains the observed warm anomalies of TEX^{L}_{86} -derived temperature when using the original linear regression calibration. Instead of the global linear calibration, a polynomial one seems to be a better option in these regions (Fig. 9). When excluding one data point in the winter sea ice-covered Southern Ocean, the correlation coefficient of the polynomial correlation is encouraging (R^2 = 0.63).

The data points of the flux-weighted mean TEX_{86}^{L} in the FEVI16 trap and TEX_{86}^{L} in the underlying surface sediment against ma SSTs are both closely located to the linear regression line. It illustrates the applicability of the linear TEX_{86}^{L} calibration in the eastern Fram Strait (Figure 3.9). At the site PF3, the TEX_{86}^{L}-derived temperatures based on the polynomial calibration yield -0.1 °C, 1.9 °C, and 2.2 °C at the shallow and deep trap, and in the underlying surface sediment, respectively (Figure 3.9), which are colder than the estimates based on the linear calibration. The polynomial TEX_{86}^{L} temperatures at the deep trap and on the sediment are slightly colder than ma SST (2.4 °C, the data can be found in Tierney and Tingley, (2015)), but less biased compared to the reconstructed temperatures based on the linear TEX_{86}^{L} calibration (see Section 3.5.2.2). To test this polynomial calibration in the southern ocean (>50° S), a further assessment needs to be made with down-core sediments in similar regions, where the original TEX_{86}^{L} estimate displays a warm bias.

3.5.4 Applicability of OH-GDGT related calibrations for SST estimates in the high latitude Atlantic Ocean

OH-GDGTs were determined in sinking particles of the eastern Fram Strait and of the APF. The proportions of OH-GDGTs to total GDGTs (sum of OH- and iso-GDGTs) ranged between 7−14% in the eastern Fram Strait and 4−7% in the APF (Figure 3.4a and 6a, c). This is a relatively smaller portion than in the Nordic Seas (~16%; Fietz et al., 2013).

Several OH-GDGT based calibrations for SST have been suggested for the global ocean and the Nordic Seas (Fietz et al., 2013; Huguet et al., 2013; Lü et al., 2015). We applied those calibrations suggested by Fietz et al., (2013) and Lü et al., (2015). Only two calibrations (Eq. 4 and 6) yield realistic temperature estimates, which varied within a similar range of satellite-derived SSTs or TEX_{86}^{L}-derived temperatures (Figure 3.4b and 6b, d). The former calibration considers relative abundances of OH-GDGT-0 and Crenarchaeol (Eq. 4). The latter is based on the RI-OH-GDGTs (Eq. 5 and 6). In the eastern Fram Strait, both OH-GDGTs based temperatures showed similar changes with an increasing trend until late-April 2008 and decreasing temperatures in May 2008 except for the last two samples (Figure 3.4b). In the APF, both OH-GDGTs based temperatures were also close to the satellite-derived SSTs and the TEX_{86}^{L}-derived temperatures at the shallow trap (Figure 3.6b). Warm biases with the TEX_{86}^{L} calibration did not occur with those OH-GDGTs calibrations at the deep trap (Figure 3.6d). We speculated in Section 3.5.2.2 that the warm-biased TEX_{86}^{L} temperatures relative to SSTs may be caused by GDGTs synthesized by Euryarchaeota dwelling in deep waters of the APF. The methanogenic Euryarchaeota are known to produce GDGT-1, -2 and -3 and may alter the TEX_{86} signal derived from pelagic Thaumarchaeota (Weijers et al., 2011). This might explain why only calibrations (OH-GDGT/Cren and RI-OH′), which do not contain GDGTs potentially originated from Euryarchaeota, show a correspondence to regional SSTs. At this stage, however, this has to be

considered speculative. Moreover, it is not clear yet if OH-GDGTs are exclusively produced by Thaumarchaeota since OH-GDGTs were also detected in a culture of Euryarchaeota (*Methanothermococcus thermolithotrophicus*) (Liu et al., 2012). Therefore, further research is needed to clarify various aspects of distribution, production, and modification of OH-GDGTs in response to physicochemical changes in the global ocean. Nonetheless, OH-GDGTs appear to be a potential temperature proxy in our two high latitude regions.

3.6 Summary and conclusion

Sinking particles collected using time-series sediment traps allowed us to determine the variability of the downward GDGT export and the environmental influence on TEX_{86}^{L} thermometry in northern and southern high latitude regions of the Atlantic Ocean. We observed fundamentally different patterns between the eastern Fram Strait and the Antarctic Polar Front.

In the eastern Fram Strait, the seasonally different composition of sinking materials resulted in different sinking velocities of GDGTs, and thus the temporal offsets between TEX_{86}^{L} -derived temperatures and SSTs may vary by season. Although increased flux of terrestrial matter transported by sea-ice in intermediate and deep waters is well known in the region (Lalande et al., 2016), TEX_{86}^{L} thermometry does not seem to be affected by lateral advection of particles. The flux-weighted mean TEX_{86}^{L} temperature in sinking particles was similar to the one in the underlying surface sediment, indicating that the TEX_{86}^{L} signal did not experience substantial changes while sinking. The flux-weighted mean TEX_{86}^{L} temperature corresponded to temperatures in water depths ranging between 30 and 80 m, where nutrient profiles suggest favorable conditions for Thaumarchaeota.

In the Antarctic Polar Front, changes in GDGT fluxes and TEX_{86}^{L} temperatures are different between the two traps moored at different depths. At the shallow trap, TEX_{86}^{L} estimates do not co-vary with satellite-derived SSTs, and its flux-weighted mean temperature is 4.6 °C. The warm-biased TEX_{86}^{L} at the deep trap and in the underlying surface sediment may be caused by GDGT contributions from Euryarchaeota, which is dominant in the deeper part of the water column of CDW at the Antarctic Polar Front. Alternatively, a systematic warm bias of the linear calibration in the high latitude southern ocean could explain the discrepancy between TEX_{86}^{L} reconstructed and observed temperatures. The discrepancies can be reduced by using a non-linear TEX_{86}^{L} calibration developed for high latitude samples from the Southern Hemisphere.

Our findings offer insights into the potential factors governing TEX_{86}^{L} thermometry such as nutrient availability or archaeal community composition in high latitude regions. In the high latitude North Atlantic, regional TEX_{86}^{L} calibrations can be an additional option next to the global calibration, while in the high latitude Southern Ocean, the benefit of a polynomial TEX_{86}^{L} calibration needs to be

further tested. Our studies suggest that OH-GDGTs based calibrations are also worth to be further investigated in the polar oceans. Accordingly, our study highlights that multiple approaches of global versus regional calibrations, polynomial relationships, or OH-related calibrations are beneficial to overcome the limitations of a single TEX_{86}^{L} calibration in high latitude ocean regions.

Acknowledgments

We acknowledge the captain, crew and scientists who participated in the expeditions for collecting sediment trap samples used in this study. This project is funded through the DFG-Research Center/Cluster of Excellence “The Ocean in the Earth System” at the MARUM and supported by GLOMAR−Bremen International Graduate School for Marine Sciences, University of Bremen. The trap samples were supplied by the MARUM Centre of Marine Environmental Research at the University of Bremen (PF3) and Alfred Wegener Institute, Helmholtz Center for Polar and Marine Research (FEVI16). MHI received funding for the Helmholtz Young Investigator Group SeaPump “Seasonal and regional food web interactions with the biological pump (VH-NG-1000)” at the Alfred Wegener Institute.

Data availability

The data presented here are available on the PANGAEA database (https://doi.pangaea.de/10.1594/PANGAEA.897268).

Appendix A

Table A 3.1 Index values for assessing the terrestrial and/or methanogen GDGT inputs at FEVI16 and PF3 sediment traps. The exact sampling interval of each sample number at FEVI16 and PF3 can be found in PANGAEA (https://doi.pangaea.de/10.1594/PANGAEA.897268).

Cup no.	FEVI16				PF3							
	(1296 m)				(614 m)				(3196 m)			
	BIT [a]	MI [b]	%GDGT-0[c]	|ΔRI| [d]	BIT	MI	%GDGT-0	|ΔRI|	BIT	MI	%GDGT-0	|ΔRI|
1	0.01	0.09	60	0.15	0.00	0.15	58	0.05	0.00	0.34	62	0.23
2	0.01	0.11	60	0.22	0.02	0.14	58	0.08	0.00	0.30	61	0.17
3	0.01	0.11	60	0.21	0.00	0.14	64	0.24	0.00	0.21	58	0.09
4	0.01	0.10	60	0.20	0.00	0.16	61	0.16	-	-	-	-
5	0.01	0.11	61	0.30	0.00	0.19	62	0.17	0.00	0.22	58	0.06
6	0.01	0.10	60	0.23	0.00	0.15	63	0.19	0.00	0.21	56	0.05
7	0.01	0.11	60	0.23	0.00	0.20	65	0.24	0.00	0.19	55	0.08
8	0.01	0.11	60	0.09	0.00	0.19	60	0.08	0.00	0.21	56	0.01
9					0.00	0.19	62	0.16				
10	0.01	0.13	61	0.14	0.00	0.23	64	0.20	-	-	-	-
11					0.00	0.20	59	0.06	-	-	-	-
12	0.01	0.15	59	0.19	0.00	0.21	64	0.26	-	-	-	-
13	0.01	0.13	59	0.10	0.00	0.21	62	0.19	-	-	-	-
14					0.00	0.16	61	0.16	-	-	-	-
15	0.02	0.14	59	0.13	0.00	0.15	60	0.15	-	-	-	-
16	0.02	0.13	61	0.22	0.00	0.14	60	0.11	0.00	0.21	56	0.04
17	0.01	0.11	61	0.20	0.00	0.16	62	0.16	-	-	-	-
18	0.01	0.09	63	0.26								
19	0.01	0.10	64	0.31								
20	-	-	-	-								
	Total 20 samples				Total 17 samples							

[a]: BIT (Hopmans et al., 2004; Weijers et al., 2006) for terrestrial input when >0.3
[b]: MI (Zhang et al., 2011) for methanotrophic archaeal input when >0.5 and normal oceanic signal when <0.3
[c]: %GDGT-0 (Blaga et al., 2009; Inglis et al., 2015) for methanogenic archaeal input when >67%
[d]: |ΔRI| (Zhang et al., 2016) for both methanotrophic archaeal and terrestrial input >0.3

CHAPTER 4

GDGTs in sinking particles of the oligotrophic ocean: TEX_{86}^{H} thermometry in the central Brazil Basin

In preparation for Organic Geochemistry

4 Manuscript III

GDGT in sinking particles of the oligotrophic ocean: TEX_{86}^{H} thermometry in the central Brazil Basin

Eunmi Park[1,2,3], Jens Hefter[1], Gerhard Fischer[2,3], Gesine Mollenhauer[1,2,3]

[1]Alfred Wegener Institute, Helmholtz Center for Polar and Marine Research, D-27570 Bremerhaven, Germany
[2]MARUM Centre for Marine Environmental Sciences, University of Bremen, D-28334 Bremen, Germany
3Department of Geosciences, University of Bremen, D-28334 Bremen, Germany

Abstract

The TEX_{86} temperature proxy, based on the relative abundance of glycerol dialkyl glycerol tetraethers (GDGT) in marine sediments, is calibrated to the overlying water temperature in the global ocean. Most TEX_{86} studies focus on high productivity or high latitude regions, which experience rapid climate change, albeit the important role of the oligotrophic zone in the global heat distribution. In this study, the seasonal trends of GDGT flux and TEX_{86}^{H}-derived temperature are examined in sinking particles collected by time-series sediment traps at two sites in the central Brazil Basin of the South Atlantic oligotrophic gyre (WA9 at 7.50° S/ 28.10° W; WAB1 at 11.53° S/ 28.52° W). At each study site, traps were moored in two depths. Mass and GDGT flux at 591 and 4456 m depth of site WA9 are highest when the trade winds are strong in July. At site WAB1, both fluxes are lower than at WA9, with multiple flux maxima at 727 m depth and a smoothed pattern at 4515 m depth. Good correlations between fluxes of GDGTs and opal/carbonate at both shallow traps reveal the preferential incorporation of GDGTs in opal- and carbonate-rich aggregates. TEX_{86}^{H} -derived temperatures resemble the satellite-derived SST without seasonality at 591 m of site WA9, while they display warm-biases consistently at the 727 m trap of site WAB1. It has been shown in laboratory experiments and in field studies that higher RI and thus TEX_{86} values occur under energy-stress conditions like low ammonia oxidation rates (Hurley et al., 2016). This accounts for the warm-biased TEX_{86} temperature at the shallow trap of site WAB1 in the oligotrophic gyre. In both deep traps of sites WAB1 and WA9, the TEX_{86}^{H}-derived temperatures reflect subsurface temperatures. We speculate that *in situ* GDGT production in deep waters presenting colder signals imprint the relatively warm surface signal in deep waters and surface sediments. It suggests that TEX_{86} thermometry in the oligotrophic oceans is governed by the complex interplay of factors including nutrient conditions, sinking pathways, and the deep production.

4.1 Introduction

An organic paleothermometer for sea surface temperature (SST), TEX_{86}, is based on the relative abundance of isoprenoid glycerol dialkyl glycerol tetraether (GDGT) lipids. GDGTs are produced by ammonia-oxidizing Thaumarchaeota (formerly Group I Crenarchaeota), one phylum of Archaea (Schouten et al., 2002). The ubiquity of these organisms in the ocean allows the TEX_{86} proxy to be applied in high (polar and sub-polar) and low latitude (tropical) regions, an advantage compared to the other organic temperature proxies, including $U^{k'}_{37}$ (Delong, 2003; Schouten et al., 2002). For the tropical regions (>28 °C), $U^{k'}_{37}$ is problematic because the proxy saturates and the lack of sensitivity to temperature diminishes (Prahl and Wakeham, 1987).

The original linear calibration of TEX_{86} with SSTs is based on values obtained from surface sediments and has been refined using an expanded database to the base 10 logarithmic scale "$\log_{10}(TEX_{86})$" named TEX^{H}_{86} for the regions with mean SST above 15 °C (Kim et al., 2010). Recently, the Bayesian, Spatially-Varying regression (BAYSPAR) SST prediction model is developed (Tierney and Tingley, 2015). This model based calibration reconstructs temperatures with a consideration of spatially varying uncertainties and TEX_{86}-temperature relationships by each 20° x 20° latitude-longitude grid. Several studies for both modern oceans (Chen et al., 2016; Park et al., 2018; Richey and Tierney, 2016) and paleoenvironments (Kim et al., 2012b; Lopes dos Santos et al., 2010; McClymont et al., 2012) have shown that TEX^{H}_{86} based temperature estimates reflect subsurface temperatures rather than mean annual (ma) SSTs in highly productive upwelling regions. Reflection of subsurface temperature is often explained by the contribution of deeper dwelling planktonic Archaea.

The main synthesizers of GDGTs in the ocean are ammonia-oxidizing Archaea, which nitrify ammonia to nitrite (Horak et al., 2013; Könneke et al., 2005). With notable energy efficiency (Horak et al., 2013; Könneke et al., 2014), Archaea can adapt to nutrient-limited marine conditions. This agrees with the high activity and abundance of Archaea at the depth of the nitrite maximum in the oligotrophic oceans (Horak et al., 2017; Sintes et al., 2013). Notably, Horak et al., (2017) showed that the community structure of Thaumarchaeota is changed from near the subtropical transition zone toward the oligotrophic gyre. This might lead to an additional factor in determining water column TEX_{86} signals.

Recent culture studies have documented an increase in TEX_{86} values under low nitrification rates (Hurley et al., 2016) and low oxygen conditions (Qin et al., 2015), indicating a potential non-thermal influence on the relative abundance of isoprenoid GDGTs and TEX_{86} thermometry.

The TEX_{86} calibration based on the Bayesian model collected TEX_{86} values from 1095 locations in the global ocean (Tierney and Tingley, 2015 and reference therein). In this dataset, most points are

from the continental shelf and slope sites with relatively few samples from true deep-sea sites in the north and south subtropical oligotrophic gyres of the Pacific and the Atlantic Oceans, and the southern Indian Ocean. These oligotrophic subtropical oceans are characterized by a deep thermocline and depleted nutrients in the surface mixed layer coinciding with deep chlorophyll maxima (DCM) and year-round low primary production (Mignot et al., 2014). However, the sheer size of the oligotrophic oceans makes their contribution to the carbon export substantial. Moreover, the gradual expansion of the oligotrophic gyres in response to global warming calls for continuous attention to these regimes (Polovina et al., 2008).

To provide insight into the environmental variables influencing the GDGT composition and the interpretation of TEX_{86} temperature signals in the water column and in the sediments of the South Atlantic oligotrophic gyre region, we investigate the variability of seasonal GDGT flux and TEX_{86}^{H}-derived temperature in sinking particles collected using moored sediment traps in the central Brazil Basin.

4.2 Oceanographic setting

In the South Atlantic Ocean, the anticyclonic subtropical gyre is formed by boundary currents: the Benguela Current (BC) flowing along the southwestern coast Africa as the eastern boundary, westward flowing South Equatorial Current (SEC) fed by the Benguela current in the north, the Brazil Current flowing southward along the northeastern Brazil in the west, and the South Atlantic Current flowing eastward in the South (Figure 4.1) (Peterson and Stramma, 1991; Stramma and England, 1999). Near the equator, the seasonal trade winds and the location of the Intertropical Convergence Zone (ITCZ) are responsible for the variability of surface currents and upwelling. During the austral winter (June−September), the southeasterly (SE) trade winds stimulate the SEC and thus the eastern equatorial upwelling (Figure 4.1) (Shannon and Nelson, 1996). During the austral summer (boreal winter) when the ITCZ is situated in the southernmost part, Saharan dust can be transported over long distances and reach the equatorial Atlantic (Wefer and Fischer, 1993).

The physical restriction caused by the gyre leads to nutrient-depleted environments in the open oceans. Despite of the low biological productivity in these oceans (e.g. North and South Atlantic, and North and South Pacific central ocean), the concern regarding their significant contribution to the C- and N- cycles has risen due to their sizes covering approximately 40% of the world oceans (Mignot et al., 2014; Polovina et al., 2008). The Atlantic Meridional Transect (AMT) programme provided important insights into the temporal and spatial variability of planktonic ecosystems in relation with biogeochemical parameters in the Atlantic Ocean between 50° N and 52° S including the North and South Atlantic oligotrophic gyres (Robinson et al., 2006). The central South Atlantic Tropical Gyre (SATL) region was defined as autotrophic, and nutrients play a role as limiting factors for phytoplankton biomass and growth rate in that region. Nutrients are supplied by the lateral transport

near the gyre edges and by convection or mesoscale eddies across the thermocline into the euphotic zone (Robinson et al., 2006 and references therein). The south Atlantic oligotrophic ocean is characterized by extremely low chlorophyll a concentrations (<0.1 mg m^{-3}) with a deep chlorophyll maximum (DCM) and permanently stratified surface water masses. When the WAB1 tap was recovered in May 1998, the DCM was recorded at around 200 m water depth with only 0.12 mg m^{-3} chlorophyll-a concentration (METEOR-Cruise 41/4 cruise report; Fischer, G. et al., 1999). Daily SSTs measured by AVHRR varied in the range of 24.6−29.1 °C near site WAB1 and 25.5−28.8 °C near site WA9 while the traps were deployed. According to WOA13 data, the nitrate-depleted upper water column extends down to 125 m depth at site WAB1 and 100 m at site WA9 (Garcia et al., 2013).

4.3 Material and methods

4.3.1 Sample collection

Two mooring systems were deployed in the oligotrophic central Brazil Basin situated within the South Atlantic subtropical gyre (Figure 4.1, Table 4.1). Sinking particles were collected using time-series sediment traps (Kiel type, opening area: 0.5 m^2) equipped with a rotation plate at two different water depths. The rotating carousel for the collection of 20 samples was programmed. WA9 trap was programmed for a 17 day sampling interval for each sample bottle. WAB1 trap had a sampling interval of 22.5 days, with 20.5 days of intervals for the first and the last sample bottle. The location and deployment period of each trap can be found in Table 4.1. A detailed method for the trap sample handling is described in Fischer and Wefer, (1991). Each sample cup was poisoned with $HgCl_2$ before and after the deployment to avoid further biological activity. After the recovery, large swimmers were picked out using forceps and later samples were sieved with a 1 mm mesh in the home laboratory. Samples were split into 5 parts for further chemical and biological analysis in the home laboratory. Surface sediments (GeoB 5201-8; 28.5° W, 11.5° S) sampled at the WAB1 trap location was also analyzed.

4.3.2 Mass flux

Freeze-dried particle samples were ground and homogenized for the following chemical analysis at the University of Bremen. Total carbon (TC) and total nitrogen (TN) were directly measured using a CHN-analyzer (Fischer and Karakaş, 2009). Total Organic Carbon (TOC) was analyzed after treatment with 2N HCl. Carbonate was obtained by subtracting OC from TC. Opal (biogenic silica) was analyzed with a sequential leaching technique according to Müller and Schneider, (1993). The lithogenic component was determined as follows: total flux − (opal + carbonate + 2×TOC). “2×TOC” is assumed to approximate the mass of organic matter.

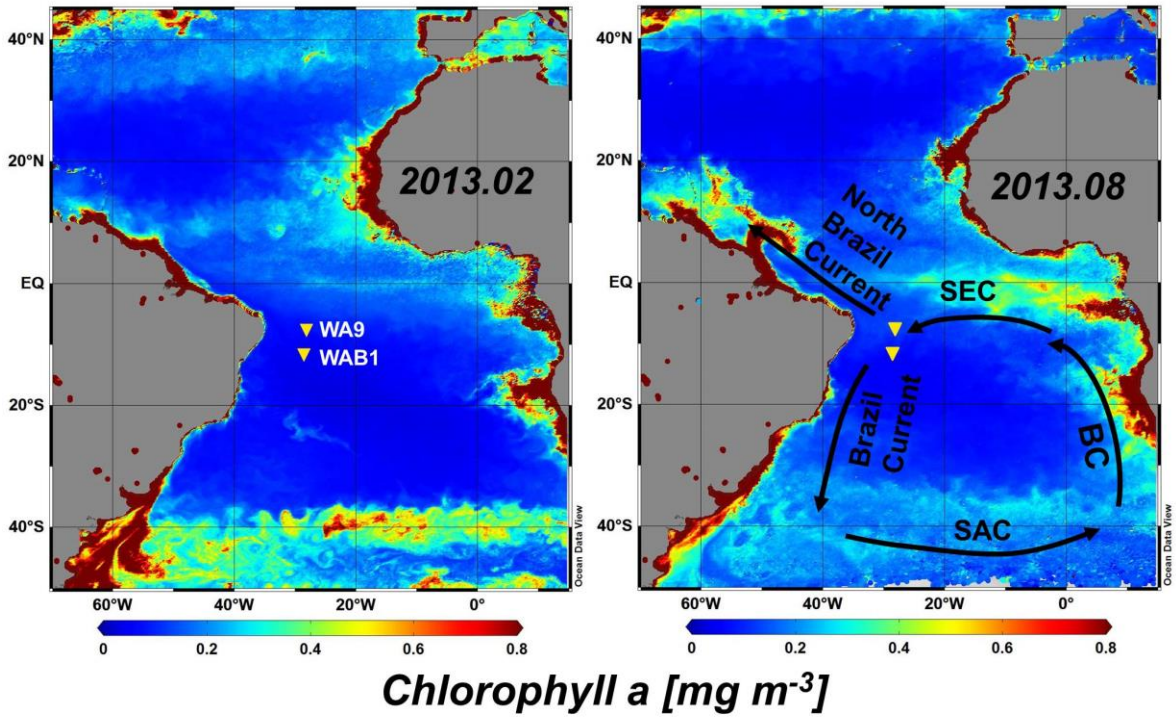

Figure 4.1 Two mooring systems (WA9 and WAB1) were deployed to collect sinking particles in the northeast oligotrophic central Brazil Basin. The background represents the monthly chlorophyll-a concentrations in February and August 2013. The data was extracted from Ocean color Climate change Initiative dataset, European Space Agency (available online at http://www.esa-oceancolour-cci.org/). Four major currents in the South Atlantic Ocean (Benguela Current (BC), westerly South Equatorial Current (SEC), southerly Brazil Current, and easterly South Atlantic Current (SAC)) develop the south Atlantic oligotrophic gyre. Parts of the SEC also feed the North Brazil Current. The map is created based on the Ocean Data View (Available online http://odv.awi.de; Schlitzer, 2017).

4.3.3 Lipid extraction and analysis

5−160 mg of sediment trap samples and 5 g of the surface sediment sample were extracted. Total lipids (TLE) were extracted three times with an ultrasonic bath for 10 minutes using 2 mL for sinking particles and 10 mL for surface sediment of a solvent mixture (9:1 v/v dichloromethane (DCM) to methane (MeOH)). The samples were centrifuged after each extraction, and the supernatants were combined into 4 mL vials. Before the extraction, a known amount of C_{-46} GDGT was added as an internal standard to achieve the lipids quantification. The TLEs were dried under a stream of N_2 gas and then saponified using 1 mL of 0.1 M potassium hydroxide in methanol and water (9:1 v/v) at 80 °C for two hours. Neutral lipids recovered in *n*-hexane (Hex) were separated into three different polarity fractions via deactivated silica gel column chromatography (mesh size: 70−230 µm) eluting with 2 mL Hex, 4 mL DCM: Hex (2:1 v/v), and 4 mL DCM: MeOH (9:1 v/v) for apolar, ketone, and polar fractions, respectively. The polar fractions were filtered through a 0.45 µm pore size polytetrafluoroethylene (PTFE) syringe filter and re-dissolved in Hex: isopropanol (99:1 v/v) at a 2 mg ml^{-1} concentration prior to GDGT analysis according to Hopmans et al., (2000).

Table 4.1 Sampling details of the sediment trap moorings and core-top sediment. Exact dates for the opening and closing of each sampling cup can be found along with fractional GDGT data on www.pangaea.de (the exact address will be followed).

Name	Location		Water depth	Trap depth	Deployment period		Flux-weighted mean TEX_{86}^{H} temperature	Intervals	Cruise name	References
	Latitude (° S)	Longitude (° W)			Start	End				
			(m)	(m)	(dd.mm.yyyy)		(°C)	(no × days)		
WA9	7.5	28.1	4996	591 4456	23.03.1996	26.02.1997	27.4 24.9	20×17	M34/4 M38/1	Fischer, G. et al., (1996) Fischer, G. et al., (1998)
WAB1	11.55	28.52	5483	727 4515	27.02.1997	19.05.1998	29.2 24.6	2×20.5, 18×22.5	M38/1 M41/4	Fischer, G. et al., (1998) Fischer, G. et al., (1999)
GeoB 5201-8	11.53	28.52	5461	-	-	-	24.7	-	M41/4	Fischer, G. et al., (1999)

* The exact sampling interval of each sample at WA9 and WAB1 can be found in PANGAEA

GDGTs were analyzed using high performance liquid chromatography (HPLC) coupled with an atmospheric pressure chemical ionization interface to the single quadrupole mass selective detector (APCI-MS). GDGT separation was achieved on an Alltech Prevail Cyano column (2.1 × 150 mm, 3 μm, with flow rate at 0.2 ml min^{-1}). The contents of isoprenoids (GDGT-1, -2, -3, Crenarchaeol, Crenarchaeol regio-isomer) and branched GDGTs ([I], [II], [III]) were determined by integrating the peak areas of masses (*m/z*) 1302, 1300, 1298, 1296 and 1292 and 1050, 1036 and 1022, respectively. Detailed conditions for GDGT analysis followed the methods described by Schouten et al., (2007) and Chen et al., (2016)

4.3.4 Temperature estimate and GDGT flux

Chromatogram peak areas of GDGTs were used to calculate TEX_{86} and TEX_{86}^{H} values according to Schouten et al., (2002) and Kim et al., (2010), respectively :

$$TEX_{86} = ([GDGT\text{-}2]+[GDGT\text{-}3]+[Cren']) / ([GDGT\text{-}1]+[GDGT\text{-}2]+[GDGT\text{-}3]+[Cren']) \quad (1)$$

$$TEX_{86}^{H} = Log_{10}(TEX_{86}) \quad (2)$$

The numbers refer to the number of cyclopentane moieties in the isoprenoid GDGTs, and Cren′ is the regio-isomer of Crenarchaeol containing four cyclopentane rings and one cyclohexane ring.

TEX_{86}^{H} values were converted to water temperature using the following calibration according to Kim et al., (2010):

$$SST\ (°C) = 68.4 \times TEX_{86}^{H} + 38.6\ (R^2 = 0.87,\ n = 255) \quad (3)$$

As an alternative calibration, the Bayesian regression model (BAYSPAR) (Tierney and Tingley, 2015) with default settings in the standard prediction mode was also applied to covert TEX_{86} values to water temperature (available online at http://bayspar.geo.arizona.edu/).

The GDGT flux represents a sum of all GDGT fluxes, which are used to calculate TEX_{86} ratios.

The Flux-weighted mean TEX_{86} value was calculated as follows:

$$\text{Flux-weighted mean } TEX_{86} = \sum\{TEX_{86i} \times \text{GDGT flux}_i \times \text{sampling interval (days)}_i\} / \sum\{\text{GDGT flux}_i \times \text{sampling interval (days)}_i\} \quad (4)$$

4.3.5 Indices for non-thaumarchaeotal GDGT source

BIT, the Branched and Isoprenoid Tetraether index, was calculated according to Hopmans et al., (2004):

$$BIT = ([I]+[II]+[III]) / ([I]+[II]+[III]+[Cren]) \quad (5)$$

Roman numbers I, II, and III refer to branched GDGTs with m/z 1022, 1036, and 1050. A possible impact of terrestrial organic matter on TEX_{86} is considered when the BIT value is >0.3.

MI, the methane index, was calculated to assess the relative input of GDGTs synthesized by methanotrophic Euryarchaeota against by Thaumarchaeota as follows (Weijers et al., 2011; Zhang et al., 2011):

$$MI = ([GDGT\text{-}1] + [GDGT\text{-}2] + [GDGT\text{-}3]) / ([GDGT\text{-}1] + [GDGT\text{-}2] + [GDGT\text{-}3] + [Cren] + [Cren´]) \quad (6)$$

when MI value is lower than 0.3, it indicates the normal marine GDGT distribution while when the MI value is higher than 0.5, it could mark the hydrate-impacted sediments.

%GDGT-0 can be used to assess the sedimentary methanogenic Archaea mainly producing GDGT-0 (Blaga et al., 2009; Sinninghe Damsté et al., 2012):

$$\%GDGT\text{-}0 = \{([GDGT\text{-}0]) / ([GDGT\text{-}0] + ([Cren])\} \times 100 \quad (7)$$

The %GDGT-0 can exceed 67% when there is an additional source of GDGTs produced by methanogenesis.

The Ring Index (RI) is defined as follows (Zhang et al., 2016):

$$RI = 0 \times [GDGT\text{-}0] + 1 \times [GDGT\text{-}1] + 2 \times [GDGT\text{-}2] + 3 \times [GDGT\text{-}3] + 4 \times [Cren] + 4 \times [Cren´] \quad (8)$$

where each bracket indicates the relative proportion of GDGT in the sum of total GDGTs.

RI has a correlation with TEX_{86} values on the modern surface sediment dataset as follows:

$$RI_{calculated} = -0.77(\pm0.38) \times TEX_{86} + 3.32(\pm0.34) \times (TEX_{86})^2 + 1.59(\pm0.10) \ (R^2 = 0.87, n = 531) \quad (9)$$

when the difference of RI values ($|\Delta RI|$) between the calculated one by eq. 9 and the measured one in geological samples is larger than 0.3, the authors suggest that it likely indicates the influence of soil-derived GDGTs or methanotrophic archaeal GDGTs (Zhang et al., 2016).

$$|\Delta RI| = RI_{calculated} - RI_{sample} \quad (10)$$

4.3.6 Environmental data

Daily SSTs were extracted from the data set measured by the Advanced Very High Resolution Radiometer (AVHRR) of the National Oceanic and Atmospheric Administration (NOAA) (Reynolds et al., 2002). The temperatures were averaged over each sampling time to compare with the TEX_{86}^{H}-derived temperatures. The AVHRR has a 0.25° grid of spatial resolution. Chlorophyll-a concentrations were extracted from the Ocean Color Climate Change Initiative dataset, European Space Agency (available online at http://www.esa-oceancolour-cci.org/) to show the seasonal difference of chlorophyll-a concentration in the study region (Figure 4.1). The spatially averaged (8 days)

chlorophyll-a (Chl-a) concentration with a grid size of 1° around the trap location was also extracted and averaged over 10 years (2001−2010) to show the seasonal variation. This satellite data is only available since September 1997, which does not cover the time period of the trap deployment.

4.4 Results

4.4.1 WA9

4.4.1.1 Mass and GDGTs fluxes

Mass fluxes at the northern site WA9 (7.5° S) range from 6.1 to 103.2 mg m^{-2} d^{-1} and from 16.3 to 82.5 mg m^{-2} d^{-1} at the shallow (591 m) and deep trap (4456 m), respectively (Figure 4.2b, e). Maximum fluxes occur in early July 1996 at both depths. Carbonate accounts for 35−86% and 56−81% of total mass fluxes at the shallow and deep depth, respectively. GDGT fluxes vary between 24.7 and 306.1 ng m^{-2} d^{-1} at the shallow trap and between 87.1 and 184.8 ng m^{-2} d^{-1} at the deep trap (Figure 4.2c, f). GDGT flux at the shallow trap has the best correlation with opal flux (R^2 = 0.85) followed by carbonate flux (R^2 = 0.72) and TOC flux (R^2 = 0.70, not shown) (Figure 4.3). Each variable shows a weaker correlation with GDGTs at the deep trap (R^2 = 0.56 for opal, R^2 = 0.50 for carbonate, and R^2 = 0.45 for TOC) relative to the shallow trap.

4.4.1.2 TEX_{86}^H estimations

In particles collected at the shallow trap, TEX_{86} values range between 0.66 and 0.70 (Figure 4.2c). The TEX_{86}^H-derived temperature according to Kim et al. (2010) ranges between 26.2 and 28.1 °C and resembles the satellite-derived SSTs (26.1−28.0 °C) even though TEX_{86}^H estimates in sinking particles do not display the seasonality observed at the surface (Figure 4.2c). BAYSPAR SSTs vary between 30.3 and 33.7 °C for these samples (not shown). At the deep trap, TEX_{86} values range between 0.61 and 0.65 and their estimated TEX_{86}^H temperatures range between 23.8 and 25.7 °C Figure 4.2f, g). BAYSPAR SSTs vary between 26.3 and 29.6 °C (Figure 4.2g). The Flux-weighted mean TEX_{86}^H temperatures are 27.4 °C and 24.9 °C at the shallow and deep trap, respectively (Table 4.1).

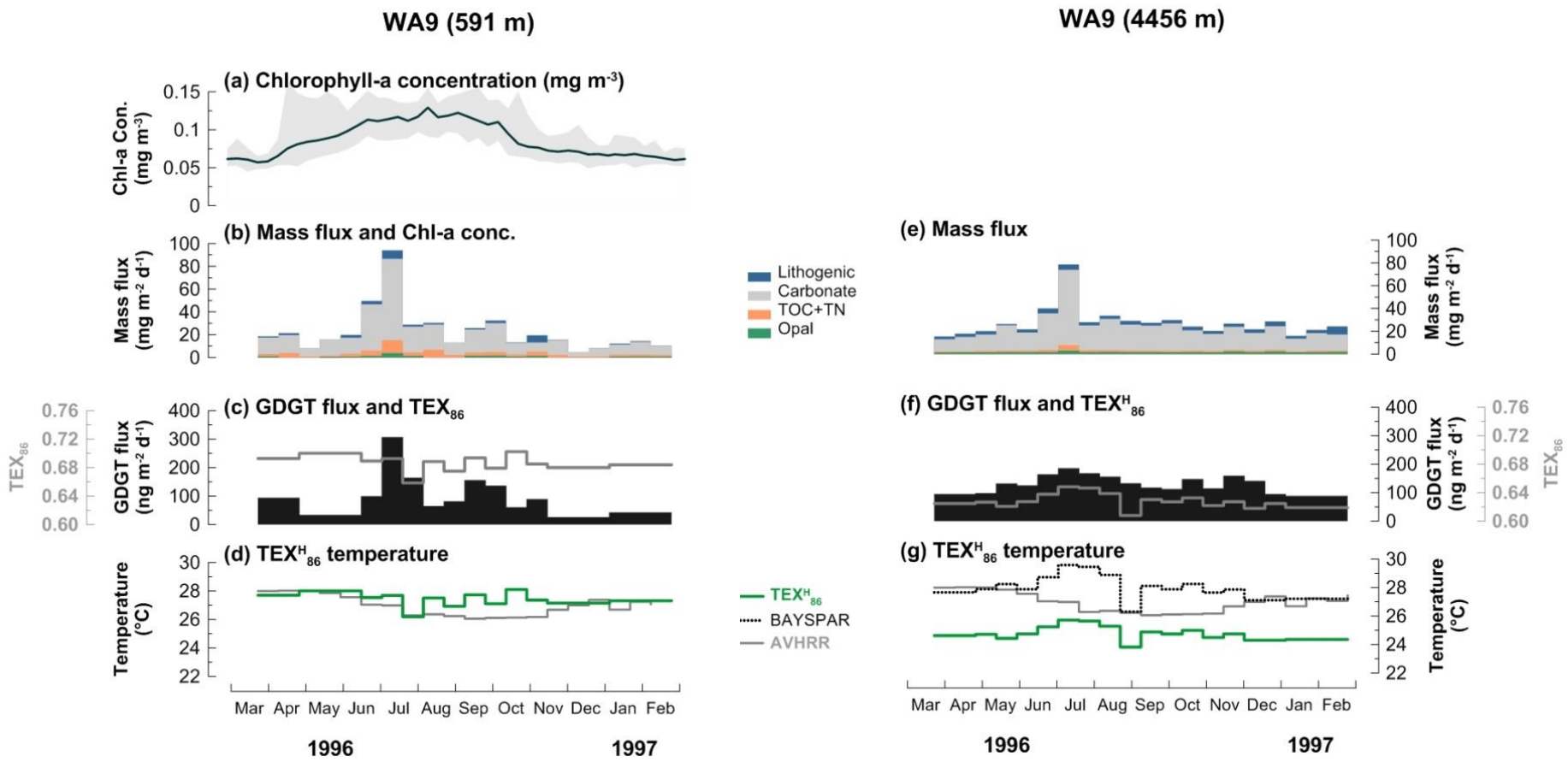

Figure 4.2 Changes in (a) satellite-derived chlorophyll-a concentration, (b, e) mass flux, (c, f) GDGT flux and TEX_{86}, (d, g) TEX_{86}^{H}-derived temperatures in sinking particles collected at the shallow (at 591 m, on the left panel) and at the deep trap (at 4456 m, on the right panel) of WA9 in the central Brazil Basin. Note that the Y-axis scale of each parameter is the same between the shallow and deep traps.

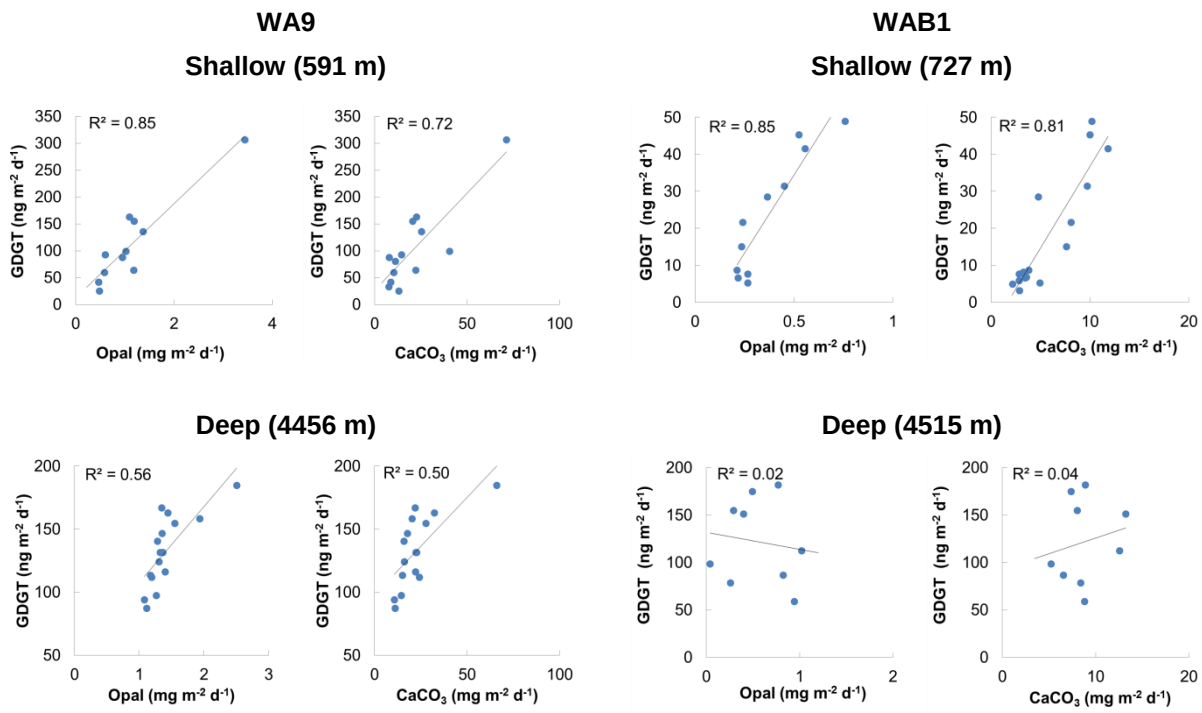

Figure 4.3 . Correlations of GDGT flux with opal and carbonate fluxes at the shallow and deep traps of the sites WA9 (left panel) and WAB1 (right panel).

4.4.2 WAB1

4.4.2.1 Mass and GDGT s fluxes

Mass fluxes at the southern site WAB1 (11.5° S) range between 3.7 and 19.3 mg m^{-2} d^{-1} and between 4.6 and 18.5 mg m^{-2} d^{-1} at the shallow (727 m) and deep trap (4515 m), respectively (Figure 4.4b, e). Multiple peaks occur in late February to April, August, November 1997, and March 1998 at the shallow trap while the changes in mass fluxes are rather smoothed at the deep trap with a maximum in June 1997. Mass fluxes are dominated by carbonate accounting for 37−68% of mass flux at the shallow trap and 66−79% at the deep trap. Over the trap deployment period, GDGT fluxes are higher in the deep trap (58.9−181.9 ng m^{-2} d^{-1}) than in the shallow trap (3.1−48.9 ng m^{-2} d^{-1}) (Figure 4.4c, f). Maxima in GDGT flux occur when mass fluxes are enhanced at the shallow trap while they are not paralleled by mass flux maxima at the deep trap. GDGT flux is correlated with opal (R^2 = 0.85) and carbonate (R^2 = 0.81) fluxes at the shallow trap (Figure 4.3). At the deep trap, no correlations between GDGTs and other components are found (Figure 4.3; R^2 = 0.02 for opal, R^2 = 0.04 for carbonate).

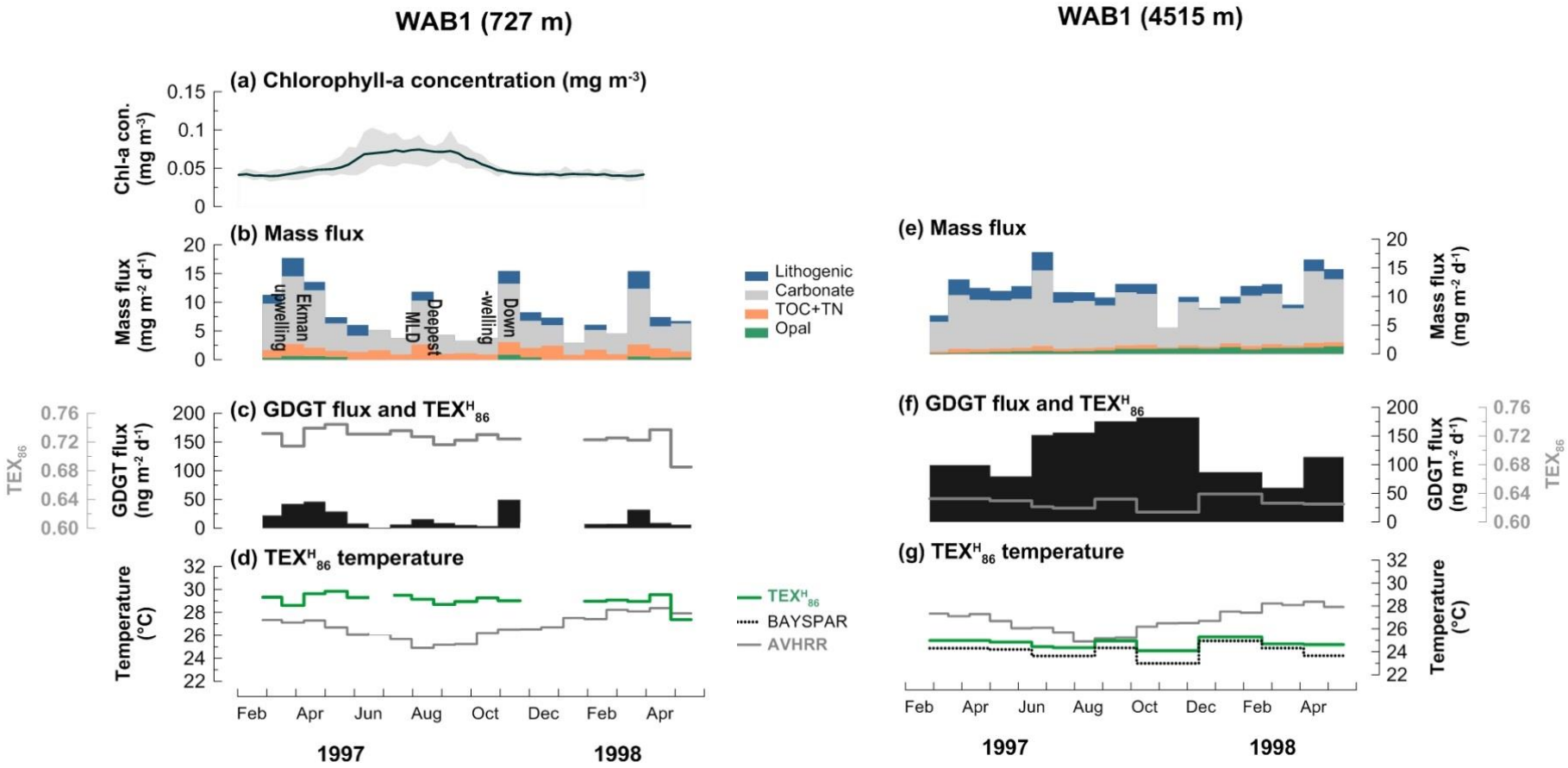

Figure 4.4 Changes in (a) satellite-derived chlorophyll-a concentration, (b, e) mass flux, (c, f) GDGT flux and TEX_{86}, (d, g) TEX_{86}^{H}-derived temperatures in sinking particles collected at the shallow (at 727 m, on the left panel) and at the deep trap (at 4515 m, on the right panel) of WAB1 in the oligotrophic Brazil Basin. Note that the Y-axis scale of each parameter is the same between the shallow and deep traps.

4.4.2.2 TEX_{86}^{H} estimations

At the shallow trap, TEX_{86} values range between 0.69 and 0.74 (Figure 4.4c). TEX_{86}^{H} -derived temperatures vary between 27.4 and 29.8 °C while the satellite-derived SSTs change between 24.9 and 28.4 °C when daily satellite SSTs are averaged according to the periods of each sample cup (Figure 4.4d). BAYSPAR SSTs exhibit higher temperatures (28.1−34.1 °C) compared to the TEX_{86}^{H} calibration (not shown). At the deep trap, TEX_{86} values vary between 0.61 and 0.64 and the TEX_{86}^{H}-derived temperatures range between 24.1 and 25.3 °C (Figure 4.4f, g). The Flux-weighted mean TEX_{86}^{H} temperatures are 29.2 °C and 24.6 °C at the shallow and deep trap, respectively. The TEX_{86}^{H}-derived temperature in the underlying surface sediment (GeoB 5201-8; 28.5° W, 11.5° S) of the WAB1 trap is 24.7 °C (Table 4.1).

4.5 Discussion

4.5.1 Flux: seasonal mesotrophic (WA9) vs. oligotrophic (WAB1) condition

Seasonal variability in mass and GDGT fluxes are more pronounced in the shallow traps at both sites WA9 and WAB1, with more smoothed patterns at both deep traps compared to the shallow ones (Figure 4.2 and 4.4). The relative mass and GDGT fluxes are higher at site WA9 than at site WAB1 by a factor of 2.5 (Figure 4.2 and 4.4). No big difference in the GDGT fluxes are found between deep traps, but the GDGT flux recorded in the shallow trap at WA9 was almost 5 times higher than the one at WAB1 (Figure 4.2c and 4.4c). This might be due to the different oceanographic regimes of the two sites; WA9 was moored in near the boundary region of the oligotrophic gyre while the WAB1 trap was located more towards the gyre interior (Table 4.1). When the SEC is enhanced by the seasonal trade wind near the equator in austral winter, a deepened mixed layer and relatively higher primary production can be found across the Atlantic expanding from the east to the west as a result of the upwelling (Figure 4.1). This could lead the enhanced nutrient supply into surface waters at site WA9 stimulating primary production in the euphotic zone and, hence, export of the organic matter (Figure 4.2b, c). The seasonal lateral nutrient inflow at the gyre fringe is a well-known mechanism in the oligotrophic gyre (McClain et al., 2004). Instead, the more often enhanced fluxes in mass and GDGTs recorded at the shallow trap of the more southern location of WAB1 show the dynamics of physical forcing and biological response in the gyre center; the seasonal production in March when the Ekman upwelling occurs, in August when the mixed layer is deepest, and in October-November when the downwelling is strongest (Figure 4.4b, c) (McClain et al., 2004).

The Chl-a concentration averaged over 2001-2010 also showed the seasonal maxima in austral winter time at both trap locations (Figure 4.2a and 4.4a) with relatively higher concentrations at WA9 than at WAB1. Although the Chl-a concentration is extracted from 2001−2010 due to the

unavailability of Chl-a data for most of the trap sampling time (only available from September 1997), different from the exact period of the trap deployment, a 10 years period can probably show the general seasonal variation of this parameter in these regions. Some studies use Chl-a concentration in the surface water of the tropical ocean to define the level of productivity; oligotrophic (Chl-a <0.1 mg m^{-3}), mesotrophic (0.1 < Chl-a < 1 mg m^{-3}), eutrophic (1 < Chl-a < 10 mg m^{-3}) condition (Franz, 2012; Vedernikov et al., 2007). As shown in Figure 4.2a and Figure 4.4a, most of Chl-a values in austral winter fell in the range of mesotrophic conditions at site WA9 while stayed below 0.1 mg m-3 assigned to oligotrophic conditions at site WAB1. This allows site WA9 to be described as being seasonally mesotrophic.

At the seasonally mesotrophic northern site WA9, a notable seasonal peak of GDGT flux in July 1996 co-occurs with a mass flux maximum at the shallow trap and with a coeval slight increase at the deep trap (Figure 4.2c, d, f, g). A co-variation of GDGT flux with opal and carbonate flux with good correlations (R^2 = 0.85 for opal, R^2 = 0.72 for carbonate) at the shallow trap and relatively weaker correlations at the deep trap (R^2 = 0.56 for opal, R^2 = 0.50 for carbonate) are observed (Figure 4.3). Several studies have reported similar results with good correlations of GDGT with total fluxes (e.g. opal, carbonate, TOC, or TN) in various oceanic regimes; in Santa Barbara Basin (with total flux; Huguet et al., 2007), in the western North Pacific (with OC, opal, and lithogenic material; Yamamoto et al., 2012), in the Cariaco Basin (with TOC and carbonate; Turich et al., 2013), off northwest Africa (with TOC and opal; Mollenhauer et al., 2015), in the eastern Indian Ocean (with opal and carbonate; Chen et al., 2016), and in the equatorial Guinea Basin (with opal; Park et al., 2018). By contrast, a recent study by Richey and Tierney, (2016) using a mooring system found no correlation between GDGTs and TOC or mass flux in the northern Gulf of Mexico.

Strong correlations of GDGT flux with opal (R^2 = 0.85) and carbonate flux (R^2 = 0.81) are also observed at the shallow trap of the southern more oligotrophic site WAB1 while no correlations are found between the respective fluxes at the deep trap (Figure 4.3). Our results support previous findings that opal- and carbonate-rich aggregates play an important role in transporting GDGTs from the upper water column, where lipids are produced and aggregates formed, to the deep waters. However, it is unclear at this stage what causes the weak correlations at the deeper traps (4456 m for WA9; 4515 m for WAB1) and how GDGTs are exported to deep waters (below the depth of the shallow trap) at both study sites (Figure 4.3).

At the oligotrophic site WAB1, given the higher mass and GDGT fluxes at the deep trap relative to the shallow one and the lack of correlation between them (Figure 4.3), a significant contribution of allochthonous sinking particles from regions with relatively higher productivity to the deep sediment trap could explain the observations. The deep trap likely has a wider catchment area than the shallow trap. Higher fluxes at deeper depth traps have been observed in other ocean regimes before; in the

eastern Atlantic (Fischer and Wefer, 1996), in the Porcupine Abyssal Plain (Lampitt et al., 2001), in the Arabian Sea (Wuchter et al., 2006b), in the eastern Fram Strait (Lalande et al., 2016), and in the equatorial Guinea Basin (Park et al., 2018). By using the concept of "a larger catchment" (the statistical funnel) with increased depth (Siegel and Deuser, 1997), Lampitt et al., (2001) suggest that catchment of a trap moored at 3,000 m could include the primary production from the euphotic zone covering a diameter of 400 km. Thus, a larger catchment seems a reasonable scenario for explaining the higher flux at the deeper ocean with little or no reflection of seasonal production in the directly overlying water layers at site WAB1. However, this scenario would be realistic only if this large catchment includes regions with higher productivity around the trap site, which is not the case in the oligotrophic center.

There are two approaches to calculate a sinking rate of particles in the water column using parameters measured in the sediment mooring system. In the first one, used when there is no time delay between peaks in mass flux between two traps, the distance between traps is divided by half the sampling interval (Fischer and Karakaş, 2009 and reference therein). In the second approach applied when SST and proxy-based temperature estimates exhibit a pronounced seasonality, sinking rate is determined by the time delay between the satellite-derived SST and the estimated temperature based on the lipid proxies (e.g. $U^{K'}_{37}$ or TEX_{86}) in sinking particles (e.g., Mollenhauer et al., 2015). Using the first approach, the minimum sinking rate of particles between two traps moored at two depths (591 m and 4456 m) at site WA9 is approximately 454 m d^{-1} (3865 m/ (17/2) days). Compared with values published by Fischer and Karakaş, (2009), this is the second highest after the one determined for the equatorial area in the Atlantic Ocean (see table 1 in Fischer and Karakaş, (2009)). Moreover, it is around 1.6-2.6 times higher than the ones in the following years at an almost identical location (Fischer and Karakaş, 2009). The same approach is not applicable at site WAB1 due to the absence of covariance in respective fluxes between the two traps and the different depths (Figure 4.4). The relatively higher sinking rate at WA9 in the Atlantic Ocean can be partly explained by the increasing sinking rate of particles with depth (Berelson, 2002) and/or the carbon-dominated environment (Iversen and Ploug, 2010). However, the former explanation was questioned later by Xue and Armstrong, (2009). For the latter explanation, Fischer and Karakaş, (2009) did not find a statistically significant relationship between carbonate content and particle sinking rate in the Atlantic Ocean, even though a relatively higher sinking rate in carbonate-rich aggregates than in opal-dominated ones was confirmed in laboratory experiments (Iversen and Ploug, 2010).

In summary, the different seasonal oceanographic forcing and biological response between the two locations (WA9 in the fringe of the gyre system and WAB1 in the center of the gyre) are reflected in mass and GDGT fluxes.

4.5.2 Seasonality of TEX_{86}^{H}-derived temperatures

TEX_{86}^{H}-derived temperatures in sinking particles at both sites WA9 and WAB1 vary within a relatively narrow range over the deployment time (Figure 4.2d and 4.4d) without clear seasonality. At the shallow trap of the seasonal mesotrophic site WA9, the TEX_{86}^{H}-derived temperatures mostly reflect the SSTs with warm-biases relative to the satellite-derived SSTs between mid-August and October when the SSTs reach their seasonal minimum (Figure 4.2d). Yet, the maximum temperature bias (2 °C) is within the TEX_{86}^{H} calibration error (Kim et al., 2010). At the shallow trap of the more oligotrophic WAB1 site, the TEX_{86}^{H}-derived temperatures are consistently warmer than the satellite-derived SST, except for the last sample (Figure 4.4d). The temperature differences between the estimated and measured ones are maximized (~4.2 °C) during austral winter. Unlike in the shallow traps, the TEX_{86}^{H}-derived temperatures are colder than the satellite-derived SSTs in the deep traps of both WA9 and WAB1 sites, with the smaller temperature biases occurring towards the cold season (Figure 4.2g and 4.4g).

There are a number of GDGT-based indices, including BIT index (Weijers et al., 2006), MI (Zhang et al., 2011), %GDGT-0 (Inglis et al., 2015), and $|\Delta RI|$ (Zhang et al., 2016), which were developed to obtain information on the occurrence of non-temperature-associated effects on TEX_{86} thermometry. At our sites, the BIT values, assessing the contribution of soil-derived GDGTs, as expected are far below the threshold (<0.3). MI values in the deep traps of both sites exceed the defined critical value (<0.3), albeit they are still within the range (<0.36) of the ´normal marine realm´ (Zhang et al., 2011). All %GDGT-0 values, an indicator of methanogenic sources, and $|\Delta RI|$, a comprehensive index for non-thermal impact, are below the respective thresholds of 67% and 0.3. Thus, none of the indices reveal significant non-thermal effects on GDGTs in our samples. Thus, the warm and cold biased TEX_{86}^{H} records in the study seem to be derived from other processes (see below sections), which cannot be identified with these non-thermal indices.

4.5.3 Origin of TEX_{86} signal

4.5.3.1 Shallow trap: surface water column origin vs. energy stressed production

TEX_{86}^{H} temperatures are almost identical to the SSTs in the shallow trap (591 m) of the less oligotrophic northern WA9 site, while warm biased temperature estimates occur in the shallow trap (727 m) of the more oligotrophic southern WAB1 site (Figure 4.2d and 4.4d). Both results differ from other studies that showed that temperature estimates derived from the TEX_{86}^{H} calibration reflect the subsurface temperatures in the tropical oceans where the surface water column is stratified (Chen et al., 2016; Huguet et al., 2007; Kim et al., 2012; Lee et al., 2008; Lopes dos Santos et al., 2010; McClymont et al., 2012; Park et al., 2018; Rodrigo-Gámiz et al., 2015). At several locations globally,

TEX_{86} is interpreted to reflect subsurface temperatures, which is explained by the deep habitat of source organisms. This observation is in agreement with the physiological and biological characteristic of planktonic Thaumarchaeota in the ocean. As Thaumarchaeota are ammonia-oxidizing Archaea (Könneke et al., 2005), maximum GDGT concentration and thaumarchaeal abundances, as well as maximum copy numbers of 16S rRNA genes and the ammonia monooxygenase enzyme (amoA), are often found toward the depth of maximum NO_2^- concentration near the base of the euphotic zone (Basse et al., 2014; Church et al., 2010; Horak et al., 2013; Karner et al., 2001; A. E. Murray et al., 1999; Santoro et al., 2010; Schouten et al., 2012; Turich et al., 2007). Park et al., (2018) found that the TEX_{86}^H-derived temperature in sinking particles of the equatorial Guinea Basin is similar to that in the water depth where the nutricline exists. However, these findings do not apply to the shallow traps in our study regions, where TEX_{86}^H-derived temperatures reflect ma SST, or they are warm-biased.

Instead, similar observations to the shallow trap of site WA9 were made in the other oligotrophic regions. In the oligotrophic northeastern Pacific Ocean, warm biased TEX_{86} temperatures in the larger fraction (>300 μm) of suspended particulate matter (SPM) and relatively colder TEX_{86} temperatures in smaller fraction were found, while the average temperature of both fractions resembles ma SST of the region (Wuchter et al., 2006b). In the offshore oligotrophic Gulf of Mexico, the four-years flux-weighted mean TEX_{86}^H-derived temperature in sinking particles is similar within the calibration error (± 2.5 °C; Kim et al., 2010) to the ma SST and in the surface sediment (Richey and Tierney, 2016). A previous study conducted in the South Atlantic gyre explains the relatively higher TEX_{86} values we observe at the shallow trap of site WAB1 under oligotrophic conditions: Hurley et al. (2018) examined suspended particles collected from the water column and at their station 7 with oligotrophic conditions, which is close to our study site, found that the TEX_{86}^H-derived temperatures reached the warmest values (>31.0 °C) at 250-349 m depth in two different size fractions (0.3−0.7 and 0.7−53 μm; only core (CL)-GDGTs are considered). Throughout the water column, the concentration- and depth-integrated average of TEX_{86}^H-derived temperature (125−498 m) was found to be 29.9 °C, which is approximately 10 °C warmer than measured overlying SST (see Hurley et al., 2018). This observation agrees with the warm biased TEX_{86}^H-derived temperatures we found in particles collected in the shallow trap (727 m) of WAB1. Indeed, the high affinity of Thaumarchaeota to ammonia allows them to adapt to low ammonia environments (Horak et al., 2013; Könneke et al., 2005; Martens-Habbena et al., 2009); however, the TEX_{86} values (i.e., warmer TEX_{86}-derived temperatures) were found to be higher at low ammonia oxidation rates in continuous culture experiment of marine ammonia-oxidizing Archaea than in the control experiments (Hurley et al., 2016). The ring index (RI; Zhang et al., 2016), the weighted average of cyclopentane moieties, revealed the same trend as the ammonia oxidation rate decreased. These field and laboratory studies therefore suggest that relatively

high TEX_{86} signals are to be expected in such energy limited environments, which has important implications for the interpretation of TEX_{86}-derived temperature estimates in oligotrophic gyre centers.

A vertically diversified archaeal community may also lead to different responses to environmental conditions like temperature, resulting in unconventional TEX_{86} thermometry (Agogué et al., 2008; Ingalls et al., 2006; Sintes et al., 2016, 2013). Ingalls et al., (2006) and Sintes et al., (2013) observed distinguishable thaumarchaeotal ecotypes by depth. Taylor et al., (2013) and Hernández-Sánchez et al., (2014) found that the GDGT [2]/[3] ratio increases with depth in SPM of water column samples and in marine sediments, revealing increasing input of GDGTs produced in the deep water with depth.

We modified the cross plots of GDGT [2]/[3] ratios versus depth after Taylor et al., (2013) using the latest TEX_{86} global data collection of Tierney and Tingley, (2015) and SPM data from the Arabian Sea, Black Sea, Bermuda, Equatorial Pacific, Southwest Atlantic oceans, and Northwest Africa (Basse et al., 2014; Hernández-Sánchez et al., 2014; Hurley et al., 2018; Schouten et al., 2012; Turich et al., 2007; Wakeham et al., 2003) (Figure 4.5). For 784 of the total 1095 data points both GDGT-2 and -3 fractional abundances are available. Within this newly compiled dataset, the maximum GDGT [2]/[3] value is 24.3, and approximately 90% of the data points display GDGT [2]/[3] ratios below 10.

The range of GDGT [2]/[3] ratios is wider and values are higher in SPM samples than in sediments (Figure 4.5). In the Arabian Sea, Northwest Africa, Southwest Atlantic Ocean (Basse et al., 2014; Hurley et al., 2018; Schouten et al., 2012), where both IPL- and CL-GDGTs have been analyzed in the same SPM samples, the bigger excursion of GDGT [2]/[3] ratios with depth occur in the IPL-GDGTs, representing the GDGTs recently produced by the deep archaeal community (Schouten et al., 2012) (Figure 4.5). A similar trend is observed in SPM samples of the West Atlantic ocean (Hurley et al., 2018). Although it is not clear yet what causes the change in GDGT [2]/[3] ratio with water depth, this ratio distinguishes between the longer time period and spatially integrated signals in sediments with relatively lower GDGT [2]/[3] values and the rather "freshly" produced GDGTs in SPM with higher GDGT [2]/[3] values. These studies support that the composition of GDGTs derived from *in situ* production in the deeper ocean differs from surface-derived material with a potentially important effect on TEX_{86}values, in particular in oligotrophic settings, where vertical export from the near surface is lower than in eutrophic and mesotrophic oceans.

The GDGT [2]/[3] ratios of the shallow traps (WA9 and WAB1) are relatively close to the ones of SPM samples, while the ones in the deep traps are more similar to ratios observed in surface sediments (Figure 4.5). Especially, the shallow trap of WAB1 from the center of the oligotrophic gyre is closer to the range of GDGT [2]/[3] ratios in SPMs than the one of WA9.

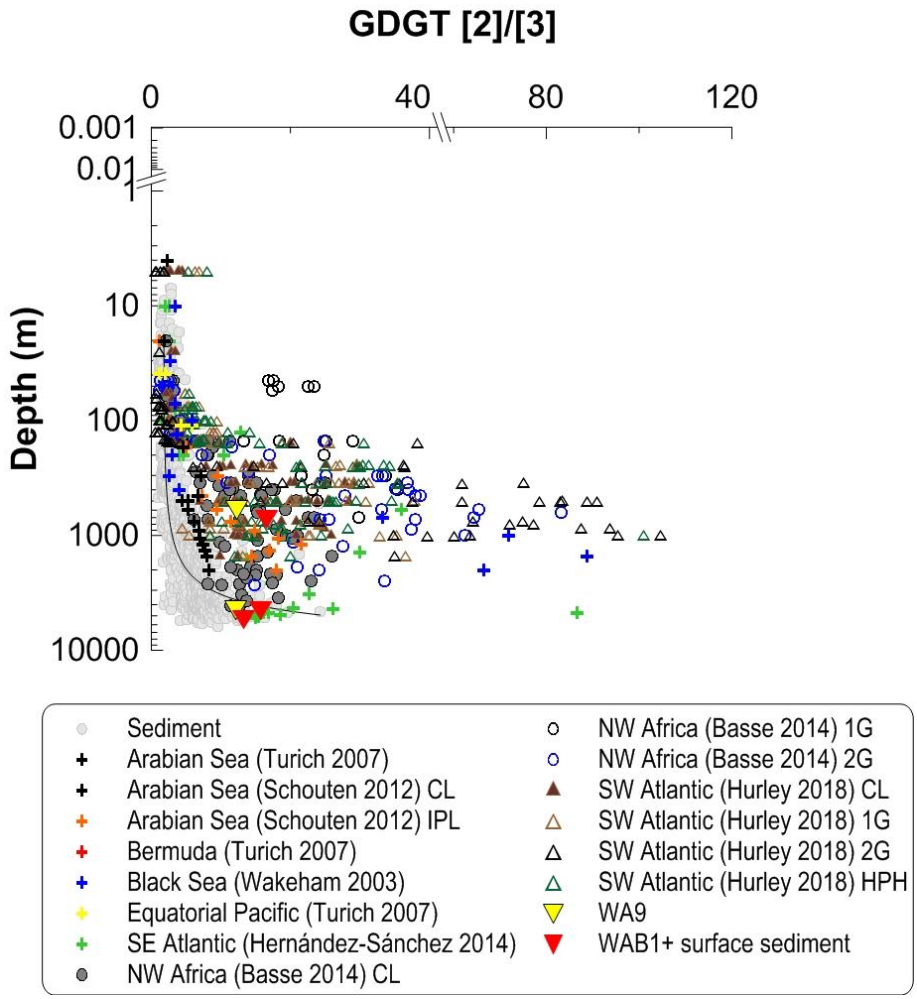

Figure 4.5 Cross plots of GDGT [2]/[3] ratio against water depth adapted after Taylor et al., (2013). The grey symbols represent the latest global core-top TEX_{86} dataset (Tierney and Tingley, 2015 and references therein). Crosses represents the GDGT [2]/[3] ratios determined in suspended particulate matter from the Arabian Sea (black), Bermuda (dark brown), and Equatorial Pacific ocean (yellow) (Turich et al., 2007), Arabian Sea (Schouten et al., 2012; black for CL-GDGTs and orange for IPL-GDGTs), Black Sea (Wakeham et al., 2003; blue), Southeast Atlantic ocean (Hernández-Sánchez et al., 2014; green), Northwest Africa (Basse et al., 2014; desert blue). Brown circles represent the ratios in the West Atlantic Ocean (Hurley et al., 2018; empty one for CL-GDGTs and filled one for IPL-GDGTs). Red triangles represent the ratios in the two traps (727 and 4515 m) and on the underlying sediment (GeoB 5201-8; 5461 m) of site WAB1 and yellow ones in two traps (591 and 4456 m) of site WA9. Note that ratios in IPL-GDGTs are available only in the Arabian Sea and West Atlantic Ocean while the remaining ratios were determined on core lipids only.

Thus, a large proportion of GDGTs derived from the ´fresh´ *in situ* GDGTs produced under energy stress conditions at site WAB1 is a plausible explanation for the observed relatively warm TEX_{86}^{H} temperature estimates, despite the absence of direct evidence (i.e., IPL-GDGTs data) in our traps. However, it still needs to be confirmed to which proportion the CL-GDGTs analyzed in our study are derived from ´fresh´ *in situ* production.

4.5.3.2 Deep trap: water column integrated TEX_{86}^{H} signals with a dominant deep *in situ* production

When the TEX_{86} signals at different depths are almost identical, it would be reasonable to argue that they are originated from the same source. However, this is not the case at both sites WA9 and WAB1 as TEX_{86}^{H}-derived temperatures at the deep traps are colder than those estimates at the respective shallow traps and SSTs (see section 4.5.3.1; Figure 4.2d, g and 4.4d, g). Lateral advection could account for differences in the proxy signals at depth, but GDGTs have been found to be less susceptible to lateral transport than other lipid biomarkers (Mollenhauer et al., 2008; Shah et al., 2008). As elaborated above, a variable archaeal source of GDGTs throughout the water column is evident from the GDGT [2]/[3] ratios by depth at both study locations (see section 4.5.3.1).

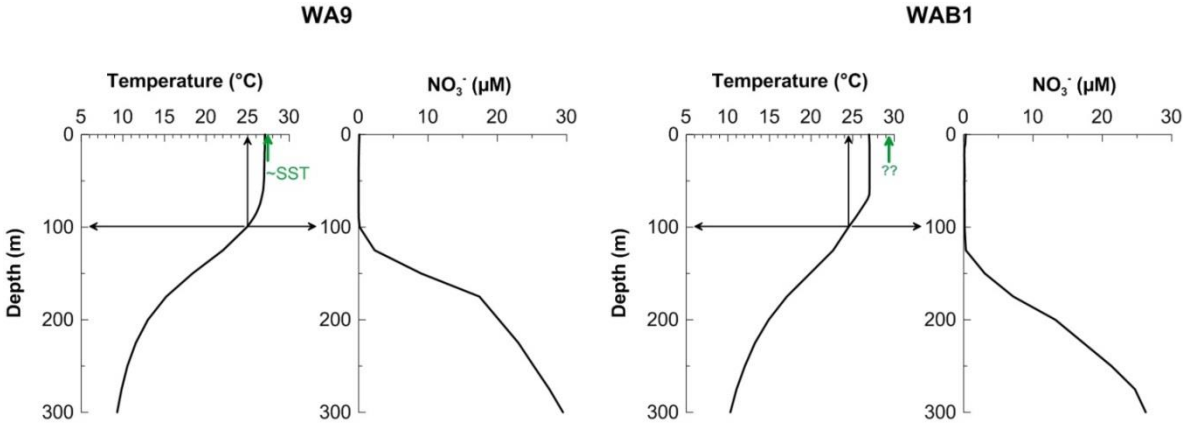

Figure 4.6 Depth profile of mean annual water temperature and nitrate concentration extracted from WOA13. Green arrows represent the flux-weighted mean TEX_{86}^{H}-derived temperatures in the shallow traps of site WA9 (27.4 ℃) and WAB1 (29.2 ℃), respectively.

We compare the flux-weighted mean TEX_{86}^{H} signal of each deep trap, which is averaged over the trap deployment period, with the depth profile of temperature and nitrate concentration to determine the potential depth of GDGT origin (Table 4.1, Figure 4.6). The flux-weighted mean TEX_{86}^{H}-derived temperature of the deep trap of WA9 is 24.9 °C, corresponding to the water temperature at 100 m depth (Table 4.1, Figure 4.6). In the seasonal mesotrophic site WA9, the nutricline occurs at around 100 m depth, above which temperatures remain relatively uniform. In analogy to other studies, the observed TEX_{86} signal is in agreement with a preferential habitat of Thaumarchaeota near 100 m depth (Meyer et al., 2016; Park et al., 2018; Seki et al., 2014). However, the discrepancy of TEX_{86}^{H} signals between 591 m and 4456 m depth traps is different from other observations, which show similar temperature estimates at multiple depths (Park et al., 2018; Wuchter et al., 2006; Yamamoto et al., 2012). The question arises why this subsurface TEX_{86}^{H} signal at the deep trap is not captured in the

shallow trap, which was deployed at far below (591 m) than the putative depth habitat of the main GDGT source (~100 m).

Active zooplankton migration can be invoked to explain the GDGT transport mechanism bypassing the shallow trap and exporting directly to the deep trap. Diel zooplankton migration is a daily pattern of vertical movement feeding in surface water at night, returning to the depth at dawn, and releasing fecal pellets in deep waters (Lampert, 1989). This scenario would be plausible only if zooplankton migrates to a depth below 591 m and excrete their pellets. Indeed, Isla et al., (2015) observed a significant contribution of total carbon flux through 500 m depth in the northwest Mediterranean. In a recent study in the Atlantic oligotrophic zone near our trap site, the active zooplankton migration was also found in lower mesopelagic layers (500−800 m; Bode, (2018)). However, the authors suggest that zooplankton feeding occurs even below these water masses based on the nitrogen isotope values, which would not carry the subsurface particles containing GDGTs from 100 m depth. Accordingly, such an active migration occurring in deep waters does not seem to explain the bypassing export scenario of GDGTs. Thus, it will remain unresolved if GDGTs in deep waters are originated from 100 m water depth until the export mechanism of GDGTs is clearly identified.

Lateral input or selective degradation is often suggested to result in alteration of organic proxy signals. However, both scenarios are not relevant to the TEX_{86} signal, which rather mirrors a local signal and has been found not to be affected by the selective degradation (Lengger et al., 2012; Mollenhauer et al., 2008). Although it remains unclear how a subsurface temperature signal is directly exported to deep waters, a subsurface temperature record is also found in the neighboring surface sediment (GeoB2212-1; 4.032° S, 25.623° W). In the surface sediment, TEX_{86}^{H}-derived temperature (22.1 °C) is approximately 4.6 °C colder than the SST (26.7 °C) of the location (data can be found in Kim et al., (2010)'s global dataset).

Similar flux-weighted mean TEX_{86}^{H}-derived temperatures at the deep trap of WAB1 (24.6 °C) and in the underlying surface sediment (24.7 °C; GeoB 5201-8 at 28.52° W, 11.53° S) were observed coincident with the water temperature at 100 m depth (Table 4.1). The above approach for the origin of TEX_{86}^{H} signals cannot be put forward for the deep trap of site WAB1 as well, where the preferred depth habitat inferred from the temperature estimates of ~100 m is shallower than the deep chlorophyll maximum (~125 m) and nutricline (~120 m) in the region. It is hard to imagine that Thaumarchaeota as ammonia oxidizer dwell at water depths, where the energy source is scarcely available (Figure 4.6). Field studies using radiocarbon of GDGTs and culture experiments have revealed that Thaumarchaeota are chemoautotrophs (Francis et al., 2005; Ingalls et al., 2006; Könneke et al., 2005; Pearson et al., 2001; Wuchter et al., 2003). Compound-specific radiocarbon data of GDGTs and an isotopic mass balance model showed that most GDGTs derive from autotrophic *in situ*

production (~83%) and only 15% are directly exported from the surface at 670 m water depth in the oligotrophic North Pacific (Ingalls et al., 2006). With a high contribution of *in situ* production at 670 m depth, the TEX_{86} temperature is only 3 °C colder than SST and far warmer than the actual temperature at 670 m, implying a different physiological response of mesopelagic Thaumarchaeota to surrounding water temperature. In the oligotrophic Atlantic water, TEX_{86}^{H} temperatures based on CL-GDGTs in SPM decreased below 250 m depth, while the estimates based on the combined (CL+IPL)-GDGTs yield far colder temperatures below 500 m due to significantly cold-biased TEX_{86}^{H} temperatures in IPL-GDGT fractions with hexose (1G) and hexose-phosphohexose (HPH) head groups (Hurley et al., 2018). If both studies are representative of oligotrophic conditions, we would assume that the relatively colder TEX_{86}^{H} based temperature estimates in the deep trap than in the shallow trap are a consequence of combined rather ´cold and dominant´ *in situ* GDGT production and relatively ´warm and less dominant´ GDGTs originated from the upper water column. This explanation may be also applicable for the deep trap of the seasonally mesotrophic site WA9. In both deep traps of WA9 and WAB1, the discrepancy between the TEX_{86}^{H} estimate and SST is minimized when chlorophyll-a concentration and GDGT flux are relatively enhanced (Figure 4.2a, g and 4.4a, g). It may show that the proportional GDGT input carrying warmer signals produced in upper waters to deep waters increases in that season. The decoupling of mass and GDGT flux pattern between the shallow and deep traps, the lack of correlation between GDGT and opal/carbonate and the observed GDGT [2]/[3] ratios also support distinct GDGT sources at depth compared to the shallow trap. Hurley et al. (2018) could calculate the export depth of GDGTs as the depth where integrated GDGT [2]/[3] values between the NO_2^- maximum depth and deeper water column agree exactly to the one in the sediment. The deepest export depth (135−180 m) is estimated for their most oligotrophic station, which coincides with the maximum GDGT concentration. This model might be suitable to reconstruct the major export depth of GDGTs. However, it needs to be considered that this water column study is only a snapshot time representing a day of sampling, while sediment reflects a longer time period. Additionally, the authors calculated TEX_{86} values in the combined (IPL+CL)-GDGT fraction even though the TEX_{86} global calibration is considered only CL-GDGTs and the proportional contributions of IPL-GDGTs in SPM and their associated TEX_{86} values have not been well constrained.

Although further investigations need to distinguish the origin of GDGTs captured in the shallow and deep waters in the central Brazil Basin, TEX_{86}^{H} signals from the upper water column do not appear in deep waters; instead cold-biased temperature estimates are dominant in deep waters. In the tropical oceans near the equator (between 5° N to 10° S), a total 123 of TEX_{86}^{H} values are available in the latest global calibration dataset (Tierney and Tingley, 2015). In agreement with our findings, most of these TEX_{86}^{H}-derived temperature estimates are colder than SSTs (n = 114), and only a few are almost identical to SSTs (n = 6).

4.5.4 BAYSPAR SST

The BAYSPAR (Tierney and Tingley, 2015) calibration model yields significantly different temperatures between particles collected at different depths and locations investigated in this study. At the shallow traps of both sites WA9 and WAB1, the BAYSPAR SSTs are remarkably warmer than the satellite-derived SST and TEX_{86}^{H}-derived temperatures (30.3−33.7 °C for WA9 and 29.1−31.4 °C for WAB1; not shown in the figure). At the deep trap of site WA9, the BAYSPAR calibration yields warm-biased temperatures in mid-June−November 1996 compared to the satellite-derived SST (Figure 4.2f), while they resemble the SSTs in remaining season. The BAYSPAR SSTs are similar to the TEX_{86}^{H} estimates at the deep trap of site WAB1 (Figure 4.4f). Warm-biased SST estimates based on BAYSPAR were also observed in sinking particles of the equatorial Guinea Basin (Park et al., 2018). In the oligotrophic northern Gulf of Mexico, the BAYSPAR SST in sinking particles varied within the range of SSTs, but resembled more the colder temperatures. Park et al., (2018) suggested that the reason of the warm bias based on the BAYSPAR SST calibration is due to the lack of reference points within a 20° × 20° grid box, which is defined for spatial dependence. Site WA9 is located within the calibration box, which covers the equator and further northern regions, with several data points. Due to the scarcity of data within, and the large size of, the calibration box, we assume that this grid box does not generate representative regression parameters for site WA9, which was situated in the fringe of the oligotrophic gyre.

4.6 Conclusion

Two time-series records of sinking particles collected in the central Brazil Basin reveal distinguishable variability in mass and GDGT flux according to the oceanographic setting. Mass and GDGT fluxes at 7.5° S at the seasonally mesotrophic WA9 station are higher than at site WAB1 at 11.5° S in the center of the oligotrophic gyre. At the shallow and deep trap of WA9, mass and GDGT flux both were enhanced in the winter time when the trade wind induced upwelling introduced nutrients into the system along the fringe of the gyre. At site WAB1, the variability of mass and GDGT flux displayed the biological response of seasonal oceanographic features like the Ekman upwelling, the deepened mixed layer, and downwelling. At the shallow traps of WA9 and WAB1, a good correlation between GDGT and opal flux suggests that GDGTs are preferably incorporated into opal-rich aggregates and transported to deep waters.

TEX_{86}^{H}-derived temperatures estimates obtained from sinking particles collected at 591 m agree well with the satellite-derived SSTs at site WA9. This coincides with the input of nutrients directly prompted by the change of surface oceanographic forcing, the consequent GDGT production and thus the export of a surface-derived TEX_{86} signal. At 727 m of WAB1, the TEX_{86}^{H}-derived temperature estimates for sinking particles are consistently warmer than the satellite-derived SSTs. This

observation is in agreement with the response of Thaumarchaeota producing GDGTs with increased TEX_{86} ratios under energy stress conditions. In the deep traps of both sites WA9 and WAB1, the colder TEX_{86}^{H}-derived temperature relative to SSTs may display an integrated signal of ´cold and dominant´ *in situ* production in deep waters with the surface-derived ´warm´ GDGTs. The almost identical TEX_{86} in the underlying surface sediment indicates a similar origin of GDGTs collected in the deep trap and deposited in sediments. The distinct TEX_{86} values by location and by depth are likely to be a reflection of oceanographic variables like nutrient conditions (less oligotrophic vs. oligotrophic) and an integrated signal from upper and deep waters.

Acknowledgments

We are grateful to the crews, scientists, and students, who were collecting the sediment trap samples used in this study. This project is funded through the DFG-Research Center/Cluster of Excellence “The Ocean in the Earth System” at the MARUM and supported by GLOMAR−Bremen International Graduate School for Marine Sciences, University of Bremen. The both WA9 and WAB1 trap samples and surface sediment (GeoB 5201-8) were supplied by the MARUM Centre of Marine Environmental Research at the University of Bremen. Gerhard Fischer at the University of Bremen is thanked for providing the unpublished mass flux data of WA9 and WAB1 traps.

Data availability

The data presented here will be archived on the PANGAEA database when the manuscript is submitted.

CHAPTER 5

Alkenone flux and $U^{k'}_{37}$ thermometry: comparison with TEX_{86} thermometry

5 Manuscript IV

Alkenone flux and the $U^{k'}_{37}$ thermometry: comparisons with the TEX_{86} thermometry

Eunmi Park[1,2,3], Jens Hefter[1], Gerhard Fischer[2,3], Gesine Mollenhauer[1,2,3]

[1]Alfred-Wegener-Institute, Helmholtz Center for Polar and Marine Research, D-27570 Bremerhaven, Germany
[2]MARUM Centre for Marine Environmental Sciences, University of Bremen, D-28334 Bremen, Germany
3Department of Geosciences, University of Bremen, D-28334 Bremen, Germany

5.1 Introduction

In previous chapters (Chapter 2, 3, 4), TEX_{86} (TEX^{H}_{86} or TEX^{L}_{86})-derived temperatures are discussed as reflecting SSTs, subsurface temperature or warm-biased temperature relative to SST in the respective regions. Variable environmental factors (e.g. nutrient distribution and level, the presence of OMZs, archaeal community structure, nutrient stress) likely play an important role in determining TEX_{86} thermometry.

Similar environmental concerns as for the TEX_{86} are also considered for the $U^{k'}_{37}$, which is based on the relative distribution of long-chain alkenones synthesized by haptophyte algae, often dominated by *Emiliania huxleyi* (see sec 1.2). Alkenone producers, haptophytes, are autotrophs which are able to produce energy using the light while planktonic Archaea, the GDGT producers, are chemoautotrophic oxidizers, which obtain energy by taking up NH_4^+. When those two proxy temperatures are compared, they are often decoupled, reflecting the different time and/or depth of the highest lipid production and export (Chen et al., 2016; Fallet et al., 2011; Jonas et al., 2017; Lee et al., 2008; Leider et al., 2010; Lopes dos Santos et al., 2013; Mollenhauer et al., 2015; Rodrigo-Gámiz et al., 2015; Rommerskirchen et al., 2011; C Turich et al., 2013). Thus, the nature of source organisms of two proxies explains parts of the discrepancy between reconstructed temperatures, although both proxy values are calibrated to ma SSTs in global calibrations.

Together with the innate biological mechanisms of those proxies, additional processes (e.g. degradation and lateral input) are also known to cause uncertainty mainly in $U^{k'}_{37}$ thermometry. In the presence of an aerobic bacterial community isolated from an *Emiliania huxleyi* culture, selective degradation of $C_{37:3}$ over $C_{37:2}$ led to the increase of $U^{k'}_{37}$ values and estimated temperatures (Rontani et al., 2005; Zabeti et al., 2010). In long-term field studies, alterations occurred only in $U^{k'}_{37}$ values

under oxic conditions, and were not detected in TEX_{86} values (Huguet et al., 2009; J.-H. Kim et al., 2009). Thus, GDGTs (TEX_{86}) are regarded to be less prone to selective degradation than alkenones ($U^{k'}_{37}$). A laterally transported allochthonous signal can overprint the local product, resulting in misleading alkenone-based temperature estimates (Benthien and Müller, 2000; Sicre et al., 2005). In contrast, lateral transport does not cause TEX_{86} biases in the sediment record (J. H. Kim et al., 2009; Mollenhauer et al., 2008).

Multiple proxy approaches provide not only independently reconstructed temperatures, but offers the advantage of complementarity between the proxies, leading to a more complete picture of the paleotemperature evolution. For instance, the relationship of $U^{k'}_{37}$ reflecting ma SST with TEX^{H}_{86} reflecting subsurface temperature were used to determine the intensity of upwelling and stratification by calculating the temperature differences between two proxies (Lopes dos Santos et al., 2010; McClymont et al., 2012). The comprehensive GDGT dataset, which is intensively discussed in previous chapters (Chapter 2, 3, 4), provide the opportunity to compare them with the $U^{k'}_{37}$-derived temperatures measured in the same sediment trap material. Here, the correlations of alkenone flux with mass flux, the maximum flux season of alkenones, and the $U^{k'}_{37}$ derived temperatures are investigated.

5.2 Methods and materials

Alkenones were extracted from the same particles used for GDGTs. Alkenone fractions are recovered by eluting DCM:Hex 2:1 (v/v) solvent with NLs throughout silica-gel column (see Section 1.8 for the lipid extraction process). To quantify the alkenones, known amounts of internal standards (nonadekan-2-one) were added to each sample before the extraction. Alkenones were analyzed using a HP-5890A gas chromatograph (GC) equipped with a DB5-MS capillary column and a flame ionization detector (FID). A gas flow rate and temperature conditions followed methods described by Chen et al., (2016). The standard deviation of a replicate analysis based on the lab-internal sediment standard was ±0.002 units of the $U^{k'}_{37}$ and 6% for alkenone concentration. $C_{37:2}$, $C_{37:3}$, and $C_{37:4}$ were integrated compared to the relative retention time of an internal standard.

U^{k}_{37}, $U^{k'}_{37}$, and $\%C_{37:4}$ indices were calculated according to Brassell et al., (1986), Prahl and Wakeham, (1987), and Rosell-Melé, (1998), respectively.

$$U^{k}_{37} = [C_{37:2} - C_{37:4}] / [C_{37:2} + C_{37:3} + C_{37:4}] \quad (1)$$

$$U^{k'}_{37} = [C_{37:2}] / [C_{37:2} + C_{37:3}] \quad (2)$$

$$\%C_{37:4} = \{[C_{37:4}] / [C_{37:2} + C_{37:3} + C_{37:4}]\} \times 100 \quad (3)$$

U^{k}_{37}, $U^{k'}_{37}$, and $\%C_{37:4}$ values were converted to temperature using the calibrations of Bendle and Rosell-Melé, (2004), Müller et al., (1998), , and Sicre et al., (2002), respectively.

$$U^{k}_{37} = 0.081(\pm0.01) \times SST\ (°C) - 0.54(\pm0.55) \quad (4)$$

$$U^{k'}_{37} = 0.033 \times SST\ (°C) + 0.044 \quad (5)$$

$$\%C_{37:4} = -3.7 \times SST\ (°C) + 43.7 \quad (6)$$

Alkenone flux is a sum of fluxes of $C_{37:2}$ and $C_{37:3}$. For the eastern Fram Strait, where $C_{37:4}$ is uniquely present in sinking particles, the alkenone flux includes all three alkenones, $C_{37:2}$, $C_{37:3}$, and $C_{37:4}$ (see Section 5.3.2.1).

5.3 Results and discussion

5.3.1 Eastern Atlantic upwelling system: the Guinea Basin and off Namibia

5.3.1.1 Guinea Basin (GBN3; 1.800° N, 11.133° W)

In the northern Guinea Basin, alkenone fluxes have relatively better correlation with $CaCO_3$ (R^2 = 0.56) at the shallow trap and with PON (R^2 = 0.65) at the deep trap rather (Table 5.1) than other components. GDGT fluxes have a good correlation with opal at both depths (Table 5.1; see Section 2.5.1), showing that opal is a major exporter of GDGTs (R^2 = 0.71 at the shallow trap and 0.62 at the deep trap;). By comparison, in the upwelling system off NW Africa, GDGT and alkenone fluxes are more strongly correlated with TOC (R^2 = 0.81 for GDGT and 0.63 for alkenone), followed by GDGT with opal (R^2 = 0.68) and alkenone with carbonate (R^2 = 0.42) fluxes (Mollenhauer et al., 2015). This implies that GDGTs and alkenones are transported into deep waters by different export mechanisms.

Table 5.1 Correlations of alkenone and GDGT fluxes with opal, $CaCO_3$, POC, PON and lithogenic component fluxes determined in sinking particles collected in the Atlantic Ocean.

R^2 Flux correlation		GBN3		LZ	[a]FEVI16	PF3		WA9		WAB1	
		853m	3921m	960m	1296m	614m	3196m	591m	4456m	727m	4515m
Alkenone	Opal	0.27	0.39	0.02	0.44	-	0.48	0.81	0.71	0.59	-
	$CaCO_3$	**0.56**	0.40	0.32	**0.71**	-	0.46	0.74	0.79	**0.81**	-
	POC	0.42	0.54	0.24	0.39	-	**0.60**	**0.93**	0.95	0.75	-
	PON	0.50	**0.65**	0.41	0.33	-	0.47	0.92	**0.97**	0.32	-
	Litho.	-	-	-	-	-	-	0.50	-	-	-
GDGTs	Opal	**0.71**	**0.62**	-	**0.82**	-	-	**0.85**	0.56	**0.85**	-
	$CaCO_3$	0.43	0.28	-	0.80	-	-	0.72	0.50	0.81	-
	POC	0.50	0.55	-	-	-	-	0.70	0.45	0.48	
	PON	0.57	0.56	-	-	-	-	0.64	-	-	-
	Litho.	-	-	-	-	-	-			-	

[a]Alkenone flux = $\sum C_{37:2} + C_{37:3} + C_{37:4}$

In the Guinea Basin, alkenone flux is higher than GDGT flux and both lipid fluxes and mass flux are relatively higher at the deep trap than at the shallow trap (Figure 5.1). Alkenone fluxes are clearly pronounced in March-April and mid-June to mid-September at both depths. GDGT flux also shows a clear seasonality at the shallow trap with multiple peaks in March-April, mid-June, and mid-August. At the deep trap, GDGT flux records minima when mass and alkenone flux decrease (Figure 5.1). It shows that the production and transport of GDGTs occur almost spontaneously when alkenones are produced and sunk into deep waters. Thus, a fast biogeochemical cycle including primary production, remineralization, ammonia release, archaeal production, the formation of aggregation with phytoplankton debris, the zooplankton grazing is expected in this upwelling system.

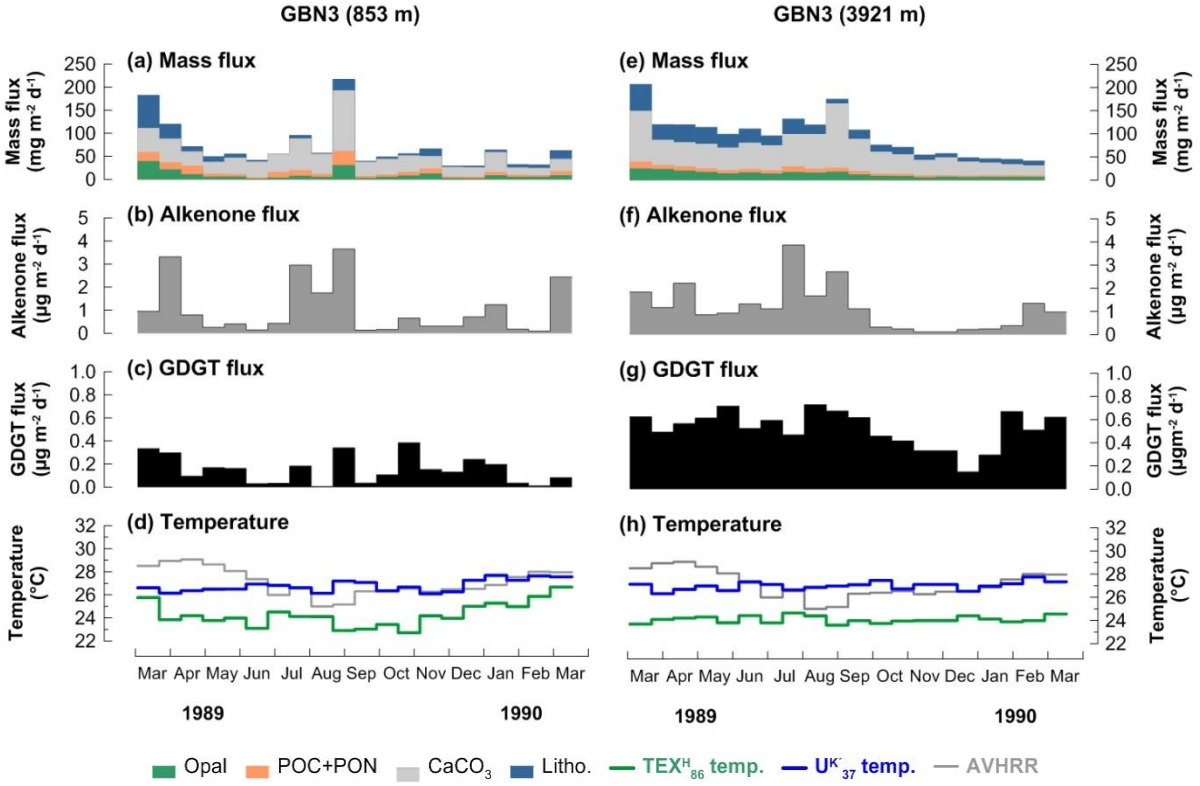

Figure 5.1 Changes in mass flux (a, e), alkenone flux (b, f), GDGT flux (c, g), and reconstructed and satellite-derived temperatures (d, h) at 853 m depth (left panel) and at 3921 m depth (right panel) in the Guinea Basin. Note that Y-axis scales are identical on the left and right panels.

No time shift of major fluxes between both depth traps indicted relatively faster sinking rates of particles in summer 1989 (~351 m d^{-1}; Fischer and Karakaş, 2009). This sinking rate can be applied for the particles alkenones and GDGTs are aggregated with. Fischer and Karakaş, (2009) reported faster sinking rates of particles nearby locations in the equator up to 530 m d^{-1}. Using the delay time of TEX_{86}^{H}-derived temperatures relative to SSTs, the sinking rate of particles carrying GDGTs is approximately 42 m d^{-1} between the depth of the major origin of the signal (~50 m) and the shallow

trap (853 m) (see Section 2.5.2). An equivalent approach is not feasible for the alkenone signal due to the lack of seasonality in the $U^{k'}_{37}$-derived temperatures. Two different approaches for assessing the sinking rate of particles do not seem to be comparable.

$U^{k'}_{37}$-derived temperatures vary in the range of 26.6−28.1 °C and 26.7−28.2 °C at the shallow and deep traps, respectively, which are continuously warmer than the TEX^{H}_{86}-derived temperatures in the traps from both depths. However, The $U^{k'}_{37}$-derived are similar to satellite-derived SSTs even though they have no seasonality. This agrees with previous findings that *Emiliania huxleyi* as major alkenone producers and autotrophs inhabit the surface waters, and thus lipid temperatures reflect SSTs (Chen et al., 2016; Fallet et al., 2011; Lee et al., 2008; Lopes dos Santos et al., 2013; Yamamoto et al., 2007). The preferential depth habitat of Thaumarchaeota, GDGT producers, governed by the nutrient distribution is probably mirrored in the TEX^{H}_{86} -derived temperature, reflecting the subsurface temperature (~50 m water depth) (see Section 2.5.2). Overall, the Guinea Basin site displays the typical lipid temperature estimates of the upwelling regions, reflecting SST in the $U^{k'}_{37}$ signal and subsurface temperatures in the TEX^{H}_{86} signal.

5.3.1.2 Lüderitz, off Namibia (LZ; 25.279° S, 13.052° E)

In the Lüderitz, maxima in alkenone and GDGT fluxes occur at different times (Figure 5.2). Alkenone flux maximum is recorded in early March, but maxima in GDGT flux occur in mid-April and mid-May. Neither alkenone nor GDGT fluxes are correlated with opal, $CaCO_3$, POC, or PON fluxes in the center of Namibian upwelling cell of Lüderitz (Table 5.1, section 2.4.2.2). Therefore, any inferences for sinking mechanisms of particles associated with alkenones or GDGTs are not available in this site.

The $U^{k'}_{37}$-derived temperatures display a 2.4 °C cold-bias in late-February and a 3.3−4.5 °C warm-bias in late-May and early-June relative to the satellite-derived SSTs. In the remaining times, the estimated temperatures resemble the SSTs. An alteration of alkenone composition is often explained by the preferential degradation of $C_{37:3}$ against $C_{37:2}$ or by lateral input. However, it is questionable if these alterations can explain such a short term period of deviation from the SST. The warm-biased TEX^{H}_{86} estimates towards the upwelling periods may be due to the production of GDGTs in the OMZs off Lüderitz, which imprints the surface signal (See Section 2.5.3; Figure 5.2). When the temporal offset of TEX^{H}_{86} estimates occur in mid-June and August-September, the $U^{k'}_{37}$-derived temperatures closely resemble the SSTs (Figure 5.2).

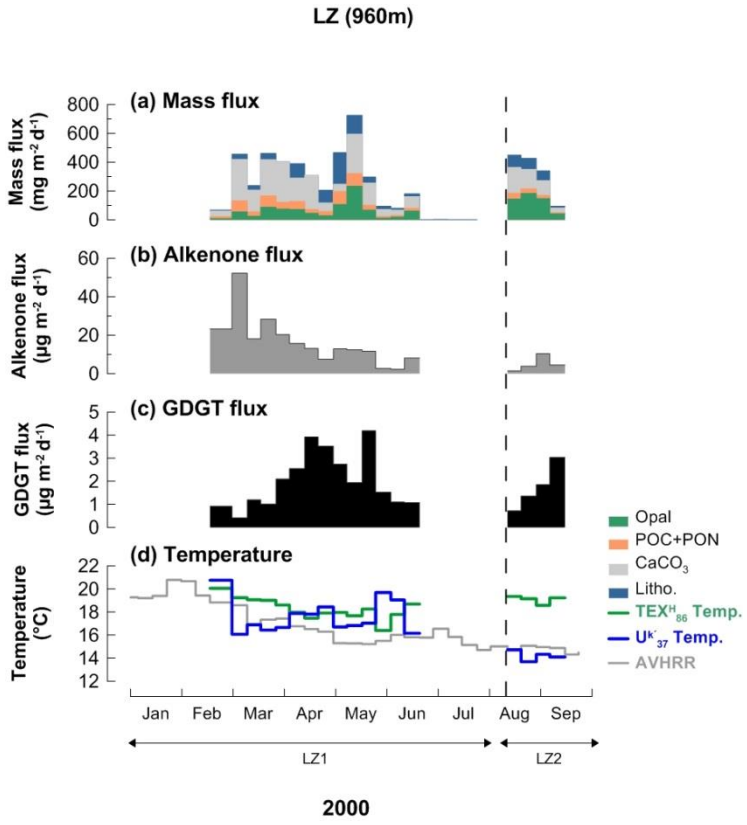

Figure 5.2 Changes in mass flux (a), alkenone flux (b), GDGT flux (c), and reconstructed and satellite-derived temperatures (d) at 960 m depth in the Lüderitz, off Namibia.

Our findings in the Lüderitz with faithful SST reflection with $U^{k'}_{37}$ and warm-biased reconstructions with TEX_{86} under the low oxygen condition are opposed to the findings in sinking particles collected in the equally oxygen deficient Cariaco Basin (C Turich et al., 2013). The authors compared temperatures based on $U^{k'}_{37}$ and TEX_{86} measured within and below the chemocline. $U^{k'}_{37}$ temperature estimates below the chemocline differed from those within the chemocline while TEX_{86} temperature estimates did not experience an alteration between the two sections of the water column. However, a permanent anoxic basin like the Cariaco Basin is not likely to be comparable with the conditions off Lüderitz, where the OMZs are seasonally present in the Lüderitz. It is assumed that the response of alkenone and GDGT producers in the Cariaco Basin, which are permanently adapted to the anoxic conditions, might be fundamentally different from those inhabiting the coastal upwelling system off Lüderitz.

Overall, both $U^{k'}_{37}$ and TEX^{H}_{86} temperature proxies reflect the SSTs, but a seasonal warm bias of TEX^{H}_{86}-derived temperature occurs when the OMZs are present. A study of a longer time scale is needed.

5.3.2 Polar oceans: eastern Fram Strait and Antarctic Polar Front

5.3.2.1 Eastern Fram Strait (FEVI16; 79.02° N, 4.35° E)

In the eastern Fram Strait, spring and summer-autumn primary production maxima are visible in mass, alkenone and GDGT fluxes (Figure 5.3). In Section 3.5.1.1, it is shown that GDGT fluxes co-vary with opal, $CaCO_3$, phytoplankton cell, and terrestrial biomarker fluxes, but are correlated differently by season, showing temporal variation of transport materials for GDGTs. Like GDGTs, biogenic and non-biogenic components can be considered as ballast materials for alkenones since both lipid fluxes have a similar seasonality. For alkenone flux, $C_{37:4}$ alkenone in addition to $C_{37:2}$ and $C_{37:3}$ are also considered since $C_{37:4}$ alkenones were identified in the eastern Fram Strait throughout the entire trap deployment period. $C_{37:4}$ alkenone accounts for 9–30% of total alkenones (the sum of $C_{37:2}$, $C_{37:3}$, and $C_{37:4}$). This alkenone compound was initially included in the temperature calibration (Brassell et al., 1986), but later was excluded due to the random presence in measured samples and the discrepancy between calibrations (Müller et al., 1998; Prahl and Wakeham, 1987; Sikes et al., 1997). However, further investigations have documented that $C_{37:4}$ is present in cold waters, while it is absent in warm waters of the North Atlantic and Nordic Sea (Bendle et al., 2005; Rosell-Melé, 1998; Rosell-Melé et al., 1995; Sicre et al., 2002). These findings agree with this study where $C_{37:4}$ is found only in the eastern Fram Strait, but not in other warm tropics (Guinea Basin, Lüderitz off Namibia, and central Brazil Basin) and cold southern oceans (Antarctic Polar Front). The alkenone fluxes are mostly correlated with $CaCO_3$ fluxes ($R^2 = 0.71$; Table 5.1). The favorable correlation of GDGT with opal and alkenone with $CaCO_3$ were also determined in the upwelling systems (NW Africa; Mollenhauer et al., (2015), Guinea Basin; see Section 5.3.1.1).

The absolute alkenone flux is higher than GDGT flux in the eastern Fram Strait (Figure 5.3). Although both lipid fluxes are pronounced in similar seasons, the maxima occur at slightly different times. The maximum alkenone flux is up to 3 times higher in summer-autumn 2007 than in spring 2008, while the GDGT flux maxima reach similar flux values in both seasons. Within the summer-autumn maxima, the GDGT peak flux appears approximately 20 days (collection time of two sample cups) after the alkenone peak (Figure 5.3). The flux values indicate new production of lipids and/or the enhanced export of lipids during the sampling period. Thus, it is reasonable to assume that the time offset between the lipid flux peaks reveal that alkenone is produced earlier than GDGT and/ or its sinking rate is faster than that of GDGT. Due to the presence of $C_{37:4}$ alkenones, it was expected that the U^{k}_{37} calibration can be used instead of $U^{k'}_{37}$ despite the fact that SSTs in the Fram Strait stays (0−4 °C) below the minimum calibration limit of the alkenone proxy (Bendle and Rosell-Melé, 2004; Sicre et al., 2002). However, both U^{k}_{37} and $U^{k'}_{37}$-derived temperatures vary between 5.3−9.4 °C, which are warmer than the satellite-derived SSTs and the TEX^{L}_{86}-derived temperatures, reflecting the water temperature at 30−80 m depth in the warm season (Figure 5.3, see Section 3.5.1).

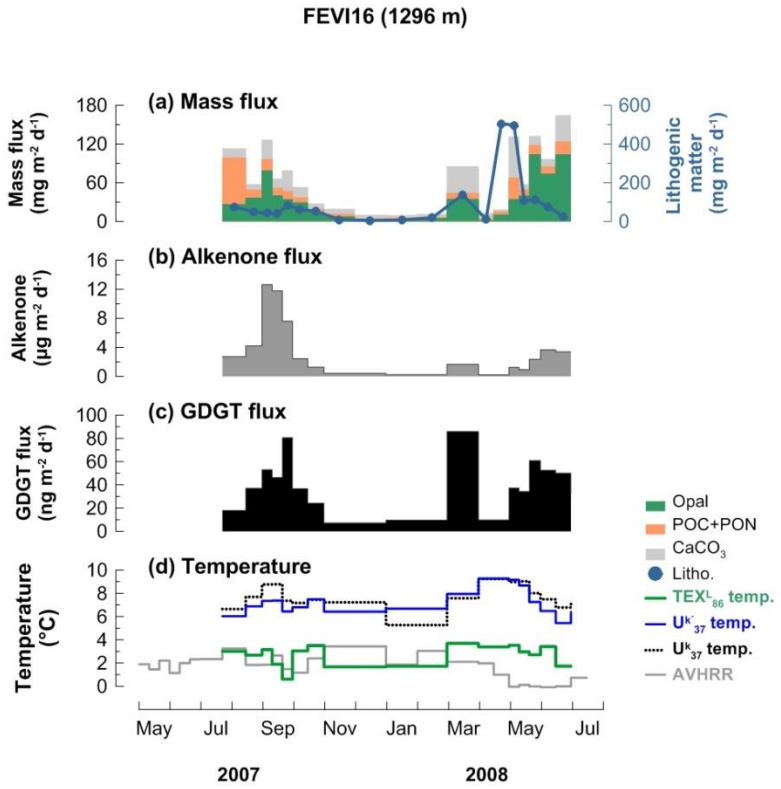

Figure 5.3 Changes in mass flux (a), alkenone flux (b), GDGT flux (c), and reconstructed and satellite-derived temperatures (d) at 1296 m depth in the eastern Fram Strait.

The reason for the warm-bias in the alkenone proxy temperatures can be found in the composition of coccolithophore species in the eastern Fram Strait and Nordic Seas. The warm water species *Emiliania huxleyi*, the primary alkenone source organism in many ocean regions, are predominant in intermediate and deep waters, where the northward current carrying warm Atlantic water flows. In contrast, the cold water species *Coccolithus pelagicus* are more dominant in surface waters, where the southward current influenced by cold Arctic water flows (Bendle et al., 2005; Lalande et al., 2016). Warm-biased temperature estimated with the U^{k}_{37} and $U^{k'}_{37}$ proxies confirms the previous finding that lateral influx of alkenones can introduce bias. Bendle et al., (2005) concluded that the relative proportion of $C_{37:4}$ in total alkenones are better for assessing the relative influence of arctic/polar versus Atlantic water masses rather than for reconstructing temperature in the Nordic Sea.

These observations confirm that the alkenone proxy is not applicable in such a high latitude region due to the significant influence of allochthonous alkenone input, while the GDGT proxy-based temperature reflects the local temperature.

5.3.2.2 Antarctic Polar Front of the Atlantic sector (PF3; 50.13° S, 5.83° E)

In the Antarctic Polar Front of the Atlantic sector, mass, alkenone, and GDGT fluxes are enhanced in different seasons at two depths. At the shallow trap (614 m), both mass and alkenone fluxes show

peaks in the austral spring and summer season, but alkenone fluxes are 5 times higher in mid-October 1990 than in December 1989 (Figure 5.4). When mass and alkenone fluxes record the minima, GDGT fluxes display multiple peaks with maxima in austral autumn and winter season (mid-May and August 1990). As discussed in Section 3.5.2.1, the temporal mismatch of maximum fluxes between alkenone (or mass flux) and GDGT implies that Thaumarchaeota may be out-competed by phytoplankton (including the haptophytes) and thus they preferentially occur in the water depth or season, which is less favorable for phytoplankton. At the deep trap, almost no flux occurs since mid-June 1990 (Figure 5.4). Mass and alkenone fluxes are pulsed in mid-December 1989 to late-January, early-March, and mid-May 1990. The last two peaks also occur in GDGT fluxes. However, the maximum of GDGT flux appears in mid-November 1989. Consequently, neither alkenone nor GDGT fluxes have a correlation with opal, $CaCO_3$, POC, or PON at the shallow trap. Only $CaCO_3$ flux showed a weak correlation with alkenone flux ($R^2 = 0.60$; Table 5.1).

The $U^{k'}_{37}$ proxy at the deep trap and the TEX^{L}_{86} proxy at both depths yielded somehow unrealistic temperature reconstructions for the region. Only the $U^{k'}_{37}$ proxy measured at the shallow trap, which was previously reported by Müller and Fischer, (2003), reflects the overlying SSTs (Figure 5.4d). Our measurements well duplicate their results, showing a clear seasonality by applying the same $U^{k'}_{37}$ calibration (Figure 5.4d). When a time lag of about 10 weeks is considered, the estimated temperatures vary fairly well with the satellite-derived SST variations. A delay time of 10 weeks can be calculated to a sinking rate of 9 m d^{-1} (=10 weeks/ 614 m). As TEX^{L}_{86}-derived temperatures of the shallow trap display a mixture of warm and cold-biased estimates relative to the SSTs, it is difficult to directly compare with the ones derived from the $U^{k'}_{37}$ proxy.

The maximum discrepancy between two proxy estimates occurs when the $U^{k'}_{37}$ proxy records relatively cold temperatures and reaches values up to 5 °C (Figure 5.4d). Greater offsets between two proxies are recorded at the deep trap because of the warm bias of TEX^{L}_{86} and cold bias of $U^{k'}_{37}$ relative to the SSTs (Figure 5.4h). The flux-weighted mean $U^{k'}_{37}$ value at the shallow trap is 0.12 and a similar value is found in the surface sediment in Müller et al., (1998)'s database (0.149 of $U^{k'}_{37}$ at PS1759-1; 50.165° S, 5.755° E). The temperature difference between the shallow trap and surface sediment is only 0.9 °C, which is below the calibration error (Müller et al., 1998; ±1 °C). Due to the short period of sampling at the deep trap, the flux-weighted mean $U^{k'}_{37}$ is meaningless. However, we can confirm that the alkenone signal corresponding to the SST at the shallow trap is propagated to the surface sediment. In contrast, a similar TEX^{L}_{86} signal was found in the deep trap and underlying surface sediment, reconstructing warm-biased temperatures, which differ from the TEX^{L}_{86} signal in the shallow trap (see Section 3.5.2.2).

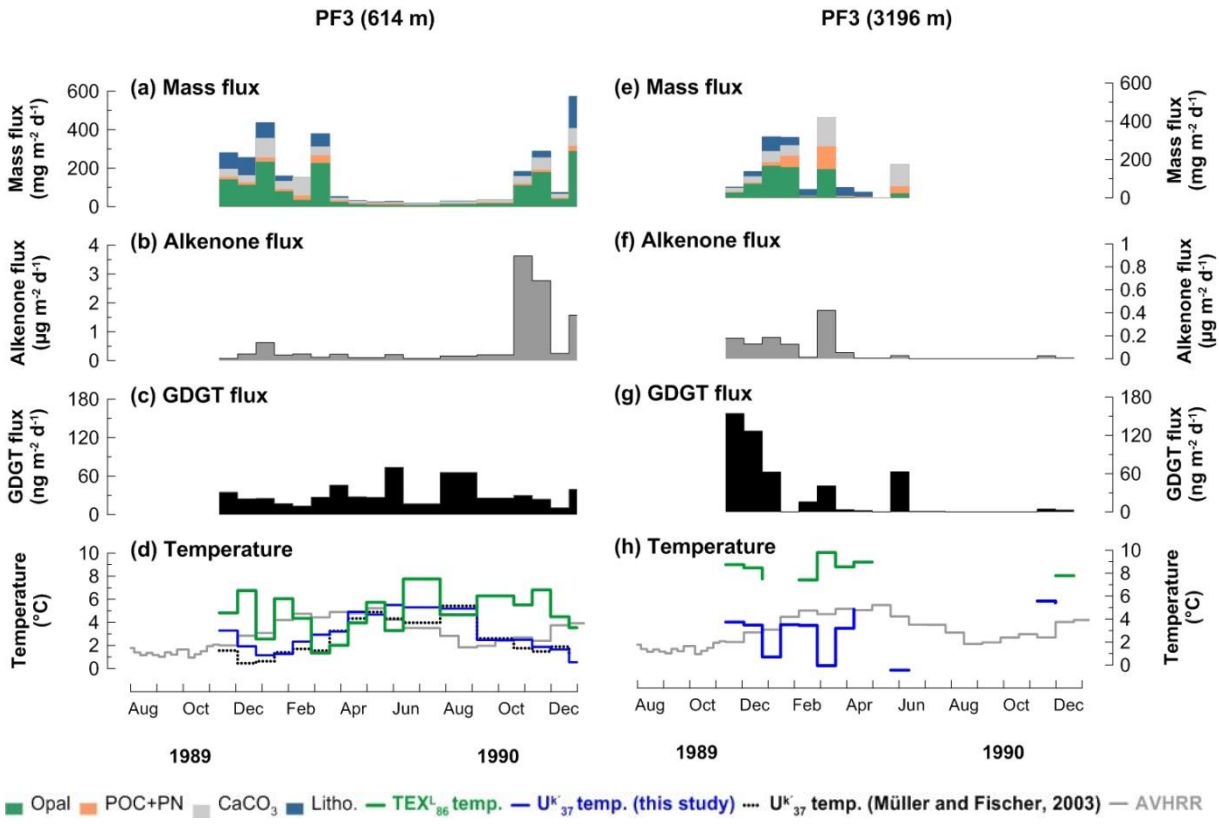

Figure 5.4 Changes in mass flux (a, e), alkenone flux (b, f), GDGT flux (c, g), and reconstructed and satellite-derived temperatures (d, h) at 614 m depth (left panel) and at 3196 m depth (right panel) in the Antarctic Polar Front of the Atlantic sector. Black dotted line (d) at the shallow trap shows the $U^{k'}_{37}$-derived temperature reported by (Müller and Fischer, 2003). Note that Y-axis scale for alkenone flux on the left panel is different from the one on the right panel.

Overall, to date, the $U^{k'}_{37}$ calibration is likely to be a better option in the Antarctic Polar Front for reconstructing SSTs than the TEX^{L}_{86} calibration. However, GDGT based calibrations seem also suited for the temperature reconstruction when the regression between TEX^{L}_{86} values and SSTs is re-defined or only certain OH-GDGTs are considered (see Section 3.5.3 and 3.5.4).

5.3.3 Oligotrophic system: central Brazil Basin

5.3.3.1 Seasonal mesotrophic region (WA9; 7.5° S, 28.1° W)

In the less oligotrophic site WA8, mass, alkenone, and GDGT fluxes covary and each shows maxima in July 1996 at the shallow trap (Figure 5.5). Alkenone fluxes are highly correlated with all ballasting components in the traps from both depths (Table 5.1). This implies that opal, $CaCO_3$, POC, and PON play roles as exporting materials for alkenones throughout the water column. The similar flux patterns in mass, alkenones, and GDGTs show that production and transport of alkenones and GDGTs occur almost at the same time.

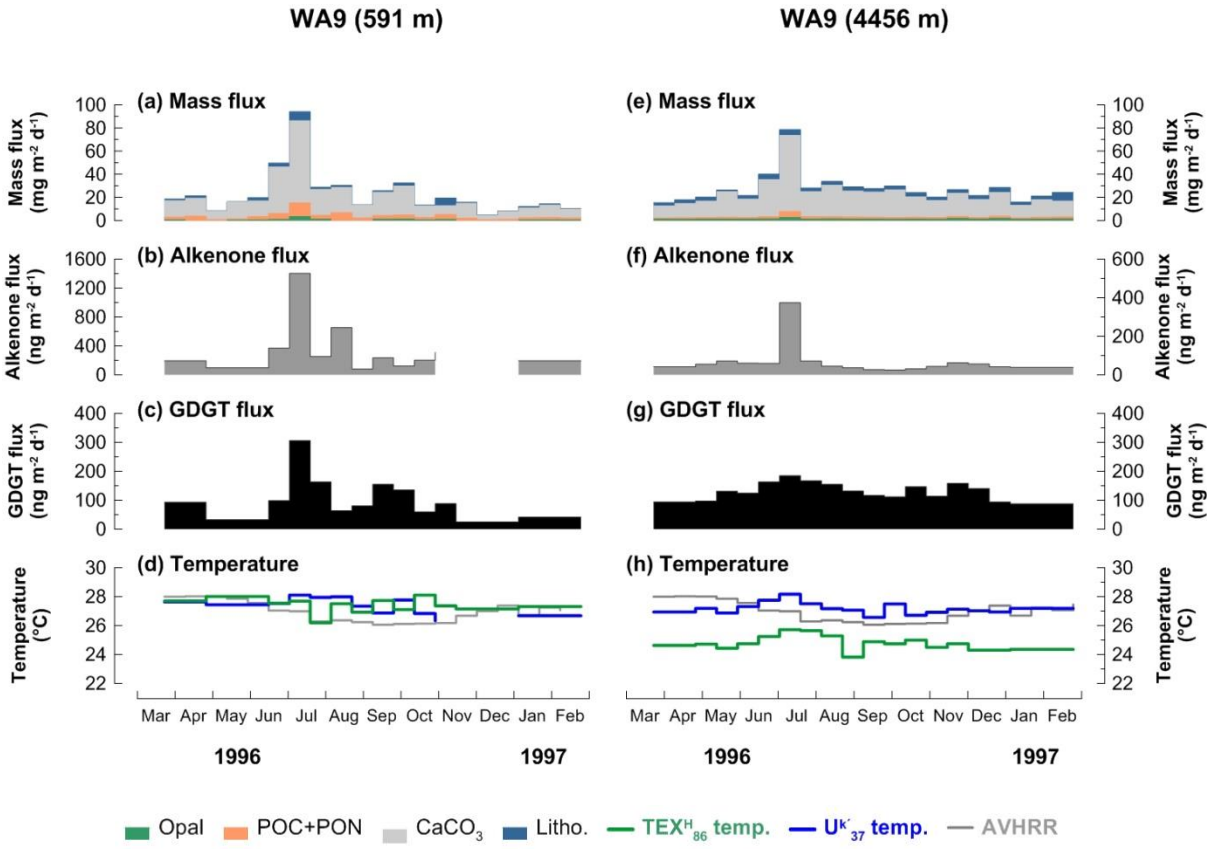

Figure 5.5 Changes in mass flux (a, e), alkenone flux (b, f), GDGT flux (c, g), and reconstructed and satellite-derived temperatures (d, h) at 591 m depth (left panel) and at 4456 m depth (right panel) in the central Brazil Basin (WA9). Note that Y-axis scale for alkenone flux on the left panel is different from the one on the right panel.

There have been concerns regarding the limited applicability of the $U^{k'}_{37}$ proxy in the tropic oceans. A maximum growth temperature of *Emiliania huxleyi* or a significantly smaller portion of $C_{37:3}$ have been previously considered, rendering the calibration inaccurate in the regions, where SSTs are warmer than 26 °C (Brassell et al., 1986; Pelejero and Grimalt, 1997). Nonetheless, $U^{k'}_{37}$ calibration can still reconstruct reasonable temperatures at the warm end of the regression up to 29 °C (Pelejero and Calvo, 2003). This is in line with the result of the central Brazil Basin.

The $U^{k'}_{37}$ -derived temperatures vary within 2 °C, with the range of 26.3−28.1 °C at the shallow trap and between 26.6−28.2 °C at the deep trap (Figure 5.5d, h). Although the signals at both traps do not follow the seasonality of the satellite-derived SSTs, the $U^{k'}_{37}$ temperature estimates reflect the SSTs. The flux-weighted mean $U^{k'}_{37}$ temperatures at both traps (27.5 °C at the shallow trap and 27.4 °C at the deep trap) are almost identical to the flux-weighted mean TEX^{H}_{86} temperature of the shallow trap (27.4 °C). The TEX^{H}_{86}-derived temperatures of the deep trap are consistently up to 3.2 °C colder than the $U^{k'}_{37}$-derived temperatures (Figure 5.5h). Whatever the reasons for this discrepancy of

GDGT abundance ratios (i.e. TEX_{86}^{H}) between two depths (see Section 4.5.3), alkenone abundance ratios (i.e. $U_{37}^{k'}$) are not affected and rather the surface signal is preserved while sinking.

5.3.3.2 Oligotrophic region (WAB1; 11.55° S, 28.52° W)

In the oligotrophic site WAB1, correlations between lipid biomarker (alkenone and GDGTs) and ballasting component fluxes are found only at the shallow trap (Table 5.1, Figure 5.6). Alkenone flux is well correlated with $CaCO_3$ (R^2 = 0.81) followed by POC (R^2 = 0.75). GDGT flux has a good correlation with opal (R^2 = 0.85) and $CaCO_3$ (R^2 = 0.81). This confirms that alkenone and GDGTs are preferentially incorporated into particles with different compositions.

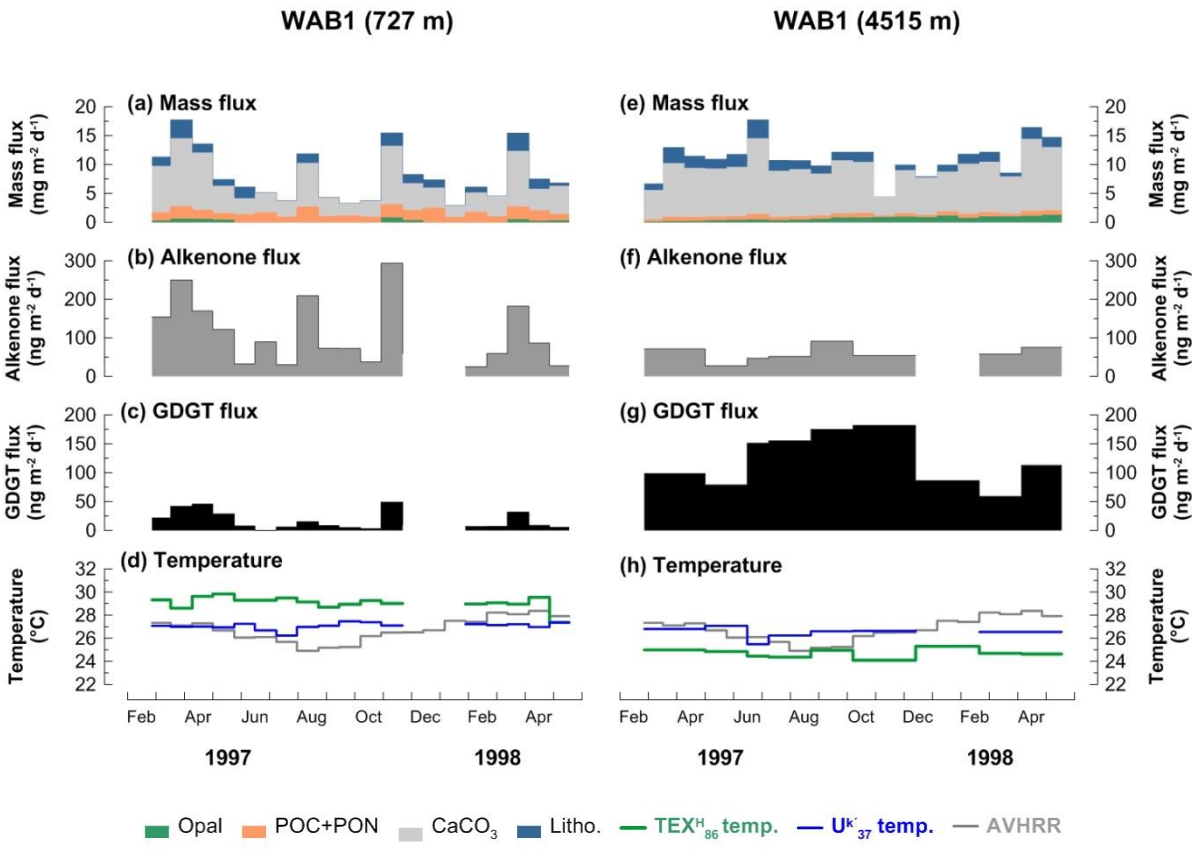

Figure 5.6 Changes in mass flux (a, e), alkenone flux (b, f), GDGT flux (c, g), and reconstructed and satellite-derived temperatures (d, h) at 727 m depth (left panel) and at 4515 m depth (right panel) in the central Brazil Basin (WAB1). Note that Y-axis scales are identical on the left and right panels.

Mass and GDGT fluxes are higher at the deep trap than at the shallow one, but the opposite trend occurs in alkenone fluxes (Figure 5.6). The seasonality of mass and alkenone fluxes are more strongly displayed at the shallow trap. At the shallow trap, mass, alkenone and GDGT fluxes are all enhanced in mid-March, August, and November 1997 and mid-March 1998. At the deep trap, the maximum

mass flux occurs in mid-June 1997, but the maxima of alkenone and GDGT flux occur in August−September and October−November 1997, respectively.

In the previous Section 4.5.3.1, it is explained that the warm-biased TEX_{86}^{H}-derived temperatures of the shallow trap relative to the satellite-derived SST are attributed to the response of Thaumarchaeota to nutrient stress (Figure 5.6, Hurley et al., 2016). For the alkenone proxy, culture and field studies have also noted that nutrient conditions may influence on the $U_{37}^{k'}$ thermometry (Conte et al., 1998; Epstein et al., 1998; Prahl et al., 2003; Sikes et al., 2005). Prahl et al., (2003) found that the $U_{37}^{k'}$ values decreased under low nutrient levels in a culture experiment. In the field, $U_{37}^{k'}$-derived temperatures have been reported to be cold biased by up to 4 °C relative to SST when the nutrient level was low (Sikes et al., 2005). However, such nutrient stress does not seem to affect $U_{37}^{k'}$ ratios at site WAB1. The $U_{37}^{k'}$-derived temperatures vary within 1.6 °C, with the range of 26.0−27.2 °C at the shallow trap and 25.5−27.1 °C at the deep one (Figure 5.6). Those reconstructed temperatures do not display seasonality, but they are similar to the satellite-derived SSTs. The flux-weighted mean $U_{37}^{k'}$ temperatures are almost identical at both traps (27.5 °C at the shallow trap and 27.4 °C at the deep trap). While the TEX_{86}^{H}-derived temperatures are warm-biased in upper waters and are cold-biased in deep waters, the $U_{37}^{k'}$-derived temperatures reconstruct the regional SST in the oligotrophic environment. Thus, a comparison of TEX_{86}^{H} and $U_{37}^{k'}$-derived temperatures in sinking particles collected in the central Brazil Basin reveals that $U_{37}^{k'}$ is a better proxy for reconstructing SST in the oligotrophic ocean and TEX_{86}^{H} is more sensitive to nutrient stress.

In order to better constrain the temperature proxy signals of oligotrophic settings, an additional site in the northeast Atlantic is investigated. This region is characterized as a typical mid-latitude ocean regime having a nutrient-limited spring production peak (Lampitt et al., 2001; 48.99° N, 16.44° W). The study site is a long-term observatory mooring region on the Porcupine Abyssal Plain (PAP) in the northeast Atlantic since 1992. In several studies it was observed that the biogeochemistry in surface waters is coupled with the benthic community of the abyssal plain (Lampitt et al., 2010 and reference therein). The flux data measured at multiple depths allow determining that the downward flux captured at 3000 m depth better represent the seasonal variability of primary production (Lampitt et al., 2010, 2001).

In this study, we analyzed alkenone and GDGTs in time-series samples of sinking particles collected at 1000 m water depth covering one year from October 1998 to September 1999 (PAP-XXV; Figure 5.7). Unfortunately, $C_{37:2}$ and $C_{37:3}$ could not be reliably quantified in the chromatogram probably due to low alkenone concentrations.

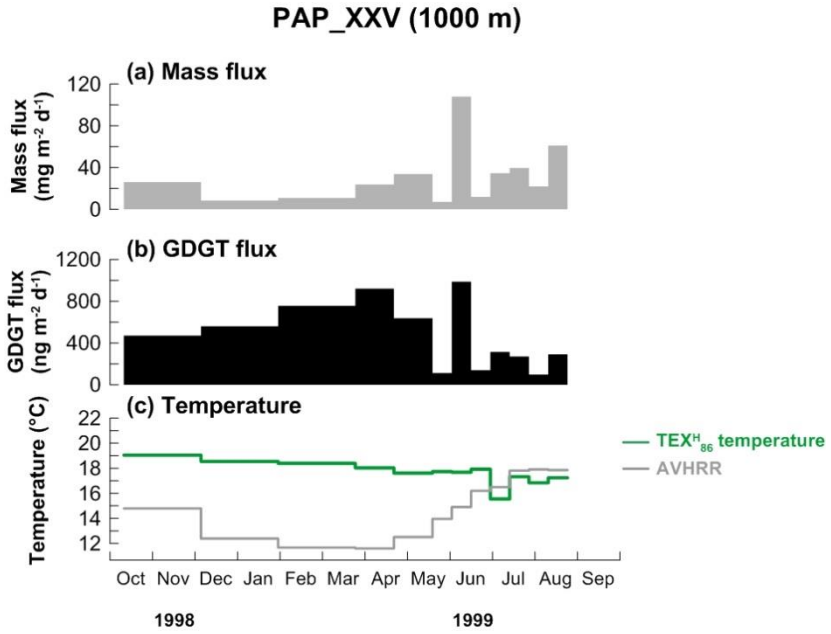

Figure 5.7 Changes in mass flux (a), GDGT flux (b), and reconstructed and satellite-derived temperatures (c) at 100 m depth in the Porcupine Abyssal Plain (PAP) of the northeast Atlantic.

Both mass and GDGT fluxes are peaked in early-June 1999 (Figure 5.7a, b). While the mass flux records minima in December to March, the GDGT flux is relatively high. The satellite-derived SSTs range between 11.6 and 17.9 °C with the lowest temperature in February when the daily SSTs are averaged according to the sampling period of each sample cup (Figure 5.7c). The TEX_{86}^{H}-derived temperatures neither display the seasonality nor reflect realistic temperatures of the region except for the last two months (July and August 1999). Between October 1998 and mid-June 1999, TEX_{86}^{H}-derived temperatures are warm-biased by up to 11 °C relative to SSTs (Figure 5.7c). Other TEX_{86} calibrations are also tested (Kim et al., 2010, 2008), but the temperature estimates display similar trends and temperature ranges (not shown in the figure). We cannot infer that the warm-biased signal at 1000 m depth represents the whole water column in the PAP. However, when taking our results from the oligotrophic SW Atlantic into account, it is noticeable that in the nutrient-limited upper oceans, TEX_{86} tends to have higher values (Figure 5.6d). Further investigations in sinking particles of deep water, especially at 3000 m depth, which according to previous studies better represent the surface water biogeochemistry, and underlying sediment are required to understand the TEX_{86} variability within the system and for a full comparison with site WAB1. Overall, the observation of warm biased TEX_{86}^{H}-derived temperatures in the PAP provides further evidence that nutrient stress has an impact on the TEX_{86} thermometry.

5.4 Summary and conclusions

The temporal and spatial variability of fluxes in mass, alkenones and GDGTs and estimated temperatures based on the $U_{37}^{k'}$ and TEX_{86} proxies are investigated throughout the Atlantic Ocean. The correlations of alkenone or GDGT fluxes with ballasting material fluxes are different by regions, implying distinct export mechanisms. When only the best correlation is considered, alkenones are better correlated with POC, PON and $CaCO_3$ while GDGTs are mostly correlated with Opal. This implies that alkenone and GDGTs are preferentially incorporated into particles containing different materials.

The seasonal maxima of alkenones and GDGTs occur in the same season in the tropical oceans (equatorial upwelling regime and oligotrophic ocean) and high northern polar ocean. However, in the coastal upwelling regime and Antarctic Polar Front, alkenone and GDGT have maxima in different seasons. This implies that the competition for nutrients between alkenone producing phytoplankton and GDGT producing archaea may differ according to the environmental conditions.

The $U_{37}^{k'}$ (and U_{37}^{k}) are relatively faithful recorders of SSTs of the study regions. However, a latitudinal limit clearly appears in the high latitude North Atlantic Ocean (in the eastern Fram Strait), where the maximum SST reaches approximately only 4 °C. The TEX_{86} seems more sensitive to environmental factors like the OMZs, archaeal community structure, or nutrient levels. Nonetheless, the TEX_{86} temperature proxy is likely more reliable than the $U_{37}^{k'}$ proxy in the high northern latitude ocean. Competitive and complementary relationships between alkenone and GDGT proxies are beneficial to reconstruct paleotemperature.

Acknowledgments

We are thankful to the crews, scientists, and students, who were collecting the sediment trap samples used in this study. This project is funded through the DFG-Research Center/Cluster of Excellence “The Ocean in the Earth System” at the MARUM and supported by GLOMAR−Bremen International Graduate School for Marine Sciences, University of Bremen.

Data availability

The data presented here will be archived on the PANGAEA database when the manuscript is submitted.

CHAPTER 6

Summary and Perspectives

6 Summary and Perspectives

The studies conducted in this thesis are primarily aimed at contributing to a better understanding of TEX_{86} thermometry using sinking particles collected in three different ocean regimes through the Atlantic Ocean including the upwelling settings, Northern and Southern polar regions, and oligotrophic settings. The seasonal variability of GDGT fluxes and TEX_{86} derived temperatures recorded in sinking particles were investigated. DifferentTEX_{86} related calibrations (TEX_{86}, TEX_{86}^{H}, TEX_{86}^{L}) were applied in the respective locations. In Polar Oceans, recently developed indices (OH-GDGTs) were also applied. In each chapter, additional GDGT based indices for assessing non-thermal signal in GDGT compositions were calculated.

The correlation between GDGT flux and potential ballasting material flux was used to identify the major export mechanism of GDGTs to deep waters. The delay in receiving TEX_{86} signals relative to overlying SST or the maximum period of GDGT flux at different depths when both parameters exhibited clear seasonality was used to investigate the sinking velocity of particles carrying GDGTs. A further aim was to obtain insights into the potential oceanographical and/or geochemical factors influencing the regional and temporal applicability of the TEX_{86} thermometry. The flux-weighted mean TEX_{86} (TEX_{86}^{H} or TEX_{86}^{L}) temperatures averaged over the trap deployment period, which covered all seasons, were compared to the depth profiles of water temperature and nutrient concentration to estimate the depth origin of GDGT signals in respective the locations. The flux-weighted mean signals in sinking particles were also compared to the TEX_{86} temperatures in underlying surface sediment to test whether the signals are changed while sinking to deep waters. $U_{37}^{k'}$ (or U_{37}^{k})-derived temperatures were also compared with temperature estimates based on TEX_{86} proxies in each study.

The main findings and perspectives are summarized as set out below:

6.1 Export mechanism of lipid signal

Correlations of GDGT fluxes with those of opal, carbonate, and other biogenic/non-biogenic components differ between regions and water depths where particles were collected. A strong correlation of GDGTs with opal fluxes was observed in the upwelling Guinea Basin (Chapter 2), in the eastern Fram Strait (Chapter 3), and in two locations of the central Brazil Basin (Chapter 4), confirming that GDGTs are probably transported by opal-dominant aggregates. In the regions where traps were available at two different depths, the correlation between the two parameters was weaker with the deep trap compared to the shallow traps, suggesting that the particle collections integrated larger spatial sources and variable temporal sources, together with a reduced seasonal amplitude of GDGT fluxes. In the oligotrophic site, in particular, a strong correlation was observed only at the

shallow trap while no correlation was found at the deep trap, which might indicate a different origin of GDGTs. Due to the relatively small number of data points in the Lüderitz, correlations between parameters are not statistically significant. In the Antarctic Polar Front, GDGT fluxes did not covary with any other parameters at either depth (Chapter 3). In addition to opal or carbonate fluxes, other available biogenic and non-biogenic parameters in the eastern Fram Strait allowed the determination of further GDGT exporters. Cell abundance of diatoms and coccolithophores, which are sources of opal and carbonate respectively, co-varied with GDGT fluxes. The flux of terrestrial biomarkers, which was probably drafted by sea-ice into the system, showed that the terrestrial component can also play a role as a ballast material. Zooplankton fecal pellet fluxes confirmed that GDGTs are incorporated into zooplankton fecal pellets and which probably lead to the rapid sinking of TEX_{86} signal.

Overall, the role of aggregates mainly associated with opal is significant in the exporting of GDGTs in various ocean regimes. As found in the eastern Fram Strait, additional investigations with more diverse components would be helpful to develop a comprehensive overview of the export mechanism of GDGTs.

When the seasonal trend of $U^{k'}_{37}$ or TEX_{86}-based temperature signal follows the SST seasonality, it allows the sinking velocity of particles containing alkenones or GDGTs to be calculated. The calculated sinking velocity may underestimate the "real" one in the water column because it probably includes the time taken for lipid production, aggregation, and transportation. In addition, the composition of ballasting materials influences the sinking velocity of aggregates and thus the proxy temperatures (Mollenhauer et al., 2015) (see Section 2 and 3). Nonetheless, determining sinking velocities helps to track the temporal and spatial origin of particles incorporated with particles (Wekerle et al., 2018). As the oceans are the carbon reservoirs for the earth, understanding the particle export transferring organic materials and the magnitude of the transfer is important in terms of the biological carbon pump. With reliable sinking velocity data, a particle trajectory study can estimate the source area of particles caught in traps. Recently, Wekerle et al., (2018) simulated the catchment area in the Fram Strait. The same approach applied to study the composition of ballasting materials carrying lipids will enhance our understanding of the origin of lipids and temperature signals.

6.2 Potential non-thermal factors influencing on TEX_{86} thermometry

The seasonal temperature records in sinking particles and the distinctive oceanographical characteristics in each region provided evidence for TEX_{86} thermometry. Additional GDGT-based proxies, which can determine the non-thermal impacts on GDGT distributions, did not reveal the input of terrigenous, methanotrophic, or methanogenic source of GDGTs. There was no latitudinal

trend of TEX_{86} temperature estimates throughout the Atlantic Ocean; rather, the reconstructed temperatures based on the lipid proxy varied according to regional conditions.

Only in the Lüderitz (Chapter 2) and in the upper water column from the seasonal mesotrophic Brazil Basin (chapter 4), did TEX_{86} thermometry reconstruct the SSTs. In the Guinea Basin (Chapter 2) and eastern Fram Strait (Chapter 3), the GDGT based (TEX_{86}^{H} or TEX_{86}^{L}) temperature estimates corresponded to the water temperature of the nutricline, where the nitrification might be active and thus GDGTs were dominantly exported. In the oligotrophic upper water column from the central Brazil Basin (Chapter 4) and the Porcupine Abyssal Plain (Chapter 5), the TEX_{86}^{H} -derived temperatures are mostly warmer than the regional SSTs, responding to low energy "nutrient" conditions. The nutrients dynamic thus seems to influence not only the depth distribution of the thaumarchaeotal community, but also the distribution of GDGT. The adaptation to low oxygen level may also dictate the ecology of Thaumarchaeota (Chapter 2). These findings are in line with batch culture experiments and field studies where the OMZs exist, showing that relatively higher TEX_{86} values are found in oxygen limited conditions (Hurley et al., 2016; Qin et al., 2015; Xie et al., 2014).

As for the delivery of lipid temperature throughout the water column, similar TEX_{86} values at the multiple depth traps were found in the Arabian Sea and in the Northwest Pacific, which is in line with the result in the equatorial upwelling Guinea Basin (Chapter 2). However, the estimated temperatures were not consistent in two different depth traps in the Antarctic Polar Front (Chapter 3) and in the central Brazil Basin (Chapter 4). In the Antarctic Polar Front, the warm-biased temperature relative to SST recorded in the deep trap and in the surface sediment may be caused by either the euryarchaeotal community or the nonlinear correlation between TEX_{86} and SST in the Southern Ocean (Chapter 3). The archaeal community in the trap location needs to be further examined and the polynomial regression suggested in this study should be applied to geological sediment record if applicable. In the central Brazil Basin, the TEX_{86} signals recording the SST or warm-biased temperatures measured in the shallow trap were not present in the deep traps. Relatively colder temperatures compared to SST were recorded both in deep traps and in the surface sediment (Chapter 4). Based on the studies that measured TEX_{86} values in IPL-GDGT fractions and compound-specific radiocarbon data of GDGTs in the oligotrophic ocean, it was hypothesized that the surface signal was imprinted by significant deep '*in situ* GDGT production' that carried colder temperature, resulting in a cold-biased temperature in the deep traps and surface sediment (Chapter 4 and references therein). The determination of radiocarbon data as conducted by Ingalls et al., (2006) and TEX_{86} value in IPL-GDGTs associated with specific head groups will give a better understanding of the origin of GDGTs and the contribution of IPL-GDGTs to CL-GDGTs composition.

6.3 Regional calibrations for high latitude oceans

In this thesis, several previously defined (U^{k}_{37}; Chapter 5 and OH-GDGT based proxy; Chapter 3) calibrations and a newly suggested calibration (polynomial TEX^{L}_{86}; Chapter 3) were also applied to compare the principal temperature record or to overcome the biased temperature record. This approach provided new insights into regionally specified calibration in the polar oceans.

In the eastern Fram Strait, the TEX^{L}_{86}-derived temperature corresponded to the water temperature at a depth of 30−80 m in the warm season (April-June) (Chapter 3). The depth profile of ammonia, nitrite, and nitrate concentrations supported the idea that Thaumarchaeota as ammonia-oxidizing chemoautotrophs preferentially dwell in that depth range during the warm season. Similar findings were made in the subpolar North Pacific, in the Sea of Okhotsk, and in the Bering Sea that TEX^{L}_{86} values-derived from the surface sediments was correlated with the water temperature at a depth of 20 m in August (Meyer et al., 2016 and references therein). Based on the reconstructed temperature, the authors defined rapid atmospheric teleconnection between the North Atlantic and the northwest Pacific/western Bering Sea in the millennial-scale climate history (Meyer et al., 2016). Interestingly, the recent study in the area of the continental edge of Newfoundland in the northwest Atlantic also showed that the TEX^{L}_{86}-derived temperatures in surface sediments resembled the average temperatures of summer months (June-August) at shallow subsurface levels (~10−15 m depth) (Schukies, 2018). The results relating to the eastern Fram Strait described in this thesis confirmed two previous findings concerning the similar development of the water column followed by the depth distribution of ammonia and the thaumarchaeotal community between the North Atlantic and the Pacific Ocean. This corroborates the expectation of a new 'latitudinal' calibration covering a defined range of latitudes from the North Atlantic to the North Pacific Ocean. In order to evaluate this hypothesis, sedimentary TEX_{86} (or TEX^{L}_{86}) values need to be archived in the subarctic Atlantic regions, where TEX_{86} measurements are rarely collected.

In the Antarctic Polar Front, periods of only a few months covered by the deep trap. Thus it is not clear how the lipid temperature signal developed throughout the seasons and what caused the difference in temperature records between the shallow and deep traps. In Chapter 3, it was identified that the TEX^{L}_{86} response to temperature in the southern oceans (>50° S) differed from that in the northern oceans (>50° N). A newly defined non-linear (polynomial) regression resulted in a smaller residual of temperature estimate compared to the original linear TEX^{L}_{86} calibration in the Antarctic Polar Front. Applying this new calibration in surface and down-core sediments, where the warm biased TEX^{L}_{86} estimates are recorded, would be an important step to unravel the unconventional response of Thaumarchaeota to temperature in the Southern Ocean.

The occurrence of OH-GDGTs in sinking particles only from the polar oceans and their reconstructed temperature corresponding to regional SSTs highlighted the applicability of OH-GDGTs as a potential temperature proxy in cold regions (Chapter 3). However, this requires further research, similar to that conducted for TEX_{86} into the ecology of lipid producers and the export mechanisms. Evidence of potential temperature calibrations along with the TEX_{86} proxy in the northern and southern polar oceans highlights the need for regionally specified approaches to reconstruct temperature in cold oceans.

6.4 Difference between $U^{k'}_{37}$ and TEX_{86} temperature estimate

Temperature differences between two lipid proxies ($U^{k'}_{37}$ and TEX_{86}) varied by regions (Chapter 5). For most of times and locations, $U^{k'}_{37}$-derived temperatures resembled the SSTs in each region. The reconstructed temperatures based on $U^{k'}_{37}$ and TEX^{H}_{86} in the Guinea Basin provided the additional evidence of alkenone proxy estimating SST and GDGT proxy estimating subsurface temperature as shown in other upwelling regions (Chen et al., 2016; Lee et al., 2008; Mollenhauer et al., 2015). The discrepancy between the two proxy records was used to explain the thermocline adjustment caused by the long-term nature of ocean circulation (Lopes dos Santos et al., 2010; Rommerskirchen et al., 2011). The use of two lipid proxies as a pair is beneficial especially in the warm oceans.

Even in the locations where non-thermal influences on TEX_{86} thermometry were identified, the $U^{k'}_{37}$ records were rather consistent, mirroring the SSTs. It seems, therefore, that the $U^{k'}_{37}$ proxy is less sensitive to environmental settings such as availability of nutrients or oxygen, or the depth distribution of nutrients, while the TEX_{86} proxy is useful to investigate paleotemperature during different climate events. For instance, the SST evolutions in the Cretaceous period, which is characterized by higher CO_2 concentration and warmer climate than the modern era, have been well constructed using the TEX_{86} proxy by comparison with isotope data (Littler et al., 2011; O'Brien et al., 2017; van Helmond et al., 2014; Zachos et al., 2006). Alkenones are rarely found in the Cretaceous period, so that the $U^{k'}_{37}$ proxy cannot be applied. Additionally, the $U^{k'}_{37}$ proxy and its modified calibrations containing $C_{37:4}$ failed to reconstruct temperatures below 4 °C whereas the TEX_{86} proxy successfully revealed the regional temperature.

The results described in this thesis proved that a time-series sediment trap is an excellent tool to investigate a proxy signal while sinking to the sediment. This work provides substantial improvements in the TEX_{86} thermometry in terms of its depth origin and the potential non-thermal effects on GDGT composition. In addition, it identifies the importance of regional calibrations for polar oceans. Further time-series sediment trap studies for multiple years and depths in diverse oceanic regions would improve the knowledge of regional TEX_{86} thermometry deviated from the global trend.

Appendix 1

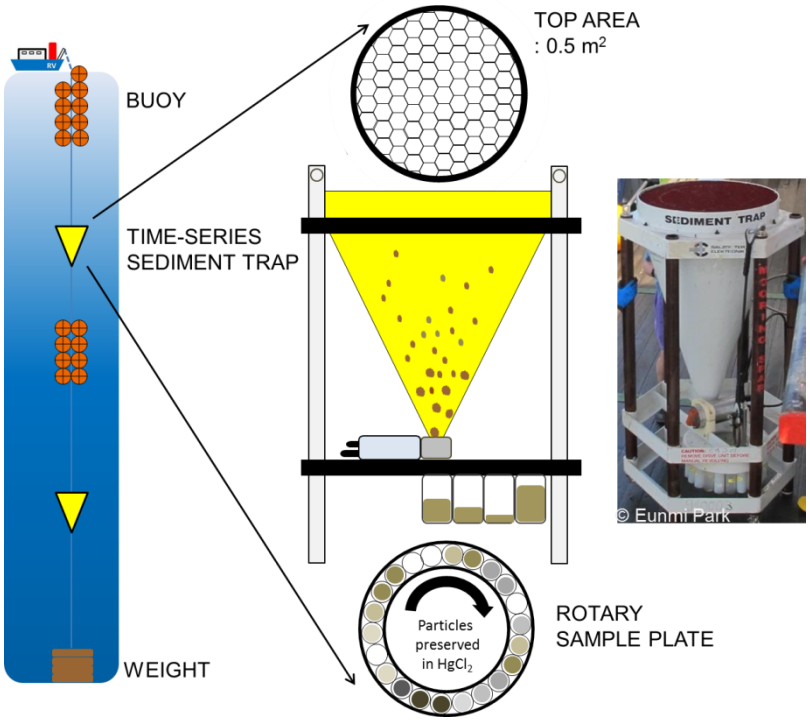

A1. Figure 1 Diagram of a time-series sediment trap used in this study. The rotary sample plate holds 20 particle collection cups (the number of cups can be different according to the model). According to the pre-programmed schedule, the tray rotates and the following cup is placed. The apparatus has the top with an opening of 0.5 m^2 covered with a honeycomb baffle to prevent the large objects and turbulence (a figure was modified after http://www.whoi.edu/page.do?pid=8415&tid=7342&cid=10286).

References

Abbott, M.R., Richman, J.G., Nahorniak, J.S., Barksdale, B.S., 2001. Meanders in the Antarctic Polar Frontal Zone and their impact on phytoplankton. Deep. Res. Part II Top. Stud. Oceanogr. 48, 3891–3912. doi:10.1016/S0967-0645(01)00073-X

Agogué, H., Brink, M., Dinasquet, J., Herndl, G.J., 2008. Major gradients in putatively nitrifying and non-nitrifying Archaea in the deep North Atlantic. Nature 456, 788–792. doi:10.1038/nature07535

Alonso-Sáez, L., Andersson, A., Heinrich, F., Bertilsson, S., 2011. High archaeal diversity in Antarctic circumpolar deep waters. Environ. Microbiol. Rep. 3, 689–697. doi:10.1111/j.1758-2229.2011.00282.x

Basse, A., Zhu, C., Versteegh, G.J.M., Fischer, G., Hinrichs, K.-U., Mollenhauer, G., 2014. Distribution of intact and core tetraether lipids in water column profiles of suspended particulate matter off Cape Blanc, NW Africa. Org. Geochem. 72, 1–13. doi:10.1016/j.orggeochem.2014.04.007

Bauerfeind, E., Kattner, G., Ludwichowski, K.-U., Nöthig, E.-M., Sandhop, N., 2014. Inorganic nutrients measured on water bottle samples at AWI HAUSGARTEN during POLARSTERN cruise MSM29. doi:10.1594/PANGAEA.834685

Bauerfeind, E., Nöthig, E.M., Beszczynska, A., Fahl, K., Kaleschke, L., Kreker, K., Klages, M., Soltwedel, T., Lorenzen, C., Wegner, J., 2009. Particle sedimentation patterns in the eastern Fram Strait during 2000-2005: Results from the Arctic long-term observatory HAUSGARTEN. Deep. Res. Part I Oceanogr. Res. Pap. 56, 1471–1487. doi:10.1016/j.dsr.2009.04.011

Beman, J.M., Popp, B.N., Francis, C.A., 2008. Molecular and biogeochemical evidence for ammonia oxidation by marine Crenarchaeota in the Gulf of California. ISME J. 2, 429–441. doi:10.1038/ismej.2008.33

Bendle, J., Rosell-Melé, A., 2004. Distributions of U_{37}^{k} and $U_{37}^{k'}$ in the surface waters and sediments of the Nordic Seas: Implications for paleoceanography. Geochemistry, Geophys. Geosystems 5, 1–19. doi:10.1029/2004GC000741

Bendle, J., Rosell-mele, A., Ziveri, P., 2005. Variability of unusual distributions of alkenones in the surface waters of the Nordic seas. Paleoceanography 20, 1–15. doi:10.1029/2004PA001025

Benthien, A., Müller, P.J., 2000. Anomalously low alkenone temperatures caused by lateral particle and sediment transport in the Malvinas Current regions, western Argentine Basin. Deep Sea Res. Part I Oceanogr. Res. Pap. 47, 2369–2393.

Berelson, W.M., 2002. Particle settling rates increase with depth in the ocean. Deep. Res. Part II Top. Stud. Oceanogr. 49, 237–251. doi:10.1016/S0967-0645(01)00102-3

Beszczynska-Möller, A., Fahrbach, E., Rohardt, G., Schauer, U., 2012a. Physical oceanography and current meter data from mooring F7-8. doi:10.1594/PANGAEA.800396

Beszczynska-Möller, A., Fahrbach, E., Schauer, U., Hansen, E., 2012b. Variability in Atlantic water temperature and transport at the entrance to the Arctic Ocean, 1997-2010. ICES J. Mar. Sci. 69, 852–863. doi:10.1093/icejms/fss056

Blaga, C.I., Reichart, G.J., Heiri, O., Sinninghe Damsté, J.S., 2009. Tetraether membrane lipid distributions in water-column particulate matter and sediments: A study of 47 European lakes along a north-south transect. J. Paleolimnol. 41, 523–540. doi:10.1007/s10933-008-9242-2

Bode, A., Hernández-León, S., 2018. Trophic Diversity of Plankton in the Epipelagic and Mesopelagic Layers of the Tropical and Equatorial Atlantic Determined with Stable Isotopes. Diversity 10, 1–16. doi:10.3390/d10020048

Brassell, S.C., Eglinton, G., Marlowe, I.T., Pflaumann, U., Sarnthein, M., 1986. Molecular stratigraphy: a new tool for climatic assessment. Nature 320, 129–133. doi:10.1038/320129a0

Brochier-Armanet, C., Boussau, B., Gribaldo, S., Forterre, P., 2008. Mesophilic crenarchaeota: proposal for a third archaeal phylum, the Thaumarchaeota. Nat. Rev. Microbiol. 6, 245.

Brüchert, V., Jørgensen, B.B., Neumann, K., Riechmann, D., Schlösser, M., Schulz, H., 2003. Regulation of bacterial sulfate reduction and hydrogen sulfide fluxes in the central Namibian

coastal upwelling zone. Geochim. Cosmochim. Acta 67, 4505–4518. doi:10.1016/S0016-7037(03)00275-8

Buesseler, K.O., Antia, A.N., Chen, M., Fowler, S.W., Gardner, W.D., Gustafsson, O., Harada, K., Michaels, A.F., Rutgers van der Loeff, M., Sarin, M., Steinberg, D.K., Trull, T., 2007. An assessment of the use of sediment traps for estimating upper ocean particle fluxes. J. Mar. Res. 345–416. doi:10.1357/002224007781567621

Carr, M.-E., 2002. Estimation of potential productivity in Eastern Boundary Currents using remote sensing. Deep. Res. Part II Top. Stud. Oceanogr. 49, 59–80. doi:doi.org/10.1016/S0967-0645(01)00094-7

Carr, M.-E., Kearns, E.J., 2003. Production regimes in four Eastern Boundary Current systems. Deep. Res. Part II Top. Stud. Oceanogr. 50, 3199–3221. doi:10.1016/j.dsr2.2003.07.015

Chapman, P., Shannon, L. V., 1987. Seasonality in the oxygen minimum layers at the extremities of the Benguela system. South Africa J. Mar. Sci. 5, 85–94. doi:doi.org/10.2989/025776187784522162

Chave, K.E., 1954. Aspects of the Biogeochemistry of Magnesium 1. Calcareous Marine Organisms. J. Geol. 62, 266–283. doi:10.1086/626162

Chen, W., Mohtadi, M., Schefuß, E., Mollenhauer, G., 2016. Concentrations and abundance ratios of long-chain alkenones and glycerol dialkyl glycerol tetraethers in sinking particles south of Java. Deep. Res. Part I Oceanogr. Res. Pap. 112, 14–24. doi:10.1016/j.dsr.2016.02.010

Chen, W., Mohtadi, M., Schefuß, E., Mollenhauer, G., 2014. Organic-geochemical proxies of sea surface temperature in surface sediments of the tropical eastern Indian Ocean. Deep. Res. Part I Oceanogr. Res. Pap. 88, 17–29. doi:10.1016/j.dsr.2014.03.005

Church, M.J., DeLong, E.F., Ducklow, H.W., Karner, M.B., Preston, C.M., Karl, D.M., 2003. Abundance and distribution of planktonic Archaea and Bacteria in the waters west of the Antarctic Peninsula. Limnol. Oceanogr. 48, 1893–1902. doi:10.4319/lo.2003.48.5.1893

Church, M.J., Wai, B., Karl, D.M., Delong, E.F., 2010. Abundances of crenarchaeal amoA genes and transcripts in the Pacific Ocean. Environ. Microbiol. 12, 679–688. doi:10.1111/j.1462-2920.2009.02108.x

Conley, K.R., Sutherland, K.R., 2017. Particle shape impacts export and fate in the ocean through interactions with the globally abundant appendicularian Oikopleura dioica. PLoS One 12, 1–17. doi:10.1371/journal.pone.0183105

Conte, M.H., Thompson, A., Lesley, D., Harris, R.P., 1998. Genetic and Physiological Influences on the Alkenone/Alkenoate Versus Growth Temperature Relationship in Emiliania huxleyi and Gephyrocapsa oceanica. Geochim. Cosmochim. Acta 62, 51–68. doi:10.1016/S0016-7037(97)00327-X

de Bar, M.W., Stolwijk, D.J., McManus, J.F., Sinninghe Damste, J.S., Schouten, S., 2018. A Late Quaternary climate record based on long chain diol proxies from the Chilean margin. Clim. Past Discuss. 1–34. doi:10.5194/cp-2018-88

Delong, E.F., 2003. Oceans of Archaea. ASM News 69, 503–511. doi:10.2307/3954521

Delong, E.F., 1992. Archaea in coastal marine environments. Proc. Natl. Acad. Sci. 89, 5685–5689.

Dwyer, G.S., Cronin, T.M., Baker, P.A., Raymo, M.E., Buzas, J.S., Corrège, T., 1995. North Atlantic Deepwater Temperature Change During Late Pliocene and Late Quaternary Climatic Cycles. Science (80-.). 270, 1347–1351. doi:10.1126/science.270.5240.1347

Elling, F.J., Könneke, M., Lipp, J.S., Becker, K.W., Gagen, E.J., Hinrichs, K.-U., 2014. Effects of growth phase on the membrane lipid composition of the thaumarchaeon *Nitrosopumilus maritimus* and their implications for archaeal lipid distributions in the marine environment. Geochim. Cosmochim. Acta 141, 579–597. doi:10.1016/j.gca.2014.07.005

Elling, F.J., Könneke, M., Mußmann, M., Greve, A., Hinrichs, K.-U., 2015. Influence of temperature, pH, and salinity on membrane lipid composition and TEX_{86} of marine planktonic thaumarchaeal isolates. Geochim. Cosmochim. Acta 171, 238–255. doi:10.1016/j.gca.2015.09.004

Epstein, B.L., D'Hondt, S., Quinn, J.G., Zhang, J., Hargraves, P.E., 1998. An effect of dissolved nutrient concentrations based temperature estimates. PaleoceanographyCurrents 13, 122–126. doi:10.1029/97PA03358

Epstein, S., Mayeda, T., 1953. Variation of O^{18} content of waters from natural sources. Geochim. Cosmochim. Acta 4, 213–224. doi:10.1016/0016-7037(53)90051-9
Fahrbach, E., Cruise Participants, 1992. Report and preliminary results of the Expeditions ANTARKTIS IX/2 of the Research Vessel Polarstern in 1990/91, Punta Arenas-Cape Town, 16.11.1990-30.12-1990.
Fallet, U., Ullgren, J.E., Castañeda, I.S., van Aken, H.M., Schouten, S., Ridderinkhof, H., Brummer, G.J. a, 2011. Contrasting variability in foraminiferal and organic paleotemperature proxies in sedimenting particles of the Mozambique Channel (SW Indian Ocean). Geochim. Cosmochim. Acta 75, 5834–5848. doi:10.1016/j.gca.2011.08.009
Fhurmann, J.A., McCallum, K., Davis, A.A., 1992. Novel major archaebacterial group from marine plankton. Nature 356, 148–149.
Fietz, S., Huguet, C., Rueda, G., Hambach, B., Rosell-Melé, A., 2013. Hydroxylated isoprenoidal GDGTs in the Nordic Seas. Mar. Chem. 152, 1–10. doi:10.1016/j.marchem.2013.02.007
Fischer, G., 1999. Report and Preliminary Results of METEOR-CRUISE M 41/1, Svalvador da Bahia - Las Palmas, 18.5-13.6.1998. Bremen.
Fischer, G., 1998. Report and Preliminary Results of METEOR-Cruise M 38/1, Las Palmas - Recife, 25.1.-1.3.1997.
Fischer, G., 1996. Report and Preliminary Results of METEOR-Cruise M 34/4, Recife - Bridgetown, 19.3.-15.4.1996. Bremen.
Fischer, G., Gersonde, R., Wefer, G., 2002. Organic carbon, biogenic silica and diatom fluxes in the marginal winter sea-ice zone and in the Polar Front Region: Interannual variations and differences in composition. Deep. Res. Part II Top. Stud. Oceanogr. 49, 1721–1745. doi:10.1016/S0967-0645(02)00009-7
Fischer, G., Karakaş, G., 2009. Sinking rates and ballast composition of particles in the Atlantic Ocean: implications for the organic carbon fluxes to the deep ocean. Biogeosciences 6, 85–102. doi:10.5194/bg-6-85-2009
Fischer, G., Wefer, G., 1996. Long-term Observation of Particle Fluxes in the Eastern Atlantic: Seasonality, Changes of Flux with Depth and Comparison with the Sediment Record, The South Atlantic: Present and Past Circulation. Springer-Verlag, Berlin, Heidelberg. doi:https://doi.org/10.1007/978-3-642-80353-6_18
Fischer, G., Wefer, G., 1991. Sampling, Preparation and Analysis of Marine Particulate Matter, in: C. Herd, D., W. Spencer, D. (Eds.), Marine Particles: Analysis and Characterization, Geophysical Monograph Series. American Geophysical Union, Washington, D.C, pp. 391–397. doi:10.1029/GM063p0391
Francis, C.A., Roberts, K.J., Beman, J.M., Santoro, A.E., Oakley, B.B., 2005. Ubiquity and diversity of ammonia-oxidizing archaea in water columns and sediments of the ocean. Proc. Natl. Acad. Sci. 102, 14683–14688. doi:10.1093/ije/1.3.279
Franz, B.A., 2012. Quality and Consistency of the NASA Ocean Color Data Record. J. Geophys. Res. Ocean. 106, 14015–14034. doi:10.1029/2000JC000304
Freeman, N.M., Lovenduski, N.S., 2016. Mapping the Antarctic Polar Front: Weekly realizations from 2002 to 2014. Earth Syst. Sci. Data 8, 191–198. doi:10.5194/essd-8-191-2016
Garcia, H.E., Locarnini, R.A., Boyer, T.P., Antonov, J.I., Baranova, O.K., Zweng, M.M., Reagan, J.R., Johnson, D.R., 2013. World Ocean Atlas 2013, Volume 4 : Dissolved Inorganic Nutrients (phosphate, nitrate, silicate). NOAA Atlas NESDIS 76 4, 25. doi:10.1182/blood-2011-06-357442
Gardner, W.D., 2000. Sediment trap sampling in surface waters, in: Hanson, R.B., Ducklow, H.W., Field, J.G. (Eds.), The Changing Ocean Carbon Cycle, A Midterm Synthesis of the Joint Global Ocean Flux Study. Cambridge University Press, pp. 240–281.
Gardner, W.D., 1985. The effect of tilt on sediment trap efficiency. Deep Sea Res. Part A, Oceanogr. Res. Pap. 32, 349–361. doi:10.1016/0198-0149(85)90083-4
Gersonde, R., Participants, C., 1990. Report and preliminary results of the Expeditions ANTARKTIS VIII/3 of the Research Vessel Polarstern in 1989/90, Cape Town-Punta Arenas, 01.11.1989-01.12-1989.

Hebbeln, D., 2000. Flux of ice-rafted detritus from sea ice in the Fram Strait. Deep. Res. Part II Top. Stud. Oceanogr. 47, 1773–1790. doi:10.1016/S0967-0645(00)00006-0

Hebbeln, D., Wefer, G., 1991. Effects of ice coverage and ice-rafted material on sedimentation in the Fram Strait. Nature 350, 409–411. doi:10.1038/350409a0

Herfort, L., Schouten, S., Abbas, B., Veldhuis, M.J.W., Coolen, M.J.L., Wuchter, C., Boon, J.P., Herndl, G.J., Sinninghe Damsté, J.S., 2007. Variations in spatial and temporal distribution of Archaea in the North Sea in relation to environmental variables. FEMS Microbiol. Ecol. 62, 242–257. doi:10.1111/j.1574-6941.2007.00397.x

Hernández-Sánchez, M.T., Woodward, E.M.S., Taylor, K.W.R., Henderson, G.M., Pancost, R.D., 2014. Variations in GDGT distributions through the water column in the South East Atlantic Ocean. Geochim. Cosmochim. Acta 132, 337–348. doi:10.1016/j.gca.2014.02.009

Herndl, G.J., Reinthaler, T., Teira, E., Aken, H. Van, Veth, C., Pernthaler, A., Pernthaler, J., 2005. Contribution of Archaea to Total Prokaryotic Production in the Deep Atlantic Ocean. Appl. Environ. Microbiol. 71, 2303–2309. doi:10.1128/AEM.71.5.2303

Hertzberg, J.E., Schmidt, M.W., Bianchi, T.S., Smith, R.K., Shields, M.R., Marcantonio, F., 2015. Comparison of eastern tropical Pacific TEX_{86} and Globigerinoides ruber Mg/Ca derived sea surface temperatures: Insights from the Holocene and Last Glacial Maximum. Earth Planet. Sci. Lett. 434, 320–332. doi:10.1016/j.epsl.2015.11.050

Ho, S.L., Mollenhauer, G., Fietz, S., Martínez-Garcia, A., Lamy, F., Rueda, G., Schipper, K., Méheust, M., Rosell-Melé, A., Stein, R., Tiedemann, R., 2014. Appraisal of TEX_{86} and TEX_{86}^{L} thermometries in subpolar and polar regions. Geochim. Cosmochim. Acta 131, 213–226. doi:10.1016/j.gca.2014.01.001

Hopmans, E.C., Schouten, S., Pancost, R.D., Van Der Meer, M.T.J., Sinninghe Damsté, J.S., 2000. Analysis of intact tetraether lipids in archaeal cell material and sediments by high performance liquid chromatography/atmospheric pressure chemical ionization mass spectrometry. Rapid Commun. Mass Spectrom. 14, 585–589. doi:10.1002/(SICI)1097-0231(20000415)14:7<585::AID-RCM913>3.0.CO;2-N

Hopmans, E.C., Weijers, J.W.H., Schefuß, E., Herfort, L., Sinninghe Damsté, J.S., Schouten, S., 2004. A novel proxy for terrestrial organic matter in sediments based on branched and isoprenoid tetraether lipids. Earth Planet. Sci. Lett. 224, 107–116. doi:10.1016/j.epsl.2004.05.012

Horak, R.E.A., Qin, W., Bertagnolli, A.D., Nelson, A., Heal, K.R., Han, H., Heller, M., Schauer, A.J., Jeffrey, W.H., Armbrust, E.V., Moffett, J.W., Ingalls, A.E., Stahl, D.A., Devol, A.H., 2017. Relative impacts of light, temperature, and reactive oxygen on thaumarchaeal ammonia oxidation in the North Pacific Ocean. Limnol. Oceanogr. 63, 1–16. doi:10.1002/lno.10665

Horak, R.E.A., Qin, W., Schauer, A.J., Armbrust, E.V., Ingalls, A.E., Moffett, J.W., Stahl, D.A., Devol, A.H., 2013. Ammonia oxidation kinetics and temperature sensitivity of a natural marine community dominated by Archaea. ISME J. 7, 2023–2033. doi:10.1038/ismej.2013.75

Huguet, C., Cartes, J.E., Sinninghe Damsté, J.S., Schouten, S., 2006. Marine crenarchaeotal membrane lipids in decapods: Implications for the TEX_{86} paleothermometer. Geochemistry, Geophys. Geosystems 7, Q11010. doi:10.1029/2006GC001305

Huguet, C., Fietz, S., Rosell-Melé, A., 2013. Global distribution patterns of hydroxy glycerol dialkyl glycerol tetraethers. Org. Geochem. 57, 107–118. doi:10.1016/j.orggeochem.2013.01.010

Huguet, C., Kim, J.H., de Lange, G.J., Sinninghe Damsté, J.S., Schouten, S., 2009. Effects of long term oxic degradation on the $U_{37}^{k'}$, TEX_{86} and BIT organic proxies. Org. Geochem. 40, 1188–1194. doi:10.1016/j.orggeochem.2009.09.003

Huguet, C., Schimmelmann, A., Thunell, R., Lourens, L.J., Sinninghe Damsté, J.S., Schouten, S., 2007. A study of the TEX_{86}paleothermometer in the water column and sediments of the Santa Barbara Basin, California. Paleoceanography 22, PA3203. doi:10.1029/2006PA001310

Hurley, S.J., Elling, F.J., Könneke, M., Buchwald, C., Wankel, S.D., Santoro, A.E., Lipp, J.S., Hinrichs, K.-U., Pearson, A., 2016. Influence of ammonia oxidation rate on thaumarchaeal lipid composition and the TEX_{86} temperature proxy. Proc. Natl. Acad. Sci. USA 113, 7762–7767. doi:10.1073/pnas.1518534113

Hurley, S.J., Lipp, J.S., Close, H.G., Hinrichs, K.-U., Pearson, A., 2018. Distribution and export of isoprenoid tetraether lipids in suspended particulate matter from the water column of the Western Atlantic Ocean. Org. Geochem. 116, 90–102. doi:10.1016/j.orggeochem.2017.11.010

Ingalls, A.E., Huguet, C., Truxal, L.T., 2012. Distribution of intact and core membrane lipids of archaeal glycerol dialkyl glycerol tetraethers among size-fractionated particulate organic matter in Hood Canal, Puget Sound. Appl. Environ. Microbiol. 78, 1480–1490. doi:10.1128/AEM.07016-11

Ingalls, A.E., Shah, S.R., Hansman, R.L., Aluwihare, L.I., Santos, G.M., Druffel, E.R.M., Pearson, A., 2006. Quantifying archaeal community autotrophy in the mesopelagic ocean using natural radiocarbon. Proc. Natl. Acad. Sci. USA 103, 6442–6447. doi:10.1073/pnas.0510157103

Inglis, G.N., Farnsworth, A., Lunt, D., Foster, G.L., Hollis, C.J., Pagani, M., Jardine, P.E., Pearson, P.N., Markwick, P., Galsworthy, A.M.J., 2015. Descent toward the Icehouse: Eocene sea surface cooling inferred from GDGT distributions. Paleoceanography 30, 1000–1020. doi:10.1002/2014PA002723.Received

Inthorn, M., Mohrholz, V., Zabel, M., 2006a. Nepheloid layer distribution in the Benguela upwelling area offshore Namibia. Deep. Res. Part I Oceanogr. Res. Pap. 53, 1423–1438. doi:10.1016/j.dsr.2006.06.004

Inthorn, M., Wagner, T., Scheeder, G., Zabel, M., 2006b. Lateral transport controls distribution, quality, and burial of organic matter along continental slopes in high-productivity areas. Geology 34, 205–208. doi:10.1130/G22153.1

IPCC, 2014. Climate Change 2014: Synthesis Report. Contribution to Working Groups I, II, III to the Fifth Assessment Report of the Intergovernmental Panel on Climate Change. Geneva, Switzerland. doi:10.1046/j.1365-2559.2002.1340a.x

Isla, A., Scharek, R., Latasa, M., 2015. Zooplankton diel vertical migration and contribution to deep active carbon flux in the NW Mediterranean. J. Mar. Syst. 143, 86–97. doi:10.1016/j.jmarsys.2014.10.017

Iversen, M.H., Nowald, N., Ploug, H., Jackson, G. a., Fischer, G., 2010. High resolution profiles of vertical particulate organic matter export off Cape Blanc, Mauritania: Degradation processes and ballasting effects. Deep. Res. Part I Oceanogr. Res. Pap. 57, 771–784. doi:10.1016/j.dsr.2010.03.007

Iversen, M.H., Pakhomov, E.A., Hunt, B.P.V., van der Jagt, H., Wolf-Gladrow, D., Klaas, C., 2017. Sinkers or floaters? Contribution from salp pellets to the export flux during a large bloom event in the Southern Ocean. Deep. Res. Part II Top. Stud. Oceanogr. 138, 116–125. doi:10.1016/j.dsr2.2016.12.004

Iversen, M.H., Ploug, H., 2010. Ballast minerals and the sinking carbon flux in the ocean: carbon-specific respiration rates and sinking velocity of marine snow aggregates. Biogeosciences 7, 2613–2624. doi:10.5194/bg-7-2613-2010

Jackson, G.A., Checkley Jr, D.M., 2011. Particle size distribution in the upper 100 m water column and their implications for animal feeding in the plankton. Deep Sea Res. Part I Oceanogr. Res. Pap. 58, 283–297. doi:10.1016/j.dsr.2010.12.008

Japp S. Sinninghe, D., S, S., Ellen C, H., Adri C. T., van D., Jan A.J., G., 2002. Crenarchaeol: the characteristic core glycerol dibiphytanyl glycerol tetraether membrane lipid of cosmopolitan pelagic crenarchaeota. J. Lipid Res. 43, 1641–1651. doi:10.1194/jlr.M200148-JLR200

Jonas, A.-S., Schwark, L., Bauersachs, T., 2017. Late Quaternary water temperature variations of the Northwest Pacific based on the lipid paleothermometers TEX_{86}^{H}, $U_{37}^{k'}$ and LDI. Deep. Res. Part I 125, 81–93. doi:10.1016/j.dsr.2017.04.018

Kabel, K., Moros, M., Porsche, C., Neumann, T., Adolphi, F., Andersen, T.J., Siegel, H., Gerth, M., Leipe, T., Jansen, E., Sinninghe Damsté, J.S., 2012. Impact of climate change on the Baltic Sea ecosystem over the past 1,000 years. Nat. Clim. Chang. 2, 871–874. doi:10.1038/nclimate1595

Kalvelage, T., Jensen, M.M., Contreras, S., Revsbech, N.P., Lam, P., Günter, M., LaRoche, J., Lavik, G., Kuypers, M.M.M., 2011. Oxygen Sensitivity of Anammox and Coupled N-cycle Processes in Oxygen Minimum Zones. PLoS One 6, e29299. doi:10.1371/journal.pone.0029299

Karner, M.B., DeLong, E.F., Karl, D.M., 2001. Archaeal dominance in the mesopelagic zone of the Pacific Ocean. Nature 409, 507–510. doi:10.1038/35054051

Kattner, G., Participants, C., 2009. Reports on Polar and Marine Research. The Expedition of the Research Vessel Polarstern to the Arctic in 2008 (ARK-XXIII/2), Longyearbyen-Reykjavik, 06.07-10.08.2008.

Kim, J.-H., Crosta, X., Willmott, V., Renssen, H., Bonnin, J., Helmke, P., Schouten, S., Sinninghe Damsté, J.S., 2012a. Holocene subsurface temperature variability in the eastern Antarctic continental margin. Geophys. Res. Lett. 39. doi:10.1029/2012GL051157

Kim, J.-H., Huguet, C., Zonneveld, K.A.F., Versteegh, G.J.M., Roeder, W., Sinninghe Damsté, J.S., Schouten, S., 2009. An experimental field study to test the stability of lipids used for the TEX_{86} and $U^{k'}_{37}$ palaeothermometers. Geochim. Cosmochim. Acta 73, 2888–2898. doi:10.1016/j.gca.2009.02.030

Kim, J.-H., Romero, O.E., Lohmann, G., Donner, B., Laepple, T., Haam, E., Sinninghe Damsté, J.S., 2012b. Pronounced subsurface cooling of North Atlantic waters off Northwest Africa during Dansgaard–Oeschger interstadials. Earth Planet. Sci. Lett. 339–340, 95–102. doi:10.1016/j.epsl.2012.05.018

Kim, J.-H., Schouten, S., Rodrigo-Gámiz, M., Rampen, S., Marino, G., Huguet, C., Helmke, P., Buscail, R., Hopmans, E.C., Pross, J., Sangiorgi, F., Middelburg, J.B.M., Sinninghe Damsté, J.S., 2015. Influence of deep-water derived isoprenoid tetraether lipids on the TEX^{H}_{86} paleothermometer in the Mediterranean Sea. Geochim. Cosmochim. Acta 150, 125–141. doi:10.1016/j.gca.2014.11.017

Kim, J.-H., van der Meer, J., Schouten, S., Helmke, P., Willmott, V., Sangiorgi, F., Koç, N., Hopmans, E.C., Sinninghe Damsté, J.S., 2010. New indices and calibrations derived from the distribution of crenarchaeal isoprenoid tetraether lipids: Implications for past sea surface temperature reconstructions. Geochim. Cosmochim. Acta 74, 4639–4654. doi:10.1016/j.gca.2010.05.027

Kim, J.H., Crosta, X., Michel, E., Schouten, S., Duprat, J., Sinninghe Damsté, J.S., 2009. Impact of lateral transport on organic proxies in the Southern Ocean. Quat. Res. 71, 246–250. doi:10.1016/j.yqres.2008.10.005

Kim, J.H., Schouten, S., Hopmans, E.C., Donner, B., Sinninghe Damsté, J.S., 2008. Global sediment core-top calibration of the TEX_{86} paleothermometer in the ocean. Geochim. Cosmochim. Acta 72, 1154–1173. doi:10.1016/j.gca.2007.12.010

Kim, J.H., Villanueva, L., Zell, C., Sinninghe Damsté, J.S., 2016. Biological source and provenance of deep-water derived isoprenoid tetraether lipids along the Portuguese continental margin. Geochim. Cosmochim. Acta 172, 177–204. doi:10.1016/j.gca.2015.09.010

Kinsman, D.J.J., Holland, H.D., 1969. The co-precipitation of cations with CaCO3,-IV. The co-precipitation of Sr2+ with aragonite between 16 °C and 96 °C. Geochim. Cosmochim. Acta 33, 1–17.

Klages, M., Participants, C., 2007. Reports on Polar and Marine Research, The Expedition of the Research Vessel Polarstern to the Arctic in 2007 (ARK-XXII/1a-c, Bremerhaven-Tromso-Longyarbyen-Tromso, 29.05-25.07.2007, Alfred-Wegener Institute.

Könneke, M., Bernhard, A.E., de la Torre, J.R., Walker, C.B., Waterbury, J.B., Stahl, D.A., 2005. Isolation of an autotrophic ammonia-oxidizing marine archaeon. Nature 437, 543–546. doi:10.1038/nature03911

Könneke, M., Schubert, D.M., Brown, P.C., Hügler, M., Standfest, S., Schwander, T., Schada von Borzyskowski, L., Erb, T.J., Stahl, D.A., Berg, I.A., 2014. Ammonia-oxidizing archaea use the most energy-efficient aerobic pathway for CO_2 fixation. Proc. Natl. Acad. Sci. 111, 8239–8244. doi:10.1073/pnas.1402028111

Kuypers, M.M., Lavik, G., Woebken, D., Schmid, M., Fuchs, B.M., Amann, R., Jorgensen, B.B., Jetten, M.S., 2005. Massive nitrogen loss from the Benguela upwelling system through anaerobic ammonium oxidation. Proc Natl Acad Sci U S A 102, 6478–6483. doi:10.1073/pnas.0502088102

Lalande, C., Bauerfeind, E., Nöthig, E.M., Beszczynska-Möller, A., 2013. Impact of a warm anomaly on export fluxes of biogenic matter in the eastern Fram Strait. Prog. Oceanogr. 109, 70–77. doi:10.1016/j.pocean.2012.09.006

Lalande, C., Nöthig, E.M., Bauerfeind, E., Hardge, K., Beszczynska-Möller, A., Fahl, K., 2016. Lateral supply and downward export of particulate matter from upper waters to the seafloor in

the deep eastern Fram Strait. Deep. Res. Part I Oceanogr. Res. Pap. 114, 78–89. doi:10.1016/j.dsr.2016.04.014

Lampert, W., 1989. The Adaptive Significance of Diel Vertical Migration of Zooplankton. Funct. Ecol. 3, 21–27. doi:10.2307/2389671

Lampitt, R.S., Bett, B.J., Kiriakoulakis, K., Popova, E.E., Ragueneau, O., Vangriesheim, A., Wolff, G.A., 2001. Material supply to the abyssal seafloor in the northeast Atlantic. Prog. Oceanogr. 50, 27–63. doi:10.1016/S0079-6611(01)00047-7

Lampitt, R.S., Billett, D.S.M., Martin, A.P., 2010. The sustained observatory over the Porcupine Abyssal Plain (PAP): Insights from time series observations and process studies. Deep. Res. Part II Top. Stud. Oceanogr. 57, 1267–1271. doi:10.1016/j.dsr2.2010.01.003

Lange, C.B., Romero, O.E., Wefer, G., Gabric, A.J., 1998. Offshore influence of coastal upwelling off Mauritania, NW Africa, as recorded by diatoms in sediment traps at 2195 m water depth. Deep. Res. Part I Oceanogr. Res. Pap. 45, 985–1013. doi:10.1016/S0967-0637(97)00103-9

Lange, C.B., Treppke, U.F., Fischer, G., 1994. Seasonal diatom fluxes in the Guinea Basin and their relationships to trade winds, hydrography and upwelling events. Deep. Res. Part I Oceanogr. Res. Pap. 41, 859–878. doi:10.1016/0967-0637(94)90080-9

Laubscher, R.K., Prissinotto, R., McQuaid, C.D., 1993. Phytoplankton production and biomass at frontal zones in the Atlantic sector of the Southern Ocean. Polar Biol. 13, 471–481.

Lea, D.W., 2014. Elemental and Isotopic Proxies of Past Ocean Temperatures, in: H.D., H., K.K., T. (Eds.), Treatise on Geochemistry: Second Edition. Elsevier Ltd., Oxford, pp. 373–397. doi:10.1016/B978-0-08-095975-7.00614-8

Leclerc, A.J., Labeyrie, L., 1987. Temperature dependence of the oxygen isotopic fractionation between diatom silica and water. Earth Planet. Sci. Lett. 84, 69–74.

Lee, K.E., Kim, J.-H., Wilke, I., Helmke, P., Schouten, S., 2008. A study of the alkenone, TEX_{86}, and planktonic foraminifera in the Benguela Upwelling System: Implications for past sea surface temperature estimates. Geochemistry, Geophys. Geosystems 9, 1–19. doi:10.1029/2008GC002056

Leider, A., Hinrichs, K.U., Mollenhauer, G., Versteegh, G.J.M., 2010. Core-top calibration of the lipid-based $U^{k'}_{37}$ and TEX_{86} temperature proxies on the southern Italian shelf (SW Adriatic Sea, Gulf of Taranto). Earth Planet. Sci. Lett. 300, 112–124. doi:10.1016/j.epsl.2010.09.042

Lengger, S.K., Hopmans, E.C., Reichart, G.-J., Nierop, K.G.J., Sinninghe Damsté, J.S., Schouten, S., 2012. Intact polar and core glycerol dibiphytanyl glycerol tetraether lipids in the Arabian Sea oxygen minimum zone: II. Selective preservation and degradation in sediment and consequences for the TEX_{86}. Geochim. Cosmochim. Acta 98, 244–258. doi:10.1016/j.gca.2012.05.003

Lincoln, S.A., Wai, B., Eppley, J.M., Church, M.J., Summons, R.E., DeLong, E.F., 2014. Planktonic Euryarchaeota are a significant source of archaeal tetraether lipids in the ocean. Proc. Natl. Acad. Sci. USA 111, 9858–9863. doi:10.1073/pnas.1409439111

Littler, K., Robinson, S.A., Bown, P.R., Nederbragt, A.J., Pancost, R.D., 2011. High sea-surface temperatures during the Early Cretaceous Epoch. Nat. Geosci. 4, 169–172. doi:10.1038/ngeo1081

Liu, X., Lipp, J.S., Hinrichs, K.-U., 2011. Distribution of intact and core GDGTs in marine sediments. Org. Geochem. 42, 368–375. doi:10.1016/j.orggeochem.2011.02.003

Liu, X.L., Lipp, J.S., Simpson, J.H., Lin, Y.S., Summons, R.E., Hinrichs, K.U., 2012. Mono- and dihydroxyl glycerol dibiphytanyl glycerol tetraethers in marine sediments: Identification of both core and intact polar lipid forms. Geochim. Cosmochim. Acta 89, 102–115. doi:10.1016/j.gca.2012.04.053

Liu, Z., Pagani, M., Zinniker, D., Deconto, R.M., Huber, M., Brinkhuis, H., Shah, S.R., Leckie, R.M., Pearson, A., 2009. Global cooling during the Eocene-Oligocene calimate transition. Science (80-.). 323, 1187–1990. doi:10.1126/science.1166368

Locarnini, R.A., Mishonov, A. V., Antonov, J.I., Boyer, T.P., Garcia, H.E., Baranova, O.K., Zweng, M.M., Paver, C.R., Reagan, J.R., Johnson, D.R., Hamilton, M., Seidov, D., 2013. World Ocean Atlas 2013, Volume 1: Temperature. S. Levitus, Ed.; A. Mishonov, Tech. Ed.; NOAA Atlas NESDIS 73, 40. doi:10.1182/blood-2011-06-357442

Lopes dos Santos, R.A., Prange, M., Castañeda, I.S., Schefuß, E., Mulitza, S., Schulz, M., Niedermeyer, E.M., Sinninghe Damsté, J.S., Schouten, S., 2010. Glacial-interglacial variability in Atlantic meridional overturning circulation and thermocline adjustments in the tropical North Atlantic. Earth Planet. Sci. Lett. 300, 407–414. doi:10.1016/j.epsl.2010.10.030

Lopes dos Santos, R.A., Spooner, M.I., Barrows, T.T., De Deckker, P., Sinninghe Damsté, J.S., Schouten, S., 2013. Comparison of organic ($U^{k'}_{37}$, TEX^{H}_{86}, LDI) and faunal proxies (foraminiferal assemblages) for reconstruction of late Quaternary sea surface temperature variability from offshore southeastern Australia. Paleoceanography 28, 377–387. doi:10.1002/palo.20035

López-García, P., Rodriguez-Valera, F., Pedrós-Alió, C., Moreira, D., 2001. Unexpected diversity of small eukaryotes in deep-sea Antarctic plankton. Nature 409, 603–607. doi:10.1038/35054537

Louw, D.C., van der Plas, A.K., Mohrholz, V., Wasmund, N., Junker, T., Eggert, A., 2016. Seasonal and interannual phytoplankton dynamics and forcing mechnisms in the Northern Benguela upwelling system. J. Mar. Syst. 157, 124–134. doi:http://dx.doi.org/10.1016/j.jmarsys.2016.01.009

Lü, X., Liu, X.L., Elling, F.J., Yang, H., Xie, S., Song, J., Li, X., Yuan, H., Li, N., Hinrichs, K.U., 2015. Hydroxylated isoprenoid GDGTs in Chinese coastal seas and their potential as a paleotemperature proxy for mid-to-low latitude marginal seas. Org. Geochem. 89–90, 31–43. doi:10.1016/j.orggeochem.2015.10.004

Manley, T.O., 1995. Branching of Atlantic Water within the Greenland-Spitsbergen Passage: An estimate of recirculation. J. Geophys. Res. 100, 20627–20634. doi:10.1029/95JC01251

Martens-Habbena, W., Berube, P.M., Urakawa, H., de la Torre, J.R., Stahl, D.A., 2009. Ammonia oxidation kinetics determine niche separation of nitrifying Archaea and Bacteria. Nature 461, 976–979. doi:10.1038/nature08465

Martin-Cuadrado, A.-B., Rodriguez-Valera, F., Moreira, D., Alba, J.C., Ivars-Martínez, E., Henn, M.R., Talla, E., López-García, P., 2008. Hindsight in the relative abundance, metabolic potential and genome dynamics of uncultivated marine archaea from comparative metagenomic analyses of bathypelagic plankton of different oceanic regions. ISME J. 2, 865–886. doi:10.1038/ismej.2008.40

Massana, R., Murray, A.E., Preston, C.M., DeLong, E.F., 1997. Vertical distribution and phylogenetic characterization of marine planktonic Archaea in the Santa Barbara Channel. Appl. Environ. Microbiol. 63, 50–56.

McClain, C.R., Signorini, S.R., Christian, J.R., 2004. Subtropical gyre variability observed by ocean-color satellites. Deep. Res. Part II Top. Stud. Oceanogr. 51, 281–301. doi:10.1016/j.dsr2.2003.08.002

McClymont, E.L., Ganeshram, R.S., Pichevin, L.E., Talbot, H.M., van Dongen, B.E., Thunell, R.C., Haywood, A.M., Singarayer, J.S., Valdes, P.J., 2012. Sea-surface temperature records of Termination 1 in the Gulf of California: Challenges for seasonal and interannual analogues of tropical Pacific climate change. Paleoceanography 27, PA2202. doi:10.1029/2011PA002226

Méjanelle, L., Sanchez-Gargallo, A., Bentaleb, I., Grimalt, J.O., 2003. Long chain n-alkyl diols, hydroxy ketones and sterols in a marine eustigmatophyte, Nannochloropsis gaditana, and in Brachionus plicatilis feeding on the algae. Org. Geochem. 34, 527–538. doi:10.1016/S0146-6380(02)00246-2

Meyer, V.D., Max, L., Hefter, J., Tiedemann, R., Mollenhauer, G., 2016. Glacial-to-Holocene evolution of sea surface temperature and surface circulation in the subarctic northwest Pacific and the Western Bering Sea. Paleoceanography 31, 916–927. doi:10.1002/2015PA002877

Mignot, A., Claustre, H., Uitz, J., Poteau, A., Ortenzio, F.D., Xing, X., 2014. Understanding the seasonal dynamics of phytoplankton biomass and the deep chlorophyll maximum in oligotrophic environments: A Bio-Argo float investigation. AGU. Glolal Biogeochem. Cycles 856–876. doi:10.1002/2013GB004781.Received

Mincer, T.J., Church, M.J., Taylor, L.T., Preston, C., Karl, D.M., DeLong, E.F., 2007. Quantitative distribution of presumptive archaeal and bacterial nitrifiers in Monterey Bay and the North Pacific Subtropical Gyre. Environ. Microbiol. 9, 1162–1175. doi:10.1111/j.1462-2920.2007.01239.x

Mollenhauer, G., Basse, A., Kim, J.-H., Sinninghe Damsté, J.S., Fischer, G., 2015. A four-year record of $U^{k'}_{37}$- and TEX_{86}-derived sea surface temperature estimates from sinking particles in the filamentous upwelling region off Cape Blanc, Mauritania. Deep. Res. Part I Oceanogr. Res. Pap. 97, 67–79. doi:10.1016/j.dsr.2014.11.015

Mollenhauer, G., Eglinton, T.I., Hopmans, E.C., Sinninghe Damsté, J.S., 2008. A radiocarbon-based assessment of the preservation characteristics of crenarchaeol and alkenones from continental margin sediments. Org. Geochem. 39, 1039–1045. doi:10.1016/j.orggeochem.2008.02.006

Mollenhauer, G., Inthorn, M., Vogt, T., Zabel, M., Sinninghe Damsté, J.S., Eglinton, T.I., 2007. Aging of marine organic matter during cross-shelf lateral transport in the Benguela upwelling system revealed by compound-specific radiocarbon dating. Geochemistry, Geophys. Geosystems 8. doi:10.1029/2007GC001603

Mollenhauer, G., Schneider, R.R., Jennerjahn, T., Müller, P.J., Wefer, G., 2004. Organic carbon accumulation in the South Atlantic Ocean: Its modern, mid-Holocene and last glacial distribution. Glob. Planet. Change 40, 249–266. doi:10.1016/j.gloplacha.2003.08.002

Mollenhauer, G., Schneider, R.R., Müller, P.J., Spieß, V., Wefer, G., 2002. Glacial/interglacial variablity in the Benguela upwelling system: Spatial distribution and budgets of organic carbon accumulation. Global Biogeochem. Cycles 16, 1134. doi:10.1029/2001GB001488

Monteiro, P.M.S., Dewitte, B., Scranton, M.I., Paulmier, A., van der Plas, A.K., 2011. The role of open ocean boundary forcing on seasonal to decadal-scale variability and long-term change of natural shelf hypoxia. Environ. Res. Lett. 6, 025002. doi:10.1088/1748-9326/6/2/025002

Monteiro, P.M.S., van Der Plas, A., Mohrholz, V., Mabille, E., Pascall, A., Joubert, W., 2006. Variability of natural hypoxia and methane in a coastal upwelling system: Oceanic physics or shelf biology? Geophys. Res. Lett. 33, L16614. doi:10.1029/2006GL026234

Monteiro, P.M.S., van der Plas, A.K., Mélice, J.L., Florenchie, P., 2008. Interannual hypoxia variability in a coastal upwelling system: Ocean-shelf exchange, climate and ecosystem-state implications. Deep. Res. Part I Oceanogr. Res. Pap. 55, 435–450. doi:10.1016/j.dsr.2007.12.010

Moore, J.K., Abbott, M.R., 2002. Surface chlorophyll concentrations in relation to the Antarctic Polar Front: seasonal and spatial patterns from satellite observations. J. Mar. Syst. 37, 69–86. doi:10.1016/S0924-7963(02)00196-3

Moore, J.K., Abbott, M.R., 2000. Phytoplankton chlorophyll distributions and primary production in the Southern Ocean. J. Geophys. Res. Ocean. 105, 28,709-28,722. doi:10.1029/1999JC000043

Moore, J.K., Abbott, M.R., Richman, J.G., 1999. Location and dynamics of the Antarctic Polar Front from satellite sea surface temperature data. J. Geophys. Res. 102, 3059–3074. doi:10.1029/97JC01705

Moreau, R.A., Whitaker, B.D., Hicks, K.B., 2002. Phytosterols, phytostanols, and their conjugates in foods: structural diversity, quantitative analysis, and health-promoting uses. Prog. Lipid Res. 41, 457–500. doi:10.1016/S0163-7827(02)00006-1

Moreira, D., Rodríguez-Valera, F., López-García, P., 2004. Analysis of a genome fragment of a deep-sea uncultivated Group II euryarchaeote containing 16S rDNA, a spectinomycin-like operon and several energy metabolism genes. Environ. Microbiol. 6, 959–969. doi:10.1111/j.1462-2920.2004.00644.x

Müller, P.J., Fischer, G., 2003. C_{37}-Alkenones as Paleotemperature Tool: Fundamentals Based on Sediment Traps and Surface Sediments from the South Atlantic Ocean, in: Wefer, G., Mulitza, S., Ratmeyer, V. (Eds.), The South Atlantic in the Late Quaternary. Springer, Berlin, Heidelberg, pp. 167–193. doi:doi.org/10.1007/978-3-642-18917-3_9

Müller, P.J., Kirst, G., Ruhland, G., von Storch, I., Rosell-Melé, A., 1998. Calibration of the alkenone paleotemperature index $U^{k'}_{37}$ based on core-tops from the eastern South Atlantic and the global ocean (60° N-60° S). Geochim. Cosmochim. Acta 62, 1757–1772. doi:10.1016/S0016-7037(98)00097-0

Müller, P.J., Schneider, R., 1993. An automated leaching method for the determination of opal in sediments and particulate matter. Deep. Res. Part I Oceanogr. Res. Pap. 40, 425–444. doi:10.1016/0967-0637(93)90140-X

Murray, A.E., Blakis, A., Massana, R., Strawzewski, S., Passow, U., Alldredge, A., DeLong, E.F., 1999. A time series assessment of planktonic archaeal variability in the Santa Barbara Channel. Aquat. Microb. Ecol. 20, 129–145. doi:10.3354/ame020129

Murray, A.E., Wul, K.Y., Moyer, C.L., Karl, D.M., Delong, E.F., 1999. Evidence for Circumpolar Distribution of Planktonic Archaea in the Southern Ocean. Aquat. Microb. Ecol. 18, 263–273.

Nöthig, E.-M., Bracher, A., Engel, A., Metfies, K., Niehoff, B., Peeken, I., Bauerfeind, E., Cherkasheva, A., Gäbler-Schwarz, S., Hardge, K., Kilias, E., Kraft, A., Kidane, Y.M., Lalande, C., Piontek, J., Thomisch, K., Wurst, M., 2015. Summertime plankton ecology in Fram Strait-a compilation of long-and short-term observations. Polar Res. 34, 1–18. doi:10.3402/polar.v34.23349

O'Brien, C.L., Robinson, S.A., Pancost, R.D., Sinninghe Damsté, J.S., Schouten, S., Lunt, D.J., Alsenz, H., Bornemann, A., Bottini, C., Brassell, S.C., Farnsworth, A., Forster, A., Huber, B.T., Inglis, G.N., Jenkyns, H.C., Linnert, C., Littler, K., Markwick, P., McAnena, A., Mutterlose, J., Naafs, B.D.A., Püttmann, W., Sluijs, A., van Helmond, N.A.G.M., Vellekoop, J., Wagner, T., Wrobel, N.E., 2017. Cretaceous sea-surface temperature evolution: Constraints from TEX_{86} and planktonic foraminiferal oxygen isotopes. Earth-Science Rev. 172, 224–247. doi:10.1016/j.earscirev.2017.07.012

Orsi, A.H., Whitworth III, T., Nowlin Jr, W.D., 1995. On the meridional extent and fronts of the Antarctic Circumpolar Current. Deep. Res. Part I Oceanogr. Res. Pap. 42, 641–673. doi:10.1016/0967-0637(95)00021-W

Park, E., Hefter, J., Fischer, G., Mollenhauer, G., 2018. TEX_{86} in sinking particles in three eastern Atlantic upwelling regimes. Org. Geochem. 124, 151–163. doi:10.1016/j.orggeochem.2018.07.015

Pearson, A., Ingalls, A.E., 2013. Assessing the Use of Archaeal Lipids as Marine Environmental Proxies. Annu. Rev. Earth Planet. Sci. 41, 359–384. doi:10.1146/annurev-earth-050212-123947

Pearson, A., McNichol, A.P., Benitez-Nelson, B.C., Hayes, J.M., Eglinton, T.I., 2001. Origins of lipid biomarkers in Santa Monica Basin surface sediment: A case study using compound-specific $\Delta^{14}C$ analysis. Geochim. Cosmochim. Acta 65, 3123–3137. doi:10.1016/S0016-7037(01)00657-3

Pelejero, C., Calvo, E., 2003. The upper end of the $U_{37}^{k'}$ temperature calibration revisited. Geochemistry, Geophys. Geosystems 4, 1–12. doi:10.1029/2002GC000431

Pelejero, C., Grimalt, J.O., 1997. The correlation between the U_{37}^{k} and sea surface temperatures in the warm boundary: The South China Sea. Geochim. Cosmochim. Acta 61, 4789–4797.

Peng, X., Jayakumar, A., Ward, B.B., 2013. Community composition of ammonia-oxidizing archaea from surface and anoxic depths of oceanic oxygen minimum zones. Front. Microbiol. 4, 1–12. doi:10.3389/fmicb.2013.00177

Pérez, V., Fernández, E., Marañón, E., Serret, P., García-Soto, C., 2005. Seasonal and interannual variability of chlorophyll a and primary production in the Equatorial Atlantic: in situ and remote sensing observations. J. Plankton Res. 27, 189–197. doi:10.1093/plankt/fbh159

Peterson, R.G., Stramma, L., 1991. Upper-level circulation in the South Atlantic Ocean. Prog. Oceanogr. 26, 1–73. doi:10.1016/0079-6611(91)90006-8

Pitcher, A., Wuchter, C., Siedenberg, K., Schouten, S., Sinninghe Damsté, J.S., 2011. Crenarchaeol tracks winter blooms of ammonia-oxidizing Thaumarchaeota in the coastal North Sea. Limnol. Oceanogr. 56, 2308–2318. doi:10.4319/lo.2011.56.6.2308

Ploug, H., Iversen, M.H., Fischer, G., 2008a. Ballast, sinking velocity, and apparent diffusivity within marine snow and zooplankton fecal pellets: Implications for substrate turnover by attached bacteria. Limnol. Oceanogr. 53, 1878–1886. doi:10.4319/lo.2008.53.5.1878

Ploug, H., Iversen, M.H., Koski, M., Buitenhuis, E.T., 2008b. Production, oxygen respiration rates, and sinking velocity of copepod fecal pellets: Direct measurements of ballasting by opal and calcite. Limnol. Oceanogr. 53, 469–476. doi:10.4319/lo.2008.53.2.0469

Podlaska, A., Wakeham, S.G., Fanning, K.A., Taylor, G.T., 2012. Microbial community structure and productivity in the oxygen minimum zone of the eastern tropical North Pacific. Deep. Res. Part I Oceanogr. Res. Pap. 66, 77–89. doi:10.1016/j.dsr.2012.04.002

Polovina, J.J., Howell, E.A., Abecassis, M., 2008. Ocean's least productive waters are expanding. Geophys. Res. Lett. 35. doi:10.1029/2007GL031745

Prahl, F., Herbert, T., Brassell, S.C., Ohkouchi, N., Pagani, M., Repeta, D., Rosell-Melé, A., Sikes, E., 2000. Status of alkenone paleothermometer calibration: Report from Working Group 3. Geochemistry Geophys. Geosystems 1. doi:10.1029/2000GC000058

Prahl, F.G., Sparrow, M.A., Wolfe, G. V., 2003. Physiological impacts on alkenone paleothermometry. Paleoceanography 18. doi:10.1029/2002PA000803

Prahl, F.G., Wakeham, S.G., 1987. Calibration of unsaturation patterns in long-chain ketone compositions for palaeotemperature assessment. Nature 330, 367–369. doi:10.1038/330367a0

Qin, W., Amin, S.A., Martens-Habbena, W., Walker, C.B., Urakawa, H., Devol, A.H., Ingalls, A.E., Moffett, J.W., Armbrust, E.V., Stahl, D.A., 2014. Marine ammonia-oxidizing archaeal isolates display obligate mixotrophy and wide ecotypic variation. Proc. Natl. Acad. Sci. U. S. A. 111, 12504–12509. doi:10.1073/pnas.1324115111

Qin, W., Carlson, L.T., Armbrust, E.V., Devol, A.H., Moffett, J.W., Stahl, D.A., Ingalls, A.E., 2015. Confounding effects of oxygen and temperature on the TEX_{86} signature of marine Thaumarchaeota. Proc. Natl. Acad. Sci. USA 112, 10979–10984. doi:10.1073/pnas.1501568112

Rampen, S.W., Willmott, V., Kim, J.-H., Uliana, E., Mollenhauer, G., Schefuß, E., Sinninghe Damsté, J.S., Schouten, S., 2012. Long chain 1,13- and 1,15-diols as a potential proxy for palaeotemperature reconstruction. Geochim. Cosmochim. Acta 84, 204–216. doi:10.1016/j.gca.2012.01.024

Read, J.F., Pollard, R.T., Bathmann, U., 2002. Physical and biological patchiness of an upper ocean transect from South Africa to the ice edge near the Greenwich Meridian. Deep. Res. Part II Top. Stud. Oceanogr. 49, 3713–3733. doi:10.1016/S0967-0645(02)00108-X

Reynolds, R.W., Rayner, N.A., Smith, T.M., Stokes, D.C., Wang, W., 2002. An improved in situ and satellite SST Analysis for climate. J. Clim. 15, 1609–1625.

Reynolds, R.W., Smith, T.M., Liu, C., Chelton, D.B., Casey, K.S., Schlax, M.G., 2007. Daily high-resolution-blended analyses for sea surface temperature. J. Clim. 20, 5473–5496. doi:10.1175/2007JCLI1824.1

Richey, J.N., Tierney, J.E., 2016. GDGT and alkenone flux in the northern Gulf of Mexico: Implications for the TEX_{86} and $U_{37}^{k'}$ paleothermometers. Paleoceanography 31, 1547–1561. doi:10.1002/2016PA003032

Robinson, C., Poulton, A.J., Holligan, P.M., Baker, A.R., Forster, G., Gist, N., Jickells, T.D., Malin, G., Upstill-Goddard, R., Williams, R.G., Woodward, E.M.S., Zubkov, M. V., 2006. The Atlantic Meridional Transect (AMT) Programme: A contextual view 1995-2005. Deep. Res. Part II Top. Stud. Oceanogr. 53, 1485–1515. doi:10.1016/j.dsr2.2006.05.015

Rodrigo-Gámiz, M., Rampen, S.W., de Haas, H., Baas, M., Schouten, S., Sinninghe Damsté, J.S., 2015. Constraints on the applicability of the organic temperature proxies $U_{37}^{k'}$, TEX_{86} and LDI in the subpolar region around Iceland. Biogeosciences 12, 6573–6590. doi:10.5194/bgd-12-6573-2015

Rommerskirchen, F., Condon, T., Mollenhauer, G., Dupont, L., Schefuß, E., 2011. Miocene to Pliocene development of surface and subsurface temperatures in the Benguela Current system. Paleoceanography 26, PA3216. doi:10.1029/2010PA002074

Rontani, J.-F., Bonin, P., Jameson, I., Volkman, J.K., 2005. Degradation of alkenones and related compounds during oxic and anoxic incubation of the marine haptophyte *Emiliania huxleyi* with bacterial consortia isolated from microbial mats from the Camargue, France. Org. Geochem. 36, 603–618. doi:10.1016/j.orggeochem.2004.10.010

Rosell-Melé, A., 1998. Interhemispheric appraisal of the value of alkenone indices as temperature and salinity proxies in high-latitude locations. Paleoceanography 13, 694–703. doi:10.1029/98PA02355

Rosell-Melé, A., Eglinton, G., Pflaumann, U., Sarnthein, M., 1995. Atlantic core-top calibration of the U_{37}^{k} index as a sea-surface palaeotemperature indicator. Geochim. Cosmochim. Acta 59, 3099–3107. doi:10.1016/0016-7037(95)00199-A

Rosell-Melé, A., Prahl, F.G., 2013. Seasonality of $U_{37}^{k'}$ temperature estimates as inferred from sediment trap data. Quat. Sci. Rev. 72, 128–136. doi:10.1016/j.quascirev.2013.04.017

Santoro, A.E., Casciotti, K.L., Francis, C.A., 2010. Activity, abundance and diversity of nitrifying archaea and bacteria in the central California Current. Environ. Microbiol. 12, 1989–2006. doi:10.1111/j.1462-2920.2010.02205.x

Schlitzer, R., 2017. Ocean Data View [WWW Document]. URL odv.awi.de

Scholten, J.C., Fietzke, J., Vogler, S., Rutgers van der Loeff, M.M., Mangini, A., Koeve, W., Waniek, J., Stoffers, P., Antia, A., Kuss, J., 2001. Trapping efficiencies of sediment traps from the deep Eastern North Atlantic: The ^{230}Th calibration. Deep. Res. Part II Top. Stud. Oceanogr. 48, 2383–2408. doi:10.1016/S0967-0645(00)00176-4

Schouten, S., Forster, A., Panoto, F.E., Sinninghe Damsté, J.S., 2007. Towards calibration of the TEX_{86} paleothermometer for tropical sea surface temperatures in ancient greenhouse worlds. Org. Geochem. 38, 1537–1546. doi:10.1029/2004PA001041

Schouten, S., Hopmans, E.C., Pancost, R.D., Damste, J.S., 2000. Widespread occurrence of structurally diverse tetraether membrane lipids: evidence for the ubiquitous presence of low-temperature relatives of hyperthermophiles. Proc. Natl. Acad. Sci. U. S. A. 97, 14421–14426. doi:10.1073/pnas.97.26.14421

Schouten, S., Hopmans, E.C., Schefuß, E., Damsté, J.S.S., 2002. Distributional variations in marine crenarchaeotal membrane lipids: a new tool for reconstructing ancient sea water temperatures? Earth Planet. Sci. Lett. 204, 265–274. doi:doi.org/10.1016/S0012-821X(02)00979-2

Schouten, S., Hopmans, E.C., Sinninghe Damsté, J.S., 2013. The organic geochemistry of glycerol dialkyl glycerol tetraether lipids: A review. Org. Geochem. 54, 19–61. doi:10.1016/j.orggeochem.2012.09.006

Schouten, S., Hopmans, E.C., Sinninghe Damsté, J.S., 2004. The effect of maturity and depositional redox conditions on archaeal tetraether lipid palaeothermometry. Org. Geochem. 35, 567–571. doi:10.1016/j.orggeochem.2004.01.012

Schouten, S., Middelburg, J.J., Hopmans, E.C., Sinninghe Damsté, J.S., 2010. Fossilization and degradation of intact polar lipids in deep subsurface sediments: A theoretical approach. Geochim. Cosmochim. Acta 74, 3806–3814. doi:10.1016/j.gca.2010.03.029

Schouten, S., Pitcher, A., Hopmans, E.C., Villanueva, L., van Bleijswijk, J., Sinninghe Damsté, J.S., 2012. Intact polar and core glycerol dibiphytanyl glycerol tetraether lipids in the Arabian Sea oxygen minimum zone: I. Selective preservation and degradation in the water column and consequences for the TEX_{86} . Geochim. Cosmochim. Acta 98, 228–243. doi:10.1016/j.gca.2012.05.002

Schouten, S., van der Meer, M.T.J., Hopmans, E.C., Sinninghe Damsté, J.S., 2008. Comment on "Lipids of marine Archaea: Patterns and provenance in the water column and sediments" by Turich et al. (2007). Geochim. Cosmochim. Acta 72, 5342–5346. doi:10.1016/j.gca.2008.03.028

Schouten, S., Villanueva, L., Hopmans, E.C., van der Meer, M.T.J., Sinninghe Damsté, J.S., 2014. Are Marine Group II Euryarchaeota significant contributors to tetraether lipids in the ocean? Proc. Natl. Acad. Sci. U. S. A. 111, E4285. doi:10.1073/pnas.1416176111

Schukies, J.L., 2018. Prüfung der Anwendbarkeit des TEX_{86} in Proben partikulären organischen Materials und Oberflächensedimenten im Bereich des Zusammentreffens von Nordatlantik - und Labradorstrom am Kontinentalhang vor. Universität Bremen.

Seki, O., Bendle, J.A., Harada, N., Kobayashi, M., Sawada, K., Moossen, H., Inglis, G.N., Nagao, S., Sakamoto, T., 2014. Assessment and calibration of TEX_{86} paleothermometry in the Sea of Okhotsk and sub-polar North Pacific region: Implications for paleoceanography. Prog. Oceanogr. 126, 254–266. doi:10.1016/j.pocean.2014.04.013

Shah, S.R., Mollenhauer, G., Ohkouchi, N., Eglinton, T.I., Pearson, A., 2008. Origins of archaeal tetraether lipids in sediments: Insights from radiocarbon analysis. Geochim. Cosmochim. Acta 72, 4577–4594. doi:10.1016/j.gca.2008.06.021

Shannon, L. V., Nelson, G., 1996. The Benguela: Large Scale Features and Processes and System Variability, in: Wefer, G., Berger, W.H., Siedler, G., Webb, D.J. (Eds.), The South Atlantic: Present and Past Circulation. Springer-Verlag, Berlin, Heidelberg, pp. 163–210. doi:10.1007/978-3-642-80353-6_9

Shevenell, A.E., Ingalls, A.E., Domack, E.W., Kelly, C., 2011. Holocene Southern Ocean surface temperature variability west of the Antarctic Peninsula. Nature 470, 250–254. doi:10.1038/nature09751

Shimokawara, M., Nishimura, M., Matsuda, T., Akiyama, N., Kawai, T., 2010. Bound forms, compositional features, major sources and diagenesis of long chain, alkyl mid-chain diols in Lake Baikal sediments over the past 28,000 years. Org. Geochem. 41, 753–766. doi:10.1016/j.orggeochem.2010.05.013

Sicre, M.-A., Bard, E., Ezat, U., Rostek, F., 2002. Alkenone distributions in the North Atlantic and Nordic sea surface waters. Geochemistry Geophys. Geosystems 3, 1–13. doi:10.1029/2001GC000159

Sicre, M.A., Labeyrie, L., Ezat, U., Duprat, J., Turon, J.L., Schmidt, S., Michel, E., Mazaud, A., 2005. Mid-latitude Southern Indian Ocean response to Northern Hemisphere Heinrich events. Earth Planet. Sci. Lett. 240, 724–731. doi:10.1016/j.epsl.2005.09.032

Siegel, D.A., Deuser, W.G., 1997. Trajectories of sinking in the Sargasso Sea: Modeling of statistical funnel above deep-ocean sediment traps. Deep Sea Res. Part I Oceanogr. Res. Pap. 44, 1519–1541.

Sikes, E.L., O'Leary, T., Nodder, S.D., Volkman, J.K., 2005. Alkenone temperature records and biomarker flux at the subtropical front on the chatham rise, SW Pacific Ocean. Deep. Res. Part I Oceanogr. Res. Pap. 52, 721–748. doi:10.1016/j.dsr.2004.12.003

Sikes, E.L., Volkman, J.K., Robertson, L.G., Pichon, J.-J., 1997. Alkenones and alkenes in surface waters and sediments of the Southern Ocean: Implications for paleotemperature estimation in polar regions. Geochim. Cosmochim. Acta 61, 1495–1505. doi:10.1016/S0016-7037(97)00017-3

Sinninghe Damsté, J.S., Ossebaar, J., Schouten, S., Verschuren, D., 2012. Distribution of tetraether lipids in the 25-ka sedimentary record of Lake Challa: Extracting reliable TEX_{86} and MBT/CBT palaeotemperatures from an equatorial African lake. Quat. Sci. Rev. 50, 43–54. doi:10.1016/j.quascirev.2012.07.001

Sinninghe Damsté, J.S., Schouten, S., Hopmans, E.C., van Duin, A.C.T., Geenevasen, J.A.J., 2002. Crenarchaeol: the characteristic core glycerol dibiphytanyl glycerol tetraether membrane lipid of cosmopolitan pelagic crenarchaeota. J. Lipid Res. 43, 1641–1651. doi:10.1194/jlr.M200148-JLR200

Sintes, E., Bergauer, K., De Corte, D., Yokokawa, T., Herndl, G.J., 2013. Archaeal amoA gene diversity points to distinct biogeography of ammonia-oxidizing Crenarchaeota in the ocean. Environ. Microbiol. 15, 1647–1658. doi:10.1111/j.1462-2920.2012.02801.x

Sintes, E., De Corte, D., Haberleitner, E., Herndl, G.J., 2016. Geographic distribution of archaeal ammonia oxidizing ecotypes in the Atlantic Ocean. Front. Microbiol. 7, 1–14. doi:10.3389/fmicb.2016.00077

Sluijs, A., Schouten, S., Pagani, M., Woltering, M., Brinkhuis, H., Damsté, J.S.S., Dickens, G.R., Huber, M., Reichart, G.-J., Stein, R., Matthiessen, J., Lourens, L.J., Pedentchouk, N., Backman, J., Moran, K., the Expedition 302 Scientists, 2006. Subtropical Arctic Ocean temperatures during the Palaeocene/Eocene thermal maximum. Nature 441, 610–613. doi:10.1038/nature04668

Soltwedel, T., Bauerfeind, E., Bergmann, M., Bracher, A., Budaeva, N., Busch, K., Cherkasheva, A., Fahl, K., Grzelak, K., Hasemann, C., Jacob, M., Kraft, A., Lalande, C., Metfies, K., Nöthig, E.M., Meyer, K., Quéric, N.V., Schewe, I., Włodarska-Kowalczuk, M., Klages, M., 2016. Natural variability or anthropogenically-induced variation? Insights from 15 years of multidisciplinary observations at the arctic marine LTER site HAUSGARTEN. Ecol. Indic. 65, 89–102. doi:10.1016/j.ecolind.2015.10.001

Stramma, L., England, M., 1999. On the water masses and mean circulation of the South Atlantic Ocean. J. Geophys. Res. 104, 20863–20883.

Taylor, K.W.R., Huber, M., Hollis, C.J., Hernandez-Sanchez, M.T., Pancost, R.D., 2013. Re-evaluating modern and Palaeogene GDGT distributions: Implications for SST reconstructions. Glob. Planet. Change 108, 158–174. doi:10.1016/j.gloplacha.2013.06.011

Thornton, D.C.O., 2002. Diatom aggregation in the sea: Mechanisms and ecological implications. Eur. J. Phycol. 37, 149–161. doi:10.1017/S0967026202003657

Tierney, J.E., Tingley, M.P., 2015. A TEX_{86} surface sediment database and extended Bayesian calibration. Sci. data 2, 150029. doi:10.1038/sdata.2015.29

Tolar, B.B., Ross, M.J., Wallsgrove, N.J., Liu, Q., Aluwihare, L.I., Popp, B.N., Hollibaugh, J.T., 2016. Contribution of ammonia oxidation to chemoautotrophy in Antarctic coastal waters. ISME J. 10, 2605–2619. doi:10.1038/ismej.2016.61

Treppke, U.F., Lange, C.B., Wefer, G., 1996. Vertical fluxes of diatoms and silicoflagellates in the eastern equatorial Atlantic, and their contribution to the sedimentary record. Mar. Micropaleontol. 28, 73–96.

Trommer, G., Siccha, M., van der Meer, M.T.J., Schouten, S., Sinninghe Damsté, J.S., Schulz, H., Hemleben, C., Kucera, M., 2009. Distribution of Crenarchaeota tetraether membrane lipids in surface sediments from the Red Sea. Org. Geochem. 40, 724–731. doi:10.1016/j.orggeochem.2009.03.001

Turich, C., Freeman, K.H., Bruns, M.A., Conte, M., Jones, A.D., Wakeham, S.G., 2007. Lipids of marine Archaea: Patterns and provenance in the water-column and sediments. Geochim. Cosmochim. Acta 71, 3272–3291. doi:10.1016/j.gca.2007.04.013

Turich, C., Schouten, S., Thunell, R.C., Varela, R., Astor, Y., Wakeham, S.G., 2013. Comparison of TEX_{86} and $U^{k'}_{37}$ temperature proxies in sinking particles in the Cariaco Basin. Deep. Res. Part I Oceanogr. Res. Pap. 78, 115–133. doi:10.1016/j.dsr.2013.02.008

Urakawa, H., Martens-Habbena, W., Huguet, C., de la Torre, J.R., Ingalls, A.E., Devol, A.H., Stahl, D.A., 2014. Ammonia availability shapes the seasonal distribution and activity of archaeal and bacterial ammonia oxidizers in the Puget Sound Estuary. Limnol. Oceanogr. 59, 1321–1335. doi:10.4319/lo.2014.59.4.1321

Urey, H.C., 1947. The thermodynamic properties of isotopic substances. J. Chem. Soc. 562–581. doi:10.1039/JR9470000562

van Helmond, N.A.G.M., Sluijs, A., Reichart, G.J., Damsté, J.S.S., Slomp, C.P., Brinkhuis, H., 2014. A perturbed hydrological cycle during Oceanic Anoxic Event 2. Geology 42, 123–126. doi:10.1130/G34929.1

Vedernikov, V.I., Gagarin, V.I., Demidov, A.B., Burenkov, V.I., Stunzhas, P.A., 2007. Primary production and chlorophyll distributions in the subtropical and tropical waters of the Atlantic Ocean in the autumn of 2002. Oceanology 47, 386–399. doi:10.1134/S0001437007030113

Versteegh, G.J.M., Bosch, H.-J., de Leeuw, J.W., 1997. Potential palaeoenvironmental information of C24 to C36 mid-chain diols, keto-and mid-chain hydroxy fatty acid; a critical review. Or 27, 1–13.

Villanueva, L., Schouten, S., Sinninghe Damsté, J.S., 2014. Depth-related distribution of a key gene of the tetraether lipid biosynthetic pathway in marine Thaumarchaeota. Environ. Microbiol. 6, 1–32. doi:10.1111/1462-2920.12508

Volkman, J.K., Barrett, S.M., Dunstan, G. a., Jeffrey, S.W., 1992. C_{30}–C_{32} alkyl diols and unsaturated alcohols in microalgae of the class Eustigmatophyceae. Org. Geochem. 18, 131–138. doi:10.1016/0146-6380(92)90150-V

Vorrath, M.-E., Lahajnar, N., Fischer, G., Libuku, V.M., Schmidt, M., Emeis, K.-C., 2017. Spatiotemporal variation of vertical particle fluxes and modelled chlorophyll a standing stocks in the Benguela Upwelling System. J. Mar. Syst. 180, 59–75. doi:10.1016/j.jmarsys.2017.12.002

Wakeham, S.G., Lewis, C.M., Hopmans, E.C., Schouten, S., Sinninghe Damsté, J.S., 2003. Archaea mediate anaerobic oxidation of methane in deep euxinic waters of the Black Sea. Geochim. Cosmochim. Acta 67, 1359–1374. doi:10.1016/S0016-7037(02)01220-6

Walczowski, W., 2013. Frontal structures in the West Spitsbergen current margins. Ocean Sci. 9, 957–975. doi:10.5194/os-9-957-2013

Walter, H.J., Geibert, W., Rutgers Van Der Loeff, M.M., Fischer, G., Bathmann, U., 2001. Shallow vs. deep-water scavenging of ^{231}Pa and ^{230}Th in radionuclide enriched waters of the Atlantic sector of the Southern Ocean. Deep. Res. Part I Oceanogr. Res. Pap. 48, 471–493. doi:10.1016/S0967-0637(00)00046-7

Wassmann, P., Reigstad, M., Haug, T., Rudels, B., Carroll, M.L., Hop, H., Gabrielsen, G.W., Falk-Petersen, S., Denisenko, S.G., Arashkevich, E., Slagstad, D., Pavlova, O., 2006. Food webs and carbon flux in the Barents Sea. Prog. Oceanogr. 71, 232–287. doi:10.1016/j.pocean.2006.10.003

Weber, J.N., Woodhead, P.M.J., 1972. Temperature dependence of oxygen-18 concentration in Reef Coral Carbonates. J. Geophys. Res. 77, 463–473. doi:10.1029/JC077i003p00463

Wefer, G., Fischer, G., 1993. Seasonal patterns of vertical particle flux in equatorial and coastal upwelling areas of the eastern Atlantic. Deep Sea Res. Part I Oceanogr. Res. Pap. 40, 1613–1645. doi:10.1016/0967-0637(93)90019-Y

Weijers, J.W.H., Lim, K.L.H., Aquilina, A., Damsté, J.S.S., Pancost, R.D., 2011. Biogeochemical controls on glycerol dialkyl glycerol tetraether lipid distributions in sediments characterized by diffusive methane flux. Geochemistry, Geophys. Geosystems 12, 1–15. doi:10.1029/2011GC003724

Weijers, J.W.H., Schouten, S., Spaargaren, O.C., Sinninghe Damsté, J.S., 2006. Occurrence and distribution of tetraether membrane lipids in soils: Implications for the use of the TEX_{86} proxy and the BIT index. Org. Geochem. 37, 1680–1693. doi:10.1016/j.orggeochem.2006.07.018

Wekerle, C., Krumpen, T., Dinter, T., von Appen, W.-J., Iversen, M.H., Salter, I., 2018. Properties of Sediment Trap Catchment Areas in Fram Strait: Results From Lagrangian Modeling and Remote Sensing. Front. Mar. Sci. 5. doi:10.3389/fmars.2018.00407

Woebken, D., Fuchs, B.M., Kuypers, M.M.M., Amann, R., 2007. Potential interactions of particle-associated anammox bacteria with bacterial and archaeal partners in the Namibian upwelling system. Appl. Environ. Microbiol. 73, 4648–4657. doi:10.1128/AEM.02774-06

Wuchter, C., Abbas, B., Coolen, M.J.L., Herfort, L., van Bleijswijk, J., Timmers, P., Strous, M., Teira, E., Herndl, G.J., Middelburg, J.J., Schouten, S., Sinninghe Damsté, J.S., 2006a. Archaeal nitrification in the ocean. Proc. Natl. Acad. Sci. USA 103, 12317–12322. doi:10.1073/pnas.0701630104

Wuchter, C., Schouten, S., Boschker, H.T.S., Sinninghe Damsté, J.S., 2003. Bicarbonate uptake by marine Crenarchaeota. FEMS Microbiol. Lett. 219, 203–207. doi:10.1016/S0378-1097(03)00060-0

Wuchter, C., Schouten, S., Coolen, M.J.L., Sinninghe Damsté, J.S., 2004. Temperature-dependent variation in the distribution of tetraether membrane lipids of marine Crenarchaeota: Implications for TEX_{86} paleothermometry. Paleoceanography 19, 1–10. doi:10.1029/2004PA001041

Wuchter, C., Schouten, S., Wakeham, S.G., Sinninghe Damsté, J.S., 2006b. Archaeal tetraether membrane lipid fluxes in the northeastern Pacific and the Arabian Sea: Implications for TEX_{86} paleothermometry. Paleoceanography 21, 1–9. doi:10.1029/2006PA001279

Wuchter, C., Schouten, S., Wakeham, S.G., Sinninghe Damsté, J.S., 2005. Temporal and spatial variation in tetraether membrane lipids of marine Crenarchaeota in particulate organic matter: Implications for TEX_{86} paleothermometry. Paleoceanography 20, 1–11. doi:10.1029/2004PA001110

Xie, S., Liu, X.-L., Schubotz, F., Wakeham, S.G., Hinrichs, K.-U., 2014. Distribution of glycerol ether lipids in the oxygen minimum zone of the Eastern Tropical North Pacific Ocean. Org. Geochem. 71, 60–71. doi:10.1016/j.orggeochem.2014.04.006

Xue, J., Armstrong, R.A., 2009. An improved “benchmark” method for estimating particle settling velocities from time-series sediment trap fluxes. Deep. Res. Part II Top. Stud. Oceanogr. 56, 1479–1486. doi:10.1016/j.dsr2.2008.11.033

Yamamoto, M., Shimamoto, A., Fukuhara, T., Naraoka, H., Tanaka, Y., Nishimura, A., 2007. Seasonal and depth variations in molecular and isotopic alkenone composition of sinking particles from the western North Pacific. Deep. Res. Part I Oceanogr. Res. Pap. 54, 1571–1592. doi:10.1016/j.dsr.2007.05.012

Yamamoto, M., Shimamoto, A., Fukuhara, T., Tanaka, Y., Ishizaka, J., 2012. Glycerol dialkyl glycerol tetraethers and TEX_{86} index in sinking particles in the western North Pacific. Org. Geochem. 53, 52–62. doi:10.1016/j.orggeochem.2012.04.010

Yang, Y., Gao, C., Dang, X., Ruan, X., Lü, X., Xie, S., Li, X., Yao, Y., Yang, H., 2018. Assessing hydroxylated isoprenoid GDGTs as a paleothermometer for the tropical South China Sea. Org. Geochem. 115, 156–165. doi:10.1016/j.orggeochem.2017.10.014

Yu, E.F., Francois, R., Bacon, M.P., Honjo, S., Fleer, A.P., Manganini, S.J., Loeff, R.V.D.M.M., Ittekot, V., 2001. Trapping efficiency of bottom-tethered sediment traps estimated from the intercepted fluxes of ^{230}Th and ^{230}Pa. Deep. Res. Part I Oceanogr. Res. Pap. 48, 865–889. doi:10.1016/S0967-0637(00)00067-4

Zabeti, N., Bonin, P., Volkman, J.K., Jameson, I.D., Guasco, S., Rontani, J.-F., 2010. Potential alteration of $U^{k'}_{37}$ paleothermometer due to selective degradation of alkenones by marine bacteria isolated from the haptophyte Emiliania huxleyi. FEMS Microbiol. Ecol. 73, 83–94. doi:10.1111/j.1574-6941.2010.00885.x

Zachos, J.C., Schouten, S., Bohaty, S., Quattlebaum, T., Sluijs, A., Brinkhuis, H., Gibbs, S.J., Bralower, T.J., 2006. Extreme warming of mid-latitude coastal ocean during the Paleocene-Eocene Thermal Maximum: Inferences from TEX_{86} and isotope data. Geology 34, 737–740. doi:10.1130/G22522.1

Zhang, Y.G., Pagani, M., Wang, Z., 2016. Ring Index: A new strategy to evaluate the integrity of TEX_{86} paleothermometry. Paleoceanography 31, 220–232. doi:10.1002/2015PA002848

Zhang, Y.G., Zhang, C.L., Liu, X.-L., Li, L., Hinrichs, K.-U., Noakes, J.E., 2011. Methane Index: A tetraether archaeal lipid biomarker indicator for detecting the instability of marine gas hydrates. Earth Planet. Sci. Lett. 307, 525–534. doi:10.1016/j.epsl.2011.05.031

.

Acknowledgements

The completion of this PhD would not have been possible without help and encouragement from a number of people to whom I am extremely grateful.

I would like to give special thanks to my supervisor Gesine Mollenhauer. Gesine, thank you for giving me a chance to my new scientific career under such a great circumstance as well as your valuable times of supervision, for getting me into the topic and sharing your knowledge and passion for building up my own ideas. I still remember your acceptance email me as a PhD student in your group. That has changed my life a lot. A special thank also goes to you, Jens Hefter, for mentoring me in the lab and most figures in this thesis were possible only with your help for last years. I would like to thank Ann Pearson for reviewing my thesis. I am honored that you review my thesis and attend my defense.

Particular thanks must also be recorded to Gesine's working group members Maria Winterfeld, Vera Meyer, Célia Santos, Shuwen Sun, and Hendrik Grotheer, Binging Wei, Torben Gentz, Elizabeth Bonk for their support and encouragement over the years. Maria, it was possible with your help that I got integrated into our group so easily. I always remember your big welcome when I started my PhD in Bremen. I learned your passion for science. Vera, Celia, Shuwen, and Bingbing I enjoyed the time we spent together and our conversation to help each other through our PhD life. I wish you a great future of your life whatever you do and wherever you live. Hendrik, thank you for accompanying while I was writing. You have overcome the boring time sitting next to me. The window seat is yours from now on. Torben and Liz, your laugh and smile gave me positive energy every day.

I would also like to thank Gerhard Fischer, Morten Iverson, and Martin Könneke for their work in my thesis committee. With all the valuable discussions we have, I could have different perspectives on my research and it helped me a lot to develop new ideas.

I deeply thank to Jin-Hyung Kim. Your simple question ´where is your dream?´ made me to pursue my PhD. As a friend and a mentor, you inspire me to learn something new. Thank you to all my friends in Korea that are not mentioned here for supporting me mentally. The physical distance between Korea and Germany is not a big matter for our friendship.

Finally, and most importantly, I want to thank my family in Korea whose support has been constant despite the distance. Mom and dad, I appreciate your endless love. I always miss you. 엄마 아빠 항상 감사하고 사랑합니다. My brother, Sung-Jin, I wish I could support you as much as you do for me. I am always proud of you. Renate and Volker, danke für alles. I learn your unconditional love every day. I am glad to be part of this family.

Axel, thank you for your endless love and great patience over the years this thesis has taken. I cannot say “thank you” enough. This thesis does exist only because you are always by my side. You have encouraged and helped me get through this tough time. You have made such a huge impact on my life. We always move forward together. Let´s start our new journey.

Versicherung an Eides Statt / *Affirmation in lieu of an oath*

gem. § 5 Abs. 5 der Promotionsordnung vom 18.06.2018 /
according to § 5 (5) of the Doctoral Degree Rules and Regulations of 18 June, 2018

Ich / I, EUN MI, PARK, Nansenstrasse 11 A, 27711 Osterholz-Scharmbeck, 3019543

(Vorname / First *Name*, Name / *Name*, Anschrift / *Address*, ggf. Matr.-Nr. / *student ID no., if applicable)*

versichere an Eides Statt durch meine Unterschrift, dass ich die vorliegende Dissertation selbständig und ohne fremde Hilfe angefertigt und alle Stellen, die ich wörtlich dem Sinne nach aus Veröffentlichungen entnommen habe, als solche kenntlich gemacht habe, mich auch keiner anderen als der angegebenen Literatur oder sonstiger Hilfsmittel bedient habe und die zu Prüfungszwecken beigelegte elektronische Version (PDF) der Dissertation mit der abgegebenen gedruckten Version identisch ist. / *With my signature I affirm in lieu of an oath that I prepared the submitted dissertation independently and without illicit assistance from third parties, that I appropriately referenced any text or content from other sources, that I used only literature and resources listed in the dissertation, and that the electronic (PDF) and printed versions of the dissertation are identical.*

Ich versichere an Eides Statt, dass ich die vorgenannten Angaben nach bestem Wissen und Gewissen gemacht habe und dass die Angaben der Wahrheit entsprechen und ich nichts verschwiegen habe*. / I affirm in lieu of an oath that the information provided herein to the best of my knowledge is true and complete.*

Die Strafbarkeit einer falschen eidesstattlichen Versicherung ist mir bekannt, namentlich die Strafandrohung gemäß § 156 StGB bis zu drei Jahren Freiheitsstrafe oder Geldstrafe bei vorsätzlicher Begehung der Tat bzw. gemäß § 161 Abs. 1 StGB bis zu einem Jahr Freiheitsstrafe oder Geldstrafe bei fahrlässiger Begehung. / *I am aware that a false affidavit is a criminal offence which is punishable by law in accordance with § 156 of the German Criminal Code (StGB) with up to three years imprisonment or a fine in case of intention, or in accordance with § 161 (1) of the German Criminal Code with up to one year imprisonment or a fine in case of negligence.*

Ort / *Place*, Datum / *Date*

Unterschrift / *Signature*